Neutrino Oscillations in Astrophysics

A thesis submitted in partial fulfilment

of the requirements for the degree of

Doctor of Philosophy in Physics

in the

University of Canterbury

by

Giles Adrian Reid

May 2010

Contents

List of Figures

List of Tables

Acknowledgements

Throughout the long process of this thesis many people have provided tremendous assistance. Thanks to my supervisors, Jenni Adams and Suruj Seunarine, for their steady guidance and confidence in me. Thanks also to the other academic staff and administrators of the Department of Physics and Astronomy for making the administrative and organizational aspects of my thesis work seem very simple. I also must express my deepest gratitude to all the interesting and lively people I have been lucky enough to know during the past several years. Their companionship and support enabled me to overcome the challenges and stresses of completing this project, a goal which frequently felt like an impossible dream.

Abstract

A survey of the theory of neutrino oscillations in dense matter and neutrino backgrounds is presented. We discuss collective neutrino systems using the gyroscopic pendulum analogy and describe the motion that results from self-induced parametric resonances. The effects of dense matter on the flavour oscillations of neutrinos are also detailed. This theory is applied to the case of continuous supernova neutrino spectra and explanations of the spectral swapping behaviour seen in numerical studies are summarized.

The results of numerical simulations of supernova oscillations in turbulent supernova backgrounds are presented and discussed. We study the motion of two example supernova neutrino spectra and examine the differences in the dynamics and flavour evolution that results from adding turbulent fluctuations to the supernova matter background. We also investigate the effect that fluctuations in the neutrino density can have on the oscillation behaviour. We find that in general the final neutrino spectra emerging from the inner supernova regions are quite robust to fluctuations in the backgrounds in our model, while the intermediate dynamics can be very strongly altered. Some significant changes in the final spectra are also found to occur when the neutrino background density fluctuations are large.

We give a detailed review of the resonant matter effects that determine the survival probabilities of atmospheric muon neutrinos. The differences between various Earth density models are described, and these models are then used to predict the flux of muon-type neutrino events in the Deep Core extension to the IceCube detector. We use recent results from the detector collaboration and build on previous work which considered the sensitivity of the detector to the mass hierarchy, and show that uncertainties in the Earth's density can have a significant influence on the event rates.

Introduction

In recent years the theoretical and experimental understanding of neutrino flavour oscillations has increased enormously. Most of the mixing parameters are accurately measured, and it is likely that future detectors will be able to use neutrinos from astrophysical sources such as supernovae as a probe of the properties of these sources. However, in order to correctly interpret the results from future detectors we require a thorough understanding of the behaviour of neutrinos in dense matter and neutrino backgrounds. This thesis concentrates on the collective flavour transformations of neutrinos in the neutrino-dense regions near supernova cores, and the effects of matter resonances on atmospheric neutrinos that pass through the Earth. In both cases, there is the possibility of using future observations to determine one of the remaining unknown parameters in neutrino physics: the neutrino mass hierarchy.

Neutrino flavour oscillations were first considered in 1957 by Bruno Pontecorvo [1], who was inspired by the oscillations of neutral kaons. He developed the quantitative theory of neutrino oscillations in a 1967 paper [2], and shortly afterwards, in 1968, the results of an experiment by Ray Davis which measured the Solar neutrino flux were announced [3]. The experiment found that there were significantly fewer neutrinos arriving at Earth than expected from theoretical predictions of nuclear reaction rates in the Sun's core. This deficit, dubbed the Solar neutrino problem, provided some evidence for neutrino flavour change, but the problem was only fully resolved with very accurate measurements from the SNO and Kamiokande detectors [4, 5]. The flux and flavour mixture measured by these detectors could only be explained by considering the effect of the dense matter in the Sun on the flavour oscillations of neutrinos created in the core. This effect was named the Mikheyev-Smirnov-Wolfenstein (MSW) effect after the authors of the two major papers which first described it [6, 7], and it provides a full explanation of how the observed deficit arises from the addition of a matter term to the Hamiltonian describing neutrino oscillations in vacuum.

Shortly after the existence of neutrino flavour oscillations was definitively proved, interest in the effects of neutrino–neutrino scattering on neutrino oscillations grew. The behaviour of very dense neutrino gases had been considered as long ago as 1992 [8–11], but the recent surge of interest in this area is mainly a result of numerical simulations of supernova neutrino oscillations, which show that neutrino–neutrino scattering can cause unexpected and novel effects where the neutrino ensemble oscillates as a collective entity and can undergo drastic flavour changes completely unlike those seen in solar or atmospheric neutrinos [12–17]. The best chance we have of observing these effects is in supernovae, where the density of neutrinos is high enough for the neutrino-neutrino interactions to become significant. The neutrino density in the early universe was also high enough for collective oscillations to be important, but the effects are more subtle and are only indirectly observable [10, 11, 18–20].

The effects of the ordinary matter surrounding the supernova core on neutrino oscillations are also complex, and must be considered along with the more dramatic collective neutrino effects. As well as the now-standard MSW effect, recent numerical simulations have explored the effects of expanding supernova shockwaves and their time-dependent effects on neutrino signals on Earth, as well as the role of turbulence [21–27]. Earlier works [28, 29] considered the effect of turbulence in the Sun as part of the explanation of the Solar neutrino problem, but these effects turned out not to be important for Solar neutrinos. It is only very recently that the combined effects of neutrino-neutrino interactions and adiabatic matter profiles resulting from shocks and turbulent fluctuations have been studied for supernova neutrinos.

In chapter 1 we give a survey of the current theoretical understanding of neutrino oscillations. We discuss the effects of dense matter on neutrinos, and the collective oscillation behaviour that occurs in regions where the neutrino density is high enough for neutrino-neutrino scattering to be an important process. Several approximate and limiting cases are studied analytically and numerically to provide a basis for the interpretation of our supernova neutrino simulations.

Chapter 2 presents the results of our simulations of supernova neutrinos travelling through the dense matter and neutrino background that surrounds the supernova core. In the initial phase of a supernova explosion the neutrino luminosities are so high that neutrino-neutrino scattering is the dominant effect. We give a detailed description of the flavour oscillations that occur using two representative supernova neutrino spectra, and discuss the effects of the matter

background. We also examine the effects of turbulent fluctuations in the matter background and non-adiabaticity in the neutrino density, and consider the effects of the neutrino hierarchy on the transformations.

In the final chapter we consider a different system in which neutrino oscillations play an important role. The oscillations of atmospheric neutrinos as they pass through the dense matter in the Earth are strongly influenced by resonances resulting from the structure of the Earth's density profile [30–37]. The jump in density between the core and mantle results in significant modifications of the neutrino survival probabilities compared to a smoothly changing density profile. We discuss the implications of these resonances on atmospheric neutrino measurements with the Deep Core extension to the IceCube neutrino telescope [38–40]. We also build upon the work of Mena *et al.* [41] and use recent results from the collaboration to update the predicted flux rates and the possibility of using these rates to measure the neutrino mass hierarchy. We extend their efforts by considering the errors induced by uncertainties in the Earth's density profile and their effects on the sensitivity of the detector to the neutrino mass hierarchy and the structure of the Earth generally.

Chapter 1

Neutrino Oscillation Theory

In this chapter we summarize and explain the current theoretical understanding of neutrino oscillations, and examine several neutrino systems and their analytic solutions. In particular, we discuss the effects of very high neutrino densities on flavour oscillations, and describe the collective behaviours that occur in simple cases. These solutions provide important insights into the complex behaviour seen in more realistic numerical simulations of supernova neutrinos, such as those we describe in chapter 2.

1.1 Neutrino Flavour Mixing

As neutrinos propagate their flavour state changes due to the fact that the flavour eigenstates are not eigenstates of the vacuum Hamiltonian. To explain experimental results such as the Solar neutrino deficit it is necessary for the three neutrino flavour eigenstates to be linear combinations of three different mass eigenstates. In general,

$$|\nu_\alpha\rangle = \sum_{\beta=1}^{3} U_{\alpha\beta}|m_\beta\rangle, \tag{1.1}$$

where the notation $|\nu_x\rangle$ is used to represent flavour eigenstates and $|m_x\rangle$ refers to the mass eigenstates. The absolute values of the masses of the eigenstates are presently unknown, although the sum of the three neutrino masses is constrained by cosmological observations to be less than 0.58 eV [42]. As will be shown below, it is actually the squared differences in mass of these eigenstates that are typically measurable in neutrino oscillation experiments.

U is a mixing matrix whose components are conventionally written as

$$U = \begin{bmatrix} c_{12}c_{13} & s_{12}c_{13} & s_{13}e^{-i\delta} \\ -s_{12}c_{23} - c_{13}s_{23}s_{13}e^{i\delta} & c_{12}c_{23} - s_{12}s_{23}s_{13}e^{i\delta} & s_{23}c_{13} \\ s_{12}s_{23} - c_{12}c_{23}s_{13}e^{i\delta} & -c_{12}s_{23} - s_{12}c_{23}s_{13}e^{i\delta} & c_{23}c_{21} \end{bmatrix} \times \mathrm{diag}(e^{i\alpha_1/2}, e^{i\alpha_2/2}, 1), \tag{1.2}$$

where $c_{ab} \equiv \cos\theta_{ab}$ and $s_{ab} \equiv \sin\theta_{ab}$. The terms involving alphas and delta are CP-violating terms, and the alpha terms only appear in the equations if neutrinos are Majorana particles. The three angles in the mixing matrix, together with the two independent mass squared differences between the three mass eigenstates, determine the flavour oscillation behaviour of neutrinos in vacuum. Many oscillation experiments can be quite accurately modelled as a two-state oscillation using only one of these mass squared differences because the best-fit value of the atmospheric mass squared difference is about 25 times larger than the solar value. This means that the corresponding oscillation frequencies are very different, so in most cases only one of them is significant for a particular experimental measurement.

The atmospheric mass squared difference, $\Delta m^2_{\mathrm{atm}}$, is approximately 2×10^{-3} eV^2, and as its name suggests it is determined from measurements of neutrinos created by cosmic rays in the Earth's atmosphere. By combining measurements of cosmic ray fluxes made with surface detectors with measurements of the flavours and fluxes of neutrinos that have passed through the Earth it is possible to determine the flavour change probability as a function of zenith angle and hence path length. This allows the mixing angle and mass squared difference to be calculated quite accurately. Other experiments measuring the fluxes of muon neutrinos from accelerators and the fluxes of electron antineutrinos from nuclear reactors find that only a small fraction of the atmospheric muon neutrinos are oscillating into electron neutrinos. This means that the effective mixing angle θ_{atm} that fits the atmospheric data alone is very close to θ_{23} in the mixing matrix above.

The mass squared difference that explains the Solar neutrino problem, often written $\Delta m^2_{\odot}$, is much smaller, having a value of approximately $8 \times 10^{-5}\mathrm{eV}^2$. The nuclear processes in the Sun's core produce only electron neutrinos, so by measuring the flavour ratio of neutrinos coming from the Sun an independent set of mixing parameters can be determined. The accuracy of the comparison

Regime	Symbol	Δm^2 (eV^2)	θ
Atmospheric	$_{\text{atm}} \simeq {}_{23}$	$(2.4 \pm 0.5) \times 10^{-3}$	$(45 \pm 7)^\circ$
Solar	$_{\odot} \simeq {}_{12}$	$(7.59 \pm 0.21) \times 10^{-5}$	$(33.9^{+2.4}_{-2.2})^\circ$
Small angle	$_{13}$	$\Delta m^2_{\odot} \pm \Delta m^2_{\text{atm}}$	$< 10.3^\circ$

Table 1.1: Neutrino oscillation parameters.

of the total Solar neutrino flux in all flavours with the theoretical prediction further strengthens the evidence for Solar neutrino oscillations. To fully explain the Solar neutrino flux measurements the effect of the matter in the Sun resulting from the Large Mixing Angle Mikheyev-Smirnov-Wolfenstein (LMA-MSW) effect must also be included [6, 7]. The resulting analysis allows for the determination of the Solar mixing angle, $\theta_{\odot}$, which is approximately equal to θ_{12} in the mixing matrix above.

Current experimental values of the mixing angles and mass squared differences are shown in Table 1.1 [43]. A few major uncertainties remain in the neutrino mixing parameters. The mixing angle θ_{13} is known to be very small compared to the other two mixing angles (which are almost maximal), but there is not enough evidence to decide whether θ_{13} is precisely zero or very small but non-zero. Another difficult experimental problem is determining the hierarchy of the neutrino mass states. Vacuum oscillation probabilities do not depend on the sign of Δm^2, so the sign of the atmospheric Δm^2 parameter is currently unknown. Because of the nature of the LMA-MSW effect on Solar neutrinos, it is possible to determine which of the two more closely-spaced neutrino mass eigenstates is the heavier one, but the current data does not allow us to say whether the third mass state is heavier or lighter than two Solar mass eigenstates. The case where it is heavier is called the "normal hierarchy", while the case where it is lighter is known as the "inverted hierarchy". As we will show, measurements of supernova and atmospheric neutrinos and their oscillations may be able to distinguish the two mass hierarchies.

The values of the CP-violating terms in the mixing matrix are unknown at present, in large part because they are proportional to the unmeasured small mixing angle. We have not considered the effect of non-zero CP-violation in our study. The identity of neutrinos as either Majorana or Dirac particles is also unknown, but is not relevant to our study.

In this work, the parameters of interest are the value of θ_{13} and the sign of the neutrino mass hierarchy. In supernovae the effect of the mass difference is

dependent on the magnitude of Δm^2, so it is sensible in most cases to ignore the small $\Delta m^2_\odot$ and consider the two closely-spaced mass eigenstates as a single state widely separated from the third mass eigenstate. Then we have an effective two-flavour mixing scenario, where the small mixing angle θ_{13} is the important one because it determines the mixing from $\nu_e \leftrightarrow \nu_x$, where ν_x is a mixture of μ and τ neutrinos. As will be demonstrated, any non-zero value of θ_{13}, no matter how small, can result in large flavour mixing due to the strong amplifying effect of collective oscillations and matter resonances.

The sign of the neutrino hierarchy is also a very important parameter for supernova neutrinos. Experiments to date have not made any determination of the hierarchy, but supernova neutrino collective effects are dramatically different in the two hierarchies. It is possible that measurements of supernova neutrino spectra could resolve this difficult experimental question. Throughout this work we will discuss the differences in behaviour that result from changing the hierarchy.

The two-flavour approximation allows us to represent the flavour of any given neutrino as a normalized two-component complex vector

$$\psi_\alpha = \begin{pmatrix} a_e \\ a_x \end{pmatrix}, \tag{1.3}$$

where the components are the coefficients of the electron and x flavours, that is, an arbitrary neutrino flavour state is represented as

$$|\nu_a\rangle = a_e|\nu_e\rangle + a_x|\nu_x\rangle. \tag{1.4}$$

With this definition the equation of motion for any neutrino can be written as

$$i\frac{\mathrm{d}}{\mathrm{d}t} = \mathcal{H}\begin{pmatrix} a_e \\ a_x \end{pmatrix}, \tag{1.5}$$

where $\mathcal{H}$ is a 2×2 matrix that in general contains the effects of vacuum mixing, background matter, and neutrino-neutrino interactions.

For vacuum oscillations, we can use the mixing parameters to calculate the probability that a neutrino created in a certain flavour eigenstate will be detected in the same state. In the rest frame of a given mass eigenstate the total energy

is m, so if we decompose a flavour state ν_α into its mass eigenstates we have

$$|\nu_\alpha(\tau)\rangle = M_1 e^{-im_1\tau}|m_1\rangle + M_2 e^{-im_2\tau}|m_2\rangle, \tag{1.6}$$

where τ is the proper time in the neutrino's rest frame, $m_{1,2}$ are the mass eigenstates and $M_{1,2}$ are the appropriate matrix elements that determine the ratio of mass eigenstates that make up the flavour eigenstate ν_α. Because neutrinos are created and detected as flavour eigenstates, we are usually most interested in the oscillation probability: the probability that a neutrino created in flavour state α will be detected in flavour state β. If we transform Equation 1.6 into the lab frame and use suitable relativistic approximations, we can calculate this probability as a function of neutrino energy and distance travelled. The result is the standard formula [43]

$$P(\nu_\alpha \to \nu_\beta) = \sin^2 2\theta \sin^2\left[1.27\Delta m^2(\text{eV})\frac{L(\text{km})}{E(\text{GeV})}\right], \tag{1.7}$$

where L is the propagation length, E is the neutrino energy, and Δm^2 and θ are the two-flavour mixing parameters appropriate to the particular experiment. This formula accounts for neutrino oscillations in vacuum, and can be fairly simply understood as interference between two different frequency modes. However, in practice most experiments deal with neutrinos that have passed through matter, whether in the Earth, the Sun, or both. The solution to the Solar neutrino problem, for instance, depends entirely on the MSW effect caused by the matter in the Sun and its slow decrease in density. Depending on the physical environment through which the neutrinos propagate, the vacuum formula may become completely inaccurate. Near the core of a supernova, for example, the vacuum term in the Hamiltonian is only a small perturbation compared to the much larger matter and neutrino background terms. In general, these background interaction effects result in much more complex dynamics than the simple, regular vacuum oscillations. The complex flavour evolution in dense backgrounds is the major focus of this chapter.

1.2 The Effects of Matter

In the presence of matter the neutrino potentials gain an additional term. Because the interaction of neutrinos with baryons is the same for all flavours it is

only the electron density which is relevant for neutrino oscillations. The resulting Hamiltonian for neutrinos in matter is given by:

$$\mathcal{H} = \frac{\Delta m^2}{4E_\nu} \begin{bmatrix} -\cos 2\theta_V & \sin 2\theta_V \\ \sin 2\theta_V & \cos 2\theta_V \end{bmatrix} + \frac{V(x)}{2} \begin{bmatrix} 1 & 0 \\ 0 & -1 \end{bmatrix}, \tag{1.8}$$

where Δm^2 is the mass squared difference of the vacuum eigenstates, θ_V is the vacuum mixing angle, E_ν is the neutrino energy, and $V(x) = \sqrt{2} G_F \rho_e(x)$ is the matter term which takes the electron neutrino charged-current interactions into account through the number density of neutrinos ρ_e. The first term in the Hamiltonian is the two-flavour vacuum mixing term which will always be present regardless of the background.

As described in [44], we can also recast the Schrödinger equation in a convenient form by transforming from the flavour basis to the mass basis. Instead of considering the neutrino as a mixture of flavour eigenstates, we can represent it as a mixture of mass eigenstates, so Equation 1.4 becomes, in this basis,

$$|\nu_a\rangle = a_H |m_H\rangle + a_L |m_L\rangle, \tag{1.9}$$

where H and L refer to the higher and lower mass eigenstates. The Hamiltonian including the matter term can be diagonalized into

$$\mathcal{H} \longrightarrow \mathcal{H}' = \mathcal{V}\mathcal{H}\mathcal{V}^\dagger = \begin{pmatrix} -\omega_m & 0 \\ 0 & \omega_m \end{pmatrix}. \tag{1.10}$$

The eigenvalues $\pm\omega_m$ are calculated from the characteristic equation derived from Equation 1.8:

$$(V - \omega_V \cos 2\theta_V - \omega_m)(-V + \omega_V \cos 2\theta_V - \omega_m) - \omega_V^2 \sin^2 2\theta_V = 0, \tag{1.11}$$

where $\omega_V = \Delta m^2 / 4E_\nu$ is the vacuum oscillation frequency, θ_V is the vacuum mixing angle, and V is the magnitude of the matter term in Equation 1.8. Solving for ω_m we find

$$\omega_m = \pm\sqrt{V^2 - 2V\omega_V \cos 2\theta_V + \omega_V^2}. \tag{1.12}$$

If we now write $\mathcal{V}$ as a rotation matrix

$$\mathcal{V} = \begin{pmatrix} \cos\theta_m & -\sin\theta_m \\ \sin\theta_m & \cos\theta_m \end{pmatrix} \tag{1.13}$$

and solve Equation 1.10 we can write the matter mixing angle in terms of the vacuum parameters:

$$\begin{aligned} \omega_m \sin 2\theta_m &= \omega_V \sin 2\theta_V, \\ \omega_m \cos 2\theta_m &= \omega_V \cos 2\theta_V - V, \\ \tan 2\theta_m &= \frac{\sin 2\theta_V}{\cos 2\theta_V - V/\omega_V}. \end{aligned} \tag{1.14}$$

With all of these transformations in hand, we can now rewrite the Schrödinger equation for the neutrinos in the mass eigenstate basis rather than the usual flavour basis. We will label the mass basis components a_H and a_L, where the subscripts label the higher and lower mass states. We define ψ_m in a similar way to ψ_α above. In the flavour basis we then have

$$i\frac{\mathrm{d}\psi_\alpha}{\mathrm{d}t} = \mathcal{H}\psi_\alpha. \tag{1.15}$$

Since supernova neutrinos are always ultra-relativistic the time derivative is equivalent to a space derivative (since we set $c = 1$), and using $\mathcal{V}$ we can write

$$\begin{aligned} i\frac{\mathrm{d}}{\mathrm{d}x}\left(\mathcal{V}^\dagger\psi_m\right) &= \mathcal{H}\left(\mathcal{V}^\dagger\psi_m\right) \\ i\mathcal{V}^\dagger\frac{\mathrm{d}\psi_m}{\mathrm{d}x} + i\frac{\mathrm{d}\mathcal{V}^\dagger}{\mathrm{d}x}\psi_m &= \mathcal{H}\left(\mathcal{V}^\dagger\psi_m\right) \end{aligned} \tag{1.16}$$

We multiply both sides by $\mathcal{V}$ to obtain

$$i\mathcal{V}\mathcal{V}^\dagger\frac{\mathrm{d}\psi_m}{\mathrm{d}x} = \left(i\mathcal{V}\frac{\mathrm{d}\mathcal{V}^\dagger}{\mathrm{d}x} + \mathcal{V}\mathcal{H}\mathcal{V}^\dagger\right)\psi_m \tag{1.17}$$

From Equation 1.13 we find

$$\begin{aligned} \mathcal{V}\frac{\mathrm{d}\mathcal{V}^\dagger}{\mathrm{d}x} &= \begin{pmatrix} \cos\theta_m & -\sin\theta_m \\ \sin\theta_m & \cos\theta_m \end{pmatrix} \frac{\mathrm{d}\theta_m}{\mathrm{d}x} \begin{pmatrix} -\sin\theta_m & \cos\theta_m \\ -\cos\theta_m & -\sin\theta_m \end{pmatrix} \\ &= \begin{pmatrix} 0 & 1 \\ -1 & 0 \end{pmatrix} \theta_m', \end{aligned} \tag{1.18}$$

where the prime denotes the spatial derivative. Using Equation 1.10 we can now express Equation 1.16 as

$$\frac{\mathrm{d}\psi_m}{\mathrm{d}x} = \begin{pmatrix} i\omega_m & -\theta'_m \\ \theta'_m & -i\omega_m \end{pmatrix} \psi_m, \tag{1.19}$$

which leads to the evolution equation

$$i\frac{d}{dx}\begin{pmatrix} a_H \\ a_L \end{pmatrix} = \begin{pmatrix} \omega_m & i\theta'_m \\ -i\theta'_m & -\omega_m \end{pmatrix} \begin{pmatrix} a_H \\ a_L \end{pmatrix}, \tag{1.20}$$

where a_H and a_L are the higher and lower mass eigenstate components of the neutrino state. ω_m, the effective freqency in the presence of matter, is calculated from

$$\omega_m(x) = \omega_V \frac{\sin 2\theta_V}{\sin 2\theta_m(x)}, \tag{1.21}$$

where θ_m is found using

$$\tan 2\theta_m(x) = \frac{\sin 2\theta_V}{\cos 2\theta_V - V(x)/(2\omega)}. \tag{1.22}$$

In these equations θ' is shorthand for $\mathrm{d}\theta/\mathrm{d}x$.

From this equation of motion we can see that the off-diagonal terms that drive the conversion of neutrinos from one mass state to the other are large when the matter density is changing quickly. Large changes in density occur at shock fronts in the supernova envelope, but small-scale turbulence can also contribute to large off-diagonal terms even if the absolute change in density is not as dramatic. Kneller [22] describes two extreme cases that can occur in the evolution equations. "Resonances" occur when $\theta_m = \pi/4$ and ω_m is at its minimum, and "points of maximal violation of adiabaticty" occur when the adiabaticity parameter, defined as $\gamma = \omega_m/|\mathrm{d}\theta_m/\mathrm{d}x|$, is minimized. Neutrino flavour transformations in dense matter are most strongly influenced by regions where the density is changing rapidly or is near an MSW resonance where $V/2 \simeq \omega_V \cos 2\theta_V$.

1.3 Neutrino–Neutrino Interactions

Neutrinos are able to scatter off other neutrinos via the weak force. These interactions have an extremely small cross section, but in supernovae and the early

universe the neutrino density is so high that this scattering has a powerful influence on the flavour evolution of the neutrinos. The strength of these neutrino scattering interactions can be roughly quantified by a parameter κ, defined as [12]

$$\kappa \equiv \frac{2\sqrt{2}G_F n_\nu \langle E \rangle}{\Delta m^2}, \tag{1.23}$$

where G_F is Fermi's constant, n_ν is the number density of neutrinos, and $\langle E \rangle$ is the average neutrino energy. Unsurprisingly, the neutrino density is the most important parameter in neutrino–neutrino interactions. In a non-isotropic situation there can also be important effects due to the relative motion of the neutrinos, which will tend to decrease the interaction strength.

When κ is large, continuous elastic scattering of neutrinos from each other exchanges momenta between different neutrino flavours. This has the effect of coupling the oscillations of neutrinos of all energies together. This is radically different from the behaviour of neutrinos in low-density environments, where each neutrino oscillates with a frequency which depends only on its energy. In various works many of the novel effects of these neutrino interactions have been understood through a formal analogy to spin precession in a magnetic field or a classical gyroscopic pendulum [13, 14, 45, 46]. Expressed in a suitable basis, neutrino flavour can be represented by a three-vector, where the $\hat{\mathbf{z}}$ axis represents the flavour of the neutrino, with $+1$ representing a ν_e state and -1 representing a ν_x state. The other components of the vector represent the phase of the neutrino state. The vacuum mixing, matter term, and neutrino interaction term can also be represented by vectors in this abstract space which act upon the neutrino vectors like external force fields on a classical body. In a vacuum the equations of motion are analogous to those of a pendulum in a fixed gravitational field.

The matter term can vary as a function of position and time but can be represented by a single vector in a fixed direction with changing magnitude. In the pendulum analogy, this vector acts as a second gravitational field with a different orientation and magnitude. The MSW effect explaining the Solar neutrino problem can be understood as being due to the neutrino flavour vectors precessing around and following the slowly changing matter term. All of the neutrinos transition smoothly from a mass and flavour eigenstate in the centre of the Sun to a vacuum eigenstate at the surface.

Constructing an analogy for the neutrino–neutrino term is more difficult because the neutrino background is not independent of the flavour states of the

neutrinos themselves as the other two terms are. The strength and orientation of the neutrino-generated 'field' is essentially the sum of all of the individual neutrino flavour vectors. Because of the non-linear nature of this background interaction it can cause a wide variety of interesting effects, which we will discuss in section 1.4.

In the general case, the combination of vacuum mixing with the neutrino and matter background results in a complex system of flavour vectors, and background 'field' vectors in the three-dimensional flavour space. For instance, depending on the relative sizes of the terms in the particular physical scenario, the neutrinos can end up locked in a fixed flavour state, or they can undergo periodic, large amplitude flavour transformations in the form of so-called bipolar oscillations. The collective neutrino effects can amplify the oscillations and cause complete flavour conversion even when θ_{13} is very small. The general behaviour of realistic initial supernova spectra can consist of various types of motion, but typically results in spectral swaps, where all neutrinos in a certain energy range swap flavour. The enormous neutrino density near a supernova and the consequent neutrino interaction term causes novel effects that are unique to supernova neutrinos and could provide many unique insights into both supernova physics and fundamental neutrino physics.

To complete the description of neutrino flavour interactions and evolution, we will discuss the general form of the neutrino interaction term in the Hamiltonian. In the two-flavour case the interaction can be written as [47]

$$\begin{aligned}\mathcal{H}_{\nu\nu} = \sqrt{2}G_F \sum_{\alpha} \Bigg[\int \left(1 - \hat{\mathbf{q}} \cdot \hat{\mathbf{q}}'\right) \rho_{\nu_{\underline{\alpha}}}(\mathbf{q}') \, \mathrm{d}n_{\nu_{\underline{\alpha}}}(\mathbf{q}') \, \mathrm{d}\mathbf{q}' \\ - \int \left(1 - \hat{\mathbf{q}} \cdot \hat{\mathbf{q}}'\right) \rho^*_{\bar{\nu}_{\underline{\alpha}}}(\mathbf{q}') \, \mathrm{d}n_{\bar{\nu}_{\underline{\alpha}}}(\mathbf{q}') \, \mathrm{d}\mathbf{q}' \Bigg] . \end{aligned} \tag{1.24}$$

Here $\rho(\mathbf{q})$ is the flavour density matrix, defined as

$$\rho_\nu = \begin{pmatrix} |a_e|^2 & a_e a_x^* \\ a_e^* a_x & |a_x|^2 \end{pmatrix}, \tag{1.25}$$

of a neutrino with momentum $\mathbf{q}$, and n is the total number density of neutrinos. Hats denote unit vectors. The index α is either e or x flavour, and underlines refer to initial flavour, so for example $n_{\nu_{\underline{e}}}$ refers to the number density of neutrinos which were created as electron neutrinos. Bars denote anti-neutrino terms,

so ignoring the direction-dependent dot product the neutrino background term is essentially the integral of the neutrino density matrices for every neutrino in the ensemble, minus the complex conjugate of the similar integral of the all antineutrino density matrices. Because $\mathcal{H}_{\nu\nu}$ is a weighted sum of density matrices it is unitary, and it can be useful to write it as [48]

$$\mathcal{H}_{\nu\nu} = \frac{1}{2}\begin{bmatrix} D_{ee} & D_{ex} \\ D_{ex}^{*} & -D_{ee} \end{bmatrix}, \tag{1.26}$$

where the diagonal term D_{ee} is real and the off-diagonal term D_{ex} is complex. These terms can then be simply converted to the components of the polarization vector $\mathbf{D}$ that describes the neutrino background potential. This vector formalism will be described in detail in later sections.

A commonly-made assumption which greatly simplifies the calculation of the neutrino interactions is the so called "single-angle approximation". As explained by Dasgupta *et al.* [49], there is some disagreement in the literature in the form of this approximation. In several references, for example [15, 48], the assumption is that the evolution along neutrino trajectories normal to the neutrinosphere is the same as the evolution of all other trajectories. It can also be shown that this approximation is equivalent to assuming that all neutrino-neutrino interactions occur at right-angles. The analytic work of Dasgupta *et al.* derives an expression that differs by a factor of two from these other references, using a framework of streamlines and averaged radial velocities. This difference is not particularly significant for most purposes, however, since the interaction strength depends on the total fluxes which vary considerably in supernova models. Adding an extra factor of two in this density does not affect the overall evolution other than by an effective scaling of the radius.

This advantage of the single-angle approximation is that it removes the dot product in the neutrino-neutrino integral (Equation 1.24) and replaces it with a geometric factor that depends only on the radius of the neutrinosphere and the radial position of the neutrino. In the single-angle approximation the neutrino-neutrino potential becomes

$$\mathcal{H}_{\nu\nu} = \frac{\sqrt{2}G_F}{2\pi R_\nu^2} D(r/R_\nu) \sum_\alpha \int \left[\rho_{\nu_{\underline{\alpha}}}(q')n_{\nu_{\underline{\alpha}}}(q') - \rho_{\bar{\nu}_{\underline{\alpha}}}(q')n_{\bar{\nu}_{\underline{\alpha}}}(q')\right] \mathrm{d}q', \tag{1.27}$$

where $D(r/R_\nu)$ is the geometric factor, defined in terms of the neutrinosphere

radius R_ν as

$$D(r/R_\nu) \equiv \frac{1}{2}\left(1 - \sqrt{1 - \left(\frac{R_\nu}{r}\right)^2}\right)^2 . \tag{1.28}$$

Adding the neutrino background term in Equation 1.26 to the vacuum and matter terms in Equation 1.8 gives us a total Hamiltonian

$$\mathcal{H} = \frac{\Delta m^2}{4E}\begin{bmatrix} -\cos 2\theta & \sin 2\theta \\ \sin 2\theta & \cos 2\theta \end{bmatrix} + \frac{V(x)}{2}\begin{bmatrix} 1 & 0 \\ 0 & -1 \end{bmatrix} + \frac{1}{2}\begin{bmatrix} D_{ee} & D_{ex} \\ D_{ex}^* & -D_{ee} \end{bmatrix} \tag{1.29}$$

which contains all of the dynamics that can occur in neutrino flavour oscillations in the two-flavour approximation. For antineutrinos the matrix has the same form, but the matter and neutrino terms must be multiplied by -1 and the terms in the neutrino-neutrino term are replaced by their complex conjugates.

1.4 Neutrino Flavour Vector Dynamics

Now that we have the form of all the neutrino interactions and can write down a full Hamiltonian for the system, we can study how the neutrino flavours evolve in various cases. In general this is an extremely complex problem, so we will begin with some simplified cases and gradually add more complications to our neutrino system.

1.4.1 Notation and Definition of Flavour Vectors

To develop the equations of motion and their solutions more fully, we use the neutrino density matrix of Equation 1.25,

$$\rho_\nu = \begin{pmatrix} |a_e|^2 & a_e a_x^* \\ a_e^* a_x & |a_x|^2 \end{pmatrix}, \tag{1.30}$$

to define a three-component "polarization" vector $\mathbf{P}$ which satisfies

$$\rho = \frac{1}{2}\left(1 + \mathbf{P}\cdot\boldsymbol{\sigma}\right). \tag{1.31}$$

This provides a more convenient representation of both the neutrino wavefunctions and the various terms in the Hamiltonian. This vector notation makes the equations of motion much simpler to understand than the standard wavefunc-

tion representation, particularly when neutrino interaction effects are significant. This is primarily because in simple cases the equations of motion in this representation turn out to be analogous to various well-studied classical systems, such as a spin in a magnetic field or a gyroscopic pendulum.

The three real polarization vector components can be calculated explicitly from the wavefunction using

$$\begin{pmatrix} \mathrm{P}_x \\ \mathrm{P}_y \\ \mathrm{P}_z \end{pmatrix} = \begin{pmatrix} a_e a_x^* + a_e^* a_x \\ i\left(a_e a_x^* - a_e^* a_x\right) \\ |a_e|^2 - |a_x|^2 \end{pmatrix}. \tag{1.32}$$

From this expression, we can see that a pure $|\nu_e\rangle$ state has $\mathbf{P} = (0, 0, 1)$ and a pure $|\nu_x\rangle$ state has $\mathbf{P} = (0, 0, -1)$. A half-and-half mixture of the two flavour states will have $\mathrm{P}_z = 0$. For a general state we can also use $\mathbf{P}$ to calculate the probability of measuring the neutrino flavour to be electron-type:

$$|\langle \nu_e | \nu_\alpha \rangle|^2 = \frac{1}{2}\left(1 + \mathrm{P}_z\right). \tag{1.33}$$

The z-component of the neutrino flavour polarization vector determines the observable flavour state of a given neutrino, while the x and y components contain the phase information.

We have chosen to define the corresponding antineutrino polarization vectors $\overline{\mathbf{P}}$ in the same way, so a pure $\bar{\nu}_e$ state has $\overline{\mathbf{P}} = (0, 0, +1)$. The equations of motion are modified for antineutrinos in this convention by the addition of a minus sign in the vacuum freqency.

1.4.2 Equations of Motion

Preliminary Definitions

The equations of motion of a general neutrino system become easier to understand and study in the flavour vector representation. We have already detailed how the neutrino wavefunctions can be represented by vectors in a three-dimensional vector space. To construct the equations of motion in this space, we must also express the various terms in the neutrino Hamiltonian as vectors which act upon the neutrino vectors.

We can express the vacuum oscillation term in the Hamiltonian as a vector in flavour space times a frequency, so it becomes $\omega\mathbf{B}$. This vacuum frequency is

defined as $\omega = \Delta m^2/4E_\nu$. Note that we have dropped the subscript V used in the matter background sections as there is no longer any ambiguity. Using the same factorization in terms of Pauli matrices as for the neutrino density matrices (Equation 1.31), we find that the unit vector $\mathbf{B}$ has flavour space components

$$\mathbf{B} = \begin{pmatrix} \sin 2\theta_V \\ 0 \\ -\cos 2\theta_V \end{pmatrix}, \tag{1.34}$$

where θ_V is the vacuum mixing angle. This expression is for the normal hierarchy. To convert to the inverted hierarchy we could flip the sign of Δm^2, resulting in $\omega \to -\omega$, but this means we need to consider two different sets of equations of motion for the two hierarchies. We find it is simpler to change the mixing angle in the inverted hierarchy. If the mixing angle in the normal hierarchy is θ_V, replacing θ_V with $\theta_V^{\text{inv}} = \pi/2 - \theta_V$ in the equations introduces the appropriate negative signs into the equations of motion. In order to continue to take advantage of the smallness of θ_V to make simplifying approximations, we define an angle $\tilde{\theta}_V \equiv \pi/2 - \theta_V^{\text{inv}}$ which is equal in magnitude to the small mixing angle in normal hierarchy. The replacement is easier to understand in terms of the effect of the orientation of $\mathbf{B}$ in flavour space. Changing the hierarchy results in a change of sign of the $\hat{\mathbf{z}}$ component of $\mathbf{B}$, so that $\mathbf{B}$ points close to the $+\hat{\mathbf{z}}$ (or ν_e) direction in the inverted hierarchy and close to the $-\hat{\mathbf{z}}$ (or ν_x) direction in the normal hierarchy. The angle between $\mathbf{B}$ and either the positive or negative $\hat{\mathbf{z}}$ axis will have the same small value in each case.

The matter term in the Hamiltonian is equal to a constant times the Pauli matrix σ_z, so it becomes a vector of magnitude V that points in the $+\hat{\mathbf{z}}$ direction. Finally, using the definitions in Equation 1.26 the neutrino background term can be written as a vector $\mathbf{D}$ with components

$$\mathbf{D} = \begin{pmatrix} \Re(D_{ex}) \\ \Im(D_{ex}) \\ D_{ee} \end{pmatrix}. \tag{1.35}$$

This $\mathbf{D}$ vector can also be expressed directly as the sum of the neutrino polarization vectors in the ensemble, because the matrix form of the neutrino background term is a sum of neutrino density matrices. We first define the

vectors $\mathbf{J}$ and $\overline{\mathbf{J}}$ as

$$\mathbf{J} = \frac{1}{N + \overline{N}} \sum_{i=1}^{N} \mathbf{P}_i \quad \text{and} \quad \overline{\mathbf{J}} = \frac{1}{N + \overline{N}} \sum_{i=1}^{\overline{N}} \overline{\mathbf{P}}_i, \tag{1.36}$$

where and N and $\overline{N}$ are the number densities of neutrinos and antineutrinos. These vectors represent the sum of the polarization vectors of all the neutrinos in the ensemble, normalized by the total neutrino density. The vector $\mathbf{D}$ above can be shown to be equal to the difference $\mathbf{J} - \overline{\mathbf{J}}$. We also define an analogous sum vector $\mathbf{S} \equiv \mathbf{J} + \overline{\mathbf{J}}$.

With these definition the total neutrino background vector in flavour space in the single-angle approximation, as in Equation 1.27, or in even simpler isotropic cases, can be rewritten as simply $\mu\mathbf{D}$. To avoid confusion due to differing definitions found in the literature, we define μ as $\mu_0 \left(N + \overline{N}\right)$ with $\mu_0 = \sqrt{2} G_F$.

Using all of these definitions it can now be shown that the Schrödinger equation for a neutrino wavefunction $\dot{\psi} = -i\mathcal{H}\psi$ is equivalent to the following equations for the corresponding neutrino polarization vector $\mathbf{P}$ or antineutrino polarization vector $\overline{\mathbf{P}}$:

$$\begin{aligned} \dot{\mathbf{P}} &= (+\omega\mathbf{B} + V\hat{\mathbf{z}} + \mu\mathbf{D}) \times \mathbf{P}, \\ \dot{\overline{\mathbf{P}}} &= (-\omega\mathbf{B} + V\hat{\mathbf{z}} + \mu\mathbf{D}) \times \overline{\mathbf{P}}. \end{aligned} \tag{1.37}$$

These equations are formally similar to those of a magnetic moment in an external field, leading to the use of terms such as 'vacuum field' or 'matter field'. The dynamics of the motion can be more complex than the analogy suggests, however, because the $\mathbf{D}$ term is a sum over all $\mathbf{P}$ vectors in the ensemble, which means that the motions of neutrinos of all flavours and energies are coupled. It has also been shown that there exist modes of motion where individual neutrino vectors change flavour periodically while $\mathbf{D}$ remains constant.

Note on Conventions

Because of the existence of various different conventions for this vector notation we will briefly explain some of the variants encountered in the literature. The vectors as defined in Equation 1.31 are generally referred to as "neutrino polarization vectors" or "flavour vectors" [13, 15, 50, 51]. An alternative convention, described as "neutrino flavour isospin" (or NFIS) [13, 48] has also been used by

some authors. The vectors in this system are related to our polarization vectors by

$$\begin{aligned} \mathbf{s}_{\nu} &= +\frac{\mathbf{P}}{2}, \\ \mathbf{s}_{\bar{\nu}} &= -\frac{\overline{\mathbf{P}}}{2}, \end{aligned} \tag{1.38}$$

so that instead of having $\mathbf{P}$ for a neutrino and $\overline{\mathbf{P}}$ for an antineutrino both pointing in the positive $\hat{\mathbf{z}}$ direction when they are in the electron flavour state an electron antineutrino NFIS vector points in the opposite direction to a electron neutrino NFIS vector. This has the advantage of allowing a single equation of motion to be used for all neutrino and antineutrino vectors.

Another difference in convention is in the use of $\mathbf{P}$ to represent either a single neutrino [15] or the sum of individual vectors $\mathbf{P}_i$ [51]. A confusing result of these differing conventions comes in the definition of a vector $\mathbf{S}$, the sum of all the flavour vectors or NFIS vectors, which in the NFIS convention is actually equivalent to the *difference* vector $\mathbf{D}$ in the polarization convention because of the additional minus sign in the definition of the antineutrino NFIS vectors.

In our work we have chosen to mostly follow the polarization vector convention and notation used in [13]. As well as having $\mathbf{P}$ vectors for single neutrinos being unit vectors, this convention generally uses definitions of vectors such as $\mathbf{J}$ and $\mathbf{S}$ which are normalized by the number density of neutrinos, so that all of our vectors are roughly unit vectors, in the sense that they are all either unit vectors or the sum or difference of two unit vectors. We find that this convention helps to avoid confusion, but we also stress that all of these conventions result in equivalent dynamics and often result in equations that look almost exactly the same, aside from an occasional minus sign or normalization constant.

It is also possible to extend this vector formalism to the full three-flavour neutrino case using Bloch vectors and Gell-Mann matrices [14]. For simplicity we have confined ourselves to the two flavour approximation. There are additional effects that arise from the full three-flavour mixing, but the general behaviour is still quite well explained in the two-flavour model, and the motion is much easier to visualize and explain with only two flavours. For more details on three-flavour effects see for example [46, 52–56].

1.4.3 Simplified Equations of Motion

The neutrino flavour evolution in a realistic supernova explosion must be calculated numerically in practice, but there are many useful insights to be gained from analytic investigation of the equations of motion in simpler cases. First we will construct the equations of motion for a neutrino system with constant (but not necessarily equal) numbers of neutrinos and antineutrinos, all with the same energy. We label the flavour vector for neutrinos $\mathbf{P}$ and for antineutrinos $\overline{\mathbf{P}}$. Because the neutrinos are monoenergetic the motion of each neutrino and antineutrino vector in the ensemble is identical, and the system can be completely described by the evolution of a one neutrino vector and one antineutrino vector. The effect of the neutrino density can be studied by changing the size of the parameter μ. The equations of motion for the two vectors in the absence of matter are:

$$\begin{aligned} \dot{\mathbf{P}} &= (\omega\mathbf{B} + \mu\mathbf{D}) \times \mathbf{P} \\ \dot{\overline{\mathbf{P}}} &= (-\omega\mathbf{B} + \mu\mathbf{D}) \times \overline{\mathbf{P}}, \end{aligned} \tag{1.39}$$

Because we only have one neutrino and one antineutrino vector, the sum and difference vectors are simply $\mathbf{S} = \mathbf{P}+\overline{\mathbf{P}}$ and $\mathbf{D} = \mathbf{P}-\overline{\mathbf{P}}$. The equations of motion of the sum and difference vectors can be found from those of the polarization vectors to be

$$\begin{aligned} \dot{\mathbf{S}} &= \omega\mathbf{B} \times \mathbf{D} + \mu\mathbf{D} \times \mathbf{S} \\ \dot{\mathbf{D}} &= \omega\mathbf{B} \times \mathbf{S}. \end{aligned} \tag{1.40}$$

By defining some new variables we can further simplify these equations, and put them in a form which allows us to apply classical analogies to study the motion [15, 50, 57]. First we define $\mathbf{Q}$ as

$$\mathbf{Q} \equiv \mathbf{S} - \frac{\omega}{\mu}\mathbf{B}. \tag{1.41}$$

Using Equation 1.40 to take the time derivative of $\mathbf{Q}$, and noting that $\mathbf{B} \times \mathbf{Q} = \mathbf{B} \times \mathbf{S}$ we obtain new equations of motion for the system in terms of $\mathbf{Q}$ and $\mathbf{D}$,

which are

$$\begin{aligned}\dot{\mathbf{Q}} &= \mu \mathbf{D} \times \mathbf{Q} \\ \dot{\mathbf{D}} &= \omega \mathbf{B} \times \mathbf{Q}.\end{aligned} \tag{1.42}$$

From these equations we find that the magnitude $Q = |\mathbf{Q}|$ is a conserved quantity, because

$$\begin{aligned}\frac{\mathrm{d}}{\mathrm{d}t}|\mathbf{Q}|^2 &= \frac{\mathrm{d}}{\mathrm{d}t}(\mathbf{Q} \cdot \mathbf{Q}) \\ &= 2\mathbf{Q} \cdot \dot{\mathbf{Q}} \\ &= \mu \mathbf{Q} \cdot (\mathbf{D} \times \mathbf{Q}) = 0.\end{aligned} \tag{1.43}$$

In a similar way, it can also be shown that $\mathbf{D} \cdot \mathbf{Q}$ and $\mathbf{D} \cdot \mathbf{B}$ are conserved according to these equations of motion.

Because the magnitude of $\mathbf{Q}$ is constant, it is constrained to move around on a sphere of fixed radius, like the bob of a spherical pendulum. The total effective flavour energy of this neutrino system can be written as [13]

$$\mathcal{E} = \omega \mathbf{B} \cdot \mathbf{Q} + \frac{\mu}{2}\mathbf{D}^2. \tag{1.44}$$

We can understand the first term as analogous to the potential energy of the pendulum in a 'gravitational field' with magnitude proportional to ω and orientation determined by the mixing angle. The second term is analogous to the kinetic energy of the pendulum, which means that $\mathbf{D}$ is like the angular momentum of the pendulum.

To make the classical analogy more explicit, we define several further parameters:

$$\begin{aligned}\mathbf{r} &\equiv \frac{\mathbf{Q}}{Q}, \\ \mathbf{L} &\equiv \mathbf{D}, \\ m &\equiv \frac{1}{\mu}, \\ \sigma &\equiv \mathbf{D} \cdot \mathbf{r}, \\ -\mathbf{g} &\equiv \omega \mu Q \mathbf{B}.\end{aligned} \tag{1.45}$$

We now divide the expression for $\dot{\mathbf{Q}}$ by Q and take the cross product with $\mathbf{r}$ on

both sides to find

$$\begin{aligned}
\mathbf{r} \times \dot{\mathbf{r}} &= \mathbf{r} \times (\mu \mathbf{D} \times \mathbf{r}) \\
m\mathbf{r} \times \dot{\mathbf{r}} &= \mathbf{D}\,(\mathbf{r} \cdot \mathbf{r}) - \mathbf{r}\,(\mathbf{D} \cdot \mathbf{r}) \\
\mathbf{D} &= m\mathbf{r} \times \dot{\mathbf{r}} + \sigma \mathbf{r}, \qquad (1.46)
\end{aligned}$$

which we can use together with the equation for $\dot{\mathbf{D}}$ to get the final equations of motion:

$$\begin{aligned}
\mathbf{L} &= m\mathbf{r} \times \dot{\mathbf{r}} + \sigma \mathbf{r}, \\
\dot{\mathbf{L}} &= m\mathbf{r} \times \mathbf{g}. \qquad (1.47)
\end{aligned}$$

These equations are formally the same as those for a spherical pendulum of length one with a bob of mass m that spins around the pendulum axis with angular momentum σ, all moving in a gravitational field $\mathbf{g}$.

To see what sort of dynamics are possible for this system we can examine the classical mechanics of a gyroscopic pendulum [57–59]. The general solution for the motion assuming no change in the mass (ie. the neutrino density) is a precession around $\mathbf{g}$ with a nutation between two limiting angles, $\vartheta_{\min}$ and $\vartheta_{\max}$, relative to this axis of precession. We will examine a few different cases to see what flavour oscillation behaviour this analogy leads to, and where the analogy breaks down.

1.4.4 Symmetric Neutrino Case

The simplest case to study first is one with equal numbers of neutrinos and antineutrinos, which are in pure electron flavour states initially, all with the same fixed oscillation frequency ω. This means that $\mathbf{S}$ has an initial magnitude of 2. Since $\mathbf{B}$ is a unit vector and $\mathbf{S} \cdot \mathbf{B} = -2 \cos 2\theta_V$, we can calculate

$$Q = \sqrt{4 + \left(\frac{\omega}{\mu}\right)^2 + 4\frac{\omega}{\mu} \cos 2\theta_V}. \qquad (1.48)$$

As mentioned earlier, $\mathbf{D} \cdot \mathbf{Q}$ is a constant of the motion, so with the initial condition of equal numbers of neutrinos and antineutrinos giving $\mathbf{D} = 0$ initially we can see that in this case $\sigma = \mathbf{D} \cdot \mathbf{r} = 0$, suggesting that the equations of motion become those of a simple pendulum rather than a gyroscopic pendulum. Indeed,

because $\mathbf{D} \cdot \mathbf{B}$ is also constant, $\mathbf{D}$ will always be constrained to the axis defined by $\mathbf{B} \times \mathbf{Q}$, which in turn means that $\mathbf{Q}$ will remain fixed in the plane defined by $\mathbf{B}$ and the $\hat{\mathbf{z}}$-axis.

We now introduce two new variables that describe the motion of the system: ϑ is the angle between $\mathbf{Q}$ and $\hat{\mathbf{z}}$, which is taken to be in the range $(0, \pi)$ when the component of $\mathbf{Q}$ along $\hat{\mathbf{z}}$ is positive and in the range $(-\pi, 0)$ when it is negative. This means that we can write $\mathbf{Q} = Q(\sin\vartheta, 0, \cos\vartheta)$. We use the magnitude of $\mathbf{D}$ as our other variable. Using the equations of motion and the vector components of $\mathbf{B}$ and $\mathbf{Q}$ we have

$$\begin{aligned}\dot{\mathbf{D}} &= \omega \mathbf{B} \times \mathbf{Q} \\ &= \omega Q(\sin 2\theta_V, 0, -\cos 2\theta_V) \times (\sin\vartheta, 0, \cos\vartheta) \\ &= -\omega Q \sin(\vartheta + 2\theta_V)\, \hat{\mathbf{y}} \end{aligned} \tag{1.49}$$

so our final equation of motion is

$$\dot{D} = -\omega Q \sin(\vartheta + 2\theta_V) \tag{1.50}$$

We can obtain an equation of motion for ϑ as follows:

$$\begin{aligned}\dot{\mathbf{Q}} &= \mu \mathbf{D} \times \mathbf{Q} \\ \frac{\mathrm{d}}{\mathrm{d}t}(\sin\vartheta, 0, \cos\vartheta) &= \mu(0, D, 0) \times (\sin\vartheta, 0, \cos\vartheta) \\ \dot{\vartheta}(\cos\vartheta, 0, -\sin\vartheta) &= \mu D(\cos\vartheta, 0, -\sin\vartheta) \\ \dot{\vartheta} &= \mu D. \end{aligned} \tag{1.51}$$

Using these equations to calculate the second derivative of ϑ we find

$$\ddot{\vartheta} = \Omega^2 \sin(\vartheta + 2\theta_V), \tag{1.52}$$

where we have defined a new frequency $\Omega \equiv \sqrt{\omega \mu Q}$. We have reduced the motion of the system to the equations of motion of a simple pendulum, where the frequency written out explicitly is

$$\Omega = \sqrt{\frac{\Delta m^2}{E_\nu} \sqrt{2} G_F n_\nu}. \tag{1.53}$$

It is clear that in this case the motion is very well-behaved and the dynamics are exactly equivalent to a simple classical pendulum. The system can be described by a Hamiltonian

$$H = \frac{\Omega^2}{\mu}\left[1 - \cos(\vartheta + 2\theta_V)\right] + \frac{\mu D^2}{2} \tag{1.54}$$

with ϑ as the coordinate and D as its conjugate momentum. The potential in the case of a small mixing angle will be

$$V(\vartheta) = \Omega^2\left[1 - \cos(\vartheta + 2\theta_V)\right] \simeq \frac{\Omega^2}{2}(\vartheta + 2\theta_V)^2 + \cdots \tag{1.55}$$

This is a simple harmonic oscillator potential with a minimum at $\vartheta = -2\theta_V$. The observable changes in flavour resulting from this solution to the equations of motion depend critically on the neutrino mass hierarchy.

Normal Hierarchy

In the normal hierarchy, $\mathbf{Q}$ has an initial position between $Q\hat{\mathbf{z}}$ and $-\mathbf{B}$, so the pendulum is near the minimum of the potential. If θ_V is small then the initial value of the $\hat{\mathbf{x}}$ component of $\mathbf{Q}$ will be approximately $\omega/\mu 2\theta_V$ and the $\hat{\mathbf{z}}$ component will be Q, so the initial value of ϑ will be approximately $2\theta_V\omega/\mu Q$, with no initial velocity. Therefore the pendulum will oscillate between two points at an angle of $(1 - \omega/\mu Q)2\theta_V$ either side of $-\mathbf{B}$. The flavour vectors will not undergo any large change from their initial pure electron neutrino states, and the observable flavour change will be negligible.

Inverted Hierarchy

In the inverted hierarchy we use a modified mixing angle $\tilde{\theta}_V = \pi/2 - \theta_V$ so that we have a small parameter to deal with in the limit of a small mixing angle. With this replacement the potential picks up a minus sign and the minimum of the potential occurs at an angle of $\pi + \tilde{\theta}_V$, which corresponds to the opposite direction in flavour space from the normal hierarchy. The initial value of ϑ can now range from zero in the large μ/ω limit to close to this minimum if the neutrino density is small. Initially the value of the $\hat{\mathbf{z}}$-component of $\mathbf{Q}$ will be approximately

$$\mathbf{Q}_z \approx \mathbf{S}_z - \frac{\omega}{\mu} = 2 - \frac{\omega}{\mu}, \tag{1.56}$$

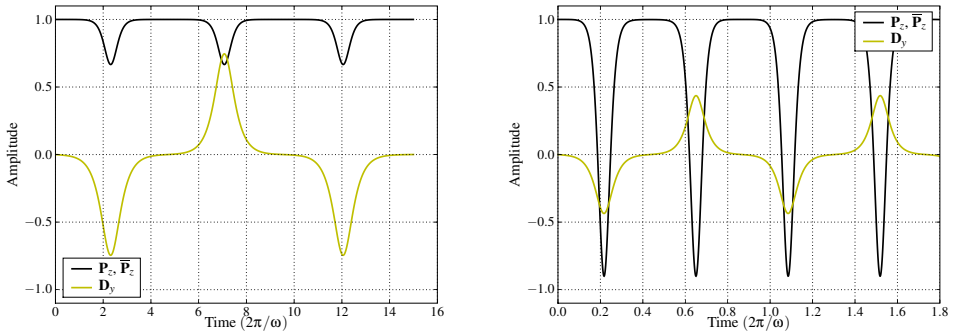

(a) $\mu = 0.6\omega$ (b) $\mu = 10\omega$

Figure 1.1: Plots of the evolution of the neutrino polarization vectors (dark curves) in the simple symmetric case discussed in the text for two different values of the neutrino interaction strength and an inverted hierarchy. The lighter curves plot the size of the difference vector $\mathbf{D}$.

which will be in the direction of the minimum of the potential if $\omega/\mu \geq 2$. For $\omega/\mu < 2$ we will get a partial conversion of flavours. The maximum allowed change in $\mathbf{S}_z$ will be determined by the requirement of conservation of Q,

$$\begin{aligned} \mathbf{Q}_z|_{\max} &= -\mathbf{Q}_z|_{\min} \\ (2 - \frac{\omega}{\mu}) &= -(\mathbf{S}_z|_{\min} - \frac{\omega}{\mu}) \\ \frac{1}{2}\mathbf{S}_z|_{\min} &= \frac{\omega}{\mu} - 1 \approx \mathbf{P}_z = \overline{\mathbf{P}}_z, \end{aligned} \tag{1.57}$$

so a periodic, complete transformation of flavour is obtained in the large μ limit. Two cases are shown in Figure 1.1, one with $\mu/\omega = 0.6$ where there is very little flavour swapping, and one with $\mu/\omega = 10$ where the flavours almost completely swap. The behaviour of the restoring force provided by $\mathbf{D}$ is also clear in these plots. Note also the difference in the time axis for these plots, showing that the frequency of the oscillation is increased by the increasing value of μ. This is expected because of the form of the frequency $\Omega = \sqrt{\omega\mu Q}$.

The High Neutrino Density Limit

To describe the motion in a very dense neutrino background a few more variables can be introduced. Firstly, to quantify the relevant limit, we define

$$n_\nu^0 \equiv \frac{\omega}{\mu_0} = \frac{\Delta m^2}{4\sqrt{2} G_F E_\nu}, \tag{1.58}$$

so that we can say that collective effects will be important when the neutrino number density $n_\nu \gtrsim n_\nu^0$.

For supernova neutrinos closer than a few hundred kilometres to the neutron star core of the explosion, $\mu \gg \omega$ because of the enormous density of neutrinos. In this limit, $\mathbf{S}$ becomes approximately equal to $\mathbf{Q}$, which means that the argument for the conserved magnitude of $\mathbf{Q}$ will also apply to $\mathbf{S}$. Thus $\mathbf{S}$, like $\mathbf{Q}$ in the general case, will remain at a constant length while rotating around $\mathbf{D}$, which points along a fixed axis. For the magnitude of $\mathbf{S}$ to remain fixed, the neutrino and antineutrino polarization vectors must remain tightly coupled throughout the motion. The term "bipolar oscillations" has been used to describe this type of motion. It originates from the fact that in the alternative convention for the polarization vectors, where electron-type antineutrinos point in the opposite direction to electron-type neutrinos, the two vectors are antialigned and their motion resembles a rotating stick with its centre fixed at the origin, so the two "poles", representing the neutrino and antineutrino vectors, remain in exactly opposed directions.

To explain the motion seen in Figure 1.1 we can solve the equation of motion for ϑ in the small $\tilde{\theta}_V$ limit [50]. The initial conditions in this case are $\dot{\vartheta}(0) = 0$ and $\vartheta(0) \simeq -(\omega/\mu Q) 2\tilde{\theta}_V$. The equation of motion is

$$\ddot{\vartheta} = \Omega^2 \sin(\vartheta - 2\tilde{\theta}_V). \tag{1.59}$$

In the case of small mixing, $\tilde{\theta}_V$ and ϑ are both small initially, so we can approximate the equation of motion by

$$\ddot{\vartheta} = \Omega^2 (\vartheta - 2\tilde{\theta}_V), \tag{1.60}$$

which is solved, together with the initial conditions, by

$$\vartheta(t) = 2\tilde{\theta}_V \left[1 - \left(1 + \frac{\omega}{\mu Q} \right) \cosh(\Omega t) \right]. \tag{1.61}$$

To estimate the timescale for the tipping of the pendulum we can use the fact that $\tilde{\theta}_V \ll 1$, which means that when $\vartheta \sim -1$ we must have $\cosh(\Omega t) \approx \exp(\Omega t)/2$. Substituting these approximations into the equation of motion we get

$$1 = -2\tilde{\theta}_V \left(1 + \frac{\omega}{\mu Q}\right) \frac{e^{\Omega t}}{2}. \tag{1.62}$$

Simplifying, and noting that $\tilde{\theta}_V \ll 1$, we get an expression for the timescale of the bipolar flips:

$$\tau_{\text{bipolar}} \approx -\Omega^{-1} \ln \left[\tilde{\theta}_V \left(1 + \frac{\omega}{\mu Q}\right)\right]. \tag{1.63}$$

So we have shown that when $\mu \gg \omega$ the time the pendulum spends close to its initial position before flipping is proportional to $\ln \tilde{\theta}_V$.

1.4.5 Decreasing Neutrino Density

It is interesting to consider what will happen to this system if we have a slowly decreasing neutrino density, since in a realistic supernova background the neutrino density will tend to zero from a very large initial value as the radius increases. As long as $n_\nu \gg n_\nu^0$ the equations of motion for ϑ and D in Equation 1.50 and Equation 1.51 will still be correct since the variables are defined to be independent of the number of neutrinos. We can most easily examine the motion by treating ϑ as a coordinate and $p_\vartheta = D$ as its conjugate momentum, which leads to the Hamiltonian

$$H = \omega \left(\frac{n_\nu}{2n_\nu^0} D^2 - \cos\vartheta\right) \tag{1.64}$$

which contains the equations of motion above. For any form of oscillation, there will be a maximum angle of excursion of the pendulum 'bob', which we label as $\vartheta_{\max}$. We can guess the general form of the motion from this Hamiltonian. Since the kinetic energy term $\left(\omega n_\nu / 2n_\nu^0\right) D^2$ has an effective mass of $n_\nu^0 / \left(\omega n_\nu\right)$ that increases as the neutrino density decreases, the kinetic energy available to lift the pendulum to high angles decreases with time. This can also be shown more rigorously in the case of a slowly changing neutrino density by using the concept of adiabatic invariants.

As described in [59], an adiabatic invariant in a system exhibiting periodic motion is the result of having a slowly changing parameter involved in the system, for instance a changing external field strength parameter. In this context,

for a parameter μ to be changing slowly means that

$$T\frac{\mathrm{d}\mu}{\mathrm{d}t} \ll \mu, \tag{1.65}$$

where T is the period of the motion. When this condition holds, even though the total energy of the system is not constant its rate of change is small, and is in proportion to the rate of change of the parameter μ. Because of this, the energy of the system can be written as a function of μ, and therefore there will be a quantity of the form $E/F(\mu)$ which remains constant throughout the motion. In general, for a one-dimensional system this quantity can be shown to be equal to

$$I \equiv \frac{1}{2\pi}\oint p\,\mathrm{d}q, \tag{1.66}$$

where q and p are the coordinate of the motion and its conjugate momentum, and the integral is over one full period of the motion. In our case, this integral gives

$$\oint D\,\mathrm{d}\vartheta = \mathcal{C}. \tag{1.67}$$

Because μ is changing adiabatically, the energy for one period is effectively constant. The Hamiltonian will be equal to this energy throughout this period, and when the system is at $\vartheta_{\max}$ it will have the value $-\omega\cos\vartheta_{\max}$ because its kinetic energy will be zero. Therefore at any given time we have

$$H = \omega\left(\frac{1}{2}\frac{n_\nu}{n_\nu^0}D^2 - \cos\vartheta\right) = -\omega\cos\vartheta_{\max}, \tag{1.68}$$

which we can solve for D to obtain

$$D = \sqrt{\frac{2n_\nu}{n_\nu^0}(\cos\vartheta - \cos\vartheta_{\max})}. \tag{1.69}$$

Because of the symmetry of the motion, the total integral in Equation 1.67 will be four times the integral for one swing from $\vartheta = \vartheta_{\max}$ to $\vartheta = 0$. This leads to

$$\mathcal{C} = 4\sqrt{\frac{2n_\nu}{n_\nu^0}}\int_0^{\vartheta_{\max}}\sqrt{\cos\vartheta - \cos\vartheta_{\max}}\,\mathrm{d}\vartheta, \tag{1.70}$$

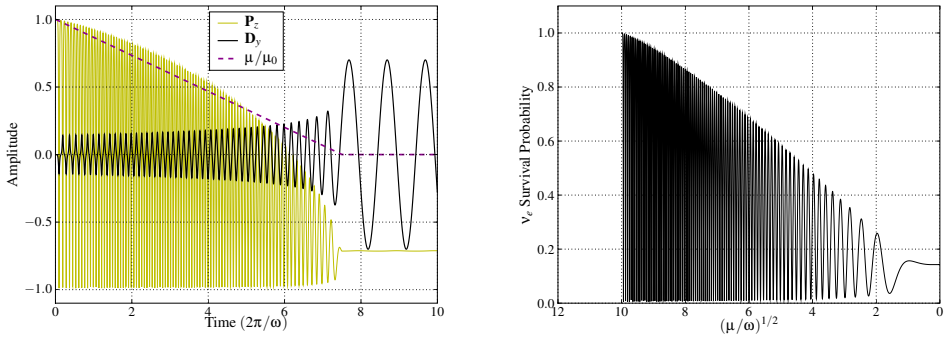

Figure 1.2: Plots of the evolution of the neutrino polarization vectors in the simple symmetric case with a linearly decreasing neutrino interaction strength. The black curve shows the value of the difference vector **D**, while the dotted line shows the decrease in μ. The right-hand figure plots the survival probability as a function of $(\mu/\omega)^{1/2}$ to demonstrate the dependence of the decline on μ.

which can be more simply written as

$$\mathcal{C} = 16\sqrt{\frac{n_\nu}{n_\nu^0}}W(\vartheta_{\max}) \tag{1.71}$$

if we define

$$W(\theta) \equiv \frac{1}{2\sqrt{2}}\int_0^\theta \sqrt{\cos\phi - \cos\theta}\,\mathrm{d}\theta, \tag{1.72}$$

which has a well-defined form in terms of elliptic integrals [57]. The factor in front of the integral means that $W(\pi) = 1$ which is convenient in the case of the inverted hierarchy when the mixing angle is almost equal to $\pi/2$.

Using Equation 1.71, and taking the initial maximum angle to be the two times the vacuum mixing angle θ_V (because the pendulum's initial angle with B is $2\theta_V$) we can obtain an idea of the behaviour of $\vartheta_{\max}$ using

$$W(\vartheta_{\max}) = W(2\theta_V)\sqrt{\frac{n_\nu(t)}{n_\nu(0)}}. \tag{1.73}$$

From the form of this equation, and noting that $W(0) = 0$, we see that the value of $\vartheta_{\max}$ will tend to zero as the neutrino density falls. This means that as $n_\nu \to 0$ the flavour vectors will be perfectly aligned with **B** with no further motion. In the normal hierarchy with a small mixing angle, the neutrino flavours will oscillate from electron to x-type with a small amplitude before settling back

to electron type in the final state. In the inverted hierarchy the neutrino vectors will eventually all be anti-aligned with their original position, representing a complete flavour conversion.

To illustrate this motion, we calculated the evolution of the same neutrino system shown in Figure 1.1 but with μ decreasing linearly as a function of time until it reaches a constant value of 0.01ω. The results are shown in Figure 1.2. The calculation used an initial value $\mu_i = 100\omega$. The gradual decrease of the maximum value of the polarization vectors discussed above is clearly seen, and we also see that though the final state of the vectors is stable, they do not completely swap, due to the factors considered in Equation 1.57. Part of this incomplete swapping is also due to the rate of decline in μ, or in other words due to non-adiabaticity. We tested this by reducing the gradient of the decline of μ to 1/10th of its value in the plot above. With this slower rate of change, the final value of $\mathbf{P}_z$ decreases from -0.712 to -0.784. This is still some way from the maximum excursion of the pendulum for the constant $\mu = 100$ case, however, which is -0.99.

We can gain a better understanding of the shape of the decline by considering the change in energy of the pendulum over one cycle [50]. The kinetic energy of the pendulum K is equal to $\mu(t)D(t)^2/2$ at any given time t. So a change in the neutrino term of $\Delta\mu$ will cause a proportional change in the kinetic energy. Assuming that the change occurs instantaneously at the lowest point of the pendulum swing, where $T = T_{\max}$, the relative change in the maximum kinetic energy will be

$$\frac{\Delta T_{\max}}{T_{\max}} = \frac{\Delta\mu}{\mu}. \tag{1.74}$$

Because the decrease in μ is actually continuous, to get an accurate result we need to include the factor $D(t)$ over one cycle, which varies approximately sinusoidally. If we assume that $D(t) \propto \sin\Omega t$ then we can use the average value of $\sin^2 x = 1/2$ over one cycle to take the variation in $D(t)$ into account. This means that if μ changes slowly (and therefore, approximately linearly) over one cycle so that $\mu \to (1-\epsilon)\,\mu$, the overall change $\Delta T_{\max}/T_{\max}$ will be $1/2 \times \Delta\mu/\mu = \epsilon/2$. So $T_{\max} \to (1-\epsilon/2)\,T_{\max} \simeq (1-\epsilon)^2$, which means that $T_{\max} \propto \mu^{1/2}$.

The decrease in the maximum kinetic energy must be reflected in a decrease of the maximum height of the pendulum's swing, since the maximum potential energy is equal to the maximum kinetic energy. The potential energy is $\omega\mathbf{B} \cdot$

$\mathbf{Q}$, which for $\mu \gg \omega$ and a small mixing angle is approximately equal to the component of $\mathbf{S}$ in the $\hat{\mathbf{z}}$ direction. So as μ decreases the maximum value of $\mathbf{P}$ and $\overline{\mathbf{P}}$, and thus the survival fraction of the initially electron-flavoured neutrinos, decreases in proportion to $\sqrt{\mu}$. The right panel of Figure 1.2 demonstrates that this approximate argument holds well in the symmetric case.

The evolution of the final state once $\mu \approx 0$ is similar to the behaviour of Solar neutrinos, which undergo an adiabatic evolution from a high matter density to vacuum and also end their evolution in a vacuum eigenstate with fixed amplitudes.

1.4.6 Asymmetric Neutrino System

The symmetric case demonstrates some of the possibilities of collective neutrino dynamics, but a more realistic approximation is necessary to explain some of the features seen in numerical simulations of supernova neutrino flavour evolution. The major aspects of the supernova neutrino spectrum that are missing are the asymmetry between the numbers of neutrinos and antineutrinos and the finite spread in energy of the neutrino beams. First of all we will drop the change in the neutrino density from the previous case, and instead consider different initial conditions, where $n_\nu \neq n_{\bar{\nu}}$. We define a new variable α such that $n_{\bar{\nu}} = \alpha n_\nu$ This means that our initial conditions are now

$$\begin{aligned} \mathbf{S}(0) &= (1+\alpha)\,\hat{\mathbf{z}} \\ \mathbf{D}(0) &= (1-\alpha)\,\hat{\mathbf{z}}, \end{aligned} \tag{1.75}$$

where we note that for a typical supernova scenario $0 < \alpha < 1$.

The non-zero initial value of $\mathbf{D}$ means that the dynamics of the system will be more complex. $\mathbf{D}\cdot\mathbf{r}$ will be non-zero, which is equivalent to adding a spinning bob to the simple pendulum, as explained in the derivation of Equation 1.47. The classical motion of a gyroscopic pendulum is generally a combination of precession and nutation. In our case, this precession is a result of the fact that $\mathbf{D}$ is no longer constrained to vary only along the $\hat{\mathbf{y}}$ axis, and can rotate in the $\hat{\mathbf{x}}$-$\hat{\mathbf{y}}$ plane, which will result in the precession of the polarization vectors in addition to the nutation that was seen in the symmetric case. This precession represents a phase shift in the neutrino oscillations, and does not cause observable flavour changes.

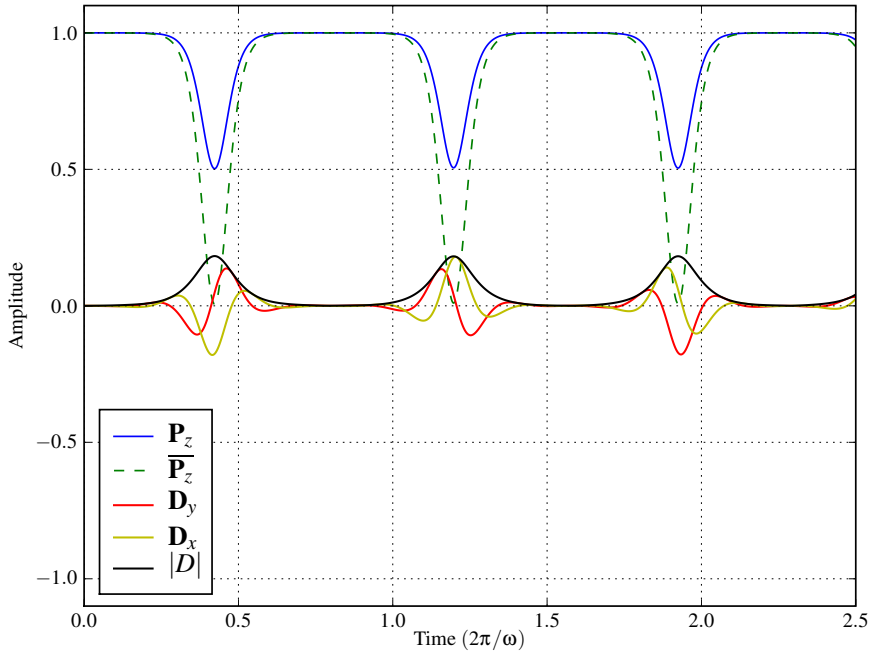

Figure 1.3: An example of the motion of the flavour vectors in the intermediate case of $\mu = 15\omega$ and flavour asymmetry $\alpha = 0.5$.

Normal Hierarchy

Using the classical pendulum analogy, we can write the energy of the flavour pendulum system as

$$\mathcal{E} = -m\mathbf{g}\cdot\mathbf{r} + \frac{m\dot{\mathbf{r}}^2}{2} + \frac{\sigma^2}{2m}. \tag{1.76}$$

Initially the neutrinos are all in pure electron states with their flavour vectors pointing in the $+\hat{\mathbf{z}}$ direction. Therefore in the normal hierarchy the flavour pendulum begins very close to its minimum potential energy position because $\mathbf{g}$ points in the same direction as $\mathbf{Q}(0)$ and $\mathbf{S}(0)$. Once again the normal hierarchy does not provide any interesting dynamics. In order to have significant flavour changes in the normal hierarchy we will need to add more complexity to our system, for instance by considering a neutrino system with a spread of energies.

Inverted Hierarchy

The inverted hierarchy is much more interesting dynamically. The initial conditions mean that the motion of the flavour vectors is analogous to the movement of a gyroscope that is spun up and released. As the gyroscope's spin slows, we expect it will eventually fall over due to gravity, but if it is spinning quickly enough it will remain in an upright position for some time and will undergo precession and nutation as it slows. For a classical gyroscope the relative sizes of the spin kinetic energy and the force of gravity quantify what is meant by a "fast enough" spin. As long as the condition

$$\frac{\sigma^2}{2m} > 2m|\mathbf{g}| \tag{1.77}$$

holds the pendulum will remain in a stable, upright position. The same condition applies to our neutrino flavour system. With the initial conditions described above we find, using $\mathbf{D}(0) = (1-\alpha)\hat{\mathbf{z}}$ and $\mathbf{Q}(0) \simeq (1+\alpha)\hat{\mathbf{z}}$, that this condition can be written as

$$\frac{\mu}{\omega} > 4\frac{1+\alpha}{(1-\alpha)^2} \tag{1.78}$$

so for instance with $\alpha = 0.5$ if $\mu/\omega \gtrsim 24$ then the system will remain stable at its initial point. The flavour vectors in this case remain at their initial points for all time and there is no flavour change, since the "gravitational" pull caused by the inverted hierarchy is not sufficient to tip the gyroscope. Note, however, that this solution depends on the assumption that $\mathbf{B}$ is exactly along the $\hat{\mathbf{z}}$ axis, which is not precisely true. Realistically there will be some motion of $\mathbf{D}$ and the polarization vectors, consisting of a very small-amplitude nutation. However, the mixing angle is small enough that this motion is practically indistinguishable from the fixed flavour vector solution.

For values of μ below this limit the system will begin to move in a combination of nutation and precession, which results in a similar flavour evolution to the simple pendulum case in the high μ limit. In Figure 1.3 we show the motion of the system in one such intermediate case. The asymmetry has several effects. The $\mathbf{D}$ vector now precesses, as shown by the non-zero $\hat{\mathbf{x}}$ and $\hat{\mathbf{y}}$ components in the plot. The flavour vectors themselves also evolve differently from each other, with the neutrino vector $\mathbf{P}$ not dipping as low as the antineutrino vector $\overline{\mathbf{P}}$. This is a result of the magnitudes of these vectors being different. The minimum value of both flavour vectors is much reduced from the minimum

in the case of no asymmetry, which would be around $1/15 - 1 = -0.93$.

The reduction in the depth of the swap in this asymmetric case can be understood in the gyroscope analogy as being a consequence of the conservation of angular momentum. From the equations of motion derived earlier for the gyroscopic pendulum, we know that both $\sigma = \mathbf{D} \cdot \mathbf{r}$ and $\mathbf{D} \cdot \mathbf{B}$ are conserved, and unlike the symmetric case these quantities are non-zero. We first write the expression for the total energy of the flavour pendulum from Equation 1.76 in a more convenient form,

$$\mathcal{E} = \omega Q \mathbf{B} \cdot \mathbf{r} + \frac{1}{2\mu}\dot{\mathbf{r}}^2 + \frac{\mu\sigma^2}{2}. \tag{1.79}$$

By taking θ_V to be small (so that $\mathbf{B} \simeq \hat{\mathbf{z}}$), and with the initial condition $\dot{\mathbf{r}}(0) = 0$, corresponding to the initially fixed neutrino states, conservation of energy requires that

$$\omega Q + \frac{\mu\sigma^2}{2} = \omega Q \cos\vartheta + \frac{1}{2\mu}\dot{\mathbf{r}}^2 + \frac{\mu\sigma^2}{2}, \tag{1.80}$$

meaning that at any position we have

$$\omega Q \left(1 - \cos\vartheta\right) = \frac{1}{2\mu}\dot{\mathbf{r}}^2. \tag{1.81}$$

We can obtain another conservation equation for the quantity $\mathbf{D} \cdot \mathbf{B}$ by taking the dot product of the expression for $\mathbf{D}$ from Equation 1.46 with $\mathbf{B}$. By also noting that by the definition of σ, initially we have $\sigma = \mathbf{D} \cdot \mathbf{r} = \mathbf{D} \cdot \mathbf{B}$, we find

$$\sigma = \frac{1}{\mu}\left(\mathbf{r} \times \dot{\mathbf{r}}\right) \cdot \mathbf{B} + \sigma \mathbf{r} \cdot \mathbf{B}. \tag{1.82}$$

Using our assumption that θ_V is small and rearranging the first term with some vector algebra, noting that $\dot{\mathbf{r}}$ is always perpendicular to $\mathbf{r}$, we obtain

$$\sigma = \frac{\dot{r}_\perp}{\mu}\sin\vartheta + \sigma\cos\vartheta, \tag{1.83}$$

where $\dot{r}_\perp$ is the component of the velocity perpendicular to $\mathbf{B}$. If we apply these expressions at the lowest point of the bob, where $\vartheta = \vartheta_{\max}$, we can use the fact that at the lowest point the motion will be a pure precession, so the motion is along a line of latitude and $\dot{\mathbf{r}}^2 = \dot{r}_\perp^2$. This lets us combine the two conservation

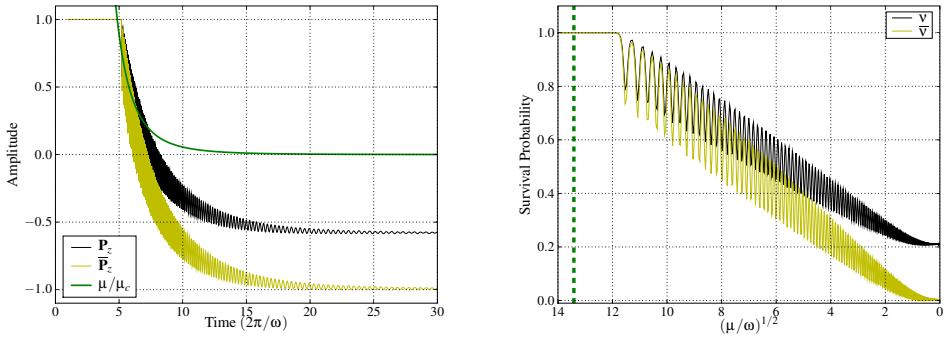

Figure 1.4: The evolution of the polarization vectors in an asymmetric case with a decreasing neutrino interaction strength. The smooth line in the left-hand figure is the value of μ as a fraction of the limiting value for bipolar oscillations to occur, while the dotted line in the right hand figure shows the point where μ crosses this threshold.

equations to arrive at the fairly simple expression

$$\cos\vartheta_{\max} = \frac{\mu\sigma^2}{2\omega Q} - 1, \tag{1.84}$$

from which we can see that large σ, corresponding to a high spin of the pendulum bob, will reduce the maximum angle, as will high μ. The condition for this equation to have a solution turns out to be the same condition as given in Equation 1.77 for the limiting value of μ that will cause the pendulum to remain upright in the synchronized mode for a given value of α. This behaviour of the gyroscopic pendulum in our analogy corresponds to the neutrinos remaining fixed in their initial flavour states.

Decreasing Neutrino Density

The asymmetric neutrino system shows somewhat similar behaviour in a decreasing neutrino density to the symmetric one described above. In particular, the argument given for the rate of decline of the pendulum swing height still applies, since the pendulum bob's spin can be assumed constant over each cycle and does not affect the other terms in the energy equation. The major difference in dynamics that is caused by the asymmetry is that the minimum swing position is no longer a full flavour conversion. For a non-gyroscopic pendulum, the swing will always pass through the minimum of the potential, but once the bob

spin is added the maximum value of ϑ is limited by conservation of momentum, as derived in Equation 1.84. Looking at this expression, we can see that as we take $\mu \to 0$ the maximum angle will get closer and closer to π, corresponding to a complete conversion. So we expect that we will have synchronized, unchanging flavour vectors until μ becomes small enough to allow bipolar oscillations. These bipolar oscillations will take the form of a small oscillation between the maximum bob height dictated by energy conservation, and the minimum bob height determined by angular momentum conservation, both of which decrease with μ. The one additional constraint on the motion is that the initial asymmetry of the two vectors must be conserved, because $\mathbf{D} \cdot \mathbf{B}$ is a constant of the motion and $\mathbf{B}$ is approximately the $\hat{\mathbf{z}}$ axis in the small-mixing angle case. So the final state will be for $\overline{\mathbf{P}}_z$ to be very close to -1, while $\mathbf{P}_z$ drops to around $-\alpha$.

In Figure 1.4 we show the results of numerically evolving the asymmetric neutrino system with $\alpha = 0.8$, $\theta_V = 0.001$, and μ decreasing smoothly as r^{-4}. The general behaviour is as expected from the arguments based on conserved energy and angular momentum, and the linear dependence of both the upper and lower points of the oscillation on $\mu^{1/2}$ is also clear.

1.4.7 The Matter Background

Until now we have assumed that the background matter density is always zero. But in a real supernova the matter density is extremely high, and so we would like to understand its effect on the neutrino evolution.

In typical analyses of supernova neutrinos the matter term is ignored, due to previous analytical and numerical results which suggest that its value and rate of decline are not particularly important when the neutrino density is very large [13, 15, 60, 61]. Because these arguments generally rely on the adiabaticity of the matter density's decline, and to illustrate why this term has such a small effect, we follow the discussion of [50] and derive in more detail the effect of the matter term.

First of all we add the matter term back into the equations of motion for our simple symmetric case to obtain

$$\begin{aligned} \dot{\mathbf{P}} &= \left(+\omega\mathbf{B} + V\hat{\mathbf{z}} + \mu\left[\mathbf{P} - \overline{\mathbf{P}}\right]\right) \times \mathbf{P}, \\ \dot{\overline{\mathbf{P}}} &= \left(-\omega\mathbf{B} + V\hat{\mathbf{z}} + \mu\left[\mathbf{P} - \overline{\mathbf{P}}\right]\right) \times \overline{\mathbf{P}}. \end{aligned} \tag{1.85}$$

The matter term is much simpler than the neutrino-neutrino term, and is similar to the vacuum term in that it acts as an external force field that causes a precession of the neutrino vectors in flavour space at the frequency V. The major difference compared to the vacuum term is that the matter term has the same sign for both neutrinos and anti-neutrinos. This means that we can effectively remove a constant matter term from the equations of motion by going to a frame that rotates with a frequency V around the $\hat{\mathbf{z}}$ axis. In this frame, the initial conditions for the polarization vectors are still the same, and the only difference in dynamics is that the formerly constant $\mathbf{B}$ vector now rotates. In the rotating frame, the constant vacuum field $\mathbf{B}$ in the normal hierarchy varies with time as

$$\mathbf{B} = \begin{pmatrix} \sin(2\theta_V) \\ 0 \\ -\cos(2\theta_V) \end{pmatrix} \Rightarrow \begin{pmatrix} \sin(2\theta_V)\cos(-Vt) \\ \sin(2\theta_V)\sin(-Vt) \\ -\cos(2\theta_V) \end{pmatrix}. \tag{1.86}$$

If $\mathbf{B}$ is time-dependent, the equations of motion will gain an additional term proportional to $\dot{\mathbf{B}}$. Equation 1.42 becomes

$$\begin{aligned} \dot{\mathbf{Q}} &= \mu\mathbf{D} \times \mathbf{Q} - \frac{\omega}{\mu}\dot{\mathbf{B}} \\ \dot{\mathbf{D}} &= \omega\mathbf{B} \times \mathbf{Q}. \end{aligned} \tag{1.87}$$

where we can calculate $\dot{\mathbf{B}}$ directly from above to be

$$\dot{\mathbf{B}} = V\sin(2\theta_V)\begin{pmatrix} \sin(-Vt) \\ -\cos(-Vt) \\ 0 \end{pmatrix}. \tag{1.88}$$

The most obvious effect of this extra term in the equations of motion is that the magnitude of $\mathbf{Q}$ is not strictly conserved any more. Another previously constant quantity, $\mathbf{D} \cdot \mathbf{B}$, will also now fluctuate with time. However, since $\mathbf{B}$ is varying with frequency V while $\mathbf{D}$ rotates with frequency ω, the time variations would be expected to average out for the $V \gg \omega$ case we are most interested in. This argument no longer holds if V itself has a significant time variation, as we might expect in a turbulent matter background.

Once again, the most relevant case for our purposes is that of the inverted hierarchy with a small vacuum mixing angle, with initial conditions such that

$\mathbf{Q}$ is aligned along the $+\hat{\mathbf{z}}$ direction. Since $\tilde{\theta}_V$ is small we then have

$$\mathbf{B} \simeq \begin{pmatrix} 2\tilde{\theta}_V \cos(-Vt) \\ 2\tilde{\theta}_V \sin(-Vt) \\ 1 \end{pmatrix}, \qquad \dot{\mathbf{B}} \simeq V 2\tilde{\theta}_V \begin{pmatrix} \sin(-Vt) \\ -\cos(-Vt) \\ 0 \end{pmatrix}. \tag{1.89}$$

Also, when $\mathbf{Q}$ is close to its initial position, we can parametrize it by two small angles ϑ_x and ϑ_y [50],

$$\mathbf{Q} \simeq Q \begin{pmatrix} \vartheta_x \\ \vartheta_y \\ 1 \end{pmatrix}, \tag{1.90}$$

where the angles are the tilts away from $\hat{\mathbf{z}}$ in the $\hat{\mathbf{x}}$ and $\hat{\mathbf{y}}$ directions. With these approximations the variation in Q is of order $\tilde{\theta}_V$ which is much less than 1 and so we can assume that Q is constant for our purposes.

This approximation results in a similar motion of $\mathbf{D}$ to the symmetric, bipolar case, where D_z was always zero. However, because of the rotation in this case D_x and D_y can both be nonzero, and $\mathbf{D}$ can rotate in the the $\hat{\mathbf{x}}$–$\hat{\mathbf{y}}$ plane. This rotation around the $\hat{\mathbf{z}}$ in this plane in flavour space represents a phase shift of the neutrino flavour states. This result follows from the equation of motion for $\dot{\mathbf{D}}$, which gives, with the above approximate forms of $\mathbf{B}$ and $\mathbf{Q}$,

$$\dot{\mathbf{D}} \simeq \omega Q \begin{pmatrix} 2\tilde{\theta}_V \sin(-Vt) - \vartheta_y \\ -2\tilde{\theta}_V \cos(-Vt) + \vartheta_x \\ 2\tilde{\theta}_V \cos(-Vt)\vartheta_y - 2\tilde{\theta}_V \sin(-Vt)\vartheta_x \end{pmatrix}, \tag{1.91}$$

where it is clear that the D_z component is of higher order in the small parameters. This suggests that the deviation from the earlier equations of motion caused by the matter background will be quite small.

By taking the derivative of Equation 1.87 and making these approximations we can obtain two independent equations of motion for the two tilt angles [50]

$$\begin{aligned} \ddot{\vartheta}_x &= \Omega^2 \left(\vartheta_x - 2\tilde{\theta}_V \left[1 - \frac{V^2}{Q^2\mu^2} \right] \cos Vt \right) \\ \ddot{\vartheta}_y &= \Omega^2 \left(\vartheta_y + 2\tilde{\theta}_V \left[1 - \frac{V^2}{Q^2\mu^2} \right] \sin Vt \right), \end{aligned} \tag{1.92}$$

where $\Omega^2 = \omega\mu Q$ as before. As well as the sign asymmetry and difference in the time dependent rotation term in these equations, there is additional asymmetry

between the two tilt angles due to the initial conditions. $\mathbf{Q}$ is initially aligned along the $+\hat{\mathbf{z}}$ axis, while $\mathbf{B}$ has a small component in the $-\hat{\mathbf{x}}$ direction. So from the definition of $\mathbf{Q}$ and again taking small angle approximations, $\vartheta_x(0) \simeq -2\tilde{\theta}_V(\omega/\mu Q)$ and $\vartheta_y(0) = 0$. From the equations of motion we can then find $\dot{\vartheta}_x(0) = 0$ and $\dot{\vartheta}_y(0) = -(\omega/\mu)\dot{\mathbf{B}}_y \simeq V 2\tilde{\theta}_V(\omega/\mu Q)$.

The equations of motion with these initial conditions are solved by

$$\vartheta_x(t) = -2\tilde{\vartheta}\frac{\Omega^2}{\Omega^2 + V^2}\left(\left[1 + \frac{\omega}{\mu Q}\right]\cosh\Omega t - \left[1 - \frac{V^2}{\mu^2 Q}\right]\cos Vt\right)$$
$$\vartheta_x(t) = -2\tilde{\vartheta}\frac{\Omega^2}{\Omega^2 + V^2}\left(\frac{V}{\Omega}\left[1 + \frac{\omega}{\mu Q}\right]\sinh\Omega t + \left[1 - \frac{V^2}{\mu^2 Q}\right]\sin Vt\right). \qquad (1.93)$$

The behaviour in the $V \ll \Omega$ limit is fairly simple, as $\ddot{\vartheta}_y \simeq -2\tilde{\theta}_V \sin Vt$, while the ϑ_x motion is similar to that in the symmetric case. Therefore $\mathbf{Q}$ will swing mostly along the $\hat{\mathbf{x}}$ direction. As we would expect, if $V = 0$ then we recover the equations of motion in the non-rotating symmetric case. In the opposite limit when V is much larger than Ω we will have the $\hat{\mathbf{y}}$ tilt being dominant. However, because the observable flavour of the neutrinos is independent of rotations in the $\hat{\mathbf{x}}$–$\hat{\mathbf{y}}$ plane this axis effect, though interesting, will not cause any directly measurable change in the flavour of the neutrinos.

The major effect of the matter term is a delay in the bipolar time scale derived in Equation 1.63. Using a similar argument to that used to arrive at that expression for τ_{bipolar}, we consider the overall magnitude $\vartheta(t) = \sqrt{\vartheta_x^2 + \vartheta_y^2}$ in the period where $t\Omega \gg 1$ so that the sin and cos terms in the equations can be ignored and $\cosh\Omega t \simeq \sinh\Omega t \simeq e^{\Omega t}/2$. Using Equation 1.93 we find

$$\vartheta(t) \simeq \tilde{\theta}_V \frac{\Omega}{\sqrt{\Omega^2 + V^2}}\left[1 + \frac{\omega}{\mu Q}\right]e^{\Omega t}, \qquad (1.94)$$

which means that ϑ will grow to order 1 on a time scale of

$$\tau_{\text{bipolar}} \simeq -\frac{1}{\Omega}\ln\left(\tilde{\theta}_V \frac{\Omega}{\sqrt{\Omega^2 + V^2}}\left[1 + \frac{\omega}{\mu Q}\right]\right). \qquad (1.95)$$

A large matter density will increase the length of the stable period between the bipolar flips of the symmetric system, but will otherwise have only a minor effect on the oscillations. Note, however, that this solution assumes a slowly-changing matter background, and therefore may not be very accurate in cases where the matter density changes rapidly.

1.5 Multiple Energies

All of the results so far have ignored the very important fact that supernovae emit neutrinos over a wide range of energies. Recent numerical studies [60, 62] have shown that the final spectra that emerge from the supernova after collective oscillations are primarily controlled by the initial conditions, such as the spectral shape, average energy, and relative flux of each neutrino and antineutrino flavour. In this section we will consider some simpler cases involving a few different neutrino and antineutrino energy modes to develop some understanding of the effects of having a spread of energies in the ensemble.

1.5.1 Symmetric Multimode System

We first consider a very simple scenario, where we have equal numbers of neutrinos and antineutrinos at a series of different energies.

The system becomes easier to study if we use the ensemble variables which integrate over all the energy modes. Firstly we define $\mathbf{J}$, the integral polarization vector, as

$$\mathbf{J} \equiv \frac{1}{N + \overline{N}} \int \mathbf{P}(E) n(E) \, \mathrm{d}E, \tag{1.96}$$

where N and $\overline{N}$ are the number densities of neutrinos and antineutrinos. We define $\overline{\mathbf{J}}$ for antineutrinos analogously. For this section, we will consider an ensemble of M distinct neutrino and antineutrino energy modes indexed as $\mathbf{P}_i$, each with equal number density, with a total number density equal to $N + \overline{N} = 2N$. So we have

$$\mathbf{J} = \frac{1}{2N} \sum_{i=1}^{M} \mathbf{P}_i, \tag{1.97}$$

and similarly for $\overline{\mathbf{J}}$. We also define

$$\mathbf{S} \equiv \mathbf{J} + \overline{\mathbf{J}} = \sum_{i=1}^{M} \mathbf{S}_i, \qquad \mathbf{D} \equiv \mathbf{J} - \overline{\mathbf{J}} = \sum_{i=1}^{M} \mathbf{D}_i, \tag{1.98}$$

where the normalization is such that

$$\mathbf{S}_i = \frac{1}{2M} \left(\mathbf{P}_i + \overline{\mathbf{P}}_i \right), \qquad \mathbf{D}_i = \frac{1}{2M} \left(\mathbf{P}_i - \overline{\mathbf{P}}_i \right). \tag{1.99}$$

We will also need one further vector

$$\mathbf{W} \equiv \frac{1}{2N} \sum_{i=1}^{M} \omega_i \mathbf{P}_i, \tag{1.100}$$

with an analogously defined $\overline{\mathbf{W}}$ for antineutrinos.

The starting point is once again the equations of motion for an individual polarization vector $\mathbf{P}_i$, representing the neutrinos in a certain frequency mode. Assuming no background matter, these equations are

$$\begin{aligned} \dot{\mathbf{P}}_i &= (+\omega_i \mathbf{B} + \mu \mathbf{D}) \times \mathbf{P}_i, \\ \dot{\overline{\mathbf{P}}}_i &= (-\omega_i \mathbf{B} + \mu \mathbf{D}) \times \overline{\mathbf{P}}_i. \end{aligned} \tag{1.101}$$

Using these equations and substituting the definitions above, we can derive the equations of motion for the individual $\mathbf{S}_i$ and $\mathbf{D}_i$ vectors, which are

$$\begin{aligned} \dot{\mathbf{S}}_i &= \omega_i \mathbf{B} \times \mathbf{D}_i + \mu \mathbf{D} \times \mathbf{S}_i, \\ \dot{\mathbf{D}}_i &= \omega_i \mathbf{B} \times \mathbf{S}_i + \mu \mathbf{D} \times \mathbf{D}_i. \end{aligned} \tag{1.102}$$

Summing over i, we obtain the corresponding equations for the total $\mathbf{D}$ and $\mathbf{S}$ vectors,

$$\begin{aligned} \dot{\mathbf{S}} &= \mathbf{B} \times (\mathbf{W} - \overline{\mathbf{W}}) + \mu \mathbf{D} \times \mathbf{S}, \\ \dot{\mathbf{D}} &= \mathbf{B} \times (\mathbf{W} + \overline{\mathbf{W}}). \end{aligned} \tag{1.103}$$

Note that in summing the total vector equations the term $\mu \mathbf{D} \times \mathbf{D}_i$ drops out. In fact, in the symmetric case considered here this term is also zero for each individual $\mathbf{D}_i$ because the only difference between the evolution of the neutrino and antineutrino in the same energy mode is in the $\pm\omega_i \mathbf{B}$ term, which restricts all of the difference vectors to move only in the $\hat{\mathbf{y}}$ direction in flavour space.

If we consider the $\mu \gg \omega$ case, the correspondence of Equation 1.103 with the single-mode asymmetric case becomes complete. The equations of motion become

$$\dot{\mathbf{S}} = \mu \mathbf{D} \times \mathbf{S} \quad \text{and} \quad \dot{\mathbf{D}} = \langle \omega \rangle \mathbf{B} \times \mathbf{S}, \tag{1.104}$$

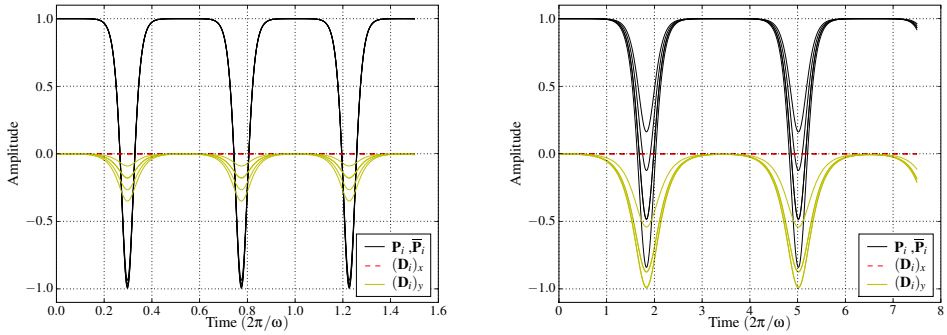

Figure 1.5: The evolution of a four-mode neutrino system with $\omega_i = i\omega_0$ for $i = 1 \ldots 4$ and $\mu = 100\omega_0$ (on the left) and $\mu = 4\omega_0$ (on the right).

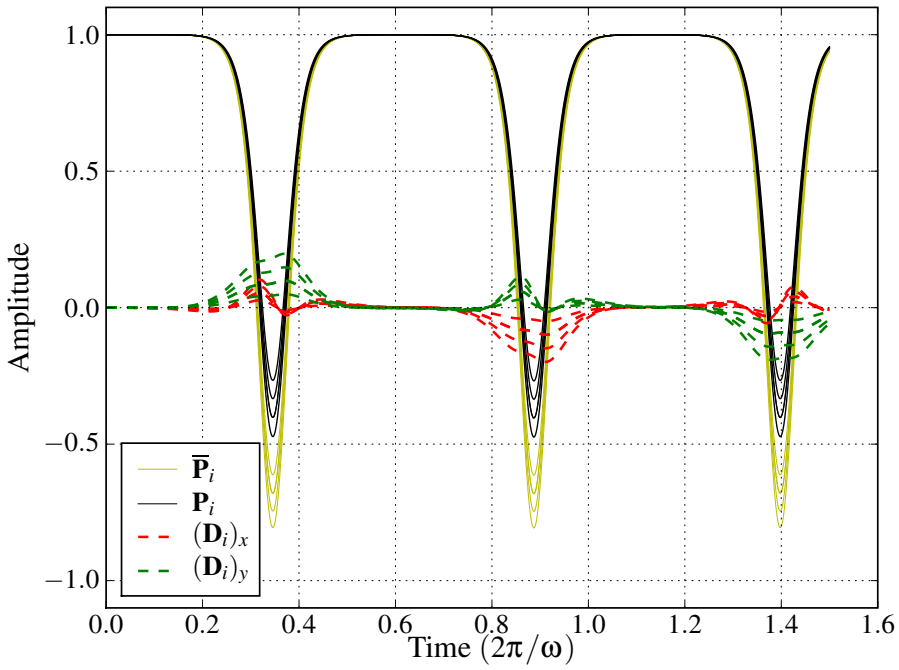

Figure 1.6: The evolution of an asymmetric four-mode neutrino system with $\alpha = 0.8$, $\omega_i = i\omega_0$ for $i = 1 \ldots 4$ and $\mu = 100\omega_0$.

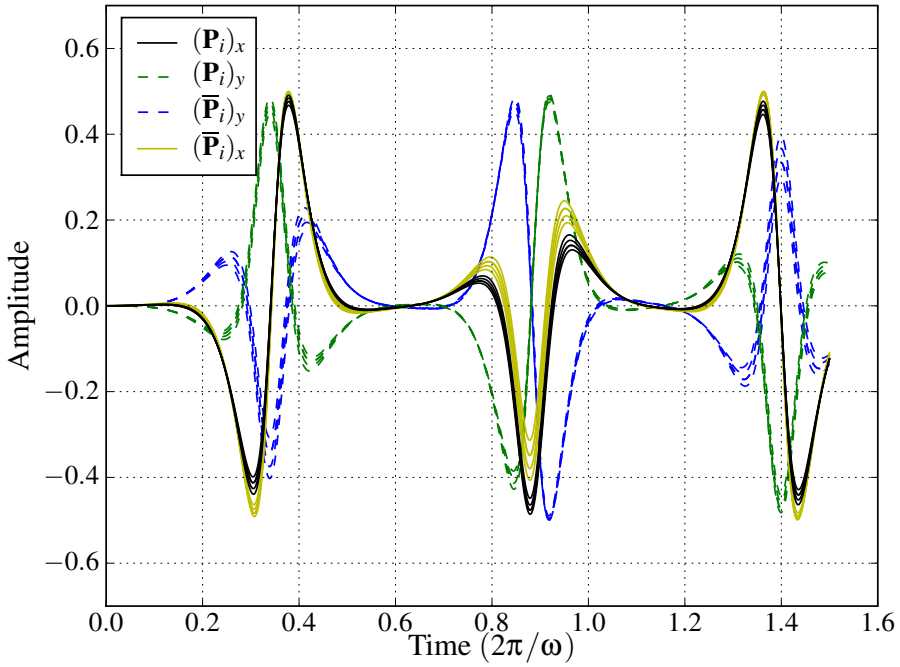

Figure 1.7: The evolution of the $\hat{\mathbf{x}}$ and $\hat{\mathbf{y}}$ components of the neutrino polarization vectors for the four-mode asymmetric neutrino system with $\alpha = 0.8$, $\omega_i = i\omega_0$ for $i = 1 \ldots 4$ and $\mu = 100\omega_0$.

where

$$\langle \omega \rangle \equiv \frac{1}{M} \sum_{i=1}^{M} \omega_i. \tag{1.105}$$

These equations are exactly equivalent to the two polarization vector equations of motion derived in Equation 1.42, with the replacement $\mathbf{Q} \to \mathbf{S}$ in the high μ limit. So the motion will be quite simple: $\mathbf{S}_i$ will move in the same way for all modes, as follows from Equation 1.103 with the first term much smaller than the second, as well as the initial condition that all $\mathbf{S}_i$ are equal. This means that $\mathbf{S}_i \simeq \mathbf{S}/2M$ for all i, with only small differences between the modes due to the relatively small but non-zero $\omega_i \mathbf{B} \times \mathbf{D}_i$ terms. There is a significant difference between the individual modes in the motion of $\mathbf{D}_i$, which can be written as

$$\dot{\mathbf{D}}_i = \frac{\omega_i}{M} \mathbf{B} \times \mathbf{S}. \tag{1.106}$$

We see that the $\mathbf{D}_i$ vectors for each mode will have different magnitudes but identical orientations. A numerical demonstration of this mode of evolution is shown in Figure 1.5. The variation of the $\mathbf{D}_i$ vectors is the result of the $\mathbf{P}_i$ vectors evolving in the $\hat{\mathbf{y}}$ direction with the opposite sign to the corresponding $\overline{\mathbf{P}}_i$ vectors.

Hannestad *et al.* [50] states that the evolution in the $\hat{\mathbf{z}}$ direction is the same for all modes, but this is only approximately true when μ is not infinite. For finite but large values of μ, modes with greater ω have a greater maximum value of $\mathbf{P}_y$, and because the $\mathbf{P}$ vectors cannot change their length this means that their $\mathbf{P}_z$ values must be correspondingly smaller. However, because this variation is small, the resulting difference in the $\hat{\mathbf{z}}$ component of the different polarization vectors is also very small. It can just be seen in the slight difference in the minimum value of the different $\mathbf{P}$ lines in the Figure 1.5. As can be seen in the plot, however, it is correct to say that the evolution of all of the energy modes is identical in phase, even for $\mu = 4$, which is certainly not in the high μ limit.

Adding an asymmetry between the number of neutrinos and antineutrinos in the multimode system has a similar effect to adding an asymmetry in the single mode case. $\mathbf{D}$ now has a conserved component in the $\mathbf{B} \simeq \hat{\mathbf{z}}$ direction which causes the vectors to precess, meaning that the motion is no longer constrained to lie in the $\hat{\mathbf{x}}$–$\hat{\mathbf{z}}$ plane. This does not result in observable changes in the flavour states because the $\hat{\mathbf{x}}$ and $\hat{\mathbf{y}}$ components just represent the phase of the oscillations. The effect of the asymmetry in this case is roughly similar to its effect in the single mode case, where the antineutrino vector had a larger amplitude of flavour oscillation. In this case the different modes each have different minima of their P_z components, but for each of the individual modes the $\mathbf{P}_i$ and $\overline{\mathbf{P}}_i$ vectors have the same amplitude difference. In Figure 1.6 we have plotted the evolution for the same system as in Figure 1.5, except with an asymmetry parameter $\alpha = 0.8$ in each mode.

In Figure 1.7 we have plotted the $\hat{\mathbf{x}}$ and $\hat{\mathbf{y}}$ components of each flavour vector, which clearly undergo much more complex motion than before despite the observable flavour behaviour still being relatively simple. The $\hat{\mathbf{y}}$ components for neutrinos and antineutrinos are out of phase, because of the difference in sign in the $\pm\omega\mathbf{B}$ cross product term in the equations of motion, while the $\hat{\mathbf{x}}$ components are in phase because they result from a common precession around the fixed $\mathbf{D}$ component in the $\mathbf{B}$ ($\simeq \hat{\mathbf{z}}$) direction. As with the P_z components,

the different modes are quite close together in amplitude and share a common frequency and remain coherent throughout their evolution.

1.5.2 Parametric Resonance in Neutrino Oscillations

As well as the large range of behaviour that is possible in the gyroscopic pendulum picture of neutrino oscillations, there also exist other types of motion that do not conform to this picture. One such motion has been described by Raffelt as "self-induced parametric resonance" [51]. This behaviour is interesting because it is independent of both the neutrino hierarchy and the neutrino interaction strength μ.

To understand this different mode of evolution, we consider a simple system consisting of three neutrino energy modes treated as an interacting dense gas. The initial state of the system consists of two electron neutrino modes and one x-type neutrino mode with equally spaced vacuum oscillation frequencies, where the ν_x has the middle frequency. So we have pure electron neutrino modes with $\omega = \omega_0 - \gamma$ and $\omega = \omega_0 + \gamma$, and a pure ν_x mode with $\omega = \omega_0$. We label the electron neutrino polarization vectors $\mathbf{P}_-$ and $\mathbf{P}_+$, and the x-type neutrino $\mathbf{P}_0$. The reason for this notation is that, as was demonstrated above in relation to the matter term, the equations of motion for polarization vectors in a rotating frame remain essentially unchanged. If we examine the equations of motion for the three neutrino polarization vectors in the unrotated frame, we have

$$\begin{aligned} \dot{\mathbf{P}}_\pm &= [(\omega_0 \pm \gamma)\mathbf{B} + \mu\mathbf{D}] \times \mathbf{P}_\pm \\ \dot{\mathbf{P}}_0 &= [\omega_0\mathbf{B} + \mu\mathbf{D}] \times \mathbf{P}_0, \end{aligned} \tag{1.107}$$

where $\mathbf{D} = \mathbf{P}_- + \mathbf{P}_0 + \mathbf{P}_+$, as per its earlier definition as the sum of all neutrino vectors minus the sum of all antineutrino vectors.

Note that in each equation there is a cross product with $\omega_0\mathbf{B}$, representing a common precession of all the flavour vectors. In a reference frame rotating around $\mathbf{B}$ with angular velocity ω_0, this term vanishes from the equations of motion. As in the matter case, this will introduce an additional precession effect, but as we showed earlier the effects are small, and so we will ignore them

in this section. In this rotating frame we have the simpler equations

$$\begin{aligned}\dot{\mathbf{P}}_\pm &= [\pm\gamma\mathbf{B} + \mu\mathbf{D}] \times \mathbf{P}_\pm \\ \dot{\mathbf{P}}_0 &= \mu\mathbf{D} \times \mathbf{P}_0.\end{aligned} \tag{1.108}$$

In this frame, $\mathbf{P}_0$ is effectively an $\omega = 0$ mode, while $\mathbf{P}_-$ and $\mathbf{P}_+$ have equal and opposite frequencies. As Raffelt points out, the apparent negative ω vector can be interpreted as an antineutrino mode [51]. This correspondence allows for simpler studies of some systems, since a mixed spectrum of neutrinos and antineutrinos can be represented as a rotated pure neutrino spectrum. Note that this rotation has removed any dependence on ω_0, and it is only the spacing of the modes that enters the equations.

Because the polarization vectors all have unit length, $\mathbf{D}$ is initially equal to $+\hat{\mathbf{z}}$. Because of the conservation of $\mathbf{D} \cdot \mathbf{B}$, it is helpful to decompose $\mathbf{D}$ into components perpendicular and parallel to $\mathbf{B}$, such that $\mathbf{D} = \mathbf{D}_\perp + \mathbf{D}_\parallel$. If we assume a small mixing angle then initially (and therefore for all time) $\mathbf{D}\cdot\mathbf{B} \simeq 1$, so the decomposition is $\mathbf{D} = \mathbf{B} + \mathbf{D}_\perp$.

This decomposition allows us to further simplify the equations of motion. First we substitute the decomposition of $\mathbf{D}$:

$$\begin{aligned}\dot{\mathbf{P}}_\pm &= [(\mu \pm \gamma)\mathbf{B} + \mu\mathbf{D}_\perp] \times \mathbf{P}_\pm \\ \dot{\mathbf{P}}_0 &= [\mu\mathbf{B} + \mu\mathbf{D}_\perp] \times \mathbf{P}_0.\end{aligned} \tag{1.109}$$

These equations once again contain a common rotation around $\mathbf{B}$, with frequency μ. If we transform into a new frame that rotates with this frequency, we get

$$\begin{aligned}\dot{\mathbf{P}}_\pm &= [\pm\gamma\mathbf{B} + \mu\mathbf{D}_\perp] \times \mathbf{P}_\pm \\ \dot{\mathbf{P}}_0 &= \mu\mathbf{D}_\perp \times \mathbf{P}_0.\end{aligned} \tag{1.110}$$

Now it is clear that there is a differential rotation caused by the splitting in ω around $\mathbf{B}$, and a common precession around $\mathbf{D}_\perp$ that acts perpendicular to $\mathbf{B}$, which will tend to flip the polarization vectors. This is very similar to spin magnetic resonance, where a small perpendicular field in phase with the fast precession of electrons around a fixed strong field can completely flip the electron spins.

To solve these equations of motion, Raffelt introduces the vector $\mathbf{P}_+ - \mathbf{P}_-$, which is similar to the general definition of $\mathbf{D}$ if we think of $\mathbf{P}_-$ as an antineutrino. Raffelt in fact calls this vector $\mathbf{D}$. However, because we have until now consistently used $\mathbf{D}$ to describe the total neutrino-neutrino field alone, we will label this new vector $\mathbf{E}$ to avoid confusion. Using the definition of $\mathbf{E}$ we can derive its equation of motion

$$\dot{\mathbf{E}} = \mu \mathbf{D}_\perp \times \mathbf{E} + \gamma \mathbf{B} \times [\mathbf{D}_\perp - \mathbf{P}_0], \tag{1.111}$$

as well as that of $\mathbf{D}_\perp$,

$$\dot{\mathbf{D}}_\perp = \gamma \mathbf{B} \times \left[\mathbf{E} - \frac{\mu}{\gamma} \mathbf{D}_\perp \right]. \tag{1.112}$$

To make further progress with the equations we can use the fact that the total energy of the system, given by $\mathbf{B} \cdot \mathbf{W} + \mu/2\mathbf{D}^2$, must be conserved. If we substitute the decomposition of $\mathbf{D}$ into this energy then we get a term of order $\gamma \mathbf{D}_\perp$ from the first part, and $\mu/2\mathbf{D}_\perp^2$ from the second part, with the other terms constant to first order. So when the vectors completely swap we must have $\mathbf{D}_\perp \lesssim \sqrt{\gamma/\mu}$ in order to conserve energy. Effectively we are just balancing the maximum potential energy, which is of order $2\gamma \mathbf{D}_\perp$, with the kinetic energy, which is of order $\mu/2\mathbf{D}_\perp^2$.

The condition $\mathbf{D}_\perp \lesssim \sqrt{\gamma/\mu}$ means that in the large μ limit $\mathbf{D}_\perp$ must be small. But because of the sign difference in the evolution of $\mathbf{P}_+$ and $\mathbf{P}_-$, we expect that $\mathbf{E}$ will be of order unity when the two vectors have precessed in opposite directions. Therefore, in order for $\dot{\mathbf{D}}_\perp$ to remain small, we must have

$$\mathbf{D}_\perp \simeq \frac{\gamma}{\mu} \mathbf{E}, \tag{1.113}$$

at least to leading order. This also requires that $\mathbf{E} \cdot \mathbf{B} = 0$, but this is expected from the symmetry of the motion of $\mathbf{P}_+$ and $\mathbf{P}_-$. If we make this substitution, we finally get the equations of motion

$$\begin{aligned} \dot{\mathbf{P}}_0 &= \quad \gamma \mathbf{E} \times \mathbf{P}_0 \\ \dot{\mathbf{E}} &= -\gamma \mathbf{B} \times \mathbf{P}_0. \end{aligned} \tag{1.114}$$

These equations of motion are exactly the same as those for the symmetric neutrino case, Equation 1.42, with $\mathbf{Q} \Rightarrow \mathbf{P}_0$, $\mathbf{D} \Rightarrow \mathbf{E}$, and $\mu = -\omega = \gamma$. The equal frequencies in this case, and the fact that both ω and μ have dropped

out of the equations, show that the resonance is generated by the system itself. The non-linear nature of the collective neutrino interactions, in which the background field is produced by the vectors it acts on, guarantees the existence of the resonant frequency γ independently of the vacuum or background parameters.

Because these equations are identical in form to the symmetric pendulum case, we can now solve them quite simply in terms of the angle ϑ that $\mathbf{P}_0$ makes with the $-\mathbf{D}$ direction and the magnitude of $\mathbf{E}$. These variables are canonically conjugate as in the earlier case, and from a similar Hamiltonian,

$$H(\vartheta, E) = \gamma \left[\frac{1}{2} E^2 + (\cos\vartheta - 1) \right], \tag{1.115}$$

their equations of motion can be obtained. These are:

$$\begin{aligned} \dot{\vartheta} &= \gamma E \\ \dot{E} &= -\gamma \sin\vartheta. \end{aligned} \tag{1.116}$$

These two equations of motion determine the motion of all the polarization vectors. If we define the coordinate system so that the motion of $\mathbf{P}_0$ is in the $\hat{\mathbf{x}}$–$\hat{\mathbf{z}}$ plane, we can parametrize the polarization vectors in terms of ϑ by

$$\mathbf{P}_0 = \begin{pmatrix} \sin\vartheta \\ 0 \\ -\cos\vartheta \end{pmatrix} \quad , \quad \mathbf{P}_\pm = \frac{1}{2} \begin{pmatrix} -\sin\vartheta \\ \pm\sqrt{2(1-\cos\vartheta)} \\ 1+\cos\vartheta \end{pmatrix}, \tag{1.117}$$

so that we always have $\mathbf{D} = +\hat{\mathbf{z}}$ in this coordinate system.

There are a range of possible initial conditions, but the most relevant ones for a small mixing angle case will be where initially $\mathbf{P}_\pm = -\mathbf{P}_0 = +\hat{\mathbf{z}}$, which gives $\mathbf{E}(0) = 0$. This initial condition corresponds to $\vartheta(0) = 0$ and therefore a maximal value of H in Equation 1.115, so the system is effectively a pendulum released from its topmost position. The small mixing angle represents a slight misalignment which will cause the pendulum to tip rather than remain exactly at this unstable equilibrium point. Note also that the motion will be the same in the inverted and neutral hierarchies, since the initial conditions and the total energy are independent of the sign of $\mathbf{B}$. A swap in hierarchy is equivalent to swapping the sign of all the vectors in the initial conditions, and has no effect on the motion relative to $\mathbf{D}$. Even a large neutrino mixing angle will not have a strong effect on the essentials of the motion, because the relevant motion is of

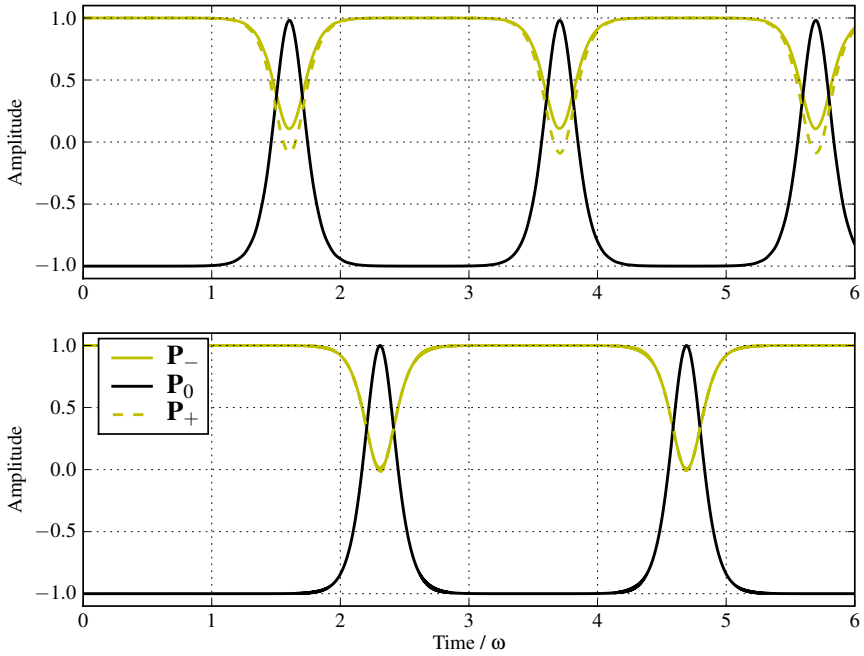

Figure 1.8: A numerical calculation of the motion of the three neutrino system. The top figure was calculated with $\mu = 10$, the bottom figure used $\mu = 1000$. The vectors in both cases have $\omega = 1, 2, 3$.

the individual vectors relative to $\mathbf{P}$, and the common motion of all the vectors along with $\mathbf{P}$ around $\mathbf{B}$ does not alter the collective interactions [51].

Despite the fact that the parametric resonance causes motion similar to the symmetric neutrino case in subsection 1.4.4, there are several unique features of this resonance solution. As mentioned above, it is independent of both the neutrino and matter backgrounds and the vacuum mixing term. This means that the commonly discussed synchronization, where all energy modes simply follow the total $\mathbf{D}$ field and remain fixed relative to each other, does not cover all the possible motions, even in this simple case. No matter how large μ is, this resonance allows large-amplitude flavour conversions of neutrinos to occur even as $\mathbf{D}$ remains constant.

The validity of this analytic study of the motion is demonstrated in Figure 1.8. The two figures are the results of a numerical calculation of the motion of the system described above with $\omega = 1, 2, 3$ for the three modes, and with two

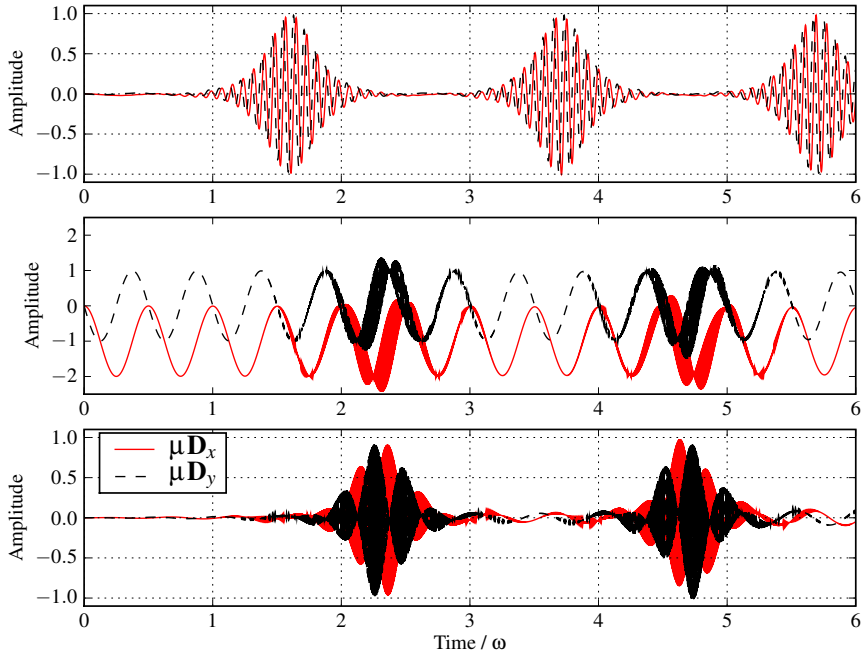

Figure 1.9: The evolution of the components of $\mathbf{D}$ during the parametric resonance of the three mode system. The top figure is for $\mu = 10$, while the bottom two are for $\mu = 1000$. The lowest figure has had constant amplitude oscillations subtracted from the motion to demonstrate that the underlying physical behaviour is unchanged.

different values of μ. There are three major differences between the large and small μ case. Firstly, the motion takes longer to start when μ is large, which is because the small mixing angle we used ($\theta_V = 0.001$) in both cases provides a relatively smaller initial tilt when the magnitude of $\mu\mathbf{D}$ is larger. Therefore it takes longer for the large amplitude motion to begin. This is similar to the behaviour in the standard bipolar case, where the timescale depended logarithmically on θ_V. However, once the motion starts the time taken for the vectors to go through their motion and return to the initial point is the same for both large and small μ. This confirms the solution above, where we found that γ is the only parameter that remains in the equations of motion.

The second difference is more interesting. The $\mathbf{P}_\pm$ vectors in the $\mu = 10$ case have a small separation at their lowest points in the evolution, which disappears in the $\mu = 1000$ case. This can be explained by the fact that at low μ the

contribution of each vector to the energy (via the $\mathbf{B} \cdot \mathbf{W}$ term) is significantly different because it is proportional to ω, which is different for the two vectors. At high μ the difference in ω is dwarfed by the very large value of the μ term in the energy. The limit on the magnitude of $\mathbf{D}_\perp$ derived earlier ($\mathbf{D}_\perp \lesssim \sqrt{\gamma/\mu}$) from conservation of energy requires that the two vectors remain very close together in $\hat{\mathbf{y}}$, which then requires that their $\hat{\mathbf{z}}$ components are also very close in order to conserve the total magnitude $\mathbf{P}^2$. Again, this is similar to the bipolar case where the two vectors were required to maintain anti-alignment to conserve the constants of the motion.

In Figure 1.9 we have plotted the value of the $\hat{\mathbf{x}}$ and $\hat{\mathbf{y}}$ components of the neutrino-neutrino term $\mu\mathbf{D}$. The top figure is for the $\mu = 10$ case and the middle figure is for the $\mu = 1000$ case. The lower figure is the $\mu = 1000$ case with constant amplitude oscillations at a frequency 2ω subtracted, corresponding to the vacuum frequency of $\mathbf{P}_0$. After adding $1 + \cos 2\omega t$ to the $\hat{\mathbf{x}}$ component and $\sin 2\omega t$ to the $\hat{\mathbf{y}}$ component we arrive at plots which are very similar to the $\mu = 10$ case. These added terms are still slightly out of phase with the numerical result, but the closeness shows that these constant oscillations are due to the precession around $\mathbf{B}$, which have been amplified by the large value of μ. The fact that the relative motion of the polarization vectors remains the same even though the total $\mathbf{D}$ vector is dominated by this constant motion shows that our use of a rotating frame to simplify the equations was justified. The plots also show the effect of a larger μ in the fast oscillations of the vectors overlaid on their overall motion.

The differences between this simple neutrino system and the other cases we have discussed are a good demonstration of the complexities that can result from neutrino background interaction effects even in apparently simple neutrino systems. Although this particular scenario is not very realistic, the observation that high neutrino density does not always result in synchronized or even small-amplitude oscillations is valuable. The analogy of the motion to spin magnetic resonance is also relevant to continuous spectra and the understanding of spectral swaps and splits. As we will show, in many realistic supernova neutrino environments the neutrino flavour oscillations cannot be explained through the gyroscopic pendulum analogy alone. In these cases the neutrino flavour swapping does appear to be driven by a resonance very similar to the simple case described above.

1.5.3 Continuous Neutrino Spectra

Real supernova spectra are continuous, and propagate through high matter and neutrino densities that decrease with radius from extremely high values near the supernova core. Therefore we expect that a realistic supernova neutrino system will have much more complicated dynamics than the cases we have considered so far with only a few energy modes. Nevertheless, there are some general results that can be obtained analytically that help to clarify the transition from discrete to continuous spectra, and to understand what causes the characteristic effects of neutrino oscillations on the overall spectra.

Simple Spectral Swaps

The main goal of studying neutrino–neutrino effects in supernovae is to develop a thorough enough theoretical model of neutrino oscillations so that any future observations of supernova neutrinos can be interpreted correctly, which could allow for measurements of the sign of the neutrino mass hierarchy and other neutrino mixing parameters. The primary determinant of the final spectra we receive on Earth will be the spectra of the neutrinos emitted from the neutrinosphere, before any oscillations take place. Although supernova models vary in their predictions of the shapes, relative fluxes, and average energies of the emitted neutrinos, two properties are common to all current models. Firstly, neutrinos of all flavours are emitted with spectra that have a thermal Fermi-Dirac shape or some other fairly similar broadly-peaked distribution, with average energies of approximately 10–30 MeV and almost all neutrinos having energies in the range 1–60 MeV. Secondly, no matter the specific choice of initial spectrum, numerical calculations in various approximate models find that the effect of neutrino oscillations on these spectra will either be negligible, or a complete swap in flavour of all neutrinos in some energy range. Here we wish to examine this swapping behaviour in detail.

No matter the complexity of the neutrino spectra, we always have the same equations of motion for each of the individual polarization vectors:

$$\begin{aligned} \dot{\mathbf{P}} &= (+\omega\mathbf{B} + \mu\mathbf{D}) \times \mathbf{P}, \\ \dot{\overline{\mathbf{P}}} &= (-\omega\mathbf{B} + \mu\mathbf{D}) \times \overline{\mathbf{P}}, \end{aligned} \tag{1.118}$$

where we have ignored the matter term because its effects are generally negligible

for a slowly changing matter density (see subsection 1.4.7). To understand the behaviour of the system as a whole we can study various integrated quantities that take into account the entire continuous spectrum. These are generalizations of the quantities defined earlier, for instance in Equation 1.36 and Equation 1.41. $\mathbf{J}$ becomes

$$\mathbf{J} \equiv \frac{1}{N + \overline{N}} \int n(E)\mathbf{P}(E)\,\mathrm{d}E, \tag{1.119}$$

where $n(E)$ contains the number of neutrinos as a function of energy, that is, the spectral shape, and the normalization factor contains N and $\overline{N}$, the total numbers of neutrinos and antineutrinos, which allows us to factor the total number density out of the variables and into μ. A similar quantity $\overline{\mathbf{J}}$ is defined using $\overline{\mathbf{P}}(E)$, the polarization vectors for antineutrinos. Note that different normalizations of of $\mathbf{J}$ can be found in some references but these do not affect the dynamics.

The definitions of $\mathbf{S}$ and $\mathbf{D}$ remain the same, although $\mathbf{J}$ now takes into account the full spectrum. We also need to define a continuous version of $\mathbf{W}$, which is

$$\mathbf{W} \equiv \frac{1}{N + \overline{N}} \int n(E)\omega(E)\mathbf{P}(E)\,\mathrm{d}E. \tag{1.120}$$

We will also make use of $\overline{\mathbf{W}}$, the analogous antineutrino integral.

With these definitions, we can integrate the single neutrino equations of motion and rearrange to obtain the equations of motion for these integral quantities [15]:

$$\begin{aligned}
\dot{\mathbf{J}} &= +\mathbf{B} \times \mathbf{W} + \mu\mathbf{D} \times \mathbf{J}, \\
\dot{\overline{\mathbf{J}}} &= -\mathbf{B} \times \overline{\mathbf{W}} + \mu\mathbf{D} \times \overline{\mathbf{J}}, \\
\dot{\mathbf{S}} &= \mathbf{B} \times \left(\mathbf{W} - \overline{\mathbf{W}}\right) + \mu\mathbf{D} \times \mathbf{S}, \\
\dot{\mathbf{D}} &= \mathbf{B} \times \left(\mathbf{W} + \overline{\mathbf{W}}\right),
\end{aligned} \tag{1.121}$$

Just as before, $\mathbf{D} \cdot \mathbf{B}$ is a constant of the motion. If we assume $\mathbf{B} \simeq \pm\mathbf{z}$ (with the plus indicating normal hierarchy and the minus inverted hierarchy) then initially when all $\mathbf{P}$ vectors are aligned in either the $+\mathbf{z}$ or $-\mathbf{z}$ direction the conserved quantity is

$$\mathbf{D} \cdot \mathbf{B} \simeq \mp \frac{N_{\nu_e} - N_{\bar{\nu}_e}}{N + \overline{N}}, \tag{1.122}$$

which is the electron lepton number of the ensemble. This demonstrates that

the equations of motion do not allow any additional lepton number violations beyond the type that occur in standard vacuum oscillations [57].

If we assume that the neutrino background density is constant, the total flavour energy of the ensemble is conserved, and can be written as

$$\mathcal{E} = \mathbf{B} \cdot \left(\mathbf{W} + \overline{\mathbf{W}}\right) + \frac{1}{2}\mu \mathbf{D}^2 = \mathcal{V} + \mathcal{T}. \tag{1.123}$$

The quantity $\mathbf{W}+\overline{\mathbf{W}}$ defines a new variable $\mathbf{M}$ that is similar to a total magnetic moment [51]. Using the equations of motion for $\mathbf{P}$ and $\mathbf{D}$ and the definition of $\mathbf{W}$ it can be shown that this quantity is exactly conserved if μ is constant. As in the simpler cases, $\mathcal{V}$ can be thought of as the total potential energy of the neutrino flavour vectors in the vacuum 'field' $\mathbf{B}$, since it is maximized when the vectors are anti-aligned with $\mathbf{B}$. $\mathcal{T}$ depends on the background neutrino density and the difference in number of neutrinos and antineutrinos $N-\overline{N}$ and can be related to the kinetic energy of the system in the gyroscopic pendulum approximation [15]. An important property of the equations of motion is that the contribution of each neutrino to $\mathbf{D}$ does not depend on energy, so the addition of a complicated spectral shape does not affect the overall strength of the neutrino background which depends only on the total number density of all neutrino flavours.

Ignoring for the moment the complexities of the motion itself, consider the case where the system evolves adiabatically from large neutrino density to vacuum, as in subsection 1.4.5. In vacuum, the energy is minimized when $\mathbf{W}$ and $\overline{\mathbf{W}}$ are antialigned with $\mathbf{B}$. In the normal hierarchy with a small mixing angle, this is already the case for the initial supernova spectrum because the number of electron neutrinos and antineutrinos is greater than the number of mu and tau neutrinos and antineutrinos. The initial value of the ensemble's total $\mathbf{M}$ is proportional to $(N_{\nu_e} - N_{\nu_x}) + (N_{\bar{\nu}_e} - N_{\bar{\nu}_x})$. Because there is an initial excess of electron neutrinos, $\mathbf{M}$ starts aligned in the $+\hat{\mathbf{z}}$ direction, while $\mathbf{B} \simeq -\hat{\mathbf{z}}$ in the normal hierarchy. Therefore we expect that in the normal hierarchy the ensemble will not drastically change its flavour as it propagates through the supernova background.

In the inverted hierarchy $\mathbf{B} \simeq +\hat{\mathbf{z}}$, so the system will tend to 'fall' towards the opposite direction from its initial position in flavour space. Because of the combination of lepton number and energy conservation, this conversion cannot be complete (just as in the simple asymmetric neutrino system), but it can cause a large fraction of the neutrinos to swap flavour. Interactions such as

$\nu_e\bar{\nu}_e \rightarrow \nu_x\bar{\nu}_x$ can convert pairs of neutrinos to lower potential energy states while conserving lepton number [15]. Inverting the initial $\mathbf{W}$ and $\overline{\mathbf{W}}$ vectors as much as allowed by lepton number conservation results in the minimum potential energy. Simulations of neutrino oscillations in supernovae typically produce a final state which has a complete inversion of antineutrino flavour vectors and the inversion of all neutrino flavour vectors above some critical energy.

The form of the final state in either hierarchy is most easily understood by looking at the equations of motion in a simplified case [57]. We begin with the equation of motion for a single neutrino flavour vector:

$$\dot{\mathbf{P}}_i = (\omega_i \mathbf{B} + \mu \mathbf{D}) \times \mathbf{P}_i. \tag{1.124}$$

We assume that the neutrinos undergo a synchronized evolution so that they all rotate together around $\mathbf{B}$ at a frequency Ω (see subsection 1.5.1). This also means that $\mathbf{D}$ will have the same rotational motion around $\mathbf{B}$ since it is just a sum of all the individual flavour vectors. We can remove the complication of this common rotation from the equations by transforming into a frame rotating with angular velocity $-\Omega\mathbf{B}$ with the previous one to obtain

$$\dot{\mathbf{P}}_i = \left([\omega_i - \Omega]\, \mathbf{B} + \mu \tilde{\mathbf{D}} \right) \times \mathbf{P}_i, \tag{1.125}$$

where $\tilde{\mathbf{D}}$ is the transformed neutrino-neutrino interaction vector which is now non-rotating. Note also that antineutrinos have the same equations of motion as neutrinos with negative ω in this picture.

For neutrinos emitted from the centre of a supernova explosion, we know that μ is initially extremely large, and much larger than the vacuum frequency, while as the radius tends to infinity μ tends to zero. If the decrease of μ is slow enough then all the neutrino vectors will end up in a final state that is anti-aligned with $(\omega_i - \Omega)\,\mathbf{B}$. In the normal hierarchy, $\mathbf{B}$ and $\mathbf{D}$ point in opposite directions, so in the final state all neutrinos with $\omega_i < \Omega$ will end up pointing in their initial directions. This means that all antineutrinos and neutrinos above a certain energy will remain in their initial flavour state. Conversely, for the inverted hierarchy $\mathbf{B}$ has the opposite sign, so only neutrinos with $\omega_i > \Omega$ will remain in their initial orientation, resulting in a complete swap in antineutrinos and a swap of neutrinos with energies less than some critical value.

So far we have avoided discussion of the value of the frequency Ω and the

swap energy E_s. Ω can be calculated explicitly, for example using Equation 65 of [57]. The swap energy can also be calculated by equating the lepton number before and after swapping, given that we know which parts of the spectrum will swap:

$$N_e - \overline{N}_e = \int_0^{E_s} n_{\nu_e} - n_{\nu_x} \, \mathrm{d}E - \int_{E_s}^{\infty} n_{\nu_e} - n_{\nu_x} \, \mathrm{d}E + \int_0^{\infty} n_{\bar{\nu}_e} - n_{\bar{\nu}_x} \, \mathrm{d}E \quad (1.126)$$

which allows us to find E_s by solving

$$\int_{E_s}^{\infty} n_{\nu_e} - n_{\nu_x} \, \mathrm{d}E = \int_0^{\infty} n_{\bar{\nu}_e} - n_{\bar{\nu}_x} \, \mathrm{d}E. \quad (1.127)$$

Further analytic work allows the construction of explicit solutions which show that this final state indeed obtains in reasonably realistic cases. Numerical solutions also display the spectral swap feature for a wide variety of initial conditions.

Parametric Swaps

As the title of the previous section indicated, this simple picture is not a complete one. Although the study of spectral splits has been an active field for a number of years, it was only recently [53, 60, 62] that it was realized that the final state with a single spectral swap was only a special case that depended on the choice of initial neutrino spectrum. For many plausible initial conditions, numerical calculations show that two swaps occur in the spectrum. This multiple swap phenomenon is in conflict with the gyroscopic pendulum picture presented above of the mechanism for the single swap, and suggests that there is additional physics that has not been taken into account. As demonstrated by the parametric resonance discussed in subsection 1.5.2, it is quite possible for a neutrino ensemble to undergo large flavour changes even while the overall system and its integrated variables appear stable. From our own numerical results and those of other works [53, 60, 62] it appears that the gyroscopic pendulum analogy can fully explain collective neutrino oscillations only when the initial conditions are such that these resonant oscillations are suppressed. In general the motion of the neutrino ensemble will be a combination of resonant and gyroscopic motion.

The simplest demonstration of resonant swapping behaviour is to consider

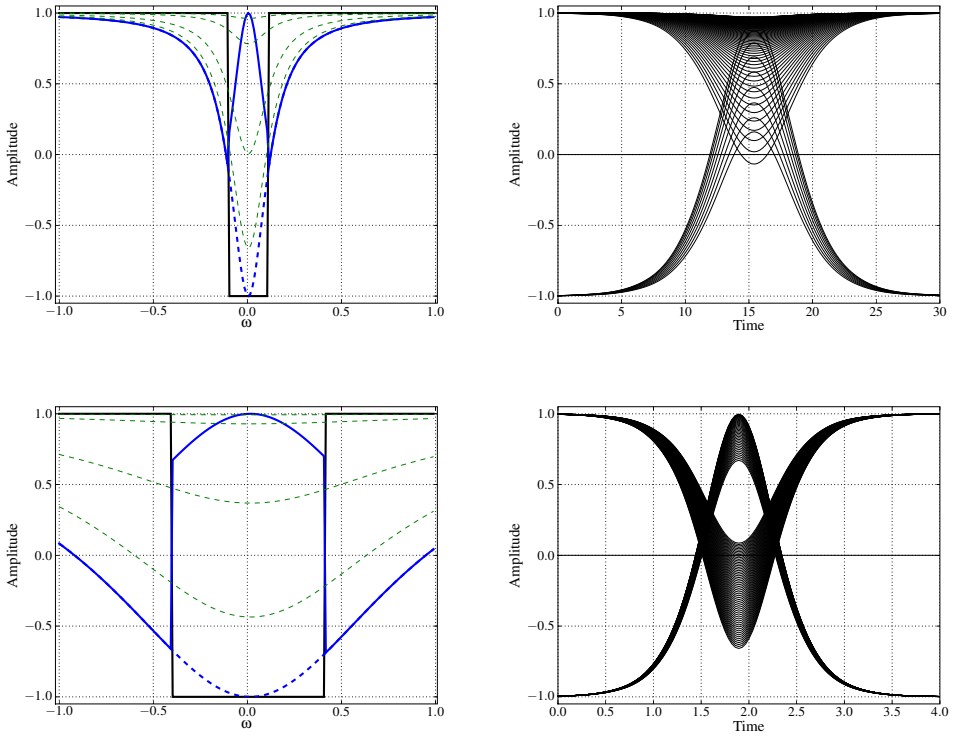

Figure 1.10: Resonant flavour swapping for a simple continuous spectra. The figures on the left show the initial spectrum (black lines) and the spectrum at the maximum of the motion (blue curve). The dashed lines show the negative spectrum in the central region to make the resonant shape of the flavour change clearer. The green dashed lines show the spectrum at a range of intermediate positions in the motion. The right hand figures plot the motion of individual frequency modes over one cycle.

the continuous analogue of the system studied in subsection 1.5.2. Instead of three separate modes with the central mode flipped, we consider a continuous spectrum which is flat over a range of ω values. The central portion of the spectrum consists of pure x-type neutrinos, while the outer parts consist of pure electron neutrinos. The system is then evolved in the same way as before with a high value of μ. The resulting motion is shown in Figure 1.10.

The motion of this system is similar to the earlier resonance case, in that the modes all move in phase with the same pendulum-like motion. The modes spread out according to their energies, with the modes closer to the central point of the spectrum having the largest amplitude and swapping completely,

while those further away are off-resonance and their amplitudes appear to follow a Lorentzian resonance curve. The timescale for the conversion is increased when the width of the swapped part of the spectrum is increased, but when the width of the flipped portion is larger than half the total width of the spectrum no flavour conversions occur. Within this constraint, the narrower the flipped portion the sharper the resonance is. All of these facts lead us to search for a resonant solution which explains the motion analytically [51].

Because our numerical code was designed to deal only with positive neutrino energies, we have normalized and shifted the values of ω in the plots. This corresponds to a rotating frame and an overall shift in the time parameter, so does not affect the dynamics. For analytic purposes we use a frequency range of $-1 \leq \omega \leq +1$ for simplicity. First we need to find the integrated equations of motion for the ensemble. We label the modes with their frequencies, so that $\mathbf{P}_\omega$ represents the mode with frequency ω. So the equation of motion for a single mode when mixing angle is small will be

$$\dot{\mathbf{P}}_\omega = \mu \mathbf{D}_\perp \times \mathbf{P}_\omega + \omega \mathbf{B} \times \mathbf{P}_\omega, \tag{1.128}$$

where $\mathbf{D}_\perp$ is the component of $\mathbf{D}$ that is perpendicular to $\mathbf{B}$. Integrating this equation over all energies we get a similar equation to Equation 1.112:

$$\begin{aligned} \int \dot{\mathbf{P}}_\omega \, \mathrm{d}E &= \mu \mathbf{D}_\perp \times \int \mathbf{P}_\omega \, \mathrm{d}E + \mathbf{B} \times \int \omega \mathbf{P}_\omega \, \mathrm{d}E, \\ \dot{\mathbf{P}} \simeq \dot{\mathbf{P}}_\perp &= \mathbf{B} \times (\mathbf{W} - \mu D \mathbf{D}_\perp), \end{aligned} \tag{1.129}$$

where $\mathbf{P}_\perp$ is the component of $\mathbf{P}$ perpendicular to $\mathbf{B}$. The magnitude of $\mathbf{D}$, D, appears because we have not normalized the vectors. We also assume that $\mathbf{D}_\perp$ is small, so that $\mathbf{D} = \mathbf{D}_\perp + (\mathbf{D} \cdot \mathbf{B})\mathbf{B} \simeq \mathbf{D}_\perp + D\mathbf{B}$. Because of conservation of energy, we can use the same reasoning as in the simpler case presented earlier to show that $\mathbf{D}_\perp \simeq \mathbf{W}/(\mu D)$ to first order in the small parameter μ^{-1}. In addition, the symmetry of the spectrum means that $\mathbf{B} \cdot \mathbf{M} = 0$ to first order. Substituting these results into Equation 1.128 we find

$$\dot{\mathbf{P}}_\omega = \left(\frac{1}{D} \mathbf{W} + \omega \mathbf{B} \right) \times \mathbf{P}_\omega, \tag{1.130}$$

where μ has been eliminated as before. From this equation, we can see that for the mode $\mathbf{P}_0$ the motion is a precession around $\mathbf{W}$, and since $\mathbf{W}$ has no

component along $\mathbf{B}$ the central mode $\mathbf{P}_0$ will undergo complete flavour conversion. The other vectors away from this resonance will precess around $\mathbf{B}$, so their conversion will be damped in an ω-dependent way.

We can now apply these equations to our numerical example. The spectrum can be represented by a function f_ω and a parameter β which determines the width of the flipped part of the spectrum, so that

$$f_\omega \equiv \begin{cases} +1 & \text{when } \beta < |\omega| \leq 1 \\ -1 & \text{when } 0 \leq |\omega| \leq \beta, \end{cases} \tag{1.131}$$

which allows us to write the initial conditions simply as

$$\mathbf{P}_\omega(0) = \begin{pmatrix} 0 \\ 0 \\ f_\omega \end{pmatrix}. \tag{1.132}$$

With this definition, we can calculate the magnitude of $\mathbf{D}$ straightforwardly to be $D = \int f_\omega \, \mathrm{d}\omega = 2(1 - 2\beta)$.

The numerical results suggest that the neutrino flavour as a function of ω will involve a Cauchy-Lorentz distribution with the form

$$L_\omega = \frac{1}{1 + (\omega/\Gamma)^2}. \tag{1.133}$$

In order for lepton number to be conserved, we must have some condition that restricts Γ. We can simply require that the integral of L_ω in the flipped part of the spectrum is equal to its integral outside this range. This means that the number of neutrinos swapping from ν_x to ν_e and vice versa will be equal. The condition can thus be written as

$$\int_{-1}^{+1} f_\omega L_\omega \, \mathrm{d}\omega = 0, \tag{1.134}$$

which, using Equation 1.131 and the symmetry of L_ω, we can write as

$$\int_{\beta}^{1} L_\omega \, \mathrm{d}\omega = \int_{0}^{+\beta} L_\omega \, \mathrm{d}\omega. \tag{1.135}$$

Using the fact that $\int L_\omega = \tan^{-1}(\omega/\Gamma)$ we obtain the condition

$$\Gamma = \frac{\beta}{\sqrt{1-2\beta}}, \tag{1.136}$$

which only has solutions for $\beta < 1/2$, which provides an explanation for the numerical result that no swap occurs when this condition is not met.

Because of the similarity of the motion to the three vector parametric case, we follow a similar method to obtain the solution. We define the coordinate system relative to $\mathbf{P}_0$ so that $\mathbf{W}$ is along the $\hat{\mathbf{y}}$ axis and $\mathbf{P}_0$ moves perpendicular to it in the $\hat{\mathbf{x}}$–$\hat{\mathbf{z}}$ plane. We use the same variable, ϑ, to write $\mathbf{P}_0$'s position as

$$\mathbf{P}_0 = \begin{pmatrix} \sin\vartheta \\ 0 \\ -\cos\vartheta \end{pmatrix}. \tag{1.137}$$

As [51] suggests, it is now possible to 'guess' a solution based on the numerically known motion and the various symmetry requirements of the system. This solution is

$$\mathbf{P}_\omega = \left[\begin{pmatrix} 0 \\ 0 \\ 1 \end{pmatrix} - \begin{pmatrix} \sin\vartheta \\ (\omega/\Gamma)\sqrt{2(1-\cos\vartheta)} \\ 1-\cos\vartheta \end{pmatrix} L_\omega \right] f_\omega. \tag{1.138}$$

This solution ensures that D is conserved because the ϑ terms cancel in the integral $\int \mathbf{P}_\omega \, \mathrm{d}\omega$. This solution also results in $\mathbf{W}$ being purely in the $\hat{\mathbf{y}}$ direction, and its magnitude is given by

$$M = \Gamma\sqrt{2(1-\cos\vartheta)} \int \left(\frac{\omega}{\Gamma}\right)^2 L_\omega f_\omega \, \mathrm{d}\omega, \tag{1.139}$$

which can be solved, using the condition in Equation 1.134, to give

$$M = \Gamma D\sqrt{2(1-\cos\vartheta)}. \tag{1.140}$$

The next step is to take the integral $\int \mathrm{d}\omega\omega$ of Equation 1.130 to find an equation of motion for $\mathbf{W}$, which gives

$$\dot{\mathbf{W}} = \mathbf{B} \times \int_{-1}^{+1} \omega^2 \mathbf{P}_\omega \, \mathrm{d}\omega. \tag{1.141}$$

Because $\mathbf{B}$ is very close to the $\hat{\mathbf{z}}$ direction, and the $\hat{\mathbf{y}}$ component of the integral

vanishes because of the odd number of factors of ω it contains in the symmetric integral, the only component remaining after the cross product is $B_y(P_\omega)_x$, whose magnitude can be obtained in the same way as that of $\mathbf{W}_y$ and is equal to $\Gamma^2 D \sin\vartheta$. The equation of motion is therefore equivalent to

$$\frac{\mathrm{d}}{\mathrm{d}t}\left(\Gamma D\sqrt{2(1-\cos\vartheta)}\right) = \Gamma^2 D\sin\vartheta, \tag{1.142}$$

which gives us a final equation of motion for ϑ

$$\dot{\vartheta} = \Gamma\sqrt{2(1-\cos\vartheta)}, \tag{1.143}$$

which is once again the same as the motion of a pendulum starting from the upright, inverted position. This equation governs the overall oscillation of the system, and the dependence of the frequency on Γ explains the shortening of the swing timescale for the spectrum with a wider flipped part. This solution for $\mathbf{P}_\omega$ clearly demonstrates that the motion is indeed like a forced resonant system, where each neutrino mode has an amplitude of oscillation that depends on how close its natural freqency is to the driving frequency provided by the neutrino-neutrino interactions.

Multiple Swaps

Despite the neatness of the previous two derivations, they cannot fully explain the motion seen in numerical simulations that result in multiple swaps. To demonstrate this, we show in Figure 1.11 the neutrino spectra before and after evolution through 400km with typical supernova conditions. These two spectra are chosen as examples of a simple single swap spectrum, shown in the upper figures, and a more complex multiple swap spectrum in the lower figures. The goal of this section is to explain some of the reasons for the very different evolution of these two seemingly similar neutrino spectra.

Dasgupta *et al.* [60] point out that in neutrino oscillations the total number of neutrinos at each energy must be conserved. Therefore, if the spectra as a function of energy are defined as $f_{\nu_e}(E)$, $f_{\nu_x}(E)$, $f_{\bar{\nu}_e}(E)$, $f_{\bar{\nu}_x}(E)$ then $f_{\nu_e}(E) + f_{\nu_x}(E)$ and $f_{\bar{\nu}_e}(E) + f_{\bar{\nu}_x}(E)$ will be constants of the motion. Therefore for the purpose of examining flavour change it is natural to use the quantity $\Delta f_\nu(E) \equiv f_{\nu_e}(E) - f_{\nu_x}(E)$ to quantify the flavour changes that occur. To allow the extension of this quantity to antineutrinos with negative ω Dasgupta *et al.*

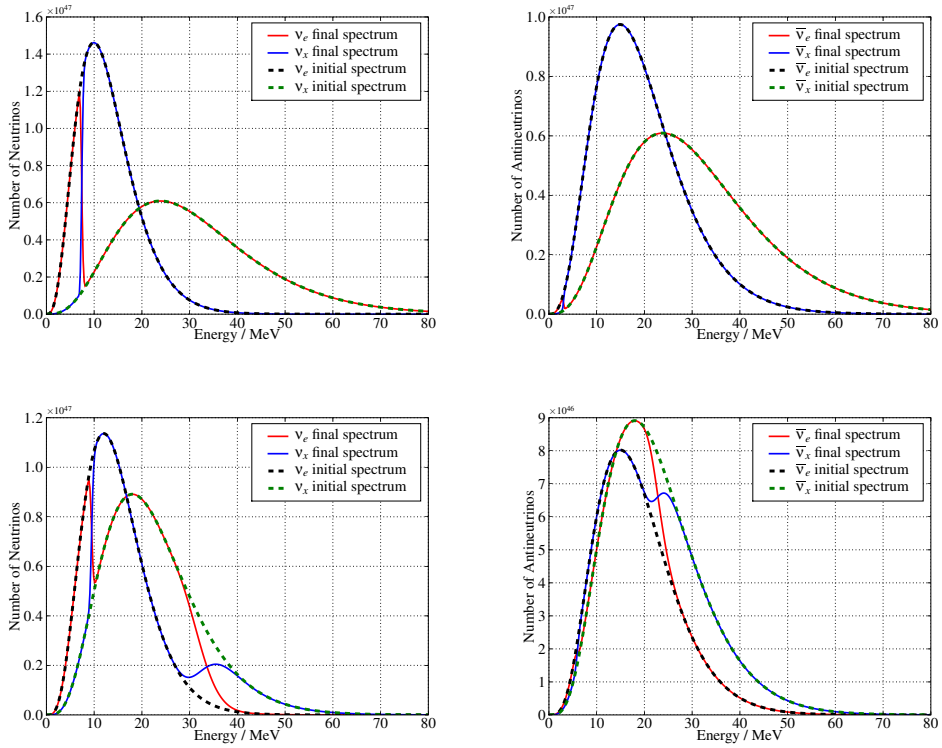

Figure 1.11: Two representative types of neutrino spectra before and after evolution through a typical supernova background. The top figures are for a Fermi-Dirac type spectrum, as used in [15], while the bottom figures are for a supernova cooling-phase spectrum, as used in [60].

define g_ω, which we will refer to as the difference spectrum, as

$$g_\omega \equiv \frac{|\Delta m^2|}{2\omega^2} \times \begin{cases} +f_{\nu_e}(E) - f_{\nu_x}(E) & \text{when } \omega > 0, \\ -f_{\bar{\nu}_e}(E) + f_{\bar{\nu}_x}(E) & \text{when } \omega < 0. \end{cases} \tag{1.144}$$

The value of g_ω is plotted in Figure 1.12 for the two spectral shapes plotted before. Also plotted in this figure is the swap factor, which is defined by

$$g_\omega^{\text{final}} = S_\omega g_\omega^{\text{initial}}. \tag{1.145}$$

The usefulness of this parameter is obvious from the plot: it reduces the complexities of the initial and final spectra into a single function which contains all the relevant information about neutrino flavour changes between the initial and

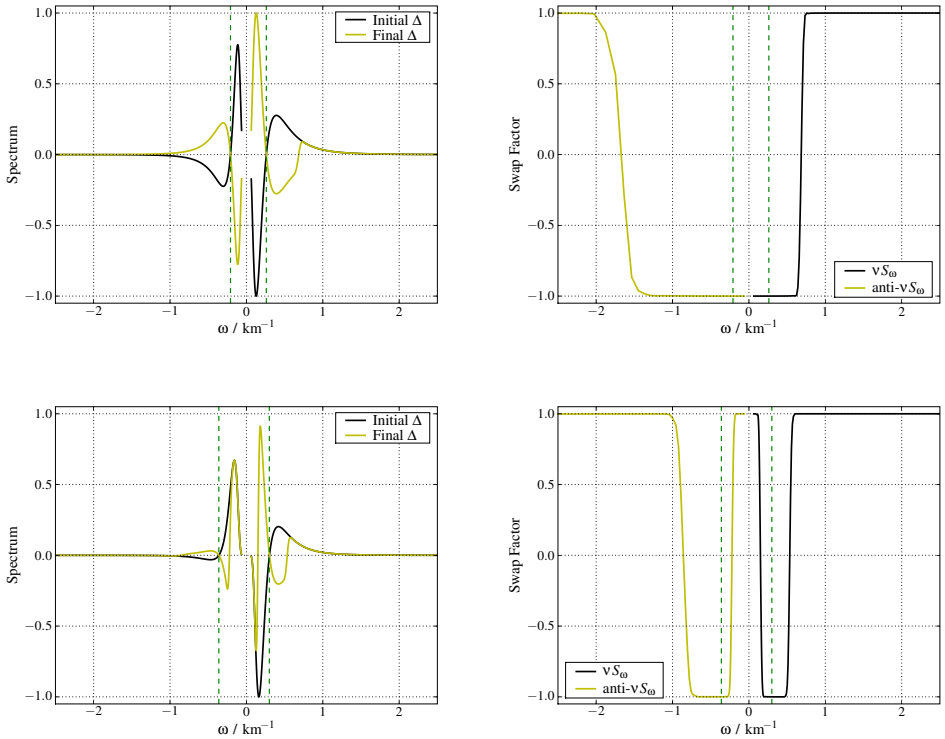

Figure 1.12: The left hand figures are plots of the difference spectrum g_ω before and after passage through supernova surroundings. The right hand figures plot the corresponding swap factor S_ω. The spectra are the same as in Figure 1.11.

final states. We see that one spectrum results in a single swap of all neutrinos below a certain value of ω, as predicted by the simple solution above. However, the other spectrum has two separate swaps separated by an unswapped portion of the spectrum. This state is not explained by the gyroscopic pendulum analogy, which predicts that all neutrinos with frequencies lower than a certain value will swap flavour.

The explanation suggested by [60] for the spectral swaps is based upon considering the points where $g_\omega = 0$. In the plots, these points are marked with vertical dashed lines. For any realistic spectrum $g_\omega = 0$ at $\omega = 0$ and $\omega = \infty$, and for the upper spectrum they also occur at $\omega = -0.209$ and $\omega = +0.261$. For the lower spectrum they are at $\omega = -0.361$ and $\omega = +0.300$. According to [60], each of these zeroes acts as the central frequency of a resonance like that studied in the previous section. The zeroes of the singly-swapped spectrum are too close

together to be driven independently, which results in a single broad swap that follows the gyroscopic swapping analogy. In the doubly-swapped spectrum there is resonant motion as well as gyroscopic motion, which produces two separate steps in the swap factor.

Summary

We have seen in this chapter that a wide range of interesting dynamics can result from the equations of motion for neutrino oscillations in dense backgrounds, even when many simplifying approximations are made. Most of the results presented above are adapted from previous works in the field, although in many cases we have converted from various alternative notations into our own unified scheme. Some of the detailed examples presented, such as the motion of the individual modes in the asymmetric neutrino system, clarify results in the literature. Others, such as the extraction of the parametric resonance from the overall motion of the neutrino system, are predicted by the equations of motion but have not been presented in this simple graphical form before. We have also emphasized that although there are very strong formal similarities between the parametric and pendulum-type motion, quite different and in some cases somewhat unrealistic approximations are required to obtain these equations of motion, and in a more realistic framework we would not expect the motion to follow one or other of these regimes precisely, particularly when adiabatic effects are important.

The major features of numerical simulations of supernova neutrino oscillations in smooth backgrounds can be explained using the analytic results of this chapter, although some details remain to be explained. In the next chapter we test the validity of these explanations for realistic neutrino spectra, and consider the effect that fluctuations in the background densites have on neutrino oscillations and the final spectra that emerge from a supernova envelope.

Chapter 2

Numerical Studies of Supernova Neutrinos

2.1 Introduction

In this chapter we consider two realistic examples of initial supernova neutrino spectra and use numerical simulations to study the flavour evolution of the neutrinos as they propagate outwards from the supernova core. We consider the evolution in smoothly changing matter and neutrino backgrounds before adding fluctuations to the background densities to simulate the turbulent and uneven flows in the supernova envelope. The validity of the analytic results presented in the previous chapter in these chaotic backgrounds is tested, and the implications for Earth-based observations of supernova neutrinos are discussed.

The flavour transformations of supernova neutrinos as they travel to Earth can be calculated in several ways. In the case of a simplified matter profile and some other approximations it is possible to find analytic solutions [52]. In more complex cases using more realistic matter profiles these analytic results can give useful insights into the results obtained from numerical simulations, but a detailed calculation of the resulting neutrino spectra must generally be done using numerical methods. Typically these numerical calculations involve a Runge-Kutta-type method, which propagates the neutrinos through the desired matter profile through a series of very small steps. The steps must be small enough to resolve all the oscillation wavelengths, which can be extremely small near the supernova surface where the neutrino potentials are very large. Many simulations use the so-called single-angle approximation, which removes the complications of the angular factor in the self-interaction potential by assuming that neutrinos evolve in a synchronized way along all trajectories. A more rigorous definition of the meaning of this approximation and its validity

is given in [49].

Due to the requirement of very small step sizes and numerical problems associated with small-scale fluctuations in the matter density, other methods have also been developed. Kneller *et al.* [22] transform the equations of motion from a differential to an integral form, and then use Monte Carlo integration to obtain the flavour swapping probability. Unfortunately this method cannot be used to calculate neutrino background effects because it relies upon randomly sampling a known background potential. In the case of self-interactions the potential can only be determined once the flavour state and hence oscillation history of the neutrinos through the supernova envelope is known. In some cases a combination of the two methods may be appropriate: once the neutrino density has fallen to a low enough value it can be ignored and the remainder of the matter interactions can be calculated with the Monte Carlo method [24].

2.2 Properties of the Initial Neutrino Flux

The collapse of the core of a massive star into a neutron star during a supernova explosion produces a vast number of electron neutrinos through the interaction $pe^- \rightarrow n\nu_e$. Because of the extremely high density and temperature in the core, neutrinos of other flavours are also produced in nucleon bremsstrahlung ($NN \leftrightarrow NN\nu_x\overline{\nu}_x$), and these neutrinos will become roughly equally distributed among the different neutrino flavours through these and other reactions such as $e^-e^+ \leftrightarrow \nu_x\overline{\nu}_x$ and $\nu_e\overline{\nu}_e \leftrightarrow \nu_x\overline{\nu}_x$. Within a few seconds most of these neutrinos escape from the core from an approximately symmetric "neutrinosphere" of about 10 km radius and are able to carry away a large fraction of the energy released in the collapse because of their very weak interactions with the supernova envelope. The precise shape of the spectrum and the relative fluxes of the neutrino flavours therefore depend on a complicated set of equilibrium reactions that exchange energy and flavour in the core. In several works, such as [15, 48], it is assumed that the amount of energy escaping in each neutrino flavour is equal, an assumption that is often called "equipartition", and that the only difference in the spectra of the different neutrino flavours is in their average energies.

However, the equipartition assumption is not necessarily accurate, as demonstrated by more detailed numerical studies of the processes governing neutrino production and propagation [63]. In addition, it has recently been noticed that

non-equipartitioned neutrino flux models can result in novel neutrino dynamics, such as multiple spectral swaps [60, 62]. In order to motivate the spectral models used in our numerical study we will briefly review the general properties expected of the neutrino spectra.

According to current models, the collapsing core of a supernova acts essentially as a blackbody emitter of neutrinos. The flavour-dependent differences in the fluxes result from several factors. The propagation of electron neutrinos through the core is dominated by two reactions,

$$\nu_e n \leftrightarrow p e^-, \text{ and}$$
$$\overline{\nu}_e p \leftrightarrow n e^+,$$

which prevent the neutrinos from freely streaming. As the density decreases with radius in the core the density eventually becomes low enough that these reactions are rare, and the neutrinos are then emitted with a thermal spectrum from an approximately spherical surface. Because there are more neutrons than protons in the core the electron antineutrinos become free streaming at a deeper, hotter layer in the core than the electron neutrinos, which is why the average energy of electron neutrinos in models of the neutrino flux are generally lower than the average energies of other neutrino flavours.

There are more complications in the case of ν_x propagation and equilibrium [63]. In the core, the dominant processes are nucleon bremsstrahlung ($NN \leftrightarrow NN\nu_x\overline{\nu}_x$), pair annihilation ($e^-e^+ \leftrightarrow \nu_x\overline{\nu}_x$ and $\nu_e\overline{\nu}_e \leftrightarrow \nu_x\overline{\nu}_x$), electron scattering ($\nu_x e^- \rightarrow e^-\nu_x$), and nucleon scattering ($\nu_x N \rightarrow N\nu_x$). As the density decreases these processes drop off at different rates. The neutrino-creating pair annihilation and nuclear bremsstrahlung processes end first, which fixes the number of neutrinos beyond a radius called the "number sphere". The energy of the neutrinos can still be changed by scattering processes until their cross sections in turn become too small. This defines an "energy sphere" beyond which both the number and the energy of the neutrinos is fixed. Finally the neutrinos become free streaming at the "transport sphere" when the energy-preserving nucleon scattering interactions become negligible. The neutrinos are then released from the neutron star into the supernova environment.

Because of this differential rate of decline in the processes, the ν_x spectrum is determined at a deeper and therefore higher temperature than the $\overline{\nu}_e$ spectrum, resulting in a higher average energy. However, because the nucleon scattering

cross section is proportional to E_ν^2, low-energy neutrinos can escape more easily, which means that the neutrinos that escape are biased towards a lower average energy than the initial temperature would suggest. This effect can lower the effective temperature to around 50–60% of the temperature at the energy sphere, and it also alters the shape of the spectrum from that of a perfect blackbody. A detailed calculation of all of these counterbalancing effects finds that the difference between the average energies $\langle E_{\overline{\nu}_e} \rangle$ and $\langle E_{\nu_x} \rangle$ is usually in the range of 0–20%, while the difference in number fluxes of the two flavours can differ by up to a factor of two [63]. These proportions also vary significantly with time after the explosion, and at late times the fluxes and energies are expected to be very similar for all flavours. For our purposes, the most valuable point is that for a wide range of initial conditions these calculations find that the equipartition assumption is violated.

Non-equipartitioned spectra such as the multiply crossed one considered in our work are interesting theoretically in illustrating the dynamics of collective neutrino oscillations, but these calculations show that they are also important for realistic models of supernova explosions. In order to observe the effects of collective neutrino oscillations in supernovae a wide range of possible initial fluxes must be considered, and the task of separating oscillation effects from model variance will be a difficult one. For our study we consider two spectra which exemplify the two common final states of supernova spectra after collective oscillations, one with a simple single swap and the other with a more complex doubly swapped final spectrum.

2.3 Supernova Matter Profiles and Neutrino Fluxes

Core-collapse supernovae form from massive stars, so the matter surrounding the core is roughly spherically symmetric and decreasing in density towards the surface of the star. The collapse causes an expanding shock to form which moves outwards through the stellar material. Hydrodynamic simulations show that large, non-symmetric density variations form near the neutron star almost instantly after the explosion begins [64]. Typical matter densities within a few tens of kilometres of the neutrinosphere are in the range $10^6 - 10^{12}$ g cm^{-3}, with corresponding electron densities of order $10^{35} - 10^{29}$ cm^{-3}.

In our simulations we have based our matter density on the fairly typical two-part profile described in [48], which consists of an exponentially falling density

close to the neutrinosphere added to a smooth profile proportional to r^{-3}. The form of the electron density profile is

$$\rho_e(r) = Y_e(\rho_b + \rho_b') \tag{2.1}$$

where Y_e is the electron fraction, taken to be 0.4, and the two parts of the baryon profile are

$$\begin{aligned} \rho_b(r) &= \rho_0 g_s \left(\frac{M_{NS}}{1.4M_\odot}\right)^3 \left(\frac{100}{S}\right)^4 \left(\frac{10\text{km}}{r}\right)^3 \\ \rho_b'(r) &= \rho_0' \exp\left(-\frac{r - R_\nu}{h_{NS}}\right). \end{aligned} \tag{2.2}$$

In our simulations we have used the base densities $\rho_0 = 4.2 \times 10^{36}$ m^{-3}, $\rho_0' = 1.63 \times 10^{42}$ m^{-3}, the neutron star mass $M_{NS} = 1.4M_\odot$, neutrinosphere radius $R_\nu = 11$ km, relativistic particle statistical weight $g_s = 11/2$, constant entropy per baryon $S = 140$, and scale height of the exponential shell $h_{NS} = 0.18$ km.

We use this simple, smooth density profile as our basic model, to which we can add inhomogeneities and fluctuations at whichever scales and amplitudes we choose.

2.3.1 Supernova Core Types

While most supernovae form from the iron cores of massive stars, a small fraction are expected to form from oxygen-neon-magnesium cores of stars of about 8-10 solar masses [65]. As discussed by Lunardini *et al.* [66], the density outside the core region decreases much more steeply in these supernovae, which causes the shock to propagate more quickly through the stellar material. Depending on the explosion parameters, the resulting change in matter potential can produce observable differences in the final neutrino spectrum that would be detected on Earth. This is one demonstration of the significant effect that turbulence and shocks can have on neutrino oscillations.

2.3.2 Time Dependence, Shocks and Turbulence

The simplest way to model the emission and evolution of supernova neutrinos is to assume that the density profile and neutrino spectrum do not vary with time. For a realistic explosion the matter density will change due to the motion

of shocks, turbulent mixing, convection, and so on. The neutrino spectrum emitted from the core will also change as the core cools and radiates energy. The static approximation will nevertheless still serve as a snapshot of the neutrino spectrum at a certain time after the explosion.

The principal time-dependent element in the matter profiles is the primary explosion shock, but the turbulent motion of the supernova material will also cause density variations on smaller time and length scales. A shock can be modelled by a large, steep drop in the matter density at a certain radius which moves outwards with time. As this shock moves outwards from the core its effect on the flavour evolution of the neutrinos that pass through it will vary. In regions where the neutrino-neutrino potential is large the shock may have a minimal effect on the neutrino oscillations, but farther from the core where the neutrino background is less significant shocks can have a powerful influence on flavour change, particularly in regions with density close to an MSW resonance. A recent study by Gava *et al.* [24] suggests that the motion of shocks can cause abrupt changes in the neutrino spectrum as a function of time.

Small-scale turbulence is a rather different phenomenon. The effect of a shock is to introduce a region in which the neutrino background potential becomes non-adiabatic, in contrast to the adiabatic decrease in potential that Solar neutrinos traverse in the Sun, or supernova neutrinos experience in a simple smooth matter envelope model. Small-scale turbulence can be thought of as introducing non-adiabaticity throughout the entire evolution. To investigate small-scale turbulence we have used a simple model (described below) based on Kolmogorov turbulence, similar to that used in [27].

In our simulations we have only considered the region within a few hundred kilometres of the supernova core. This is the region in which collective neutrino effects are significant, and our main goal was to determine the effects of turbulence on the collective neutrino system. Several studies of matter turbulence in the absence of collective neutrino effects have shown that small-scale matter fluctuations and the large density jump around the main supernova shock can become very important at larger radii where the matter density is close to the MSW resonance value [24, 27, 61]. Our work suggests that the spectrum of neutrinos that enters the shock region can be affected by turbulence at smaller radii, but we have not determined whether this significantly changes the effects of the matter resonances.

2.4 Numerical Code

We have written our own code to numerically solve the Schrödinger equation for the neutrino evolution (as shown in Equation 1.5) by taking small steps outward from the neutrino sphere. When the step size is small enough, we can calculate the change in the wavefunctions of the neutrinos using

$$\psi_{E,\alpha}(x + \delta x) \simeq \exp(-iH_{E,\alpha}\delta x)\psi_{E,\alpha}(x), \tag{2.3}$$

where δx is a small step length, and the subscripts on the wavefunction and Hamiltonian are to indicate that these quantities depend on the energy and flavour of the neutrino under consideration. In our simulations we use a two-flavour approximation where the neutrinos are divided into electron and x (that is, the combination of μ and τ) flavours and their anti-neutrinos. The Hamiltonian is the sum of vacuum, matter background and neutrino background terms, and can be written as a single 2×2 matrix as follows

$$H(x) = \frac{1}{2}\begin{bmatrix} -\Delta\cos 2\theta_{13} + V(x) + D_{ee}(x) & \Delta\sin 2\theta_{13} + D_{ex}(x) \\ \Delta\sin 2\theta_{13} + D^*_{ex}(x) & \Delta\cos 2\theta_{13} - V(x) - D_{ee}(x) \end{bmatrix}, \tag{2.4}$$

where $\Delta = \Delta m^2/2E_\nu$, the D terms are calculated from the neutrino background, and the V terms are due to the matter background. The Hamiltonian for antineutrinos is similar, but with the matter and neutrino background terms replaced with their negative complex conjugates.

A single step of the calculation consists of evolving each neutrino by a small distance δx according to its Hamiltonian. As described in section 1.3, there are three terms that must be calculated: the vacuum term, the matter term and the neutrino-neutrino term. The vacuum term simply depends on the neutrino energy and the mixing parameters (in our two-flavour case, θ_{13} and the atmospheric Δm^2). The matter term depends on the neutrino flavour and the background electron density, which comes from our density profile model. We use the simple profile shown in Equation 2.2 to calculate the matter density as a function of radius.

The neutrino potential is more complicated to calculate because it depends on integrating the neutrino flavour density matrices over all energies. Our program stores a wavefunction for each neutrino flavour in a set of energy bins. Each wavefunction is a two-component vector which represents the flavour of

all of the neutrinos and antineutrinos within the bin's energy range. These wavefunctions are combined with the function describing the spectral shape to calculate the total neutrino background term in the Hamiltonian. To obtain the results used in this chapter we used energy bins of width 0.2 MeV with energies from 1 keV to 80 MeV. We use the single angle approximation described in chapter 1 to calculate the decline in the neutrino-neutrino interaction strength as a function of radius.

Because the matter and neutrino background terms are independent of neutrino energy we calculate the sum of the two and use this as our working Hamiltonian, with the vacuum terms being added in for each neutrino individually. This means that we only need to carry out the large sum over all neutrino modes once for each step, using the neutrino wavefunctions calculated in the previous step.

Once the Hamiltonian has been calculated, it is applied via Equation 2.3 to each neutrino flavour and energy bin. Because this evolution equation is exact when the Hamiltonian is constant, we can ensure numerical accuracy by requiring that the change in the Hamiltonian over each step is within a certain small tolerance. Our runs used the condition $H(x + \delta x) - H(x) \leq 5 \times 10^{-6}$. If this condition is violated, the step is redone at 0.85 times the original size. This cycle continues until the tolerance is met. We have also tested different tolerance levels and alternative methods of testing the accuracy of each step to ensure that our results are not due to numerical quirks.

Because the potentials decrease roughly as r^{-3} for matter and r^{-4} for neutrinos their rate of change falls fairly quickly with radius. This allows us to gradually increase the step size as the radius increases to save on computation time. In each step we increase the step size by 1%. In combination with the rate of change condition this ensures that processor time is not wasted on unnecessarily small steps. Simulations can be continued to any radius, but we find that by around 400 km the oscillations are stable and the interesting collective flavour dynamics have ended.

The main result of the simulations is a record of the flavour state and number density of the neutrinos as a function of energy and radius, which can be converted into an energy spectrum and flux. We also obtain the value of the neutrino-neutrino potential at each step. While the absolute magnitude of this potential can be calculated by considering the decrease in number density as the neutrinos propagate outwards in a sphere of increasing radius around the super-

nova, the off-diagonal terms which the neutrino background term contributes to the Hamiltonian depend on the instantaneous flavour mixture at that radius. Since these terms drive the neutrino flavour swapping it is useful to have a measure of their variation which can be compared to the evolution of the neutrino flavour in the collective and bipolar regimes.

Within this computational framework we can vary the matter profile and the neutrino flux to determine the dependence of the final flavour composition on the properties of the supernova.

2.5 Neutrino Oscillations in the Supernova Environment

As we showed in chapter 1, the changes in neutrino flavour as described by the dynamics of their vectors in flavour space can be very complicated. Nevertheless, there are several common features of the evolution of supernova neutrinos across a wide range of realistic spectral and background parameters. The flavour-space motion most commonly seen is similar to that of the asymmetric two-vector evolution with a decreasing neutrino density. The initial part of the motion, from the neutrinosphere to roughly 100 km in radius, is synchronized motion where there are no flavour changes. The most interesting part of the evolution then occurs, as the collective motion of the vectors moves them towards their final states. As the neutrino background term decreases, neutrinos of different energies settle into their different final states. Motion can range from small-amplitude, apparently simple and well-behaved motion in some scenarios to large-amplitude and chaotic looking fluctuations in others depending on the parameters chosen. This more complex period continues until around 300 km, after which the neutrino density is too low to produce further collective effects and the evolution becomes rather static once more.

Because of the more complicated spectral shape in these more realistic simulations the polarization vectors in the various plots are no longer for single neutrinos. Our simulation tracks the polarization vectors of neutrinos that are initially in pure ν_e and ν_x states, so initially the total value of $n_\nu(E)\mathbf{P}_z(E)$ is equal to $n_{\nu_e}(E)\mathbf{P}_{\nu_e}(E) + n_{\nu_x}(E)\mathbf{P}_{\nu_x}(E)$. As these vectors evolve and swap flavour it is likely that these polarization vectors will not remain as pure electron neutrinos or x neutrinos, but this quantity computed with the evolved flavour vectors will remain a measure of the overall flavour of the neutrinos at each energy. Summed over all energies, this quantity is just $N\mathbf{J}$ (or for the an-

tineutrinos, $\overline{N}\,\overline{\mathbf{J}}$), as used in the analytic description of the polarization vector dynamics.

The reason this is a useful quantity is that the final state of the neutrino flavours at a given energy tends to be either unchanged from the initial state or completely reversed in flavour space. The polarization vector plots demonstrate how the different parts of the spectrum are evolving to produce the particular final state. As explained in subsection 1.5.3 the final state usually has one or two spectral swaps depending on the spectrum. We can see immediately that the doubly-swapped spectrum has undergone much more complicated dynamics, involving large-amplitude collective oscillations, whereas the singly-swapped spectrum has only small-amplitude oscillations on top of a smooth evolution to the final state. In the sections that follow, we will analyze these differences and examine the effects of matter and neutrino background effects upon them.

2.6 Neutrino Oscillations in Turbulent Environments

Numerical simulations of supernova explosions find that the radial matter density profile is not smooth, and very large fluctuations in density occur. These fluctuations can be large enough to strongly alter the neutrino evolution in the absence of collective neutrino effects. Several studies [25–27, 67] have investigated the effect of matter turbulence, focusing on how fluctuations around MSW resonances can wash out the flavour structure. In outline, the effect can be understood in terms of the standard MSW effect. In the two flavour approximation the MSW resonance occurs when the matter term, $\sqrt{2}G_F n_e$, is equal to the vacuum oscillation term $\Delta m^2/4E_\nu \cos 2\theta_\nu$. When this occurs, the diagonal terms cancel, making the off-diagonal terms in the Hamiltonian dominant. This results in a strong flavour conversion. If the matter density fluctuates around this resonance the mixing between different flavours can become very large in both directions, and with sufficiently large fluctuations the neutrinos can end up in a completely incoherent 50/50 mixture of the two eigenstates.

As we have seen, however, the addition of collective effects can completely alter the behaviour of the neutrino ensemble. Recent work by Gava et al. [24] includes the effect of shocks in the supernova matter, and the results are claimed to be robust to turbulence, although this is not tested. Just by examining the Hamiltonian shown in Equation 2.4, it might be expected that at small radii, where the D term is much larger than the V term, even quite large fluctuations

in the matter density will have little effect on the overall Hamiltonian. The usual MSW resonance is suppressed because the matter term only cancels with the vacuum term, not the neutrino-neutrino term. Therefore we could conclude that turbulence, if it has any effect, will only be important near MSW resonance densities in regions with small neutrino background effects.

Two analytic results suggest that this argument is not complete. Matter resonances can occur not only when the MSW condition is met but also when the rate of change of the matter density is high, as described in section 1.2. Furthermore, as described in subsection 1.4.7, the matter term in the presence of a high neutrino density can be shown to be equivalent to an insignificant rotation in flavour space, but only if the matter density is changing slowly. Along with the continuing discovery of novel resonance effects in neutrino oscillations, these effects mean that it is important to determine the effect of small-scale fluctuations in the matter profile, even far from the MSW resonance.

2.6.1 Background Fluctuation Modelling

To model the matter profile in the presence of turbulence we have used a model based on the Kolmogorov turbulence approximation in [27]. Kolmogorov hypothesized that the largest-scale eddies would break up into smaller ones and that this process would continues until a cutoff scale where viscosity dissipates the energy in the eddies [68]. This argument assumes that this scale depends only on the viscosity ν and the energy dissipation rate ε. Through dimensional analysis this assumption leads to a unique length scale given by

$$\eta = \left(\frac{\nu^3}{\varepsilon}\right)^{1/4}. \tag{2.5}$$

In Kolmogorov's theory, turbulence at intermediate scales between the small-scale where viscosity is important and the large-scale where energy flows are important depends only on ε and the wavenumber k. Dimensional analysis can again be used to obtain an energy spectrum of the form

$$E(k) = C\varepsilon^{2/3}k^{-5/3}. \tag{2.6}$$

This spectrum represents the distribution of the kinetic energy of the fluid flows on different length scales which result from the breakup of large-scale flows into smaller-scale turbulence. This spectrum has been experimentally verified to be a

good model of the energy spectrum of many turbulent fluids, and although it has been shown to break down in some cases it is excellent for this application since it provides an analytic formula that quite accurately models a large range of physical conditions and is easily implemented in our computational framework. We also ran some simulations with different values of the exponent of k in the fluctuations, and found that these variations did not cause any significant change in the oscillation behaviour. The effects of fluctuations appear to be quite robust to model variations.

In numerical simulations of supernova matter flows [64] we see turbulence over a wide range of length scales, mostly the result of the explosion shocks moving through the dense stellar atmosphere. We assume that these density variations are the result of velocity flows over similar length scales, as a result of a Kolmogorov-like cascade to smaller scales. Therefore we assume a spectrum of density fluctuations about the mean smooth profile in Equation 2.1 and Equation 2.2 of the Kolmogorov type. To model this spectrum in our simulations we use the sum of a large number cosines at a range of wavenumbers with random phases added, as described in [27]. Our noise function is

$$A_{\text{noise}}(r) = C\zeta \sum_{k=1}^{k_{\max}} k^{-5/6} \cos\left(kr/\lambda + \phi(k)\right), \tag{2.7}$$

where ϕ are random phases generated at the start of the simulation and $k_{\max}$ is typically around 5000. ζ is a constant which is chosen to normalize the magnitude of A to be approximately equal to C. There are two parameters we can vary to change the nature of the turbulence. We can vary the overall magnitude of the fluctuations through the constant C, and we can change the characteristic scale of the fluctuations by our choice of the length unit λ. We have chosen λ so that the largest fluctuations are of the order of 30 km, since fluctuations larger than this are most likely to be due to large-scale motions such as the shocks themselves. We also expect that fluctuations far larger than the scale of neutrino oscillations will not have a strong effect on the neutrino flavour change. The amplitude, C, of the noise is varied in separate calculations as a test parameter. We have chosen values in a wide range, so that the density variations caused by the fluctuations range from about 1–50% of the mean density. Fluctuations of this magnitude are seen in hydrodynamic supernova simulations, but we can also consider more extreme cases to help isolate the effects of turbulence.

Once we have chosen the parameters, we take our smooth matter profile $\rho(r)$ described in Equation 2.1 and compute the turbulent profile as

$$\rho(r) \longrightarrow \rho(r)\left[1 - A_{\text{noise}}(r)\right]. \tag{2.8}$$

The only random parameters in the backround are the phases, which are generated and fixed at the start of the simulation. This gives a significant computational advantage over using an uncorrelated random noise term, because it means that the potential at each radius is analytically known. The adaptive step size routine might otherwise tend to result in the selection of small fluctuations over large ones to preserve the tolerance, rather than using step sizes that allow accurate computation of a given background.

2.6.2 Neutrino Density Fluctuations

The commonly used 'bulb model' of neutrino emission from a supernova assumes that neutrinos are emitted isotropically and are free-streaming [48]. Because neutrinos are relativistic and weakly interacting we do not expect the neutrino background to undergo the same turbulent mixing and eddie breakup that causes small-scale fluctuations in the matter density. Nevertheless the assumption of a completely isotropic neutrino background is questionable. If the temperature or composition varies over the surface of the neutrinosphere or fluctuates on small time scales, or the core itself is non-spherical, it is likely that the neutrino density will not be completely smooth. For instance, if the neutrino temperatures are different on different points of the neutrinosphere then the neutrinos that cross a reference neutrino path at a given time will have a different integrated neutrino interaction potential due to differences in the spectra. There could also be variations in the rate of neutrino emission which would cause a change in the total neutrino density. Although these types of fluctuation will not be due to fluid turbulence as in the matter case, we have used the Kolmogorov spectrum as a convenient model for random fluctuations with a small cutoff scale. Adding delta-correlated noise would be the most obvious alternative, but has the disadvantage of not being analytically defined by a simple array of random phases, which makes it far less computationally convenient.

Because the neutrino background term is a 2×2 matrix there is more than one way to apply the noise term to it. The simplest choice is to multiply the entire matrix by A, which is equivalent to a changing the number density of

neutrinos without changing their flavour mixture. If the neutrinos are emitted from different regions in the neutron star that are not at equilibrium with each other the flavour mixture of the neutrinos may fluctuate in space. This can be roughly modelled by applying fluctuations to only the diagonal or off-diagonal terms in the matrix, which will have the effect of changing the relative size of the off-diagonal terms which drive the neutrino mixing. As shown in subsection 1.4.7 the orientation and timescale of the motion of the flavour vectors in the $\hat{\mathbf{x}}$ and $\hat{\mathbf{y}}$ directions can also vary depending on the size of the matter background. These components of the polarization vectors are the ones that contribute to the off-diagonal neutrino matrix terms, so the evolution of neutrinos along different paths through an inhomogeneous background could provide another source of variation in the neutrino potential.

2.6.3 The Effects of Density Fluctuations

In our simulations we find that the addition of fluctuations in the matter and neutrino terms terms can have an effect on the neutrino-neutrino mixing term, the evolution as a function of radius, and on the final spectrum and flavour mixture. However, we typically find that the effect is not a drastic one. The spectral swaps still occur with a similar structure, and the final spectrum remains roughly similar to that obtained with smooth potentials. Depending on the initial spectrum and the fluctuations added there may be a shift in the energy of a swap, or its width may be altered.

We plot several different variables in the figures to display in detail the effects of the background fluctuations and the dynamics of the neutrino evolution. Spectrum plots show the flux of neutrinos and anti-neutrinos of electron and x flavours as a function of energy before and after their passage through the matter and neutrino background. Plots of the neutrino potentials as a function of radius display the size of the potential terms in the equations of motion. The matter term is a real number proportional to electron density, and is plotted as a single curve. The neutrino-neutrino term is a 2×2 complex matrix so it is not possible to fully represent it with a single line. We have split it into three components: an overall magnitude plotted in blue which is proportional to the neutrino number density, and the real and imaginary parts of the off-diagonal part of the neutrino background term in the Hamiltonian, D_{ex}, which are plotted separately. These correspond to the components of the neutrino

background vector $\mathbf{D}$ in the $\hat{\mathbf{x}}$ and $\hat{\mathbf{y}}$ directions in flavour space, and are a measure of the mixing and coupling between different neutrino flavours.

The polarization vector evolution plots show the change in flavour of electron neutrinos at evenly-spaced intervals between 1 and 80 MeV to demonstrate how the evolution of neutrino flavour varies as a function of energy. In these plots, the y-axis value represents the $\hat{\mathbf{z}}$ component of the neutrino polarization vector in flavour space. We have chosen to display mostly unweighted values, so that the evolution of each mode is clearer. For some plots we have multiplied the flavour vectors for each mode by the number density of neutrinos at the corresponding energy. This allows us to see which modes are the most significant contributors to the total neutrino flavour change, but tends to obscure the evolution of the neutrino flavour by making the initial and final values a function of both the spectral shape and the oscillation probability.

These neutrino vector evolution plots are useful because they can be compared to those for the simple cases that we solved analytically in chapter 1, allowing us to determine which types of flavour-space motion are occurring in each of our various neutrino systems, and whether our system corresponds to any of the various analogies and approximations that have been studied.

The connection between the flavour vectors and the neutrino background potential can be seen by comparing the the off-diagonal neutrino terms in the potential plots to the evolution of the flavour vectors. The end of the static part of the polarization vector evolution usually corresponds to the region where the off-diagonal terms are of the same order as the other potential terms. This occurs roughly at the point where, in the gyroscopic pendulum analogy, the spin of the bob can no longer keep the pendulum from falling. The off-diagonal terms increase gradually as the bob begins to move slightly from its initial position, and become of comparable amplitude to the diagonal term when the mixing is large and the neutrino flavour vectors are moving away from the $\hat{\mathbf{z}}$-axis in flavour space.

We also present several difference spectrum and swap factor plots. These plots factor out the complex spectral shape and show the relative flavour changes that occur during the evolution. The swap factor, in particular, is very useful because it is effectively a plot of the survival probability as a function of energy.

2.7 Analyzing the Effects of Fluctuations

There are many quantities related to the neutrino ensemble that may vary depending on the initial conditions and background fluctuation model. In our study, we have separately considered the effects of matter density fluctuations and neutrino density fluctuations on the final neutrino spectra emerging from the supernova and the dynamics of the evolution.

2.7.1 Differences in Final Spectra

Ideally, neutrino detectors can measure three properties of supernova neutrinos: their flavour, their energy, and their arrival time. The energy resolution and flavour discrimination accuracy of current detectors is unlikely to be good enough to resolve all the fine structure of the different spectra we investigate, but large effects such as spectral swaps may be detectable. For this reason we examine the effect of density fluctuations on the final spectrum that emerges after the collective neutrino effects have ended.

For most realistic initial supernova neutrino spectra we expect to see up to two spectral swaps in the neutrino and antineutrino spectra. The number and energy range of these swaps depends on the particular shape of the spectra chosen, the background parameters, and the neutrino mixing parameters, in particular the hierarchy choice. In our simulations we generally find that the effect of the addition of either matter or neutrino density fluctuations is to alter the details of the final spectra, while retaining similar qualitative features. The requirements of conservation of lepton number and energy limit the size of the alterations, but the general blurring and broadening effects we find mean that separating the effects of the supernova background from subtle changes in the initial spectrum, even from very good Earth-based observations, may be very difficult.

2.7.2 Radial Evolution

The evolution of neutrino flavour as a function of radius in a supernova is unobservable from Earth, but it is very interesting theoretically. Although a great deal of work has been done to understand neutrino spectral swaps analytically, there is still no general framework which can fully explain the dynamics of the neutrino ensemble, particularly in the presence of non-adiabatic backgrounds.

As a byproduct of calculating the final neutrino spectrum numerically, we also obtain a complete record of the evolution to the final state.

We find that adding fluctuations to either the matter or neutrino potentials (or both together) often results in quite different flavour evolution for individual neutrino modes, even if the final state is not changed significantly. All neutrinos are initially in pure flavour states, that is, pure electron flavour or pure x-flavour. In most cases these neutrinos also have final states that are very close to pure flavour states. When fluctuations are added to the neutrino potential the flavour of the neutrinos often evolves more chaotically in the intermediate stages, but eventually settles into a similar final state. This suggests that the major influence on the final spectrum is the initial spectrum coupled with conservation laws and the minimization of the ensemble's energy. The shape and fluctuation of the background potentials contribute only second-order effects.

Despite the smallness of the effects of the background fluctuations, it is important to test our toy models of spectral swap behaviour. We find that the dynamics of our two test spectra are very different, and the effects of background fluctuations on the evolution are correspondingly different. So while our understanding of the final spectra as being minimum energy states of the neutrino ensemble subject to various restrictions seems quite robust, explaining the intervening dynamics is a much more difficult task.

2.7.3 Time Variation of Neutrino Spectra

The possibility of using detectors such as IceCube with very good timing resolution to measure the evolution of the supernova itself has been discussed in [69, 70]. Other works such as [24] have considered the effect of the shocks that move through the supernova envelope, and their effects on the observable neutrinos as a function of time. This aspect has not been studied in our work.

2.8 Singly Swapped Spectrum

The initial neutrino spectrum used in several studies by various groups [15, 48, 57, 71] is a Fermi-Dirac distribution with average neutrino energies $\langle E_{\nu_e} \rangle$, $\langle E_{\bar{\nu}_e} \rangle$, $\langle E_{\nu_x} \rangle$, and $\langle E_{\bar{\nu}_x} \rangle$ of 10, 15, 24, and 24 MeV, with the number of neutrinos scaled so that an equal amount of energy is carried by neutrinos of each species. We numerically solved the evolution equations for this initial spectrum propagating through a range of neutrino and matter backgrounds to determine

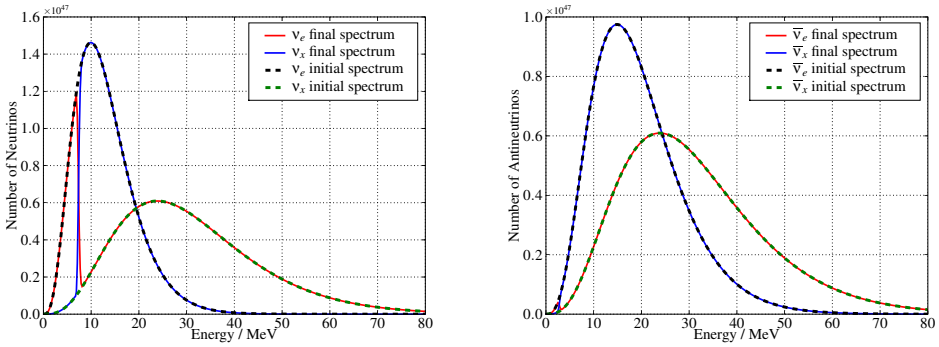

(a) Neutrino spectrum

(b) Antineutrino spectrum

Figure 2.1: The Fermi-Dirac type initial neutrino and antineutrino spectra before and after evolution through 400 km, with the matter background density set to zero.

the dependence of the the final state on the background potentials and their fluctuations.

2.8.1 Evolution in a Neutrino Background

Before we add complications such as fluctuating neutrino and matter densities to our calculations, we first examine the simplest realistic case and evolve the neutrino flux as determined by the above spectrum from the neutrinosphere to a few hundred kilometres from the supernova core. The initial neutrino and antineutrino spectra and the resulting spectra after 400 km of evolution are shown in Figure 2.1. The sharp flavour swap edge at around 8 MeV in neutrinos and the complete swap of flavour of all antineutrinos except for a small remnant at very low energy are the most obvious features of these plots. As expected from lepton and energy conservation laws the shape of the total neutrino spectra remain the same, and it is only the neutrino flavours that have changed.

In order to better understand the dynamics of the neutrino flavour changes we see in the spectrum plots we plot the flavour of the neutrinos as a function of radius in Figure 2.2. This displays the value of the **z**-component of the neutrino polarization vectors as a function of distance from the supernova. This component is the most physically relevant because it is directly related to the flavour state and hence survival probability of the neutrinos. These vectors are calculated by adding up the **P** vectors defined in Equation 1.31 for all the

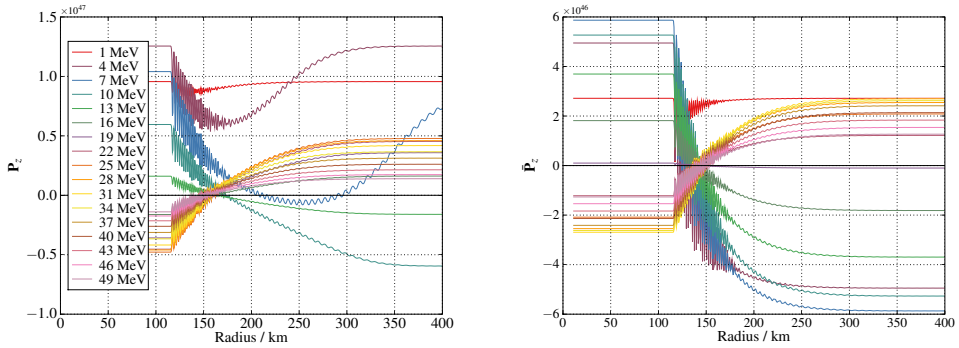

(a) $\mathbf{P}_z$ (b) $\overline{\mathbf{P}}_z$

Figure 2.2: The evolution of the $\hat{\mathbf{z}}$ components of the polarization vectors $\mathbf{P}$ for neutrinos and antineutrinos. Each line is for a single neutrino energy bin, and the magnitudes of the components have been weighted by the total number density of neutrinos at the appropriate energy.

neutrinos in a given energy bin. This quantity is then effectively equal to $n_{\nu_e} - n_{\nu_x}$ in each energy bin, although because the flavour states are in general a mixture of flavours the number of each flavour is a sum of amplitudes rather than a simple count. In the plot we see that at different energies the different relative numbers of electron and x-type neutrinos mean that the initial polarization vectors take on a range of values. For instance, it is clear from the spectra in Figure 2.1 that electron-type neutrinos dominate the flavour vectors for low energy bins while x-types are much more numerous in high energy bins.

For this spectrum and background, the neutrino flavour vectors all remain locked in their initial orientations until approximately 120 km. Over the next 100 km most vectors flip their signs and by 300 km all but the lowest-energy bins are in essentially stable final states with the same magnitude but the opposite sign. The lowest-energy bins, shown by the curves which begin uppermost on the plots, take longer to settle into a final state, and the lowest-energy neutrino bin is the only one in the plot which has not swapped sign in the final state.

The overall motion of each vector is strongly reminiscent of the simple asymmetric neutrino example with a decreasing μ, discussed in subsection 1.4.6, in particular Figure 1.4. In both cases the initial synchronized state persists for some time until some critical value of μ is reached, after which there is smooth overall motion of the vectors towards their final states, with smaller-amplitude oscillations around this smooth decrease. The motion appears to conform to

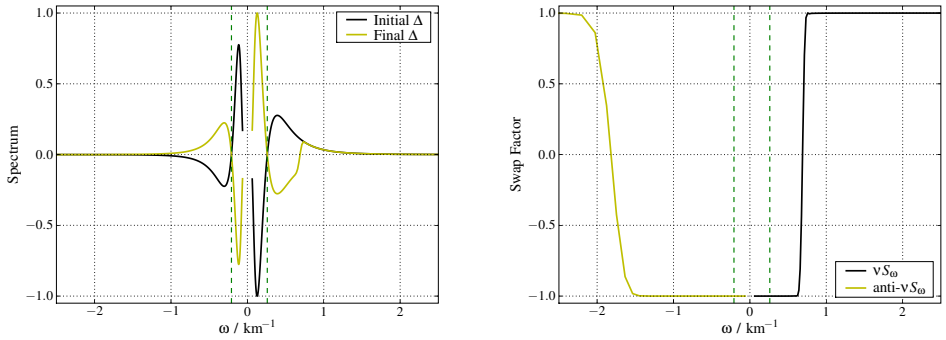

(a) Difference spectrum

(b) Swap factor

Figure 2.3: The neutrino difference spectrum and swap factor for the Fermi-Dirac spectrum before and after evolution through 400km in the absence of a matter background. The complete swapping of flavour for all neutrinos with $\omega \lesssim 0.75$ km^{-1} is clearly seen.

the adiabatic approximation and the spectrum undergoes a single spectral swap, which suggests that we can explain the dynamics of this spectrum's evolution completely using the basic spectral swap argument in subsection 1.5.3. The position of the spectral swap is dependent on the initial conditions and is fixed by lepton and energy conservation.

The anti-neutrino vectors undergo very similar motion, except that here even the lowest energy bin flips sign. The major differences from the neutrino plot are that the small-scale oscillations have greater amplitudes and continue longer, and that the final state does not emerge as quickly as for the neutrinos. However, the motion is completely consistent with the description above.

Figure 2.3 is a plot of the neutrino difference spectrum calculated from Equation 1.144 and the resulting swap factor derived from it using Equation 1.145. The swap factor is a broad step, representing a single spectral swap. Also note the asymmetry around the zero frequency point. This is as expected from the single swap argument: because there are fewer anti-neutrinos than neutrinos the swap must extend through practically the entire anti-neutrino spectrum in order for lepton number to be conserved.

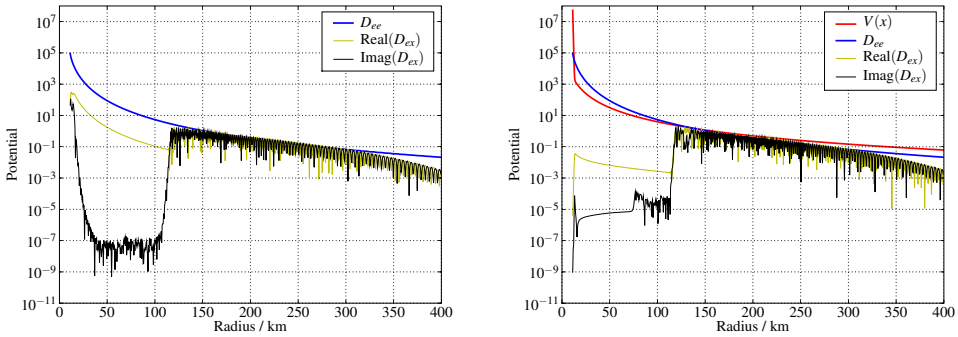

(a) No matter

(b) Matter added

Figure 2.4: Background potentials felt by neutrinos with and without matter added. The smooth upper curve on the left is the neutrino background term $\sqrt{2}G_F n_\nu$ and the lower curves are equivalent to the magnitude of the $\hat{\mathbf{x}}$ and $\hat{\mathbf{y}}$ terms of the background vector $\mathbf{D}$. The matter background term in the right-hand figure is curve that steeply descends from the top left.

2.8.2 Evolution in a Matter Background

In a real supernova there is a very high density shell of ordinary matter as well as the neutrino background. We can see the effect of this matter background by adding a smooth approximation to the matter density, according to Equation 2.1, to the system in the previous section. Analytic results (detailed in subsection 1.4.7) suggest that, at least in simple cases, a slowly changing matter background will not significantly alter neutrino flavour evolution. It is nevertheless interesting to see the subtle effects that do result from the presence of matter.

A comparison of the background potentials as a function of radius is shown in Figure 2.4. The red curve is the added matter term, which dominates the total potential at very small and very large radii because of its initial exponential fall from extremely high density to a much lower value that decreases as r^{-3}. Because the neutrino background decreases as r^{-4} it eventually becomes insignificant compared to the matter term. However, because the matter potential is strictly diagonal in the flavour basis and does not depend on the neutrino evolution, while the neutrino potential has off-diagonal terms that depend on the same neutrino states that it acts as a background for, the two potentials are fundamentally different and cannot be compared simply through their overall

magnitudes. The main D_{ee} curve in the figure is the magnitude of the diagonal term in the neutrino potential, and simply falls as r^{-4} with the neutrino density. The real and imaginary parts of the off-diagonal term in the neutrino potential are plotted as separate curves and show more interesting behaviour since they are related to the amount of mixing in the neutrino states, and reflect the dynamics of the system, such as the complex precessions and nutations of the polarization vectors, rather than just the neutrino number density.

It is notable that flavour oscillations begin at almost the same point in both cases. This is because the appearance of collective oscillations (at least in situations where the gyroscopic pendulum analogy holds to a good approximation) only requires that the value of the coupling parameter μ is less than a critical value $\mu_{\rm sync}$, above which the ensemble 'gyroscope' is in a stable inverted position held up by the 'angular momentum' of the bob that is proportional to μ^2. In the single energy asymmetric neutrino case, the critical value $\mu_{\rm sync}$ is dependent only on the relative number of neutrinos as compared to antineutrinos. We see from these numerical results that this also holds true in this more realistic example with continuous energy spectra: the same initial spectrum has the same critical value of μ and this value is not dependent on the matter background. In addition, the lengthening of the timescale of bipolar oscillations that results from the decrease in the effective mixing angle in the presence of a high matter density is not very large in this model because the scale of the collective oscillations is far smaller than the rate of decrease of μ. This means that a delay of the onset of oscillations of some fraction of a period amounts to only a small change on the scale of these plots.

The point at which the synchronized, non-moving phase of the evolution ends can be calculated in terms of the average frequency of the ensemble. If we assume that the system is acting like an inverted gyroscopic pendulum with a large but decreasing angular momentum around the pendulum axis, the condition for the pendulum to remain upright is that the spin term must be larger than difference in potential between the maximum and minimum position of the pendulum. This can be written in terms of the variables introducted in subsection 1.4.3 as [15]

$$\frac{\sigma^2}{2m} > 2m|\mathbf{g}|, \tag{2.9}$$

which, if we substitute the definitions of the parameters in terms of the neutrino

vector quantities, becomes

$$\frac{\mu\left(\mathbf{D}\cdot\mathbf{Q}\right)^2}{2Q^2} > \frac{2\langle\omega\rangle\mu Q}{\mu}, \tag{2.10}$$

where $\langle\omega\rangle$ is the average frequency of all the neutrinos in the ensemble. We assume that $\mu \gg \langle\omega\rangle$ and the vectors are all aligned along the direction of $\pm\hat{\mathbf{z}}$. This is true for the initial state, and persists until the bipolar oscillations begin. This assumption leads to $\mathbf{Q} \approx \mathbf{S}$ and $\mathbf{D}\cdot\mathbf{Q} = DQ$, which we can substitute into the previous equation to obtain an expression for the minimum value of the neutrino interaction strength which will keep the system upright. The minimum value μ_{sync} is given by

$$\mu_{\text{sync}} = \frac{4\langle\omega\rangle S}{D^2}. \tag{2.11}$$

As long as μ is greater than this μ_{sync} we expect the neutrino vectors to remain fixed in their initial configuration. To calculate the numerical value of μ_{sync}, we must in general integrate the neutrino spectrum to obtain the average frequency, and then use the initial fluxes of each neutrino flavour to calculate the magnitudes D and S. We can also calculate $\langle\omega\rangle \simeq 0.91$ km^{-1}, and from this we find that the critical value of μ_{sync} is approximately 65 km^{-1}.

To determine the radius at which this value of μ occurs, we simply use the initial value of $\mu(r)$ at the neutrinosphere and solve for the value of r at which the radial factor $D(r)$ is equal to $\mu_{\text{sync}}/\mu(R_\nu)$. With our parameters we find $\mu(R_\nu) = \sqrt{2}G_F N^{\text{eff}}_{\text{total}}(R_\nu) \simeq 4.4\times10^{-6}$ km^{-1}. Solving for $D(r) = 65/4.4\times10^{-6}$ gives $r = 106$ km. In Figure 2.5 we see that this value is approximately 15 km too small. However, there are two factors which affect the accuracy of this critical value calculation. Firstly, the smallness of the mixing angle means that the initial tilt of the pendulum is extremely small, so that it takes some time for the pendulum to fall after the bob spin drops below the critical value. This can be seen in the potential plot, Figure 2.4. In particular, the rise of the imaginary part of the off-diagonal (mixing) terms in the neutrino potential begins very soon after 105 km, but does not become of the same order as the diagonal term until about 120 km. The off-diagonal terms are analogous to the pendulum's $\hat{\mathbf{x}}$ and $\hat{\mathbf{y}}$ components, or the tilt away from the initial position.

In the presence of matter we expect an additional delay, as described in subsection 1.4.7. This small delay is difficult to see in the plots, but is visible when the evolution is plotted at a larger scale. For this spectrum we have good

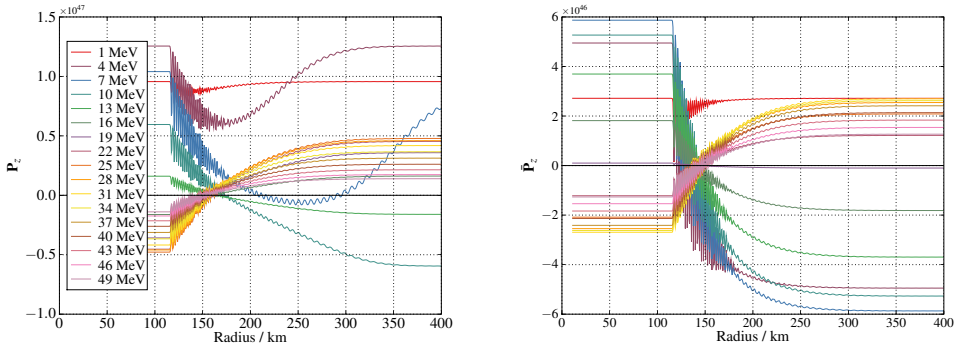

(a) $\mathbf{P}_z$ (b) $\overline{\mathbf{P}}_z$

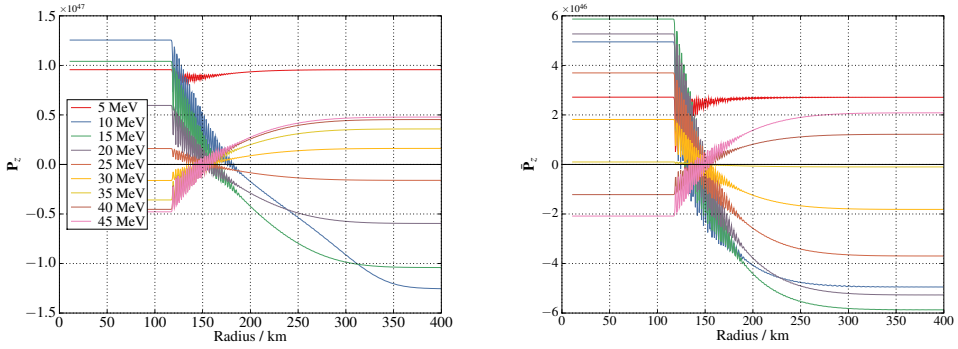

(c) $\mathbf{P}_z$ (d) $\overline{\mathbf{P}}_z$

Figure 2.5: The evolution of the neutrino and antineutrino polarization vectors. Each curve is for a single energy bin, with the magnitudes weighted by the number density of neutrinos in that bin. The lower figures are for the same initial spectrum as the upper ones but differ because they were evolved through a smooth matter background.

agreement between the predictions of the gyroscopic pendulum analogy and the dynamics seen in our simplified model of a real supernova explosion.

Comparing the plots of the neutrino potentials with and without the matter term reveals a decrease of the real part of the off diagonal term before the oscillations begin when matter is present, and a corresponding increase in the imaginary part. At the onset of oscillations the total magnitude of the off-diagonal term is slightly higher in the absence of matter. This difference in the ratio of the real and imaginary parts of the neutrino potential is one of the predicted effects of a slowly changing matter background. As described in subsection 1.4.7, the effect of a dense matter background is to cause the

pendulum-like fall of the polarization vectors to contain a component along the $\hat{\mathbf{y}}$ axis, corresponding to $\Im(B_{ex})$, as opposed to the fall that occurs in vacuum that is almost purely along the $\hat{\mathbf{x}}$ axis. The enhancement of the $\hat{\mathbf{y}}$ component is very clear in the right hand figure where matter has been added.

Figure 2.5 is the polarization vector plot for neutrino evolution with a matter background. The major difference in the neutrino side is the suppression of the small-scale oscillations of the vectors, and a flattening out of the evolution of the low energy neutrino vectors represented by the uppermost curves. We can understand the reduction of the small-scale oscillation amplitude as being due to the effective suppression of the mixing angle caused by a matter background.

On the antineutrino side there is a similar decrease in small-amplitude oscillations, and the lowest energy vector ends up with an opposite final sign. The effect of this on the final spectra is to move the edge of the spectral swap at low energy in antineutrinos to a slightly higher energy. It is interesting that the matter background increased the number of unswapped antineutrinos, since this small unswapped portion of the spectrum is not explained by the gyroscopic pendulum analogy discussed in subsection 1.5.3. The fact that matter increases the size of this effect suggests that it is the result of the small violation of adiabaticity that the smoothly decreasing neutrino background introduces. The matter background acts to suppress the effective mixing angle, which means the timescale of the system is increased and any adiabatic effects are enhanced.

In spite of the complexities of this much more realistic supernova neutrino calculation we have seen in this section that the dynamics, both in vacuum and in the presence of a large matter background, are still similar to the much simpler models examined in chapter 1. The final state is well-described by the analytic treatment of single spectral swaps. However, the small number of unswapped antineutrinos suggests that there are some subtleties that will need to be added to the basic picture in order to fully explain the system's behaviour and final state.

2.8.3 Effects of Matter Fluctuations

Next we test the effects of fluctuations in the matter background. As shown in section 1.2, flavour mixing can be driven by a rapidly-changing matter potential. In analytic work it is typically assumed that the matter background is changing slowly enough that the matter term can be removed by transform-

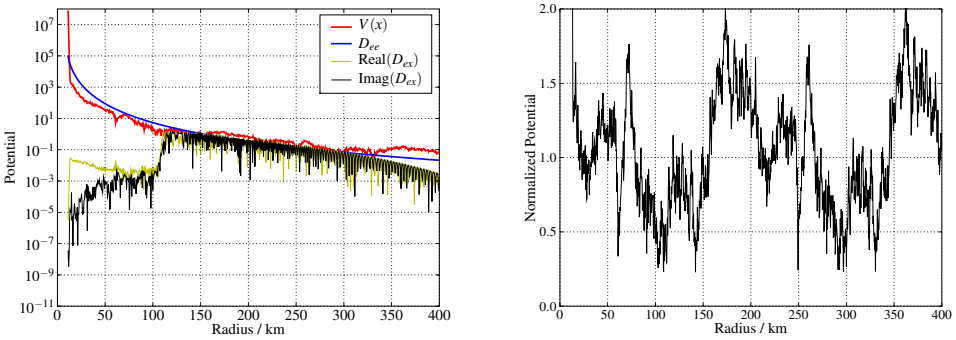

(a) Potentials

(b) Matter fluctuations

Figure 2.6: Neutrino potentials with fluctuations added to the matter density are shown on the left. The right hand figure shows the fluctuating matter background divided by the smooth profile to show the variation of the profile with respect to the standard smooth profile clearly.

ing into a rotating frame with nearly constant angular velocity, as explained in subsection 1.4.7. As we showed in the previous section, even a smooth matter background has an effect on the evolution, although it does not have large significant effect on the final neutrino spectrum. Plots for this section use the Kolmogorov spectrum described in subsection 2.6.1, with fluctuations at scales of $30\,\mathrm{km}/k$ for $1 \leq k \leq 5000$. The amplitude of the fluctuations used results in a density that varies between approximately half and double the base, smooth density profile, as shown in Figure 2.6.

The major difference in the potential plots is that the diagonal terms in the neutrino potential appear to pick up fluctuations from the matter term. The imaginary part is enhanced by the matter fluctuations and both the real and imaginary parts show non-smooth evolution beginning at the initial radius, whereas the smoothness of the neutrino potential only became disrupted beyond about 70 km in the absence of matter density fluctuations.

Evolving the same Fermi-Dirac initial neutrino spectrum through this fluctuating background gives the spectra shown in Figure 2.7. It appears that the matter fluctuations make very little difference to the final spectrum of neutrinos. This suggests that the large neutrino-neutrino interaction and the relative simplicity of the evolution in the no-fluctuation case are producing a very stable solution that is not finely balanced with any particular resonance conditions involving the matter density or its adiabaticity.

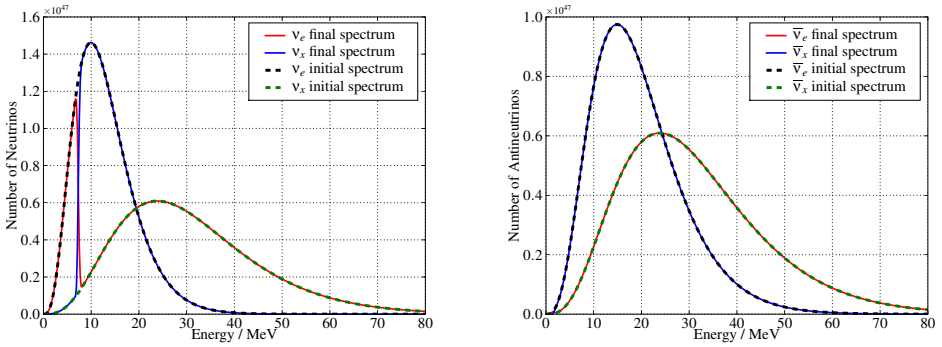

(a) Neutrino spectrum

(b) Antineutrino spectrum

Figure 2.7: The Fermi-Dirac initial spectrum and its final state after passage through the fluctuating matter background shown above.

In Figure 2.8 we have plotted the $\hat{\mathbf{z}}$ component of the neutrino and antineutrino polarization vectors for a series of neutrino energies for three different magnitudes of the matter fluctuation term. The top two plots are for the standard smooth matter profile, the middle two are for a matter profile with density fluctuations of around 0.5 to 1.5 times the smooth profile, resulting from setting the constant $C = 1.0$ in the fluctuation factor (see Equation 2.7), and the bottom two are for the profile shown in Figure 2.6, with fluctuations between 0.3 and 2.0 times the smooth profile corresponding to $C = 2.0$. These plots show that although the final spectrum is largely unaffected by matter fluctuations the dynamics and evolution of the neutrino flavours are altered in several ways.

The first difference in the matter fluctuation plots is the small shift in the end of the synchronized phase of the evolution from around 120 km to 110 km. This shift is smaller for lower matter noise cases, which suggests that there is a non-adiabatic effect that is disrupting the collective synchronized mode.

The second noticeable change caused by matter fluctuations is a strong decrease in the amplitude of the oscillations in the early region from the onset of flavour changes until about 175 km. Beyond 175 km the polarization vectors behave very similarly, but in this intermediate region the suppression of small-scale oscillations is very apparent. This suppression increases with increasing fluctuation amplitude.

As expected from the similarity of the final spectra, the final states of the flavour vectors are the same no matter the fluctuation amplitude. There are

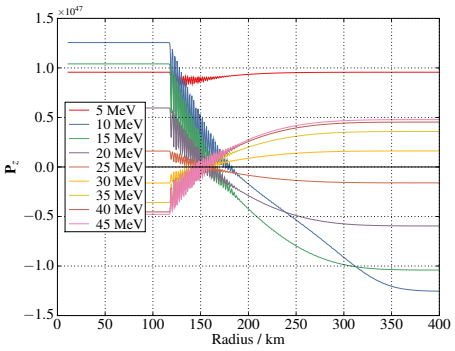

(a) $\mathbf{P}_z$ - $C = 0$

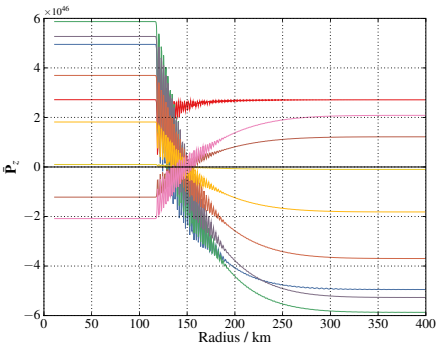

(b) $\overline{\mathbf{P}}_z$ - $C = 0$

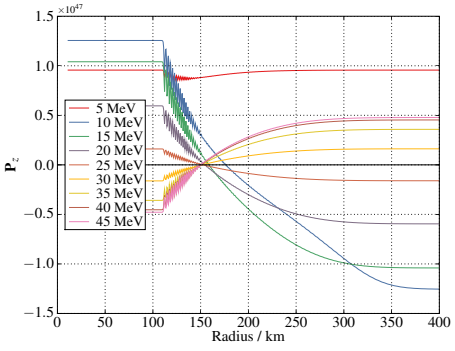

(c) $\mathbf{P}_z$ - $C = 1.0$

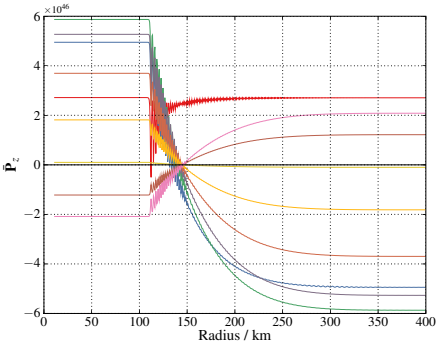

(d) $\overline{\mathbf{P}}_z$ - $C = 1.0$

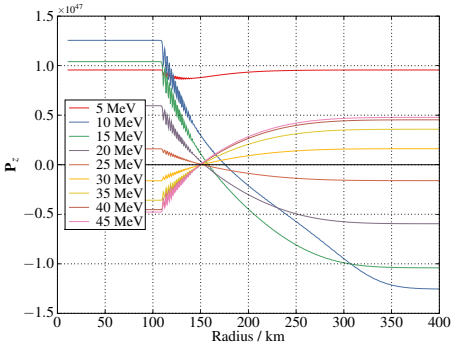

(e) $\mathbf{P}_z$ - $C = 2.0$

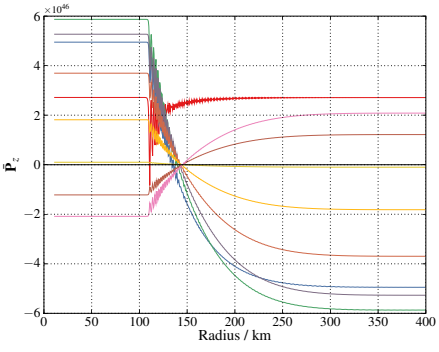

(f) $\overline{\mathbf{P}}_z$ - $C = 2.0$

Figure 2.8: The evolution of the anti-neutrino polarization vectors at a range of energies as they propagate through matter backgrounds with fluctuations of increasing amplitude C.

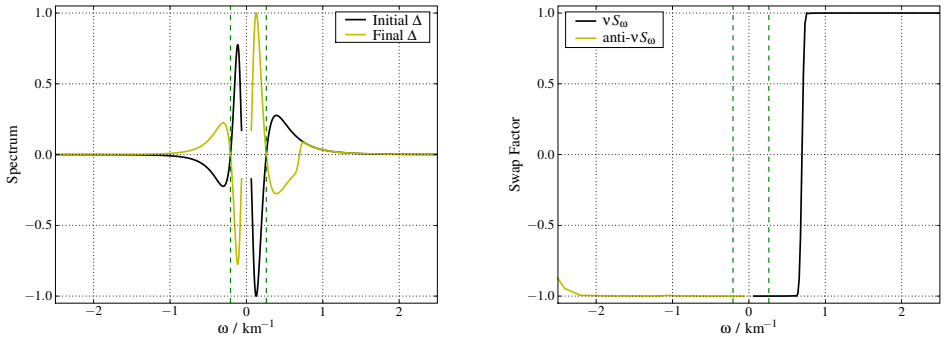

(a) Difference spectra

(b) Swap factor

Figure 2.9: The neutrino difference spectrum and swap factor for the Fermi-Dirac spectrum after evolution for 400km through a matter background with turbulent fluctuations added.

small shifts in some of the energy bins but no significant changes that appear to be proportional to the size of fluctuations. This agrees with the analysis of the single swap dynamics where the final state is a unique minimum of the flavour potential $\mathbf{B} \cdot \mathbf{M}$, which is reached as the kinetic energy (proportional to μ) goes to zero. Since the matter fluctuations do not change this minimum energy state and there is no alternative, lower-energy state that can be reached through these alterations in the dynamics, the effect is solely on the intermediate motion of the polarization vectors.

In Figure 2.9 we plot the difference spectrum and swap factor for a fluctuating matter background. The neutrino side of the swap factor remains very sharp and there is no visible difference from the no fluctuations case. On the antineutrino side the step has been broadened and now covers the full frequency range plotted. Because there are very few antineutrinos at $\omega < -1.0$ this difference is quite minor in that it represents a change in flavour of only a small number of neutrinos. It is interesting that the matter fluctuations reduce the deviation from the minimum energy state where all antineutrinos are swapped. This small difference in the antineutrino spectrum may be due to a dynamical effect. If there is some small amount of energy or polarization vector angular momentum that cannot be effectively removed in the smooth evolution, these low energy antineutrinos may be unable to reach their minimum energy state. These numerical results suggest that the matter fluctuations are functioning either as a dissipative factor allowing these few remaining unswapped antineutrinos to

relax into the lower-energy swapped state, or as a small excitation that allows the global minimum to be reached instead of a fairly stable local minimum with slightly higher energy.

2.8.4 Effects of Neutrino Density Fluctuations

In this section we examine the effect of adding fluctuations in the neutrino background density to the supernova simulation. We follow a similar procedure as we did to investigate the effects of matter fluctuations except that the neutrino potential is now multiplied by the fluctuating variable, and the scale of fluctuations is smaller. Physically the added factor corresponds to a variation in the number density of background neutrinos. Since it is an overall multiplication we are assuming that the fluctuations in the neutrino background are only in density, not in the flavour state, energy spectra or evolutionary history. We might imagine a situation where greater numbers of neutrinos are emitted at higher average energies from hot spots on the neutrinosphere, resulting in fluctuations in the magnitude and direction in flavour space of the neutrino background as the neutrinos from these hot spots cross the path of the reference neutrino. Another possible cause of fluctuations would be variations in neutrino emission on small time scales. Certainly we would not expect a real supernova explosion to emit neutrinos in a perfectly spherically symmetric way, so we expect that there will be some deviations from the smooth single-angle approximation. However, as a first step in analyzing the effects of neutrino density fluctuations we have chosen to use the simplest possible model of fluctuations. We used a maximum fluctuation scale of 10 km for these calculations, corresponding to roughly to the initial size of the neutrinosphere, and used the same method as for matter fluctuations to calculate and apply the fluctuations.

In many situations very little accuracy is lost if the matter background is ignored completely, because the magnitude of the matter term can be thought of as simply a rotation around the $\hat{\mathbf{z}}$ axis in flavour space which has little physical effect. In contrast, because the neutrino background term in the Hamiltonian (see Equation 1.26) is a sum of all the neutrino wavefunctions its direction in flavour space depends on the particular state of the neutrinos at any given radius. Removing it with a rotation around a single fixed axis is not possible even for a very slowly changing neutrino background, and there can be strong collective effects even when μ is not large (see subsection 1.5.2). Therefore we expect

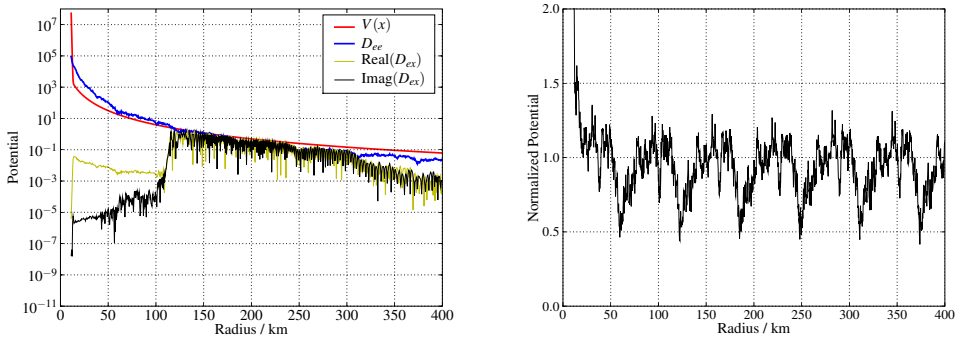

(a) $C = 1.0$ (b) $C = 1.0$

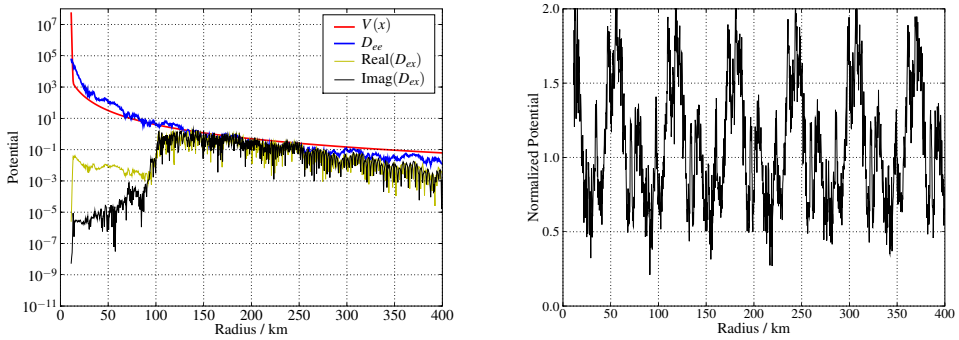

(c) $C = 2.0$ (d) $C = 2.0$

Figure 2.10: Plots of the background potentials with fluctuations of two different amplitudes added to the neutrino density are shown on the left. The right hand figures plot the background neutrino densities normalized to the smooth model to show the fluctuations that have been added.

that neutrino density fluctuations will be a much richer source of interesting phenomena.

In Figure 2.11 we show the final spectra obtained after evolving the Fermi-Dirac initial spectrum through a smooth matter background with a fluctuating neutrino background density. The variation of the neutrino background density used for these calculations is shown in Figure 2.10. We can see immediately from the plots of the spectra that the sharpness of the main spectral swap has been disrupted by the fluctuations. There is also a new swap edge introduced at high energy which is particularly noticeable in the antineutrino spectrum. This swapping behaviour is more similar to that seen in the absence of any fluctuations with the doubly-swapped spectrum described in section 2.10. In that case,

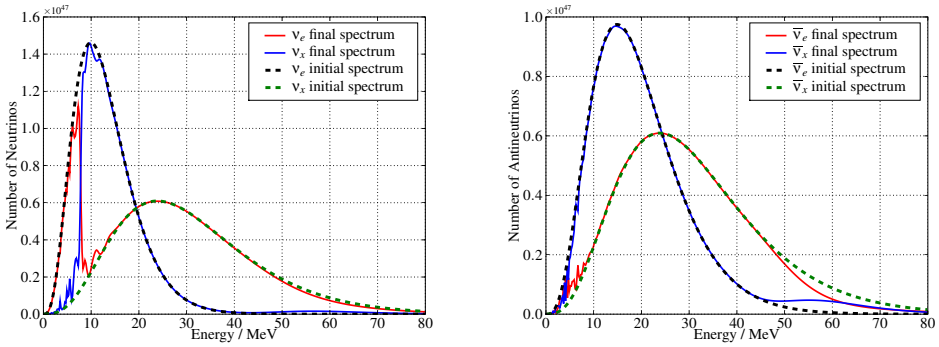

(a) Neutrino spectrum

(b) Antineutrino spectrum

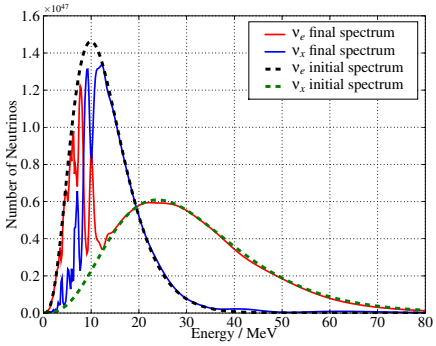

(c) Neutrino spectrum

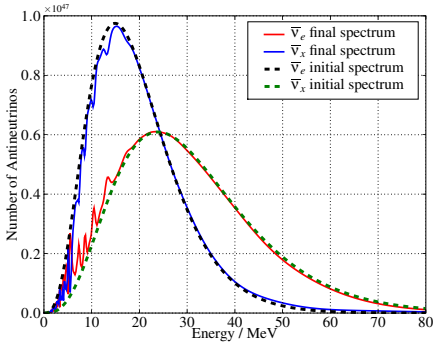

(d) Antineutrino spectrum

Figure 2.11: Neutrino and antineutrino spectra before and after evolution through 400km with a Fermi-Dirac-type initial spectrum and neutrino background fluctuations added.

it has been argued [60] that the second swap is caused by a parametric resonance produced by the neutrino background, in a similar way to the resonance seen in a simple case investigated analytically in [51]. It may be that fluctuations in the background neutrino density, which acts like a kinetic energy term in the gyroscopic pendulum approximation, can drive these secondary resonances which may be too weakly excited to have an effect in the no-fluctuation case. If this behaviour is caused by a similar type of resonance its appearance only in the presence of neutrino fluctuations suggests that it is the background fluctuations themselves that are driving the resonance.

The division of the swap at high energy can be seen in the plot of the swap factors in Figure 2.12. The single step roughly centred on $\omega = 0$ has become

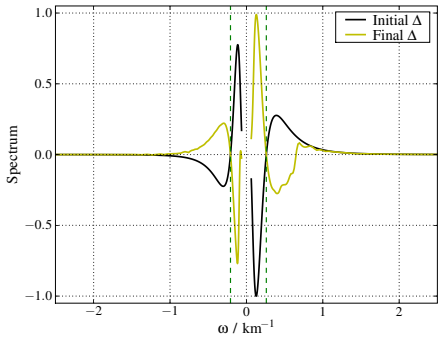

(a) Difference spectrum, $C = 1.0$

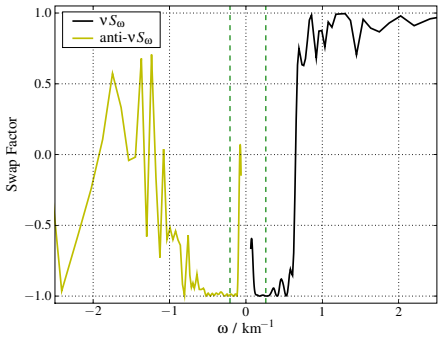

(b) Swap factor, $C = 1.0$

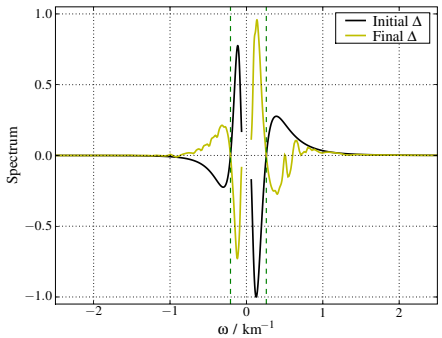

(c) Difference spectrum $C = 2.0$

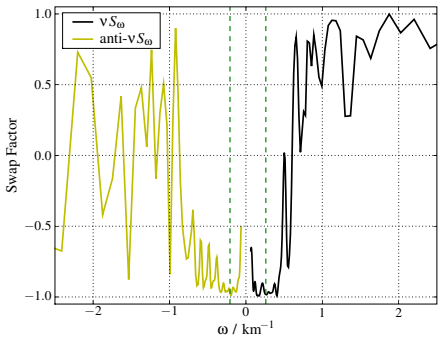

(d) Swap factor, $C = 2.0$

Figure 2.12: The neutrino difference spectrum and swap factor for the Fermi-Dirac spectrum after evolution through 400km through a fluctuating neutrino background. The upper figures are for the smaller-amplitude fluctuation case with $C = 1.0$ and the lower figures used high amplitude fluctuations with $C = 2.0$.

two separate steps, with one each on the neutrino and antineutrino sides as the swap factor tends to one at the zero point corresponding to very high energy. If we compare these swap factor results to our other spectrum studied below, which displays a doubly-swapped spectrum even in the absence of background fluctuations, the graphs are somewhat similar. The fluctuations have caused the steps themselves to become very uneven, but the general behaviour of two smaller steps around the points where the difference spectrum is zero (marked by dashed lines) is similar. Dasgupta *et al.* [60] suggests that the separation into two swaps can be washed out if the crossing frequencies are too close together. However, the explanation given for the swaps not being resolved is either a

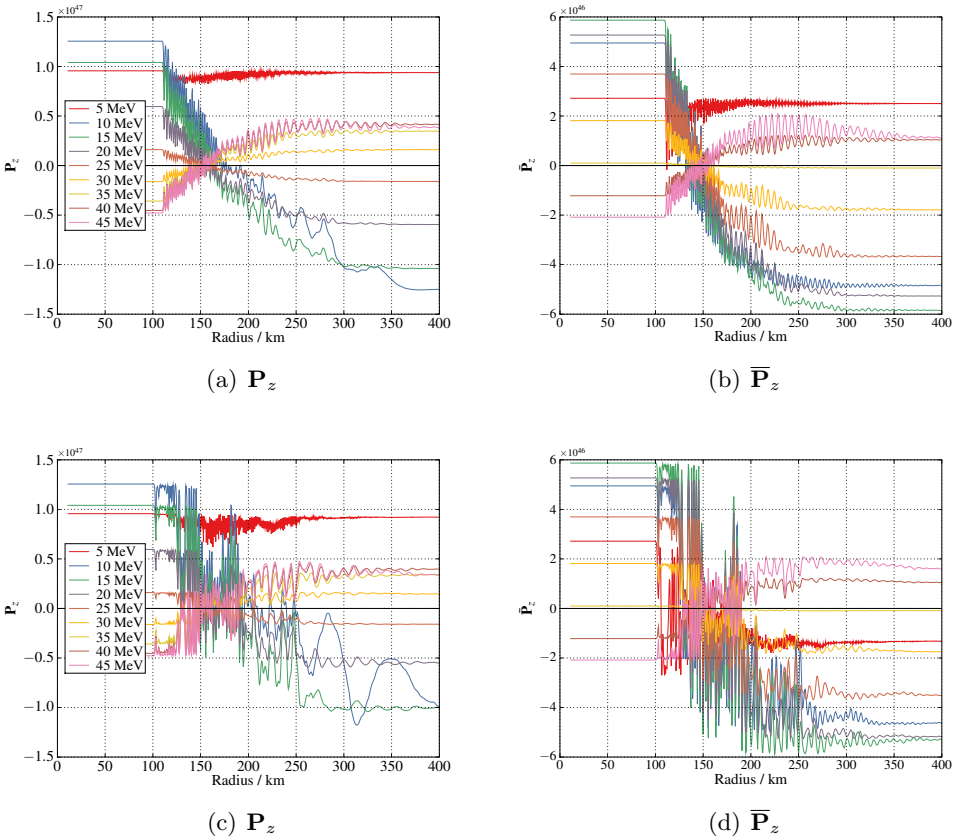

(a) $\mathbf{P}_z$ (b) $\overline{\mathbf{P}}_z$

(c) $\mathbf{P}_z$ (d) $\overline{\mathbf{P}}_z$

Figure 2.13: The evolution of the polarization vectors $\mathbf{P}$ at a range of energies, during propagation through a fluctuating neutrino background. The upper figures are for a fluctuation amplitude $C = 0.5$ and the lower figures are for $C = 2.0$.

lack of numerical resolution or adiabaticity violation. In our case, fluctuation-induced adiabaticity violation appears to decrease the width of the spectral swaps, although it also decreases their sharpness.

In Figure 2.13 we show the evolution of the flavour polarization vectors through the fluctuating neutrino background. The plots are still similar in overall form to the evolution in the smooth and fluctuating matter background, shown in Figure 2.8. Most of the vectors follow the same basic path as they do in the non-fluctuating background. As in the case of matter fluctuations, the end of the synchronized phase occurs at an earlier radius, particularly for the larger amplitude neutrino fluctuations. Since the end of synchronized motion occurs when μ falls below a certain critical value, this shift must be due to fluctuations

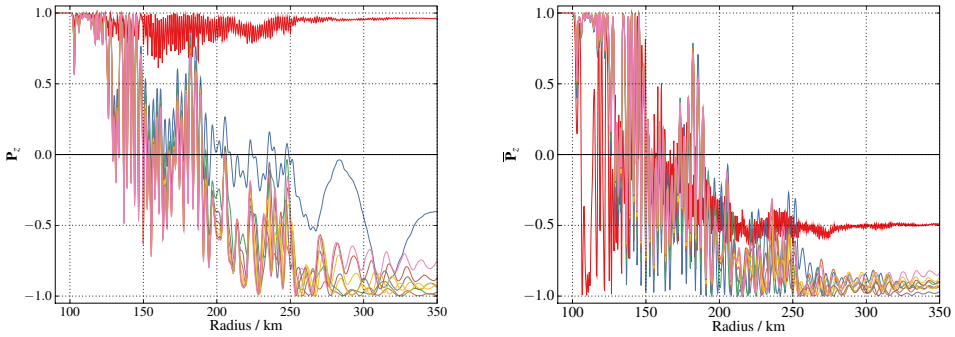

(a) $\mathbf{P}_z$

(b) $\overline{\mathbf{P}}_z$

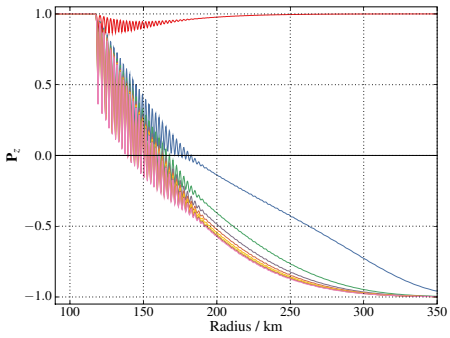

(c) $\mathbf{P}_z$

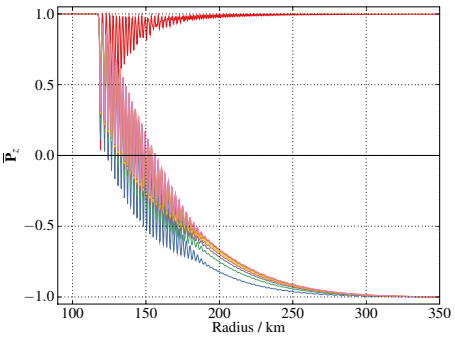

(d) $\overline{\mathbf{P}}_z$

Figure 2.14: The evolution of the unscaled polarization vectors at a range of energies during the bipolar phase. The upper figures are for large-amplitude neutrino density fluctuations with $C = 2.0$, while the lower figures are for a smooth background. The colour scheme is the same as in Figure 2.13.

in the background density causing μ to drop below the critical value for long enough to trigger the motion. Depending on the fluctuations, this dip could occur anywhere within a small range of radii before the underlying smooth average density curve reaches the critical value. However, because of the steep r^{-4} decline of the background the fluctuations will have to be extremely large to trigger motion at a much smaller radius than in the smooth case.

One new feature of the motion is seen in the lower figures for the large amplitude ($C = 2.0$) fluctuation case. Between 100 and 150 km the neutrino vectors do not immediately start their linear motion towards the final state after the end of the synchronized phase as in the smooth background case. Instead they remain at their initial positions, and undergo oscillations from

their base value to a relatively large amplitude and back several times, until they finally stop returning to their initial values past 150 km. In the no fluctuation case the oscillations were of essentially fixed, small amplitude around a linearly decreasing central point from the onset of the bipolar phase. To more clearly examine this region, we have replotted the values of $\mathbf{P}_z$ between 100 and 200 km in Figure 2.14. We also removed the scaling by number so that the individual energy modes all range between -1 and +1, and the equivalent plots for the smooth background case have been added below for comparison.

In comparing the two sets of figures, we see that the initial motion in the fluctuation case appears to be simply small-amplitude fluctuations around the initial value. In other words, the earlier start to the motion does not result in significant motion in the fluctuating background case before the onset of oscillations in the smooth background case. There is one major exception to this: the lowest energy antineutrino mode flips completely at around 105km, and finishes with a negative value after large-amplitude fluctuations. In the smooth background case, this mode remains approximately fixed at $\mathbf{P}_z = +1$ throughout the motion, with only small amplitude oscillations from this value.

Beyond 120km where neutrinos in both backgrounds undergo collective oscillations there are more differences in the motion. The smooth background modes steadily decrease towards their final values, and the amplitude of oscillations is small. As in the simple two-mode case with decreasing neutrino density, the vectors never return to their initial value once they begin to move. In contrast, the polarization vectors in the fluctuating background oscillate several times from their initial value to negative values and back. These oscillations are more reminiscent of the parametric resonance example.

Despite these differences, and the much more chaotic general appearance of the motion, there are also several similarities. Aside from the lowest-energy mode, the vectors still move together with a similar oscillation frequency in both cases. The differences resulting from the neutrino fluctuations are mostly differences in the maximum and minimum points of the collective oscillation. While the amplitude of these differences is very large, as seen from the final spectra the final state of the system is still quite resilient. This is in good accord with the gyroscopic pendulum analogy. In that analogy, we can think of μ as being the magnitude of kinetic energy of the pendulum at any given point, so the fluctuations can be thought of as 'kicks' to the pendulum at non-resonant frequencies. Because these kicks are in the end proportional to the constantly

decreasing smooth background density, the motion will eventually die out in a similar way as before no matter what the effect of the kicks was during the large amplitude phase of the motion. The differences in the final state are most pronounced in the high frequency part of the spectrum, where we expect the non-adiabaticity of the fluctuations to have a stronger effect.

The only significant violation of this relatively simple picture of the effect of neutrino fluctuations is in the apparent splitting of the single spectral swap into two closely-spaced swaps in the high-amplitude cases. This suggests that the fluctuations may be helping to drive motion more like the parametric-resonance multiple swap dynamics we will examine in detail for the doubly-swapped spectrum. However, the evolution plots still look very different to the true doubly-swapped spectrum's evolution, so it may simply be that adiabaticity violations are preventing the system from falling into its normal minimum energy state in a way that affects the highest and lowest energy neutrinos most strongly.

2.9 Singly Swapped Spectrum in Normal Hierarchy

We also ran calculations for this spectrum in the normal hierarchy to check that there are no novel effects caused by the fluctuations in neutrino background or matter background. We found that, as in the inverted hierarchy, the system's behaviour is well-explained by the pendulum analogy. The neutrino ensemble undergoes no flavour change at all in the normal hierarchy regardless of the background fluctuations. In the case of very high neutrino density fluctuations we do not see even transient flavour changes during the evolution. If the neutrino spectrum emitted from a supernova is like the singly-swapped spectrum studied here, it should be much simpler to determine the hierarchy than it would be for the doubly-swapped spectrum studied in the following sections, because of this stark difference in behaviour.

The largest differences in the spectra caused by the hierarchy are in the flavour distribution at high energy. For inverted hierarchy, there are far more electron antineutrinos than muon neutrinos at energies above 40 MeV, while the spectrum below 20 MeV is strongly dominated by $\bar{\nu}_x$. For the normal hierarchy this flavour distribution is exactly reversed. Similarly, for the neutrino spectra the inverted hierarchy causes the higher energy flux above 30 MeV to be made up almost entirely of electron neutrinos, whereas it mostly consists of x-type neutrinos in the normal hierarchy. The difference between the spectra the two

hierarchies is large, but measuring the hierarchy from supernova neutrino observations will still require very good energy resolution and flavour discrimination, as well as a large enough detector volume to observe a significant number of neutrinos from a given supernova explosion.

2.10 Doubly Swapped Spectrum

We now consider a different initial spectrum, used in [60] and based on modelling done in [63], as an example of a spectrum that results in two spectral swaps instead of the single swap seen in the spectra used in most of the earlier studies of supernova neutrinos. The shape of the spectrum as a function of β (defined by $\beta \equiv E/\langle E \rangle$, where $\langle E \rangle$ is the average energy) is given by

$$\phi(\beta) = \frac{128}{3\langle E \rangle} \beta^3 e^{-4\beta}, \tag{2.12}$$

where the factor 128/3 is for normalization. The spectrum we study in this section also has different average energies from the singly swapped spectrum. These values (in MeV) are $\langle E_{\nu_e} \rangle = 12$, $\langle E_{\bar{\nu}_e} \rangle = 15$, and $\langle E_{\nu_x} \rangle = \langle E_{\bar{\nu}_x} \rangle = 18$. A further difference from the singly swapped case is that we no longer assume equipartition of neutrino energies, so the total energy emitted in different neutrino flavours is no longer the same (see section 2.2). The total amount of energy in each neutrino flavour is distributed so that the total fluxes F emitted in each neutrino flavour are in the ratio $F_{\nu_e} : F_{\bar{\nu}_e} : F_{\nu_x} : F_{\bar{\nu}_x} = 0.85 : 0.75 : 1.00 : 1.00$. The spectrum resulting from these parameters is shown in Figure 2.15. Note that these numbers do not have to be finely tuned to obtain a doubly swapped final spectrum. The particular details we have chosen are not especially favoured or special, but simply represent a realistic initial spectrum with interesting dynamics that are quite different from the singly-swapped spectrum.

2.10.1 Evolution in the Neutrino Background

Once again we begin with the neutrino background only so that the evolution can be studied with as few complications as possible. The major features of the spectrum in this case are the two swaps, one in the neutrino spectrum between approximately 10 and 35 MeV, and one in the antineutrino spectrum between about 5 and 25 MeV. Although the initial spectral shape appears roughly similar to the Fermi-Dirac case, the relative numbers of each flavour are considerably

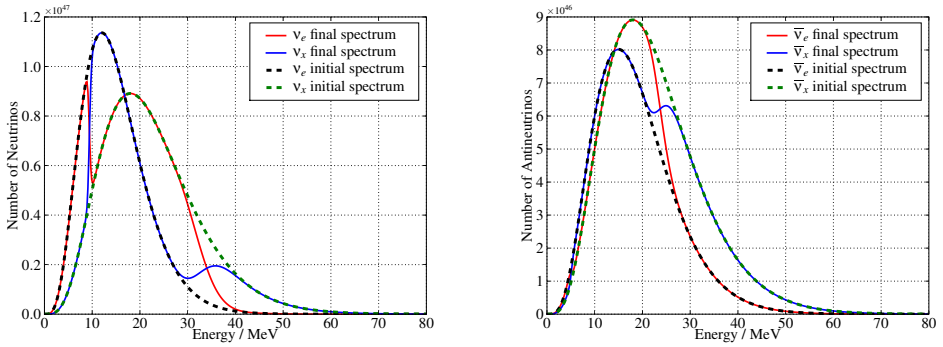

(a) Neutrino spectrum

(b) Antineutrino spectrum

Figure 2.15: The initial neutrino and antineutrino spectra and the resulting doubly-swapped spectrum that is obtained after evolution for 400km from the neutrinosphere.

different to those in the singly-swapped spectrum. The major difference between the final states of the two spectra is that, as shown in Figure 2.16, there are two sharply defined steps in the swap factor instead of the single broad step for the Fermi-Dirac spectrum. Comparing to Figure 2.3, the gap between the two swaps at low frequency is clearly seen in the difference spectrum plot. Its shape is similar to the second turning point in the final antineutrino spectrum for the singly swapped spectrum in the presence of neutrino background fluctuations, shown in Figure 2.12. This gives further evidence that one of the effects of the neutrino fluctuations in that case was to resolve the two splits that underlie the seemingly simple single swap, so that the resulting dynamics and final state became more like the doubly-swapped spectrum.

The polarization vector plots shown in Figure 2.17 show much more complex behaviour than the corresponding plots for the single-swap Fermi-Dirac spectrum. The initial period of evolution begins earlier with this initial spectrum, with fluctuations in the polarization vectors beginning at about 80 km. Between 80 and 150 km there are two very smooth, large-amplitude oscillation periods involving all neutrino energies that resemble the parametric resonance oscillations. After the third such period from around 150 km onwards the motion becomes more complicated. There is behaviour similar to that in the Fermi-Dirac case where regular oscillations are overlaid on a fairly smoothly-moving base value. However, compared to that case the overlaid oscillations have a very large amplitude. By 400 km the polarization vectors have reached a stable state.

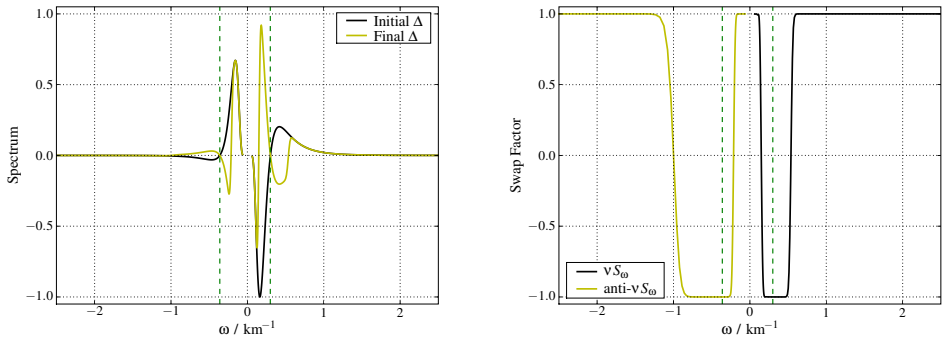

(a) Difference spectra (b) Swap factor

Figure 2.16: The neutrino difference spectrum, on the left, and swap factor obtained from evolving the doubly-swapped spectrum for 400 km with no background matter.

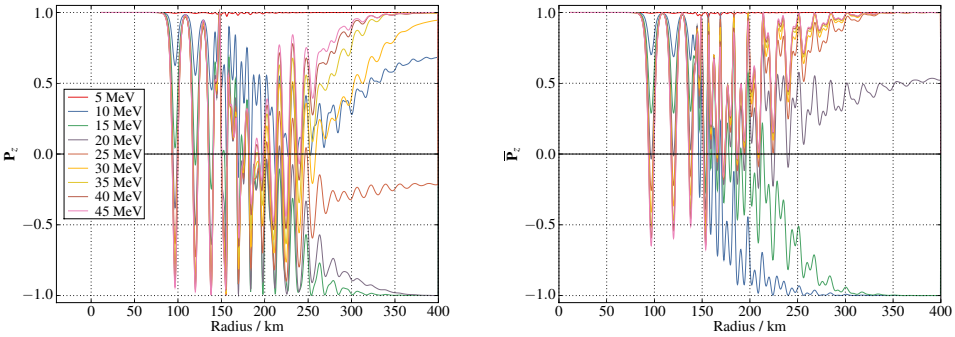

(a) $\mathbf{P}_z$ (b) $\overline{\mathbf{P}}_z$

Figure 2.17: The evolution of the $\hat{\mathbf{z}}$ component of the neutrino and antineutrino polarization vectors for the doubly-swapped spectrum.

The behaviour between 175 and 250 km is particularly complex, with several vectors undergoing approximately sinusoidal oscillations with large amplitude while others move very little. These large amplitude oscillations have almost died out by 300 km and the neutrinos end up in stable final states by 400 km.

Many of the polarization vectors oscillate with very large amplitude and repeatedly cross the $\mathbf{P}_z = 0$ axis during their evolution. Compared to the singly swapped spectrum's evolution, the decreasing neutrino background has a less obvious influence on the motion. In the earlier case, the motion of the vectors was dominated by a gradual decline caused by the decrease in μ. In this case, the motion mainly consists of large-amplitude oscillations like those that occur in the parametric resonance solutions, which gradually die out as the pendulum-type motion ends the evolution. Although the underlying smooth motion toward the final state is somewhat evident underneath the large oscillations, the motion is far less well-behaved than the smooth, monotonic evolution in the single swap case. The double swap seems to be the result of a much less constrained system, or one that is strongly influenced by resonances that did not occur in the singly swapped spectrum.

As we did for the singly-swapped spectrum, we can calculate the critical value μ_{sync} which determines the stability of the gyroscopic pendulum. The average frequency for this spectrum is found to be $\langle\omega\rangle = 0.472$ km^{-1} as compared to 0.9 km^{-1} for the singly-swapped spectrum. The critical value μ_{sync} is much lower than for the earlier spectrum, with a value of approximately 9.8 km^{-1}. The total number density of neutrinos is also decreased in this spectrum with our parameters, which results in an initial μ value of 3.10×10^6 km^{-1}. Solving for the value of r at which the oscillations should begin gives $r = 155$ km. Our simulations show that oscillations begin at a much smaller radius, around 80 km. This motion cannot be explained by the gyroscopic pendulum analogy.

This result is very interesting, however, because it indicates that there are two different regimes acting in combination to produce the flavour evolution seen in Figure 2.17. Before 80 km the system is in the familiar fixed upright position. At around 80 km a threshold is crossed which allows the system to undergo oscillations even though the gyroscopic system remains stable. These parametric-type oscillations continue until approximately 150 km, where the gyroscopic pendulum is now able to fall, resulting in a combination of the two modes of motion that gradually settles into a doubly-swapped final state.

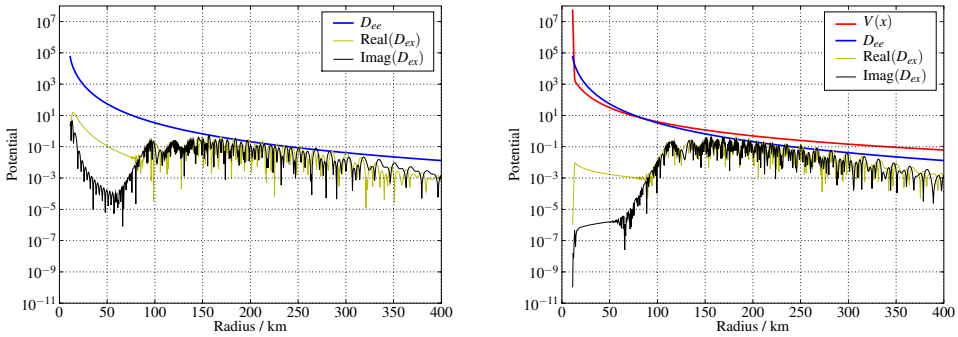

(a) No matter

(b) Matter added

Figure 2.18: The neutrino potentials for the doubly swapped spectrum with and without a matter background. The smooth upper curve on the left is the neutrino background term $\sqrt{2}G_F n_\nu$ and the lower curves are equivalent to the magnitude of the $\hat{\mathbf{x}}$ and $\hat{\mathbf{y}}$ terms of the background vector $\mathbf{D}$. The matter background term in the right-hand figure is the curve that steeply descends from the top left.

2.10.2 Evolution with a Matter Background

Adding a smooth matter background to this simulation causes several changes in the evolution. First of all, in the plots of the background potentials in Figure 2.18 we see that the matter term has smoothed out the imaginary off-diagonal component of the neutrino background. One very striking difference compared to the singly swapped spectrum is that this component is not enhanced by the matter term for this spectrum. Instead, it is suppressed at very low radius and is essentially unchanged by matter beyond 50 km. Prior to 50 km in the presence of matter the off diagonal terms are very similar for both spectra, but the increase that occurs before the onset of large-amplitude oscillations is much steeper for the singly-swapped spectrum. It is also notable that while the off-diagonal terms were approximately equal to the overall magnitude throughout the collective oscillation phase in the singly swapped spectrum, for the doubly swapped spectrum they remain significantly below the main neutrino background magnitude curve during the early parametric phase of the motion and tend to oscillate with greater amplitude throughout the motion.

The final spectra after evolution through the smooth matter background are shown in the upper panels of Figure 2.19. The only significant difference in the spectra compared to the no-matter case is a narrowing of the swap in antineu-

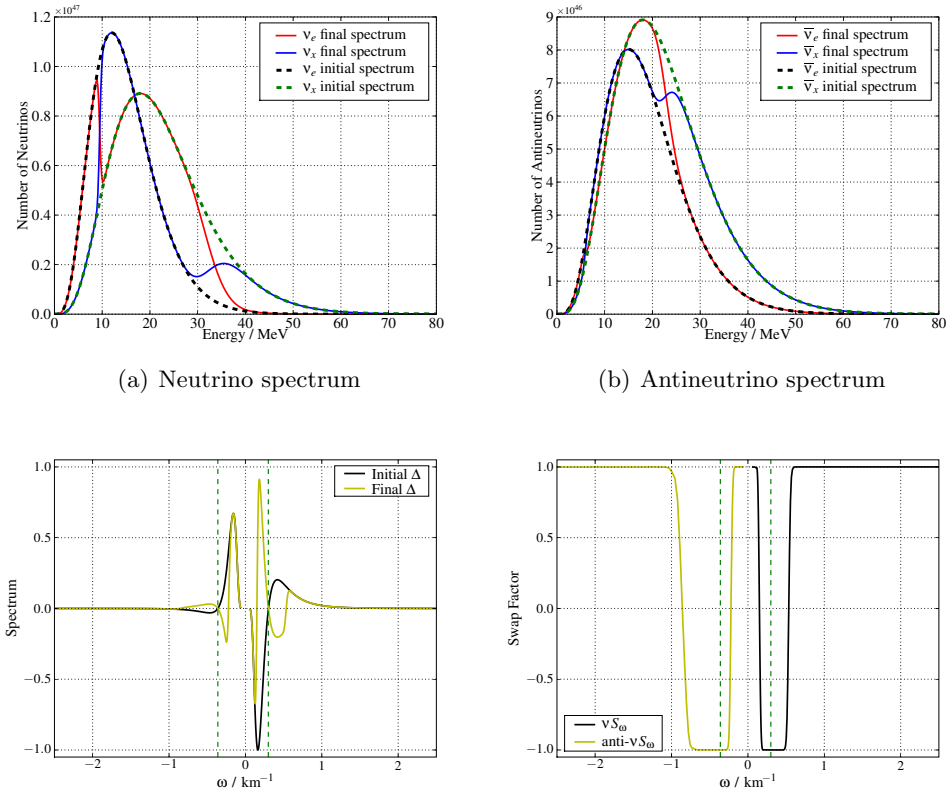

(a) Neutrino spectrum

(b) Antineutrino spectrum

(c) Difference spectra

(d) Swap factor

Figure 2.19: The initial and final states of the doubly swapped neutrino spectra and the corresponding difference spectrum and swap factor after evolution for 400 km through a smooth matter background.

trinos. The low energy edge moves to an energy about 2 MeV higher while the higher energy edge moves lower by roughly the same amount. This narrowing effect of the matter background can be most clearly seen in the anti-neutrino swap factor shown in the lower right panel of Figure 2.19. The neutrino side of the swap factor plot remains the almost the same while the step in antineutrinos becomes significantly narrower in the presence of the matter background. The neutrino step is also narrowed, but only by a barely visible amount.

The plot of the polarization vectors in Figure 2.20 shows that the matter background causes a delay of approximately 20 km in the onset of oscillations. This is much larger than the delay seen for the singly-swapped spectrum. Since the end of the stationary part of the evolution in this case does not correspond

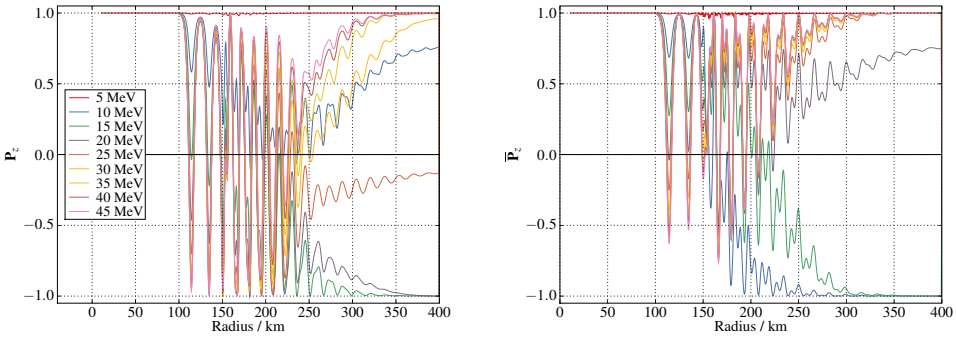

(a) $\mathbf{P}_z$ (b) $\overline{\mathbf{P}}_z$

Figure 2.20: The evolution of the polarization vectors $\mathbf{P}$ of neutrinos and antineutrinos at a range of energies for the doubly swapped spectrum in a smooth matter background.

to the gyroscopic instability point the matter background must have quite a different effect on the parametric oscillations than it does on the gyroscopic pendulum motion. The middle period of the evolution of the neutrino vectors from about 150–250 km is more well-behaved in the presence of matter. In particular, the large-amplitude symmetric oscillations appear to follow a much smoother mean central value towards their final value than in the vaccum case. The peaks of the oscillations are also smoothed out, particularly in the region from 140–200 km where the interference between the parametric and gyroscopic oscillations is strongest. This smoothing effect probably results from the same cause that led to a suppression of the small-amplitude oscillations in the singly swapped case.

In antineutrinos, there is also smoothing of the oscillations, but it is not as pronounced and the amplitudes and central points of the different modes still appear to fluctuate rather chaotically. A notable feature of the plots is the similarity in all cases of the first part of the motion. In all the plots there are two full, very smooth oscillation cycles before more complex dynamics start to disrupt the simple oscillations. The subsequent oscillations look fairly similar but they have a noticeably smaller wavelength and are less sinusoidal in shape.

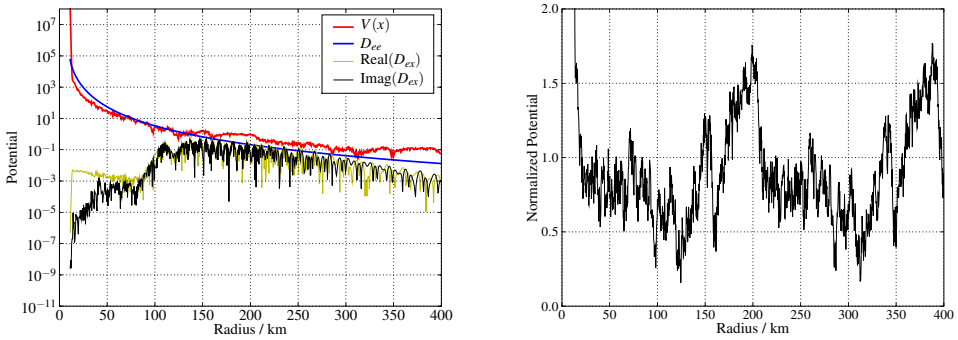

(a) Potentials

(b) Matter fluctuations

Figure 2.21: Neutrino potentials with fluctuations added to the matter density are shown on the left. The right hand figure shows the fluctuating profile divided by the smooth profile to show the variation of the profile with respect to the standard smooth profile clearly.

2.10.3 Effects of Matter Density Fluctuations

We added a fluctuating term to the matter background and evolved the doubly swapped spectrum through this background. The potentials and the normalized plot of the fluctuations added are shown in Figure 2.21. As can be seen in the potential plot the matter fluctuations disrupt the smoothness of the off-diagonal neutrino potential terms during the initial portion of the motion. The fluctuations in the matter density drive fluctuations in both the real and imaginary parts of D_{ex}, and the imaginary part is significantly larger than in the smooth background case, reaching approximately the same magnitude as the real part by 50 km radius. The rise of the off-diagonal terms that accompanies the onset of large amplitude collective oscillations remains as before, but it is shifted to a slightly lower radius. The off-diagonal terms also continue to experience significantly more fluctuations, presumably driven by the matter background, until around 220 km. The separation of the two parts seen in the no-matter case is reduced by the smooth matter background, and reduced further still by the matter fluctuations. This may be the result of the effect noted in subsection 1.4.7, where the effect of matter was shown to be a rotation in the axis of the simple pendulum motion. The smooth matter background tends to mix the $\hat{\mathbf{x}}$ and $\hat{\mathbf{y}}$ components of the neutrino motion as it acts as a steady rotation term, while the fluctuating background, equivalent to a rapidly changing rotation, results in

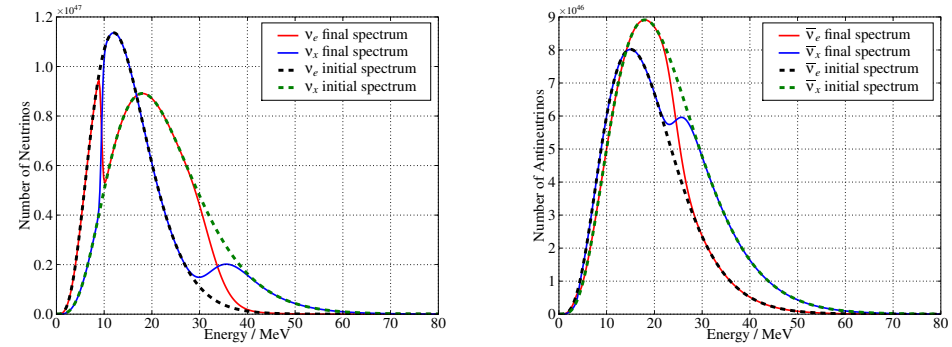

(a) Neutrino spectrum

(b) Antineutrino spectrum

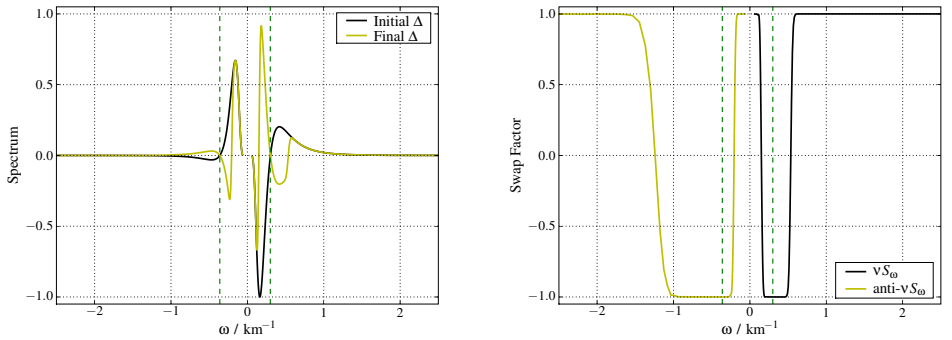

(c) Difference spectra

(d) Swap factor

Figure 2.22: The doubly-swapped neutrino spectra, difference spectrum and swap factor after evolution for 400 km in a matter background with large amplitude fluctuations, $C = 2.0$.

more mixing of the two components due to its irregular speed.

The fluctuations in the matter background, as in the single swap case, cause no major alterations in the final neutrino spectrum. The most notable change in the swap factor shown in Figure 2.22 is that the antineutrino step has been broadened. Comparing this swap factor with the smooth matter and no matter cases we see that the smooth matter background has the narrowest swap, followed by the case with no matter background, while the fluctuating matter background produces the broadest swap. The neutrino swap remains unchanged in all cases. This pattern is exactly the same as the one seen for the singly swapped case with matter fluctuation: a smooth matter background narrows the antineutrino swap, while a fluctuating matter background widens it, rela-

tive to the zero point of no matter background. The constancy of this effect despite the very different details of the evolution suggests that the effect is due solely to adiabaticity in the matter term and that this effect is independent of the details of the neutrino dynamics and initial spectral shape.

To compare the details of the differences in the evolution we have plotted the unweighted $\hat{\mathbf{z}}$ components of the neutrino polarization vectors in the central region of the evolution in Figure 2.23. In the left hand plots of the neutrino polarization vectors the most noticeable difference caused by matter fluctuations is that the polarization vectors reach much lower amplitudes during two or three cycles in the range from about 150 km to 200 km. The motion is disrupted after the second cycle and does not follow the smooth consistent oscillation pattern of the fluctuation-less plot after the vectors double back in the middle of the third cycle.

In the antineutrino plots on the right hand side, the key difference is in the doubly-peaked structure of the oscillations. In the upper figures with a smooth matter background there are two closely-spaced maxima of the bipolar oscillations which are roughly equal in magnitude. In the earlier cycles the first peak has a higher maximum, but as the evolution proceeds the second peak becomes the larger one. In contrast, the evolution in the presence of matter fluctuations shows a significant decrease in the maximum amplitude of the smaller peak. The highest peaks still reach an amplitude of $+1$, but both the minimum points and the maxima of the secondary peaks are closer to zero. This effect is more pronounced in the case of smaller matter fluctuations with $C = 1.0$ than with $C = 2.0$. It is also notable that the differences in evolution gradually decrease with radius, and the plots are very similar after about 250 kilometres. This, along with the lack of strong effects seen in the gyroscopic-type singly-swapped spectrum evolution, suggests that the matter fluctuations have their strongest influence on the parametric-type motion, and that this motion dies away by around 250 km.

There is one antineutrino mode whose final state is significantly shifted in the plots. This is also the only antineutrino mode that does not end in a very strongly polarized state with $\mathbf{P}_z = \pm 1$. In contrast, there are many neutrino modes whose states at 300 km are not pure flavour states. Another interesting difference between neutrinos and antineutrinos is that the neutrinos all depart from their synchronized motion at the same radius, about 225 km. In antineutrinos, aside from the lowest energy mode which does not move significantly

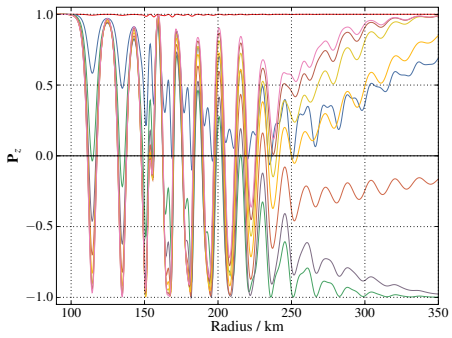

(a) 0.0, $\mathbf{P}_z$

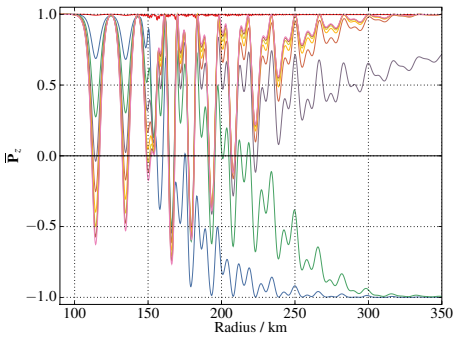

(b) 0.0, $\overline{\mathbf{P}}_z$

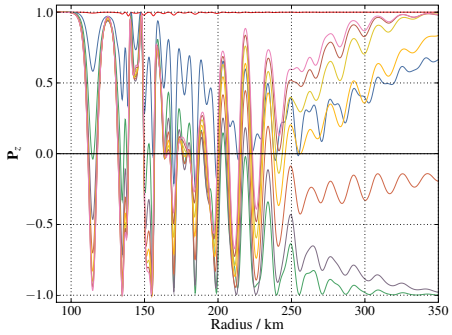

(c) 1.0, $\mathbf{P}_z$

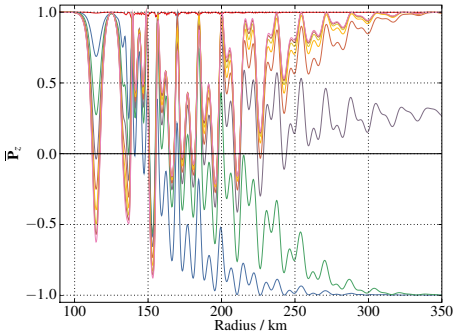

(d) 1.0, $\overline{\mathbf{P}}_z$

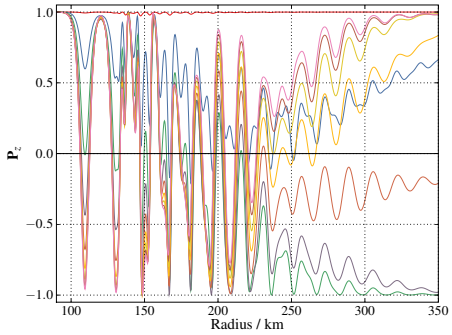

(e) 2.0, $\mathbf{P}_z$

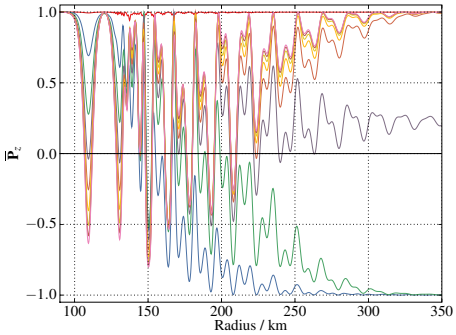

(f) 2.0, $\overline{\mathbf{P}}_z$

Figure 2.23: The evolution of the polarization vectors $\mathbf{P}$ of neutrinos and antineutrinos for the doubly swapped spectrum in a fluctuating matter background. The top figures show the evolution in a smooth matter background for comparison, the middle figures are for fluctuations with amplitude $C = 1.0$, and the lower figures used $C = 2.0$.

throughout the evolution, there are two modes which separate from the rest of the ensemble at a much smaller radius, around 150 km. These are the two next lowest energy modes, which cover the swapped central part of the antineutrino spectrum. It appears that the energy range of the antineutrino swap is determined quite early in the evolution rather than resulting from the later transition between parametric resonance and gyroscopic pendulum motion.

2.10.4 Effects of Neutrino Density Fluctuations

Finally we add fluctuations to the neutrino density during the evolution of the doubly-swapped spectrum. In Figure 2.25 we show the results of three separate simulations, which differ only in the fluctuations added to the neutrino background. The background potentials for each run are shown in the left hand figures, and exhibit broadly similar characteristics to the non-fluctuating potentials. The modifications caused by fluctuations are almost identical to those seen in the singly-swapped case, shown in Figure 2.10. The rise of the off-diagonal terms is shifted to a smaller radius, and the maximum amplitude of these terms fluctuates with the overall density rather than falling smoothly with radius. The smoothness of the initial portion of the off-diagonal terms is upset, as it was by the matter fluctuations. Of course, much of this fluctuation is simply because the terms have been multiplied by a fluctuating turbulence factor, rather than a sign of drastically different behaviour. The general shape of the evolution aside from these small-scale disturbances and the overall shift is similar in all cases, even for the very large neutrino density fluctuations in the bottom figures.

The spectra resulting from these neutrino density fluctuations are shown in Figure 2.25. We see both shifts in the position of the swaps and alterations in their shapes as compared to the swaps in the smooth background. In neutrinos, the swap is broadened for $C = 1.0$ compared to the small-fluctuation $C = 0.1$ spectrum, but the swap is then narrowed by the larger fluctuations with $C = 2.0$. The spectrum becomes more disorderly as the fluctuation amplitude is increased, although this is only obvious in the $C = 2.0$ plot in neutrinos.

In the antineutrino spectra there is a somewhat similar effect where the spectral swap becomes wider for $C = 0.1$ compared to the smooth background, but is progressively narrowed by the two higher fluctuation cases. Simulation at intermediate values (not plotted here) also fit this pattern. Although the low energy parts of the antineutrino spectra for the two flavours are very close

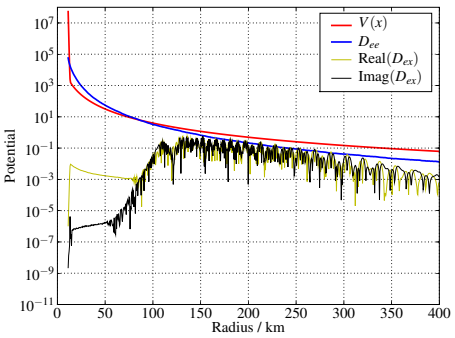

(a) Potentials, $C = 0.1$

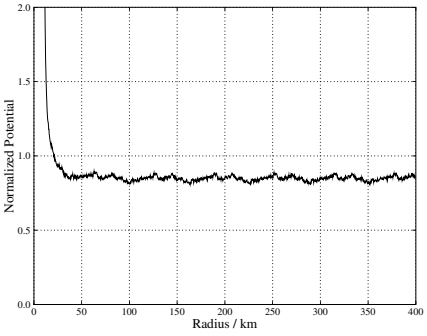

(b) Neutrino fluctuations, $C = 0.1$.

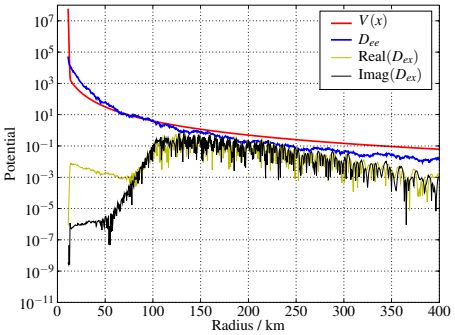

(c) Potentials, $C = 1.0$

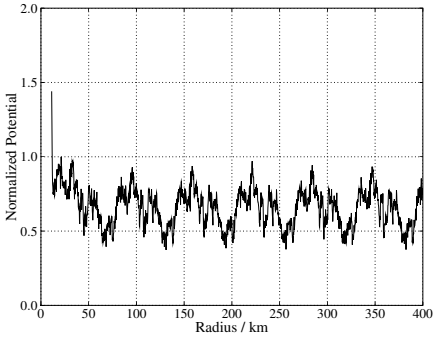

(d) Neutrino fluctuations, $C = 1.0$.

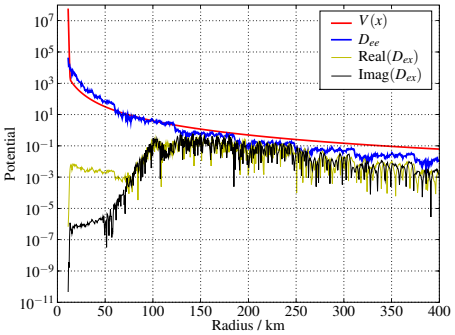

(e) Potentials, $C = 2.0$

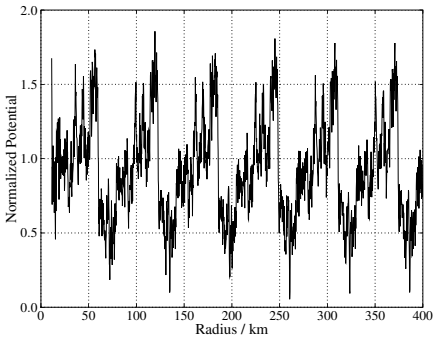

(f) Neutrino fluctuations, $C = 2.0$.

Figure 2.24: Plots of the neutrino and matter potentials for the doubly swapped spectrum evolved through three different fluctuation amplitudes. The potentials are on the left hand side, and the right hand figures show the neutrino background amplitude normalized for the smooth r^{-4} decline.

together, it is interesting to see that as the fluctuation amplitude is increased the lower edge of the swap in this region becomes extremely disordered, with the spectra crossing several times between 0 and 10 MeV. Another new feature is that the region in the centre of the swap is no longer completely swapped, as the final $\bar{\nu}_e$ spectrum does not reach all the way to the peak of the initial $\bar{\nu}_x$ spectrum. The highest-energy part of the final antineutrino spectra also peel away from the initial spectra above 40 MeV in the $C = 2.0$ simulation.

We can obtain a clearer view of these small deviations by looking at the normalized swap factor plots in Figure 2.26. For $C = 0.1$ the general structure of the two swaps is still visible, but only the neutrino swap remains sharp, while the antineutrino swap has been spread out to high negative ω. In the higher fluctuation cases the antineutrino swap is barely recognizable under the jagged fluctuations, while the neutrino swap becomes progressively more disrupted. In the $C = 2.0$ swap factor a partial third swap seems to be forming at $\omega = 0$ and another small swap in neutrinos at high ω has also appeared.

The evolution of the flavour polarization vectors in these different fluctuating backgrounds are plotted in the corresponding panels in Figure 2.27. The neutrino fluctuations have significant and complicated effects on the evolution of the neutrino flavours. Comparing the plots with the smooth background case in Figure 2.20 the evolution is much less regular. Although the evolution in the smooth matter background is less easily understood than the singly-swapped case, it appears to be comprised of only a few different collective frequencies which gradually freeze out into the final spectrum. In the presence of neutrino background fluctuations the evolution becomes more disorderly.

In the neutrino half of the plots, on the left hand side, we see a shift of the onset of oscillations toward lower radius as the fluctuation amplitude is increased. This is the same as the effect noted for the singly-swapped spectrum with neutrino fluctuations. The collective evolution begins to diverge from the smooth case after only half the first parametric oscillation period. In the lowest-amplitude case the effect is small, but in the middle and lower plots the smoothness of the familiar pendulum dip motion is upset. This disruption continues for the next few cycles, before the later stage becomes smooth again. The irregularities persist for longer in the higher noise amplitude cases, but even for extremely high amplitude fluctuations with $C = 2.0$ the motion becomes fairly smooth after 200 km. This later part of the motion seems to be in a different mode to either the gyroscopic or parametric motion, as the oscillations are

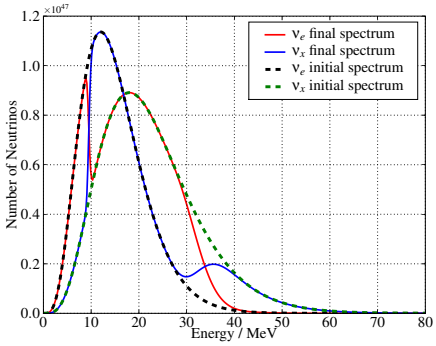

(a) Neutrino spectrum, $C = 0.1$.

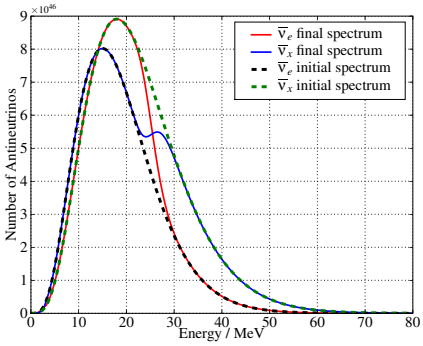

(b) Antineutrino spectrum, $C = 0.1$.

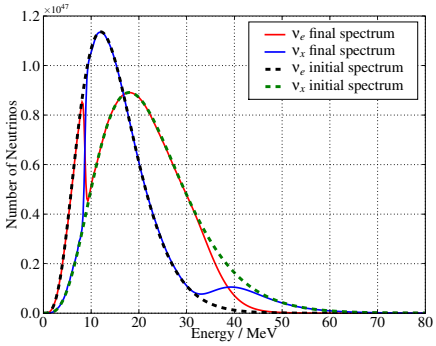

(c) Neutrino spectrum, $C = 1.0$.

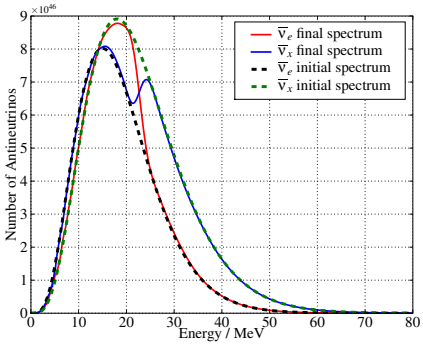

(d) Antineutrino spectrum, $C = 1.0$.

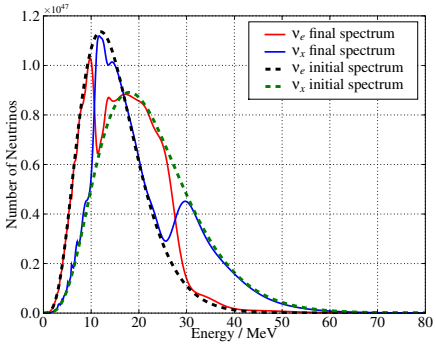

(e) Neutrino spectrum, $C = 2.0$.

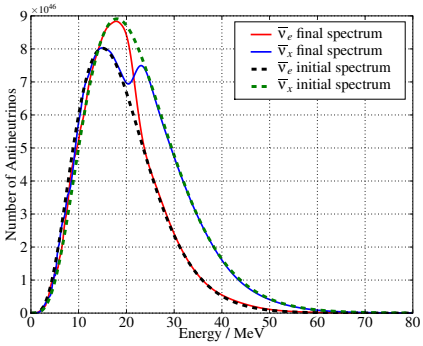

(f) Antineutrino spectrum, $C = 2.0$.

Figure 2.25: The neutrino and antineutrino spectra for the doubly-swapped spectrum after evolution for 400 km in a fluctuating neutrino background. The plots correspond to the neutrino density fluctuations plots shown in Figure 2.24 above.

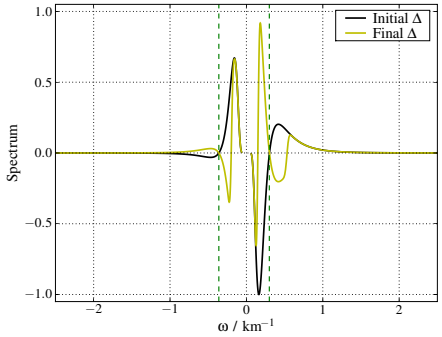

(a) $C = 0.1$

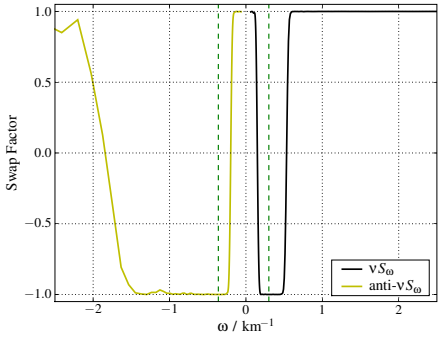

(b) $C = 0.1$

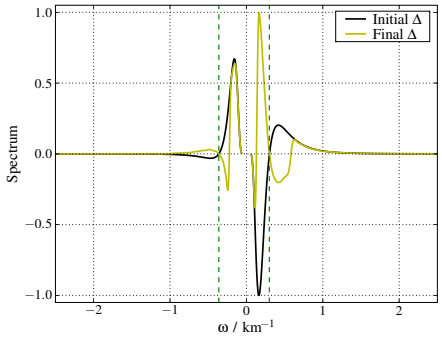

(c) $C = 1.0$

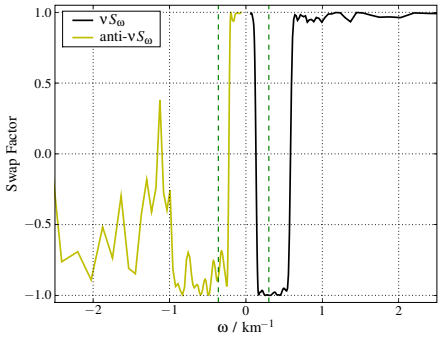

(d) $C = 1.0$

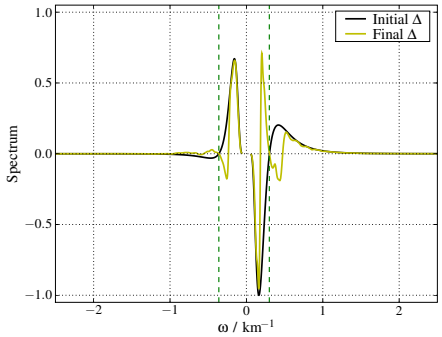

(e) $C = 2.0$

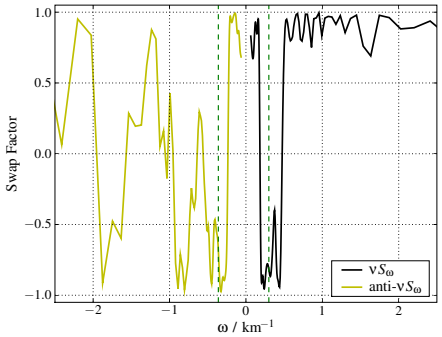

(f) $C = 2.0$

Figure 2.26: The neutrino difference spectrum and swap factor for the doubly swapped spectrum in fluctuating neutrino background densities with $C = 0.1$, 1.0, and 2.0 going down the page.

almost sinusoidal, smoothly curved at both their maxima and minima, rather than the dip and return shape seen in the early part of the evolution. This suggests that there is some strong interference or interaction between the two modes of evolution in this region.

The very last stage of the evolution beyond about 250 km is similar to the smooth case for the top two plots, although the exact order and final positions of several vectors are altered. The vectors decouple from the large-amplitude collective motion and steadily move towards a stable final state. However, in the $C = 2.0$ case the motion is rather less evenly-directed toward the final state. The vectors show an unusual evolution and continue to fluctuate well after the point where, on the other plots, the small-amplitude motions of the vectors that are superimposed on their overall motion towards the final state become smoothed out.

In all cases the neutrino modes are still strongly coupled, and although the maximum and minimum points of the collective motion are altered strongly almost all of the modes remain together until the last stage of the evolution. It is possible that this is an artifact of our single-angle approximation and the collective evolution would be completely destroyed in a similar multi-angle simulation, but it is nevertheless remarkable that the collective effects are so resilient even with very large alterations in the background potential.

The antineutrinos follow a somewhat similar pattern. The previous complex but smooth and regular evolution is upset by the fluctuations so that after the first collective dip and return the motion becomes highly irregular in all three plots. Once again, the motion becomes much more stable and smooth in the later stages, although the plots are less similar to the smooth background ones than the neutrino plots were, even after 250 km radius. There is also a disruption of the last stage of the evolution for the vectors that have final states near $\overline{\mathbf{P}}_z = +1$ in the region from 275 km onwards, just as in the neutrino plots.

One major difference in the highest fluctuation plot at the lower right of Figure 2.27 is in the motion of the lowest-energy vector. In all of the other plots with this spectrum it remains essentially fixed at $\overline{\mathbf{P}}_z = +1$ throughout the evolution. In the two other neutrino fluctuation plots it undergoes some small, high-frequency fluctuations and in the $C = 1.0$ case its final state is not exactly at $+1$. However, for $C = 2.0$ the vector falls with the rest of the ensemble apparently in association with the second collective dip, although this dip is very irregular and the low-energy vector falls significantly before the others. It

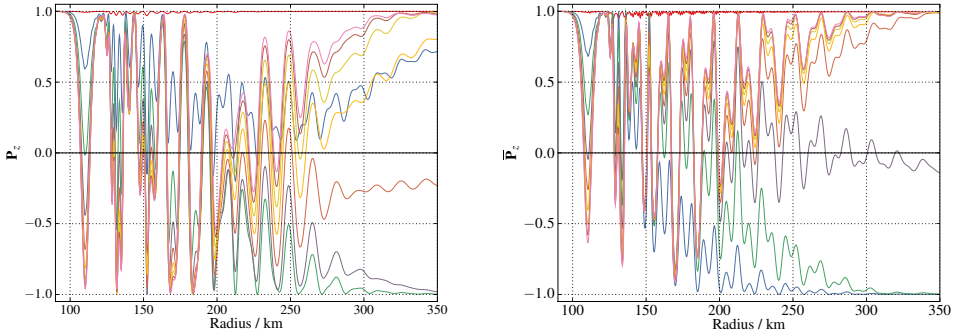

(a) $\mathbf{P}_z, C = 0.1$

(b) $\overline{\mathbf{P}}_z, C = 0.1$

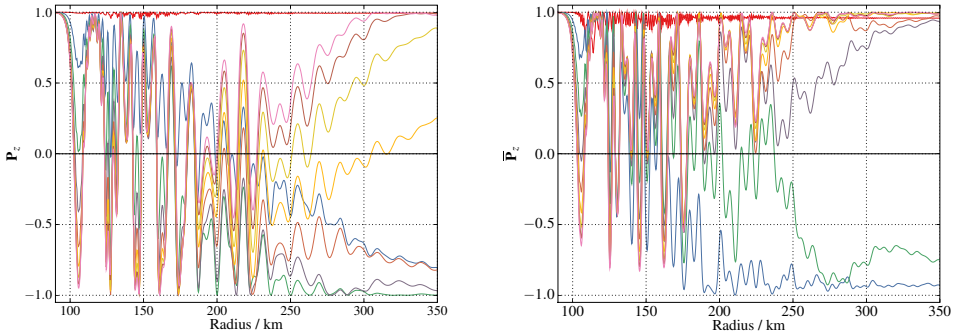

(c) $\mathbf{P}_z, C = 1.0$

(d) $\overline{\mathbf{P}}_z, C = 1.0$

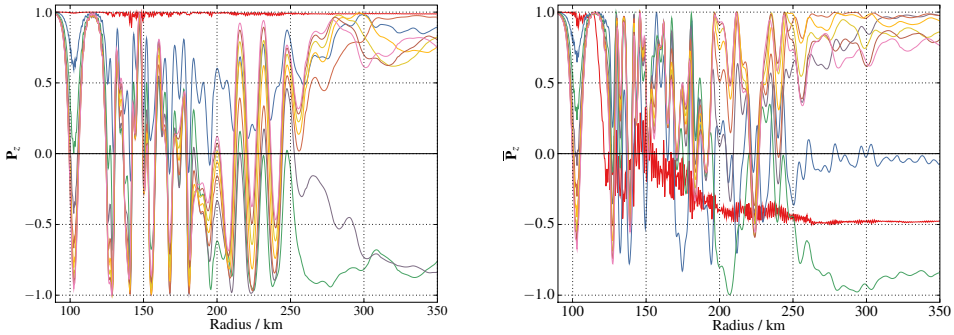

(e) $\mathbf{P}_z, C = 2.0$

(f) $\overline{\mathbf{P}}_z, C = 2.0$

Figure 2.27: The evolution of the polarization vectors $\mathbf{P}$ for neutrinos and in a fluctuating neutrino density with three different fluctuation amplitudes. The upper figures are for a background fluctuation amplitude $C = 0.1$, the middle figures are for $C = 1.0$, and the lower figures are for $C = 2.0$.

then undergoes a very unusual evolution and ends up with a stable value of about $\overline{\mathbf{P}}_z = -0.5$. In addition, the second-lowest energy vector has a final state of $\overline{\mathbf{P}}_z \simeq 0$ instead of being completely swapped to -1 as it was in the other cases.

The effect of a fluctuating neutrino background on the doubly-swapped spectrum is clearly much more complicated than in the singly-swapped case. The final state is significantly changed and the evolution itself shows new types of motion, unlike the singly-swapped case where all the motion could be understood relatively simply using an analogy with kicks to a gyroscopic pendulum. It is also striking in the doubly-swapped spectrum plots that the antineutrinos undergo very different evolution to the neutrinos in this ensemble. With the singly-swapped spectrum both neutrinos and antineutrinos appear to move in a very similar way as they evolve, with the differences being quite minor between the two sides of the plots. With this doubly-swapped spectrum the evolution of the neutrinos is only similar in the earliest and latest parts of the evolution, as the neutrinos go through sinusoidal motion that is not present in the antineutrinos. The motion of the antineutrinos suggests that there is interference between two out-of-phase collective oscillations which results in double peaks of varying amplitude being overlaid on the the simpler parametric oscillation shape.

2.11 Doubly Swapped Spectrum in Normal Hierarchy

In the simple argument explaining spectral swaps in subsection 1.5.3 the idea of the pendulum succumbing to the effect of the 'gravitational force' of the vacuum mixing vector and having a final state pointing roughly in the opposite direction is central. If we assume that the analogy still holds in this case, then we might expect very little to happen in the normal hierarchy because the system starts off at the minimum of the potential. This was indeed the case for the singly-swapped spectrum.

While the gyroscopic pendulum analogy was shown to be quite accurate for the singly-swapped spectrum in the inverted hierarchy, we have also seen that it cannot fully explain the behaviour of the doubly-swapped spectrum in the inverted hierarchy. Therefore it is important to investigate the behaviour of this spectrum in the normal hierarchy. We can also compare the predictions for the neutrino spectra that would be observed on Earth for the two different hierarchies, which may eventually lead to the determination of the hierarchy if

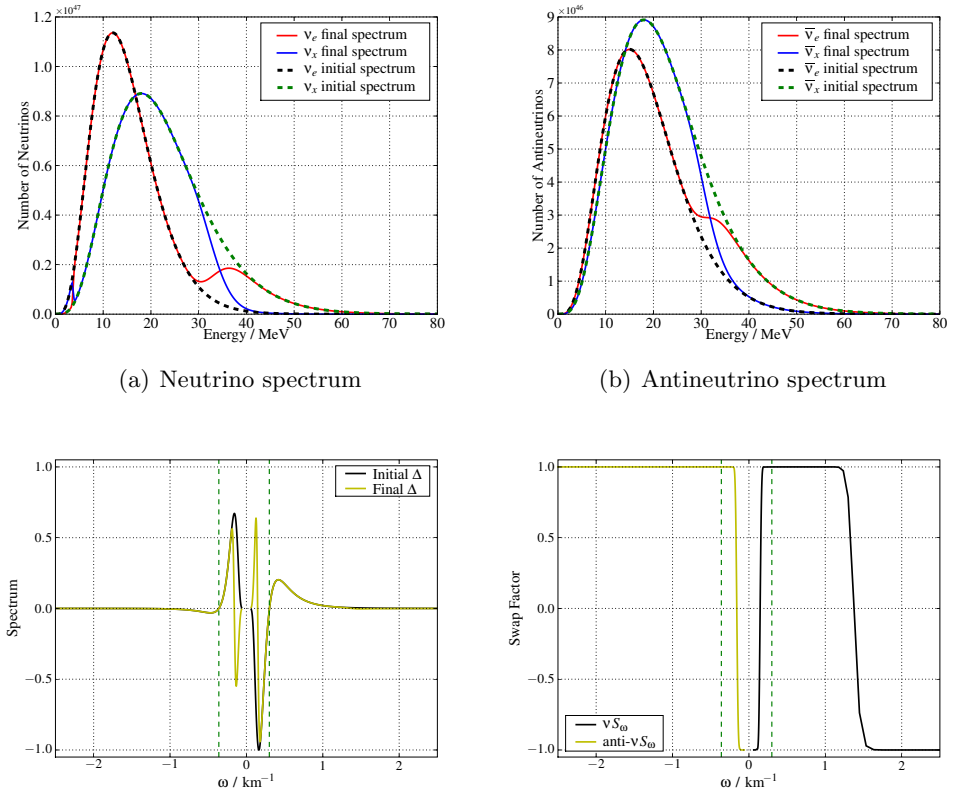

(a) Neutrino spectrum

(b) Antineutrino spectrum

(c) Difference spectra

(d) Swap factor

Figure 2.28: The doubly swapped neutrino and antineutrino spectra before and after evolution in the normal hierarchy with no matter background are shown in the upper panels. The neutrino difference spectrum and swap factor are shown in the lower panels.

a supernova fortuitously occurs in the Galaxy in the future.

2.11.1 No Matter Background

As before, we begin by examining the initial and final spectra and swap factor for evolution without a matter background. These are plotted in Figure 2.28. The most important point, as far as the behaviour in the normal hierarchy is concerned, is that we still see a spectral swap, though it resembles an inverse of the inverted hierarchy swap factor shown in Figure 2.19. The two separate swaps either side of $\omega = 0$ are replaced by a single swap centred on $\omega = 0$, with an additional swap at high frequency. The swaps in the inverted hierarchy

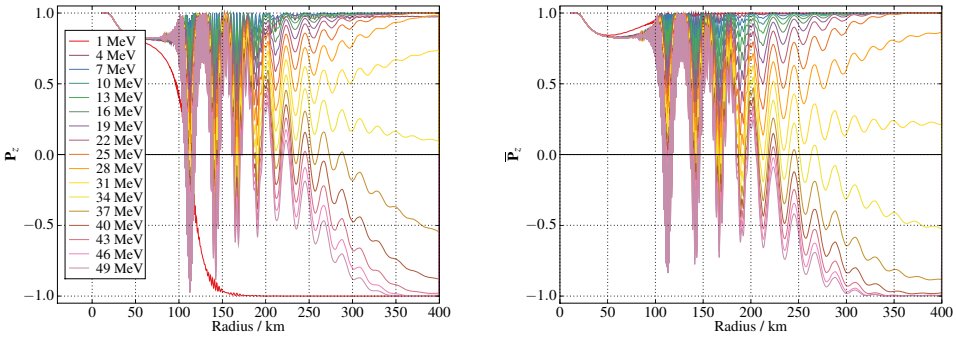

(a) $\mathbf{P}_z$ (b) $\overline{\mathbf{P}}_z$

Figure 2.29: The evolution of the $\hat{\mathbf{z}}$ component of the neutrino and antineutrino polarization vectors in the normal hierarchy with no matter background.

were centred on the crossing points of the difference spectrum. The swap here is centred on the asymptotic crossing point at $\omega = 0$, where the flux of all flavours tends to zero. Clearly there are still significant collective effects resulting in large neutrino flavour changes, although the simple picture of spectral swaps predicts no significant effect.

In [60] it is suggested that spectral swaps will occur in the inverted hierarchy at crossing points of the difference spectrum with positive slope, and in the normal hierarchy at crossing points with positive slope. The situation here agrees with their results for the same spectrum. The general principle is that swaps around the zero points of the difference spectrum provide a way for the ensemble to reach a lower total energy by swapping the flavours of a block of neutrinos of higher ω with an equal number of neutrinos of the opposite flavour with lower ω. The energy of the system is $\int \omega \mathbf{B} \cdot \mathbf{P}_\omega \, \mathrm{d}\omega$. In the normal hierarchy, this quantity can be decreased, for example, by the swap of energy of an electron neutrino with high ω with an x-type neutrino with low ω. The contribution of those two neutrinos to the energy of the system is initially $\omega_{\text{high}} - \omega_{\text{low}}$, which becomes $-(\omega_{\text{high}} - \omega_{\text{low}})$ after the exchange. Thus even when the overall $\mathbf{D}$ vector of the system starts oriented towards the minimum of the potential, changes within the ensemble can still occur, and these may decrease the total energy, for instance by altering the length of $\mathbf{D}$. This was the key insight of [51], discussed in subsection 1.5.3.

Examining the evolution of the individual polarization vectors in this sce-

nario, shown in Figure 2.29, we see that the evolution looks considerably different to what occurred in the inverted hierarchy. The main difference from the inverted hierarchy is that the vectors move together to a lower value of $\mathbf{P}_z$ almost immediately, and undergo very high-freqency oscillations in the middle period of the evolution. There is also one vector that falls to $\mathbf{P}_z = -1$ very soon after the motion starts. However, this odd motion does not occur in the presence of a smooth matter background, suggesting that it is an artifact of the unrealistic initial conditions. Nevertheless they are still interesting as they represent yet another possible mode of oscillation that can arise from the same equations of motion.

If the high-frequency oscillations are ignored, the evolution consists of fairly simple, smooth collective oscillations, which transition into the same final stage behaviour as we saw in the inverted hierarchy, though the particular vectors end up with different final values than they did before. The motion looks very similar in its essential features to the inverted hierarchy case, but the vectors return much more consistently to their initial $\mathbf{P}_z = +1$ position instead of gradually falling away from this maximum as they do in the inverted hierarchy.

2.11.2 Smooth Matter Background

Adding a smooth matter background removes the high-frequency oscillations and the early fall of the system, and makes the evolution extremely regular. In the spectrum and swap factor shown in Figure 2.30, the only difference from the no matter case is that the swap in neutrinos at high ω has vanished, so the flavour change is now entirely in the central peak. The width of this swap remains exactly the same as before.

We can see from the plots of the polarization vectors in Figure 2.31 that the evolution consists of large-amplitude parametric swaps whose maxima gradually decrease from $\mathbf{P}_z = +1$ for the vectors that end up with swapped flavours. Most of the vectors oscillate with gradually decreasing amplitudes until they return to their initial state with $\mathbf{P}_z = +1$. The vectors that swap follow similar paths to the vectors in the singly-swapped inverted hierarchy case, except that the amplitudes and periods of the oscillations overlaid on their gradual fall are much larger. It is also notable that the evolution of the antineutrinos looks almost exactly the same as the evolution for neutrinos.

Comparing with the inverted hierarchy, the evolution of the system in the

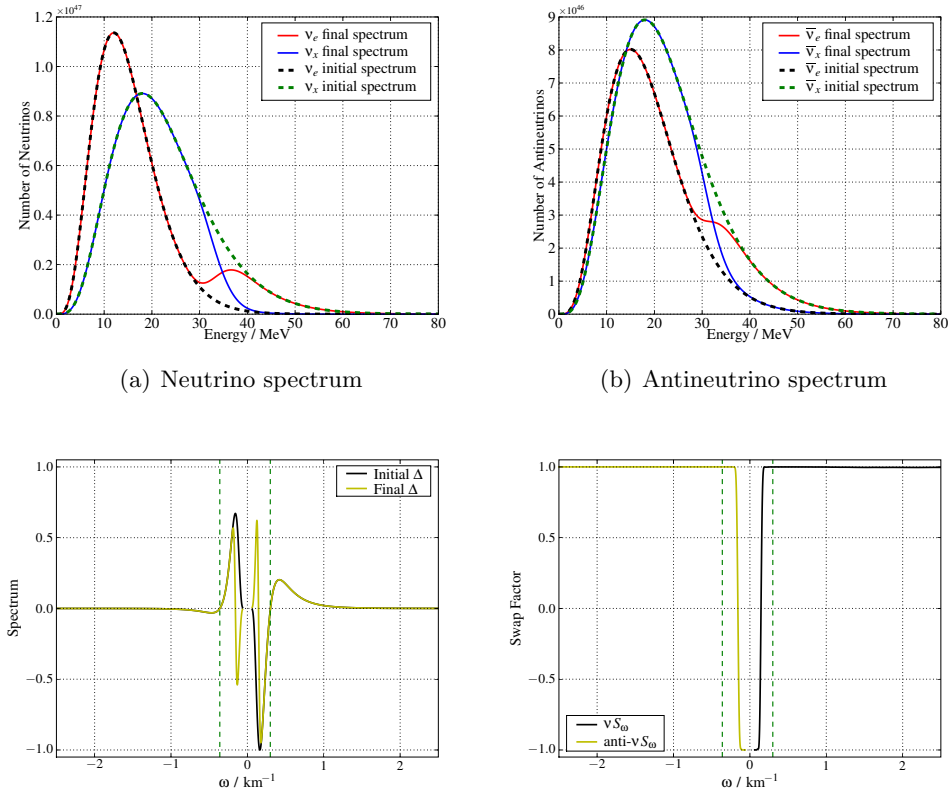

(a) Neutrino spectrum

(b) Antineutrino spectrum

(c) Difference spectra

(d) Swap factor

Figure 2.30: The neutrino and antineutrino spectra (in the top panels) for the doubly swapped spectrum in the normal hierarchy after evolution for 400 km through a smooth matter background. The neutrino difference spectrum and swap factor are shown in the lower panels

normal hierarchy is similar in the early region before the critical value of μ is reached. Oscillations begin at close to the same radius, and though the very gradual decline in the maxima of the first few oscillations caused by the decrease in μ in the inverted hierarchy is not present the motion has the same period. This is consistent with our theoretical understanding of the resonant oscillations, which do not depend on the hierarchy. In the normal hierarchy the gyroscopic pendulum motion does not occur at all, and all of the flavour change is due to the same form of motion that causes the evolution in the inverted hierarchy to start well before the critical density for the pendulum is reached.

As compared to the singly-swapped spectrum, the addition of a matter background this spectrum in inverted hierarchy caused a much larger delay in the

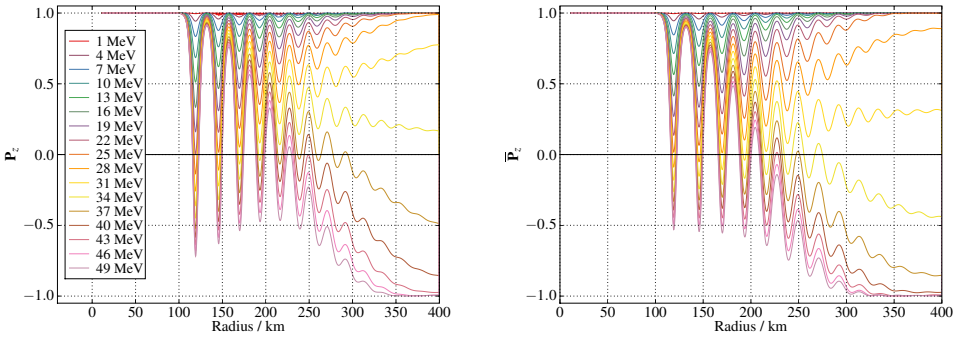

(a) $\mathbf{P}_z$ (b) $\overline{\mathbf{P}}_z$

Figure 2.31: The evolution of the $\hat{\mathbf{z}}$ component of the neutrino and antineutrino polarization vectors for the doubly swapped spectrum in the normal hierarchy with a smooth matter background.

onset of oscillations. In contrast, we find that the matter background causes no shift in the oscillation peaks in the normal hierarchy. Nevertheless, the motion of the system in the early stages of the evolution looks very similar in both hierarchies. If the delayed onset of oscillations is due to the gyroscopic pendulum argument given in subsection 1.4.7 then it appears that the initial position of the pendulum does affect the resonant motion even when the neutrino density is well above the critical value for the pendulum to begin its fall. Whatever the explanation, it is clear from our results that the simple three-mode model of parametric resonance does not fully describe the motion of the doubly-swapped neutrino spectrum in decreasing matter and neutrino backgrounds, and that there is a complicated interaction between the resonant swapping, the matter background term and the flavour gyroscope which results in the matter background having an influence on the resonant oscillations only in the inverted hierarchy.

2.11.3 Matter Background Fluctuations

The addition of matter density fluctuations has almost no visible effect on the evolution of this spectrum in the normal hierarchy. Both the final spectra and resulting swap factor and the evolution of the polarization vectors remain almost identical to the smooth background case. There is a very small shift of the final neutrino states at high energies. This shift is interesting because neutrino

fluctuations also have more of an effect on the neutrino side of the spectrum as will be shown in the next section, in contrast to the inverted hierarchy where the spectral alterations were typically stronger in the antineutrino side.

As with the lack of delay induced by the matter background discussed above, it is curious that matter background fluctuations have no effect in the normal hierarchy, even though they significantly altered the inverted hierarchy spectrum and caused a significant shift in the position of the resonant periods. Looking in detail at the changes in the spectrum, however, shows that the only significant effect in the inverted hierarchy was to extend the range of the antineutrino swap to larger negative frequencies. The central unswapped region remains exactly the same, just as it does for the normal hierarchy. So even though the final states of these low-frequency neutrinos are different, the effect of the matter background fluctuations upon them is identical for both hierarchies. The high-frequency parts of the spectrum are evidently more strongly influenced by the gyroscopic pendulum motion that only occurs in the inverted hierarchy. It appears that the matter background, the gyroscopic pendulum, and the parametric resonance interact in a rather complex way in the inverted hierarchy. In the normal hierarchy the stability of the gyroscopic pendulum quashes the effects of matter fluctuations on the pendulum motion and the consequent interactions with the resonant oscillations are also removed.

2.11.4 Neutrino Background Fluctuations

As in the inverted hierarchy, adding fluctuations to the neutrino background has a significant effect on the evolution of the neutrino flavours and the spectra. We plot the swap factor obtained from two simulations with different fluctuation amplitudes in Figure 2.32. The central swap appears to be starting to split in two at low frequency, which is reminiscent of the effect of neutrino fluctuations on the singly-swapped spectrum shown in Figure 2.12. The width of the swap is not affected and its edges remain sharp, but at higher ω the swap factor shows deviations from $+1.0$ which increase with higher neutrino background fluctuation amplitude. As noted in the previous section, the largest effect is on the neutrino side of the plot in this case, as opposed to the antineutrino side in the inverted hierarchy.

The effect of the neutrino background fluctuations on the evolution of the polarization vectors is similar to that seen for the same spectrum in the inverted

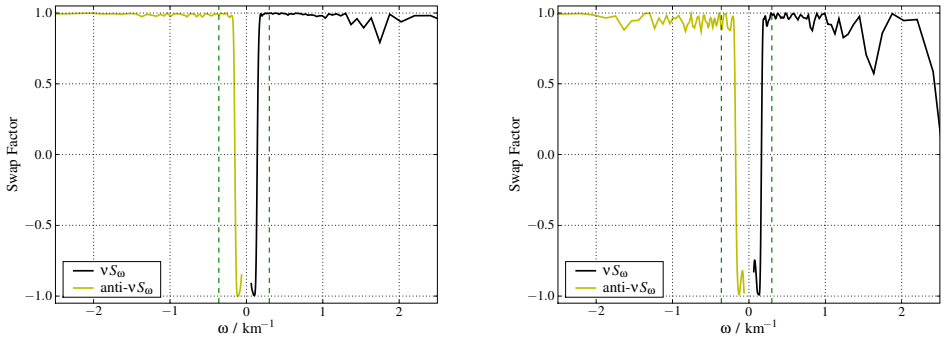

(a) $C = 1.0$ (b) $C = 2.0$

Figure 2.32: Swap factor for the doubly-swapped spectrum in the normal hierarchy with neutrino background fluctuations added with two different values of the fluctuation amplitude parameter C.

hierarchy. Examining Figure 2.33 we see that the start of the evolution occurs at a lower radius for larger amplitude fluctuations. The smoothness of the large-amplitude collective swaps is also progressively disrupted, and the lowest-energy mode undergoes a strange evolution that does not follow the rest of the ensemble. The neutrino and antineutrino modes evolve very similarly, even in their more chaotic motions, which is in contrast to the inverted hierarchy where the two plots looked quite different and did not seem to be particularly closely related. A spread of the final states from completely polarized flavour eigenstates is also apparent.

2.12 Summary

We have studied two different examples of realistic neutrino spectra in the two-flavour, single-angle approximation, and examined the effects of fluctuations in the density of both matter and neutrinos on the flavour evolution and final states. We believe this to be the first detailed study of the effect of small-scale matter and neutrino density fluctuations on the two quite different collective neutrino systems chosen.

We have reproduced previous results for smooth matter and neutrino backgrounds and have found several new effects that result from matter density fluctuations and particularly neutrino density fluctuations. Some of these effects, such as the behaviour of the singly-swapped spectrum in a fluctuating

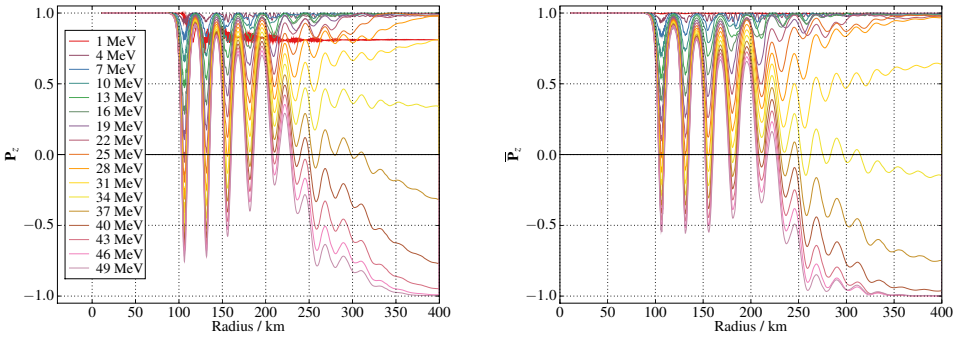

(a) $\mathbf{P}_z$ (b) $\overline{\mathbf{P}}_z$

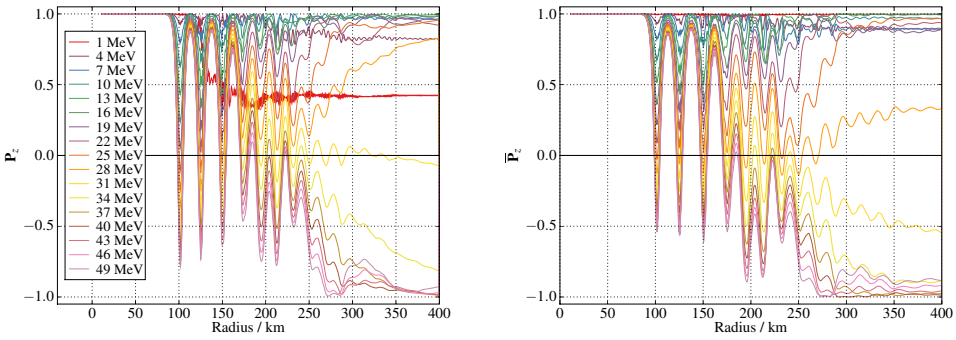

(c) $\mathbf{P}_z$ (d) $\overline{\mathbf{P}}_z$

Figure 2.33: The evolution of the $\hat{\mathbf{z}}$ component of the neutrino and antineutrino polarization vectors for the doubly swapped spectrum in normal hierarchy with a fluctuating neutrino background.

neutrino background, can be understood in the framework of the well-studied gyroscopic pendulum solutions, but we do not believe that current theoretical solutions can explain the details of the effects on the final spectrum. In the doubly-swapped spectrum the mixture of parametric resonance and simple gyroscopic pendulum swapping behaviour and the study of the relative influence of density fluctuations on each type of motion is also quite novel.

Together with previous results on the effects of matter turbulence in regions where collective neutrino effects are negligible, it appears that matching analytic expectations of the neutrino flavour transformations in smooth backgrounds with the neutrino spectra that are likely to arrive at Earth from a realistically chaotic supernova background will be difficult.

For the first example, which was chosen as an example of a spectrum with a single spectral swap in its final state, we find that the motion of the neutrino vectors can be very well explained by the gyroscopic pendulum analogy. The system acts like a pendulum with a spinning bob, with the neutrino density acting as the bob's spin. As the neutrino density falls, the pendulum falls from its upright initial position to a downward pointing final state in flavour space. The final state, with a single broad spectral swap, is the lowest-energy state that conserves both lepton number and energy in the neutrino ensemble. The evolution of the vectors is very similar to that of the simple single-energy gyroscopic pendulum studied in subsection 1.4.6.

Fluctuations in the matter background density have little effect on the final spectrum, and only a small effect on the intermediate motion of the flavour vectors. The high-frequency oscillations about the slowly-falling average position of the vectors are suppressed by matter fluctuations, and the spectral swap extends to higher-energy antineutrinos. Both spectra follow the same pattern in the broadening of the antineutrino side of the swap: a smooth matter background produces the narrowest swap, followed by no matter background, with matter fluctuations causing the broadest swap. This suggests that the effect is solely due to adiabaticity violation effects. The smooth matter background has a similar effect to a decrease in the mixing angle, which makes the motion more adiabatic, while large enough matter fluctuations add to the adiabaticity violation.

Neutrino density fluctuations have a stronger effect on the evolution than matter fluctuations, but the final spectra still retain most of the same general features. In the highest-fluctuation cases the broad, sharp swap becomes very irregular and it partially splits in two around $\omega = 0$. The evolution is very strongly affected, which we explain by viewing the density fluctuations as impulses upsetting the pendulum's motion by sudden additions or reductions in the kinetic energy term, which depends on the neutrino density. However, we also see that the system is unable to settle into its previous final state even when these fluctuations die away. We presume that this effect is the result of adiabaticity violation which causes the approximate equations of motion and the equations for the energy of the ensemble to become somewhat inaccurate.

In the normal hierarchy, the ensemble begins at the minimum of energy and we find that there is no motion of any of the modes, even in the presence of large-amplitude background fluctuations.

For the doubly-swapped spectrum, the major difference in evolution is that the flavour oscillations begin well before the gyroscopic pendulum analogy predicts. They are also of far larger amplitude and longer period than the motions in the first spectrum. This suggests that the ensemble undergoes a combination of parametric resonance oscillations and gyroscopic pendulum motion. This is supported by the abrupt change in the evolution that occurs when the critical neutrino density for the gyroscopic pendulum is crossed. The parametric motion dies away faster than the pendular motion, and the final portion of the evolution is similar to that of the singly-swapped spectrum.

The endpoint of this evolution is a spectrum with two spectral swaps. Each occurs around a zero point in the difference spectrum where the slope is negative, as predicted by the resonant swapping model of Dasgupta *et al.* [60]. As mentioned, the effect of matter density fluctuations on the final spectrum in this case is roughly similar to the behaviour of the singly-swapped spectrum. However, the effect on the intermediate motion of the neutrino vectors is more complex, and the heights of many of the oscillation peaks are altered.

Neutrino density fluctuations have a pronounced effect on both the final state and the evolution of the doubly-swapped spectrum. The swap factor becomes increasingly irregular and disorderly on the antineutrino side as the amplitude of the fluctuations is increased, with the swap becoming almost unrecognizable under random-looking variations. On the neutrino side the effect is similar, but much smaller in amplitude, and the swap remains mostly intact even with very large amplitude neutrino fluctuations.

The evolution in the presence of neutrino density fluctuations is extremely chaotic, with only the first large amplitude resonant swap remaining unaffected. The motion in the final stages of the evolution is similar to the smooth background case, but the motion in the intermediate phase becomes extremely complex. The motion is a combination of random kinetic energy kicks to the gyroscopic pendulum and large-amplitude parametric resonance motion, but still shows some smoothness and periodicity in comparison to the equivalent plots for the singly-swapped spectrum.

In the normal hierarchy, the doubly swapped spectrum still undergoes some flavour changes, but there is only one swap and it is centred on the zero of the difference spectrum with positive slope at $\omega = 0$. There appears to be no gyroscopic pendulum-type motion in this case, and the motion does not significantly change after the 150 km critical density point. Because the pendulum analogy

suggests that the system starts in the minimum of potential, the motion must be entirely due to parametric resonance oscillations that allow internal motion of the neutrino vectors even though the neutrino pendulum is not moving.

Matter background fluctuations have only extremely tiny effects on the evolution and the spectrum in this case, but neutrino density fluctuations do have a significant effect. The changes in the swap factor are similar to those seen in the inverted hierarchy, but in this hierarchy they are much more pronounced on the neutrino side rather than the antineutrino side. The fluctuations add high-frequency, small-scale fluctuations to the first few periods of the evolution, and also cause some additional disruption to some of the minima and maxima of the oscillations, but the effect is much less pronounced than in the inverted hierarchy.

Chapter 3

Parametric Oscillations in the Earth

In this chapter we examine the theory of neutrino oscillations in the Earth. In particular, we consider the strong resonant effects of the core-mantle boundary on oscillations of atmospheric neutrinos with energies between 5 and 25 GeV, and the possibility of using the Deep Core extension to the Ice Cube detector to measure them. Independently, Mena *et al.* [41] considered the effect of the neutrino mass hierarchy on the atmospheric neutrino signals expected in the detector, and found that a measurement of the hierarchy using Deep Core may be possible. We build upon their results using updated detector data and consider the effects of the Earth density model on neutrino oscillations in the detector's sensitive energy range, and how these might affect the hierarchy sensitivity. Several approximate methods of calculating the atmospheric neutrino oscillation probabilities are considered and compared.

3.1 Neutrino Oscillations and the Matter Effect

In vacuum, the oscillations of neutrinos are dependent on two Δm^2 values, usually called the Solar and atmospheric mass squared differences. As the names suggest, in most cases only one of these mass squared differences is important and we can describe neutrino oscillations using a two-state approximation. In dense matter coherent forward-scattering of neutrinos through weak interactions with electrons affects the potential energies of the mass eigenstates, which leads to significant modifications of the survival probabilities of different neutrino flavours as compared to the vacuum formulae. As described in section 1.2, the Hamiltonian describing two-state neutrino oscillations in matter can be can be

written as [43]:

$$\mathcal{H} = \frac{\Delta m^2}{4E_\nu} \begin{bmatrix} -\cos 2\theta_V & \sin 2\theta_V \\ \sin 2\theta_V & \cos 2\theta_V \end{bmatrix} + \frac{V(x)}{2} \begin{bmatrix} 1 & 0 \\ 0 & -1 \end{bmatrix}, \tag{3.1}$$

where $V(x)$ is the matter-induced potential which can depend on position, θ_V is the mixing angle in vacuum and E_ν is the neutrino energy. It is clear from this equation that if the $V(x)$ term is of a similar order to the vacuum term the flavour evolution of the neutrinos will be significantly altered.

The Solar MSW effect is the best-known instance of this matter effect. It predicts that because of the large matter density in the Sun's core, the electron neutrinos created in the centre of the Sun are simultaneously in an electron flavour eigenstate and an eigenstate of the Hamiltonian containing the matter potential. Since the matter potential term is diagonal and is much larger than the vacuum term at the centre of the Sun, and furthermore varies slowly and smoothly with radius, the neutrinos remain in the same mass eigenstate from their creation until their exit from the Sun into the vacuum. Once in the vacuum, this mass eigenstate does not oscillate because it is an eigenstate of the vacuum Hamiltonian. The result is that the fraction of solar neutrinos which are detected on Earth as electron neutrinos is smaller than would be possible if the neutrinos were created in a vacuum, even with a large mixing angle. This effect explains the Solar neutrino problem.

The matter effect also applies to neutrinos passing through the Earth, though in a different way. Atmospheric neutrinos are created in a vacuum flavour state and as they pass through the Earth they undergo weak scattering interactions with electrons just as Solar neutrinos do. In the Earth, however, the assumption that the density changes slowly enough to allow an adiabatic approximation does not hold. According to the Preliminary Reference Earth Model (PREM) shown in Figure 3.1, the density of the Earth changes very rapidly from around 5.5 g cm^{-3} in the mantle to 9.9 g cm^{-3} in the core within about 500 metres at a radius of 3480 km. [72, 73]. This sharp change can have a large effect on oscillation probabilities in certain energy ranges, due to parametric resonances resulting from the chance relationship between the oscillation phases and frequencies in the core and mantle layers that results from Earth's particular density profile and the size of the neutrino mixing parameters.

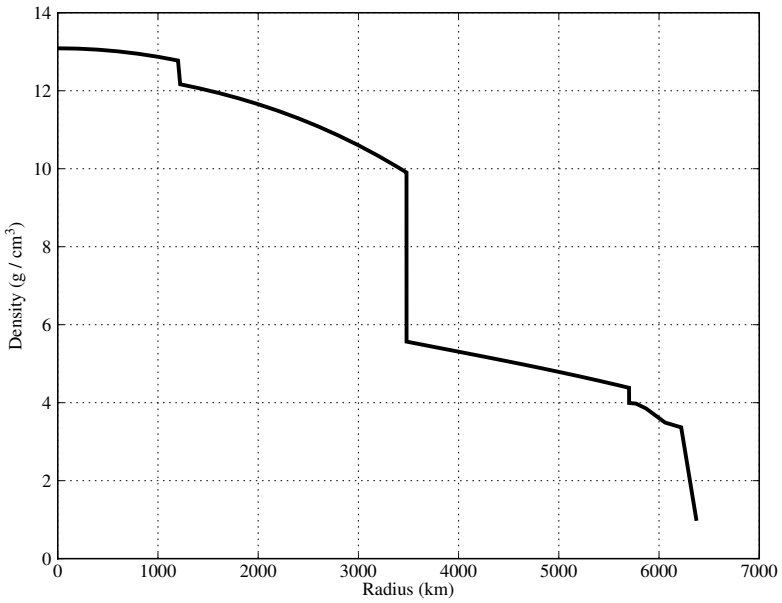

Figure 3.1: The Preliminary Reference Earth Model (PREM) values for the density of the Earth as a function of radius. The density changes abruptly at the boundary between the core and the mantle at a radius of about 3500 km.

3.2 Parametric Resonance

Following Akhmedov *et al.* [30], we will derive an approximate solution to the evolution of the the neutrino flavour. We use the Hamiltonian in Equation 3.1 and approximate the Earth's structure as being a central core of constant density ρ_{core} surrounded by a mantle with a lower density ρ_{mantle}.

We begin by defining an evolution matrix $S(x)$ such that $S(x)\psi(0) = \psi(x)$. This matrix must solve the equation

$$i\frac{\mathrm{d}S(x)}{\mathrm{d}x} = H(x)S(x), \tag{3.2}$$

where we write the Hamiltonian as

$$H(x) = \frac{V(x)}{2}\begin{pmatrix} 1 & 0 \\ 0 & -1 \end{pmatrix} + \omega_V \begin{pmatrix} -\cos 2\theta_V & \sin 2\theta_V \\ \sin 2\theta_V & \cos 2\theta_V \end{pmatrix}, \tag{3.3}$$

where the vacuum oscillation frequency $\omega_V = \Delta m^2/4E_\nu$. Although in dense

matter $V(x)$ is much larger than ω_V, over the full distance of travel through the Earth the product of the off-diagonal terms in the vacuum matrix with the path length becomes significant, and cannot be simply ignored. To simplify the equations, we split the Hamiltonian into two parts,

$$H_0 = \omega_{\rm mat}(x) \begin{pmatrix} 1 & 0 \\ 0 & -1 \end{pmatrix}, \qquad H_I = \omega_V \sin 2\theta_V \begin{pmatrix} -\epsilon & 1 \\ 1 & \epsilon \end{pmatrix}, \tag{3.4}$$

where $\pm\omega_{\rm mat}(x)$ are the eigenvalues of $H(x)$ and are the oscillation frequencies in matter. The value of $\omega_{\rm mat}(x)$ in terms of the other parameters is

$$\omega_{\rm mat}(x) = \sqrt{(V(x)/2 - \omega_V \cos 2\theta_V)^2 + \omega_V^2 \sin^2 2\theta_V}. \tag{3.5}$$

Note that the value of $\omega_{\rm mat}$ depends on position through the matter density term V. The remaining term, H_I, is found by subtracting H_0 from the total Hamiltonian, which results in

$$\epsilon(x) = \frac{\omega_V \cos 2\theta_V - V(x)/2 + \omega_{\rm mat}(x)}{\omega_V \sin 2\theta_V}. \tag{3.6}$$

From the definition of $\omega_{\rm mat}$ we know that

$$\left(\frac{\omega_{\rm mat}}{\omega_V \sin 2\theta_V}\right)^2 = 1 + \eta^2, \tag{3.7}$$

where

$$\eta \equiv \frac{V/2 - \omega_V \cos 2\theta_V}{\omega_V \sin 2\theta_V}, \tag{3.8}$$

so assuming that we are not close to an MSW resonance where $V/2 \simeq \omega_V \cos 2\theta_V$ the magnitude of η will be large, and

$$\frac{\omega_{\rm mat}}{\omega_V \sin 2\theta} \simeq \eta + \frac{1}{2\eta}. \tag{3.9}$$

Writing $\epsilon = -\eta + \omega_{\rm mat}/\omega_V \sin 2\theta_V$ we see that in the off-resonance region we have

$$\begin{aligned} \epsilon &\simeq \frac{1}{2\eta} = \frac{\omega_V \sin 2\theta}{V - 2\omega_V \cos 2\theta} \\ &\simeq \frac{\omega_V}{V} \sin 2\theta. \end{aligned} \tag{3.10}$$

Therefore ϵ is indeed a small parameter as long as the neutrino energy is high enough for V to be larger than ω_V and the MSW condition is not met. The off-diagonal terms in the two parts of the Hamiltonian are in the ratio $\omega_V \sin 2\theta/\omega_{\text{mat}}$, which we define to be equal to $\sin 2\theta_{\text{mat}}$, where θ_{mat} is an effective mixing angle in matter. Because ω_{mat} will typically be of the same order as V and $V \gg \omega_V$, the value of θ_{mat} will be much less than one, and because $\epsilon \approx \sin 2\theta_{\text{mat}}$ in this regime the diagonal terms in H_I are of an even smaller order. Therefore, as long as $\sin 2\theta_{\text{mat}} \ll 1$ only the off-diagonal terms in H_I need to be considered at first order, and they are small enough to be treated as a perturbation to H_0.

We can now find approximate solutions to Equation 3.2 by writing $S = S_0 S_I$ with S_0 a solution to the evolution equation with H_0 as the total Hamiltonian. This base solution is found by first integrating the total phase change over the path of the neutrino. This phase change is

$$\phi(x) = \int_0^x \omega_{\text{mat}}(x')\,\mathrm{d}x', \tag{3.11}$$

and leads to a fairly simple solution for S_0:

$$S_0(x) = \begin{pmatrix} e^{-i\phi(x)} & 0 \\ 0 & e^{+i\phi(x)} \end{pmatrix}. \tag{3.12}$$

This solution represents the change in the oscillation phase angle during the path if the matter density is taken to have a constant value averaged over the path. This is often called the adiabatic phase change. The perturbation term contains the effect of changes in the matter density along the path. Inserting $S = S_0 S_I$ into Equation 3.2 we find

$$i\frac{\mathrm{d}S_I}{\mathrm{d}x} = S_0^{-1} H_I S_0 S_I = \tilde{H}_I S_I. \tag{3.13}$$

The Hamiltonian $\tilde{H}_I = S_0^{-1} H_I S_0$ is now in the form of a standard perturbation Hamiltonian in the interaction picture. Therefore we can find a solution of the form $S_I = I + S_I^{(1)} + \cdots$ by the usual iterative method. The lowest order term will be equal to

$$S_I \simeq I - i\int_0^L \tilde{H}_I(x')\,\mathrm{d}x'. \tag{3.14}$$

When we substitute in the matrices from the various expressions above, we find

the expression for the total evolution matrix to be

$$S(L) = S_0(L)\left[I - i\omega_V \sin 2\theta_V \int_0^L \begin{pmatrix} 0 & e^{i2\phi(x)} \\ e^{-i2\phi(x)} & 0 \end{pmatrix} \mathrm{d}x\right]. \tag{3.15}$$

Because we are interested in flavour change, we want to find the amplitude of the off-diagonal term in this matrix, which is

$$P(\nu_e \leftrightarrow \nu_{\mu,\tau}) = \omega_V^2 \sin^2 2\theta_V \left|\int_0^L e^{-i2\phi(x)}\,\mathrm{d}x\right|^2. \tag{3.16}$$

We will label this transition probability henceforth by P_2. We can simplify this equation slightly by using the fact that the density profile is symmetric about the point closest to the core, so the integral only needs to be done from $x = 0$ to $x = L/2$. Furthermore, the antisymmetric $\sin 2\phi(x)$ part of the exponential terms cancels, so the probability becomes

$$P_2 = 4\omega_V^2 \sin^2 2\theta_V \left(\int_0^{L/2} \cos 2\phi(z)\,\mathrm{d}z\right)^2, \tag{3.17}$$

where we have defined a new integration variable $z = x - L/2$ which runs from 0 at the middle of the trajectory to $\pm L/2$ at the ends.

To simplify this expression, we can use the fact that $\mathrm{d}\phi(z)/\mathrm{d}z = \omega(z)$ and

$$\frac{\mathrm{d}}{\mathrm{d}z}\sin 2\phi(z) = \frac{\mathrm{d}\phi(z)}{\mathrm{d}z} 2\cos 2\phi(z) \tag{3.18}$$

to integrate Equation 3.17 by parts. The result is

$$P_2 = \sin^2 2\theta^0_{\mathrm{mat}}\left[\sin\phi_L + \omega_0 \int_0^{L/2} \frac{1}{\omega^2_{\mathrm{mat}}}\frac{\mathrm{d}\omega_{\mathrm{mat}}}{\mathrm{d}z}\sin 2\phi(z)\mathrm{d}z\right]^2, \tag{3.19}$$

where ω_0 represents the value of $\omega_{\mathrm{mat}}(z)$ at $z = L/2$, that is, at endpoints of the neutrino path. ϕ_L is equal to $2\phi(L/2)$, which is the same as the total adiabatic phase change. $\sin 2\theta^0_{\mathrm{mat}}$ is defined as $\omega_V \sin 2\theta_V/\omega_0$. The perturbation approximation has provided the standard adiabatic phase change term $\sin^2 2\theta^0_{\mathrm{mat}} \sin^2\phi_L$ plus a correction that depends on the rate of change of ω_{mat}.

As noted above, the density of the Earth can be well-approximated as two shells, core and mantle, with a sharp change in density at the boundary. There-

fore we can integrate Equation 3.19 by assuming that $\mathrm{d}\omega_{\mathrm{mat}}/\mathrm{d}z$ is only significant in this thin boundary layer. If we define ω_m and ω_c to be the values of ω_{mat} in the mantle and core, and ϕ_m and ϕ_c to be the adiabatic phase integrated through each of these layers separately, the probability becomes

$$P_2 = \sin^2 2\theta_m \left[\sin(\phi_c + 2\phi_m) - \frac{\omega_0}{\omega_m}\left(1 - \frac{\omega_m}{\omega_c}\right)\sin\phi_c\right]^2, \tag{3.20}$$

where θ_m is the matter mixing angle in the mantle. From this expression we can see that the transition probability depends strongly on the relative size of the phases ϕ_c and ϕ_m. If these angles are such that $\sin\phi_c = -\sin(\phi_c + 2\phi_m) = \pm 1$ then there will be a maximum of the transition probability. This is a resonance condition that involves many variables including the structure the Earth and the neutrino mixing parameters and energy. Using the PREM density profile and current best-fit neutrino parameters the resonance condition is satisfied for atmospheric neutrinos passing through the Earth's core, and results in an enhancement of the probability $P(\nu_e \rightarrow \nu_{\mu,\tau})$ of more than a factor of two in the energy range from about 5 GeV to 15 GeV. The resonance effect depends strongly on the Earth's density profile, so measurements of the oscillation probabilities in this energy range for long-baseline atmospheric experiments provide a way to both measure the structure of the Earth and test of neutrino oscillation theory.

The transition probability P_2 as a function of $\cos\Theta$, where Θ is the neutrino zenith angle, is shown in Figure 3.2 with and without the first-order non-adiabatic correction. The effect of the correction term is to significantly amplify the oscillation probabilities of the neutrinos which pass through the core. There are two peaks, one near the edge of the core and one near the centre, where the oscillation probability is approximately doubled compared to the probability calculated assuming an adiabatic density variation.

3.2.1 The Muon Neutrino Survival Probability

The transition probability P_2 calculated in the previous section is for the transformation $\nu_e \leftrightarrow \nu_{\mu,\tau}$. However, studies of the atmospheric neutrino flux in the relevant energy range (roughly 10–50 GeV) find that the flux ratio

$$\frac{F_{\nu_\mu} + F_{\overline{\nu}_\mu}/2}{F_{\nu_e} + F_{\overline{\nu}_e}/2} \tag{3.21}$$

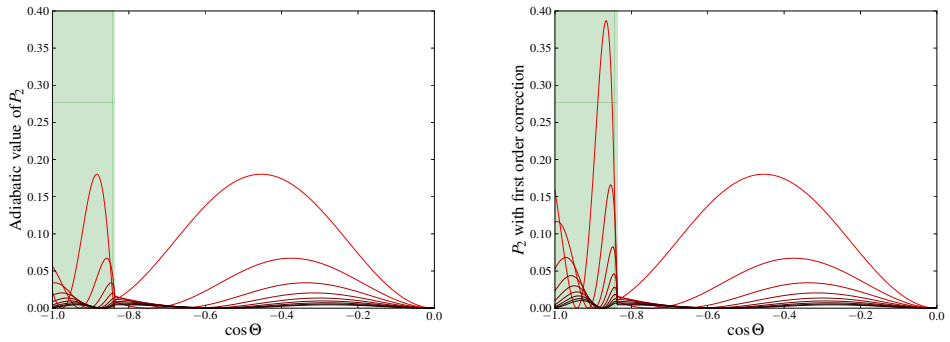

Figure 3.2: Neutrino oscillation probabilities in the Earth. Each line is for a single neutrino energy, ranging from 8 to 32 GeV in 3 GeV intervals from top to bottom. For higher energy neutrinos P_2 is negligible. The shaded region is the range of zenith angles for which the neutrino path crosses the Earth's core. The left-hand figure is the adiabatic probability, while the right-hand figure includes the first order correction term in Equation 3.20.

is around 3 at 10 GeV, increasing to 4.5 at 30 GeV [74–76]. Large neutrino detectors such as Deep Core, which is described in more detail below, are also much more suited to detecting the longer paths produced by muons in the ice than the more compact electromagnetic cascades created by electron neutrino interactions. Therefore it is the survival probability $P(\nu_\mu \rightarrow \nu_\mu)$, rather than the appearance probability, that is the most important parameter for this type of detector.

To calculate the survival probability, and obtain more accurate results for this analysis as a whole, we have used the framework described by Akhmedov *et al.* in a series of papers [31–34]. To accurately calculate the muon neutrino survival probability the $\nu_{\mu,\tau}$ mixed state must be decomposed into the true flavour states. In full, the three-flavour neutrino Hamiltonian in matter can be written as

$$H(x) = \frac{UM^2U^\dagger}{2E_\nu} + V(x), \tag{3.22}$$

where U is the standard neutrino mixing matrix (see for example [43]), $M^2 = \mathrm{diag}(0, \Delta m^2_{12}, \Delta m^2_{13})$ and $V(x) = \mathrm{diag}(V(x), 0, 0)$ where the matter term $V(x) = \sqrt{2}G_F N_e(x)$ as usual. Fortunately, this Hamiltonian can be greatly simplified because of the large difference in magnitude of Δm^2_{12} ($\sim 8 \times 10^{-5}$ eV^2) and Δm^2_{12} ($\sim 2.5 \times 10^{-3}$ eV^2). For neutrinos in the range we are interested in above

5 GeV energy, the correction due to the mass splitting Δm^2_{12} is both very small in absolute terms and much smaller than the Δm^2_{13} term.

The calculation is further simplified if we use a basis $\tilde{\nu} = (\nu_e, \tilde{\nu}_2, \tilde{\nu}_2)$, which is related to the standard flavour basis ν_f by $\nu_f = U_{23}\tilde{\nu}$, where U_{23} is the 2–3 part of the total mixing matrix U. In this basis, with the approximation that $\Delta m^2_{12}/\Delta m^2_{13} = 0$, the full three-flavour Hamiltonian is

$$\tilde{H}(x) = \begin{pmatrix} \frac{\Delta m^2_{13}}{2E_\nu}\sin^2\theta_{13} + V(x) & 0 & \frac{\Delta m^2_{13}}{2E_\nu}\sin\theta_{13}\cos\theta_{13} \\ 0 & \frac{\Delta m^2_{12}}{2E_\nu}\cos^2\theta_{12} & 0 \\ \frac{\Delta m^2_{13}}{2E_\nu}\sin\theta_{13}\cos\theta_{13} & 0 & \frac{\Delta m^2_{13}}{2E_\nu}\sin^2\theta_{13} \end{pmatrix}. \tag{3.23}$$

If we further assume that the mixing term $\frac{\Delta m^2_{12}}{2E_\nu}\cos^2\theta_{12}$ is negligible because of the smallness of the mass squared difference and the high energy of the neutrinos we are interested in then we can write a two-flavour Hamiltonian which includes the four non-zero corner terms of $\tilde{H}$ and decompose it as

$$\tilde{H}^{(13)}(x) = H(x) + \left(\frac{\Delta m^2_{13}}{4E_\nu} + \frac{V(x)}{2}\right)\mathbb{1}, \tag{3.24}$$

where H is the two-flavour Hamiltonian in Equation 3.3. So we can find the total S matrix in the $\tilde{\nu}$ basis by solving the two-flavour evolution equations using $H(x)$ and then multiplying by a phase shift term to account for the term subtracted out of $\tilde{H}(x)$. Because this extra term is a diagonal matrix, the phase shift is given by

$$\psi(L) \equiv \int_0^L \left(\frac{\Delta m^2_{13}}{4E_\nu} + \frac{V(x)}{2}\right)\mathrm{d}x, \tag{3.25}$$

so the corner terms in $\tilde{S}$ are given by the four terms in the two-flavour S-matrix multiplied by $e^{-i\psi}$. Finally, to obtain the oscillation probabilities between the three flavours in this approximation we have to convert back from the $\tilde{\nu}$ basis to the ν_f basis. The flavour-basis S matrix is given by $S_f = U_{23}\tilde{S}U^\dagger_{23}$. Once all these conversions are done, the transition probabilities between all three flavours

can be written as

$$
\begin{aligned}
P\left(\nu_e \to \nu_e\right) &= 1 - P_2, \\
P\left(\nu_e \to \nu_\mu\right) &= \sin^2\theta_{23} P_2, \\
P\left(\nu_e \to \nu_\tau\right) &= \cos^2\theta_{23} P_2, \\
P\left(\nu_\mu \to \nu_\mu\right) &= 1 - \sin^4\theta_{23} P_2 + 2\sin^2\theta_{23}\cos^2\theta_{23}\left[\mathrm{Re}\left(e^{-i\psi}S_{22}\right) - 1\right], \\
P\left(\nu_\mu \to \nu_\tau\right) &= \sin^2\theta_{23}\cos^2\theta_{23}\left[2 - P_2 - 2\mathrm{Re}\left(e^{-i\psi}S_{22}\right)\right],
\end{aligned} \tag{3.26}
$$

where $P_2 = |S_{12}|^2$ as before. To calculate any oscillation probability we need only calculate the two matrix elements P_2 and $e^{-i\psi}S_{22}$ and use the appropriate probability formula.

3.2.2 Improving the Earth Model

Armed with these three-flavour expressions we could now use a similar procedure as in the previous section to calculate the three-flavour transition probabilities in the two-layer model of the Earth's density. However, to obtain a more accurate result, and to compare the accuracy of various approximations in the energy range we are interested in we will construct a more accurate model of the Earth's density following section 4 of [33].

If we assume that the matter potential along a neutrino path of length L is equal to the average value $\bar{V}$, the Hamiltonian Equation 3.3 leads to a fairly simple expression for the evolution matrix $S(L)$, which is

$$
S(L) = \begin{pmatrix} \cos\phi + i\cos 2\bar{\theta}\sin\phi & -i\sin 2\bar{\theta}\sin\phi \\ -i\sin 2\bar{\theta}\sin\phi & \cos\phi - i\cos 2\bar{\theta}\sin\phi \end{pmatrix}, \tag{3.27}
$$

where $\phi = \bar{\omega}L$. The constant $\bar{\omega}$ is the value of ω_{mat}, as defined in Equation 3.5, at the average matter density, and $\sin 2\bar{\theta} = \omega_V \sin 2\theta_V/\bar{\omega}$. The simplest model of the Earth would be to consider the entire planet to have a constant, averaged density. The path length through the Earth is $L = 2R_\oplus\cos\Theta$, where Θ is the zenith angle and $R_\oplus$ is the radius of the Earth, which we take to be 6371 km. From the expression for the evolution matrix, the transition probability P_2 after passage through a layer of constant density is $\sin^2\bar{\theta}\sin^2\phi$. In this model the reason for the definition of the matter mixing angle and frequency is clear: these quantities can be put directly into the vacuum oscillation probability to obtain

the probability in matter. Unfortunately this model is rather inaccurate for the actual Earth density profile, because it does not capture any of the core-mantle resonance effects.

If we use the two-layer model of the earlier section, where the mantle and core each have a constant density, then the total S matrix is just $S_{\text{total}} = S_{\text{m}}^T S_{\text{c}} S_{\text{m}}$, where the subscripts m and c refer to the core and mantle layers, and each matrix is simply computed at the average density. With a core and mantle layer, the path lengths for each of the two mantle parts of the path and the length through the core are given by

$$\begin{aligned} L_m &= R_\oplus \left(-\cos\Theta - \sqrt{(R_c/R_\oplus)^2 - \sin^2\Theta} \right), \\ L_c &= 2R_\oplus \sqrt{(R_c/R_\oplus)^2 - \sin^2\Theta}, \end{aligned} \tag{3.28}$$

where R_c, the radius of the core, is 3480 km in the PREM model. For paths that do not cross the core the total path length is just $2L_m = -2R_\oplus \cos\Theta$. The results obtained in this model of the Earth are essentially the same as those obtained in section 3.2, except that this model remains accurate at the MSW resonance, where the perturbation approach of the previous section breaks down.

To improve the two-layer model, we can use the PREM density profile to calculate the average mantle and core densities as a function of zenith angle. Neutrino paths which come closer to the centre of the Earth will pass through denser layers, so the average density of the two layers becomes higher. This model is surprisingly accurate, because the density of the layers changes quite slowly so along a given path the density stays quite close to the average.

To further improve our model, we make use of the perturbation theory calculations described in [33]. This model takes the two-layer average density model as the zero-order case and corrects it for the changing density in the layers using a parametrized model of the density variation. First we will summarize the perturbation approach.

For a single layer with average matter potential $\bar{V}$ we can write the true potential as a function of position as

$$V(x) = \bar{V} + \Delta V(x), \tag{3.29}$$

which means that the Hamiltonian can be written as

$$H(x) = \bar{H} + \Delta H(x) \tag{3.30}$$

with

$$\bar{H} = \bar{\omega} \begin{pmatrix} -\cos 2\bar{\theta} & \sin 2\bar{\theta} \\ \sin 2\bar{\theta} & \cos 2\bar{\theta} \end{pmatrix}, \qquad \Delta H = \frac{\Delta V(x)}{2} \begin{pmatrix} 1 & 0 \\ 0 & -1 \end{pmatrix}. \tag{3.31}$$

The constants $\bar{\theta}$ and $\bar{\omega}$ are the values of $\omega_{\rm mat}$ and $\theta_{\rm mat}$ at the average matter density of the layer. We also use $\bar{H}$ and $\bar{S}$ to denote the Hamiltonian and the evolution matrix that are obtained assuming the layer has a constant density equal to the true average.

Next we decompose the true evolution matrix $S(x)$ into two parts,

$$S(x) = \bar{S}(x) + \Delta S(x), \qquad \Delta S(x) = -i\bar{S}(x)K(x), \tag{3.32}$$

and assume that the elements of K are small. Substituting the above definitions into the standard evolution equation $i\frac{\rm d}{{\rm d}x}S(x) = H(x)S(x)$, and discarding all but the lowest-order terms in ΔV and K we obtain

$$\frac{{\rm d}K(x)}{{\rm d}x} = \bar{S}^{\dagger}(x)\Delta H(x)\bar{S}(x). \tag{3.33}$$

Since we have already solved the evolution equation we have an exact expression for $\bar{S}(x)$, and we also know the form of $\Delta H(x)$ from Equation 3.31. Writing all of these definitions out in full and rearranging we obtain a differential equation for $K(x)$,

$$\begin{aligned} \frac{{\rm d}K(x)}{{\rm d}x} = \frac{\Delta V(x)}{2}\Bigg[&-\cos 2\bar{\theta} \begin{pmatrix} -\cos 2\bar{\theta} & \sin 2\bar{\theta} \\ \sin 2\bar{\theta} & \cos 2\bar{\theta} \end{pmatrix} \\ &+ \sin 2\bar{\theta} \begin{pmatrix} \sin 2\bar{\theta} & \cos 2\bar{\theta} \\ \cos 2\bar{\theta} & -\sin 2\bar{\theta} \end{pmatrix} \cos 2\phi(x) + \sin 2\bar{\theta} \begin{pmatrix} 0 & -i \\ i & 0 \end{pmatrix} \sin 2\phi(x) \Bigg]. \end{aligned} \tag{3.34}$$

Because the first term is constant, and the average of $\Delta V(x)$ over the entire neutrino path must be zero, this term will not affect the final expression for $S(L)$. Dropping this term and integrating along the neutrino path from $x = 0$

to $x = L$ gives

$$K(L) = \frac{\sin 2\bar{\theta}}{2}\left[\begin{pmatrix} \sin 2\bar{\theta} & \cos 2\bar{\theta} \\ \cos 2\bar{\theta} & -\sin 2\bar{\theta} \end{pmatrix}\int_0^L \Delta V(x)\cos 2\phi(x)\,\mathrm{d}x \right. \\ \left. + \begin{pmatrix} 0 & -i \\ i & 0 \end{pmatrix}\int_0^L \Delta V(x)\sin 2\phi(x)\,\mathrm{d}x\right]. \tag{3.35}$$

This expression is easier to evaluate in terms of the variable $z \equiv x - L/2$ which is the distance from the central point of the path and runs from $-L/2$ to $+L/2$. Defining two new terms

$$\Delta I \equiv \int_{-L/2}^{+L/2} \Delta V(z)\cos\left(2\bar{\omega}z\right)\,\mathrm{d}z, \\ \Delta J \equiv \int_{-L/2}^{+L/2} \Delta V(z)\sin\left(2\bar{\omega}z\right)\,\mathrm{d}z, \tag{3.36}$$

and substituting the resulting expression for $K(L)$ into the definition of ΔS in Equation 3.32 gives us

$$\Delta S(L) = -i\sin 2\bar{\theta}\left[\begin{pmatrix} \sin 2\bar{\theta} & \cos 2\bar{\theta} \\ \cos 2\bar{\theta} & -\sin 2\bar{\theta} \end{pmatrix}\Delta I + \begin{pmatrix} 0 & -i \\ i & 0 \end{pmatrix}\Delta J\right]. \tag{3.37}$$

This expression is useful because when ΔV is symmetric $\Delta J = 0$ and when ΔV is antisymmetric $\Delta I = 0$. As explained in [33], it is advantageous to define two further parameters

$$\varepsilon = \sin 2\bar{\theta}\sqrt{\Delta I^2 + \Delta J^2}, \qquad \xi = \arg(\Delta I + i\Delta J) \tag{3.38}$$

and write the evolution matrix as

$$S = \cos\varepsilon\bar{S} + \sin\varepsilon S', \tag{3.39}$$

where $\Delta S = \varepsilon S'$, so S' is explicitly

$$S' = -i\left[\begin{pmatrix} \sin 2\bar{\theta} & \cos 2\bar{\theta} \\ \cos 2\bar{\theta} & -\sin 2\bar{\theta} \end{pmatrix}\cos\xi + \begin{pmatrix} 0 & -i \\ i & 0 \end{pmatrix}\sin\xi\right]. \tag{3.40}$$

This redefinition is useful because it guarantees that the matrix S obtained through this perturbative expansion is unitary, regardless of the size of the de-

viations from the average potential. This prevents the introduction of unphysical rounding errors when the equations are solved numerically.

3.2.3 Mantle Model

For neutrinos that do not cross the core the mantle has a symmetric density profile, which means that $\Delta J = 0$. To obtain an analytic expression for S we can approximate this profile using a parabola by fitting the equation

$$\Delta V(z) \simeq V''_m \left[\left(\frac{z}{L} \right)^2 - \frac{1}{12} \right] \tag{3.41}$$

to the true density profile by varying V''_m as a function of zenith angle. This approximation leads to a formula for ΔI as a function of zenith angle alone,

$$\Delta I \simeq \frac{V''_m L}{12} \left(\frac{3\phi \cos\phi + (\phi^2 - 3)\sin\phi}{\phi^3} \right), \tag{3.42}$$

where ϕ is the adiabatic phase change $\bar{\omega} L$ which itself depends only on the zenith angle and the density model of the Earth. So given a model of the Earth's density and the neutrino oscillation parameters we can solve Equation 3.39 numerically to find the evolution matrix as a function of zenith angle and energy.

3.2.4 Core Model

For core-crossing neutrinos we must construct the approximate core and mantle matrices separately and combine them as in the constant density case using $S_{\text{total}} = S_m^T S_c S_m$. The core density can be approximated using the same parabolic formula as the mantle-only model, with the parameter labelled V''_c. The phase ϕ_c can be calculated as before using the average frequency in the core $\bar{\omega}_c$ and the path length in the core L_c.

When the neutrino path crosses the core the density profile in each mantle layer is roughly antisymmetric. A linear function of z fits the density profile quite well, so we define

$$V_m(z) = \bar{V}_m + \Delta V_m(z), \qquad \Delta V'_m \simeq V'_m \frac{z}{L_m}. \tag{3.43}$$

Because this profile is asymmetric, $\Delta I_m = 0$ and ΔJ_m can be found analytically

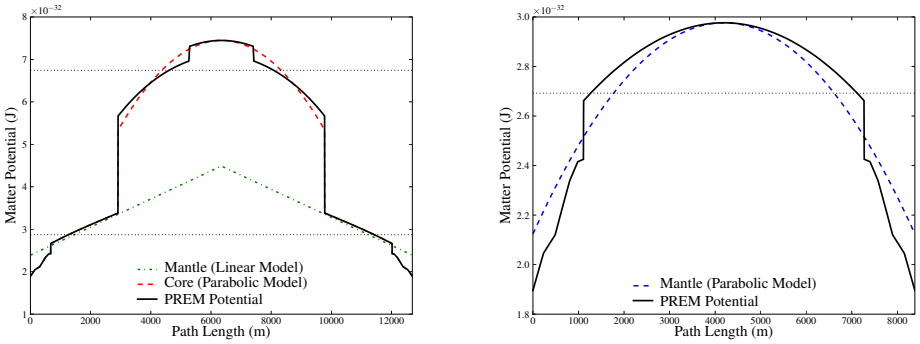

Figure 3.3: Exact density profiles and analytic approximations using linear and parabolic fits. The left-hand figure is for a core-crossing path with nadir angle 5° and the right-hand figure is for a mantle-only trajectory with nadir angle 49°. Horizontal dotted lines mark the average densities in the core and mantle.

to be

$$\Delta J_m \simeq V'_m L_m \frac{\sin\phi_m - \phi_m \cos\phi_m}{4\phi_m^2}. \tag{3.44}$$

We now have formulae for the evolution matrix for both mantle-only and core-crossing paths as a function of the neutrino energy and zenith angle and the parameters V'_m, V''_m, and V''_c, which can be computed from the PREM data. In Figure 3.3 we show two examples of the density profiles for two representative neutrino paths through the Earth, along with the density profiles computed using our approxmate formulae. In Figure 3.4 we plot our values of the correction coefficients as a function of zenith angle.

Using the parametrized density profile and the perturbation theory detailed above we can now calculate R_{33} and P_2 as a function of zenith angle and energy, and use the expressions in Equation 3.26 to calculate the probability of any flavour transition. In Figure 3.5 and Figure 3.6 we plot the most relevant probabilities for high-energy atmospheric neutrino detectors, $P(\nu_e \to \nu_e)$ and $P(\nu_\mu \to \nu_\mu)$, for three different density models and two different values of θ_{13}. It is clear that the single average-density model is not satisfactory, particularly for core-crossing neutrinos which are the easiest to measure in high energy detectors because they can be more easily separated from the very high downgoing cosmic ray background. The results of the two-layer averaged density model do not differ greatly from our more detailed perturbation model, but there are noticeable differences at the core-mantle boundary and in the shape of

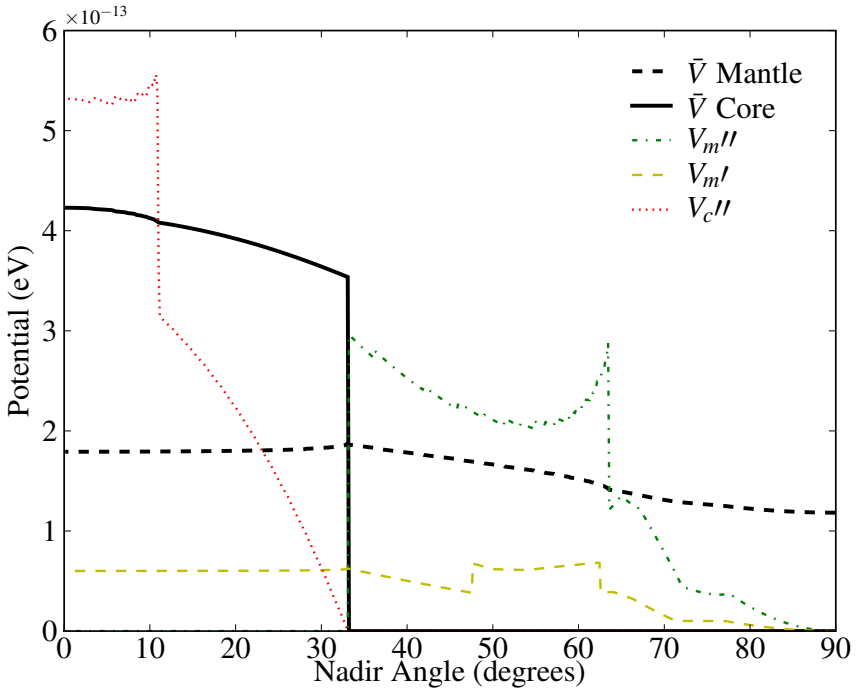

Figure 3.4: Average values and correction coefficients for the Earth density profile model used in this chapter.

the primary maximum in the core-crossing trajectories in the ν_μ survival plots. There is a significant difference in the electron neutrino survival plots at around $\cos\Theta = -0.45$, which is due to the parametrized model more accurately dealing with the jump in the mantle density that is crossed at that angle.

These plots demonstrate that the size of the mixing angle will have a considerable influence on any signal seen by Deep Core. As θ_{13} tends to zero the electron neutrino survival probabilities become smaller and the muon neutrino survival probabilities tend towards the vacuum probability. The differences between the models follow the same pattern in both cases. However, even for $\sin^2\theta_{13} = 0.05$ there is a noticeable enhancement due to the mantle-core boundary and the inner core resonance is still strong.

For antineutrinos, the calculations are very similar, except that the sign of the matter potential V must be reversed. This means that in the normal hierarchy the MSW resonance cannot occur, since the two terms $\Delta m^2/4E$ and $-V$ have the same sign, and the matter oscillation frequency never becomes

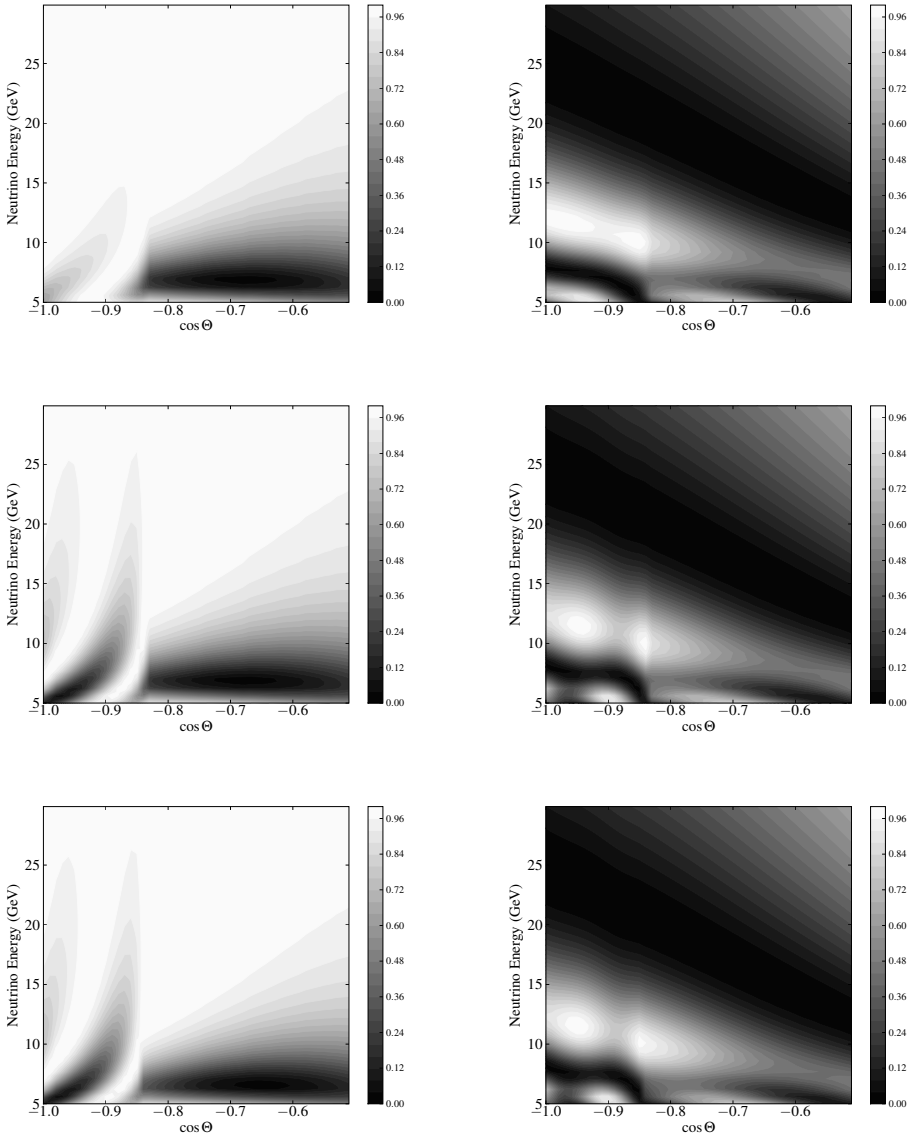

Figure 3.5: Neutrino oscillograms for $\sin^2 2\theta_{13} = 0.15$ with three density models. The left-hand figures are for the survival probability $P(\nu_e \to \nu_e)$, the right-hand figures are for $P(\nu_\mu \to \nu_\mu)$. Darker regions have lower probabilities, with black regions having probability 0. The upper figures are for the single average density model, the middle figures are for the two layer averaged-density model, and the bottom figures are for the corrected model described in the text.

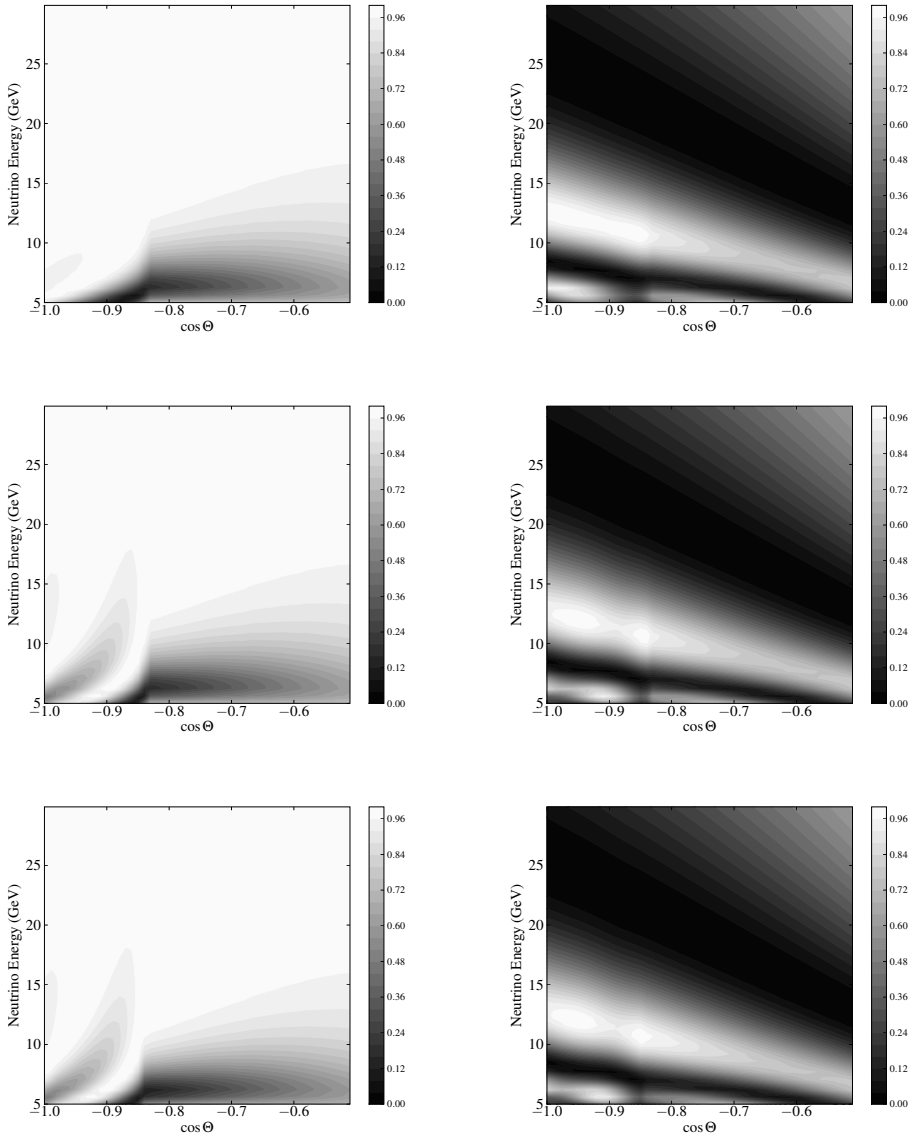

Figure 3.6: Neutrino oscillograms for $\sin^2 2\theta_{13} = 0.05$ with three density models. The ordering and colouring of the figures is the same as in Figure 3.5.

small. The matter mixing angle is also small in this case, so the probability $\bar{P}_2$ for electron antineutrino transitions is suppressed by the Earth's matter at all densities. Above 5 GeV the electron neutrino survival probability is essentially 100% and as a result the Earth's matter has practically no effect on the muon antineutrino survival probability, which follows the vacuum probability.

In the inverted hierarchy, there is a similar sign swap in the equation for the oscillation frequency since Δm^2 becomes negative. This means that with our approximations there is no difference between the transition probabilities $P(\nu_\mu \to \nu_\mu)$ in normal hierarchy and $P(\bar{\nu}_\mu \to \bar{\nu}_\mu)$ in inverted hierarchy. Note that this symmetry is broken by the Δm_{12} mixing terms at lower energies [34]. For the neutrino energy range we are interested in this symmetry breaking is extremely small. The transition probabilities for antineutrinos are shown in Figure 3.7.

3.3 The Atmospheric Neutrino Flux

Because of the symmetries of the transition probabilities described in the preceding sections, the observable differences resulting from the neutrino mass hierarchy and the density profile of the Earth are entirely dependent on the asymmetries of the incoming atmospheric neutrino flux. If the incoming fluxes of neutrinos and antineutrinos were equal then changing the hierarchy would have no effect on the flux observed in a detector such as Deep Core which has no charge discrimination capabilities. Fortunately in the energy range at which neutrino oscillations are most strongly affected by the hierarchy and matter effects there is a significant difference in the flux of neutrinos as compared to antineutrinos. In addition, the atmospheric flux of electron neutrinos and antineutrinos is much lower than the flux of muon-type neutrinos.

Our flux model is based on the results of Honda *et al.* [74]. We parametrized the fluxes of each neutrino flavour $(\nu_e, \bar{\nu}_e, \nu_\mu, \bar{\nu}_\mu)$ in the form

$$F_{\nu_\alpha} = A \times E_\nu^p. \tag{3.45}$$

One set of the parameters A and p for each flavour is sufficient to fit the model data very well across the range of energies we consider in this study. We calculated the parameters for each of three angular bins given in the model data. The parameters used are shown in Table 3.1.

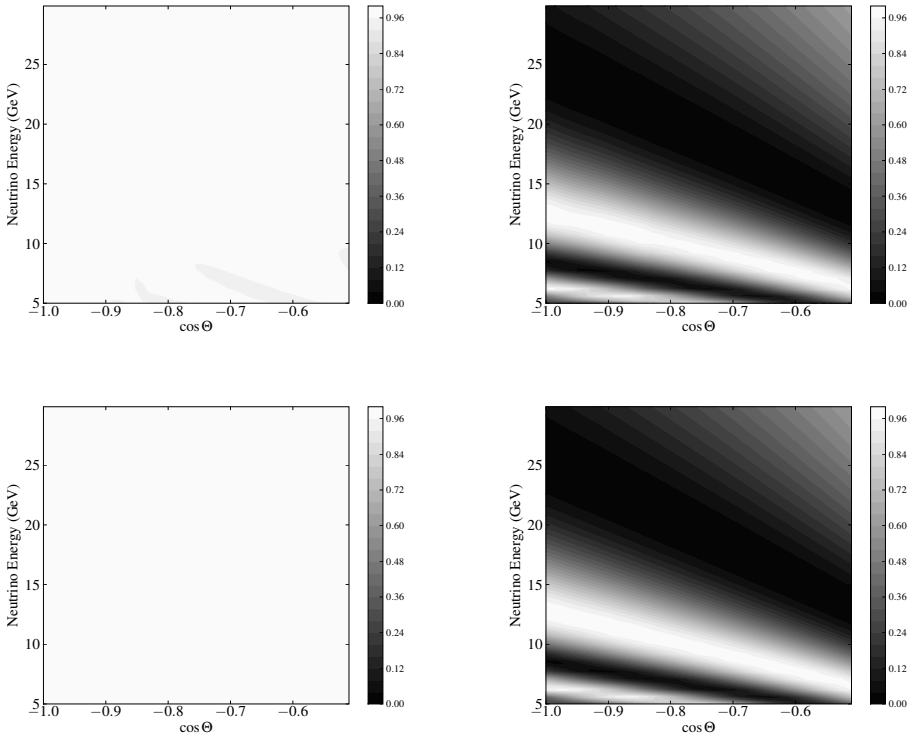

Figure 3.7: Oscillograms for antineutrinos with the corrected Earth density model in normal hierarchy. The upper pair of figures is for $\sin^2\theta_{13} = 0.15$, and the lower pair is for $\sin^2\theta_{13} = 0.05$ Note that because we set $\Delta m^2_{12} = 0$ these figures are the same as those that would be obtained for neutrinos in inverted hierarchy.

	ν_μ			$\bar{\nu}_\mu$		
$-\cos\Theta$	1.0–0.9	0.9–0.8	0.8–0.7	1.0–0.9	0.9–0.8	0.8–0.7
p	-2.993	-2.985	-2.978	-3.029	-3.025	-3.020
A	2.400	2.404	2.410	2.313	2.326	2.339
	ν_e			$\bar{\nu}_e$		
p	-3.508	-3.517	-3.524	-3.474	-3.482	-3.482
A	2.142	2.202	2.263	1.988	2.047	2.101

Table 3.1: Parameters for the atmospheric neutrino flux. The flux is computed from these fitted values of p and A using Equation 3.45.

The interaction cross section adds an additional asymmetry to the neutrino/antineutrino fluxes which is very beneficial to the measurement of the hierarchy. The charged-current cross section for neutrinos is 2.03 times the antineutrino cross section at 10 GeV, and this ratio changes only slightly over the relevant energy range, decreasing to 1.95 times at 60 GeV neutrino energy [77]. Because of this factor, the effective ν:$\bar{\nu}$ flux ratio in the detector is improved by a factor of two from the raw incident flux ratio, which provides a corresponding improvement in the sensitivity of hierarchy measurements.

Comparing the two density models in Figure 3.8 there are significant differences caused by the two-layer oscillation resonance. The two peaks in the electron neutrino survival probability that result from the resonance in the core-crossing region appear as significant decreases in the flux in the normal hierarchy, particularly for neutrinos with energies below 20 GeV. In the lowest-energy bin the flux as a function of angle has a very different shape with the inclusion of the core resonance. As explained in the next section, the lowest bin that we can expect Deep Core to be sensitive to is 10–15 GeV. The flux predicted in this bin by the corrected model in the inverted hierarchy is lower than for the single-density model in normal hierarchy. This suggests that any measurement of the hierarchy will depend crucially on the accuracy of the matter model used to interpret the results. We consider the effect of uncertainties in the densities of the layers in subsection 3.4.2.

The differences between the density models are smaller at higher energies because the matter effects decrease with energy. Thus in the 20–25 GeV energy bin the difference between the models is very small, as is the difference caused by changing the hierarchy. In the integrated flux plot in the lower left we can see that although the detector becomes less sensitive at low energies the differences in the low energy bins are still large enough for the core resonances to be visible. The corrected model's predictions are significantly different from the constant-density approximation, and also tend to increase the difference in flux between the two hierarchies. This is very clearly visible in the plot of the normal minus the inverted hierarchy interactions, which shows that the difference in count rate in the highest zenith angle bins is considerably greater in the corrected model. The shape of the angular distribution of the muon neutrino flux is also considerably altered in the corrected model, and so measurements involving the comparison of rates in different angular bins will be in error if a constant density approximation is used.

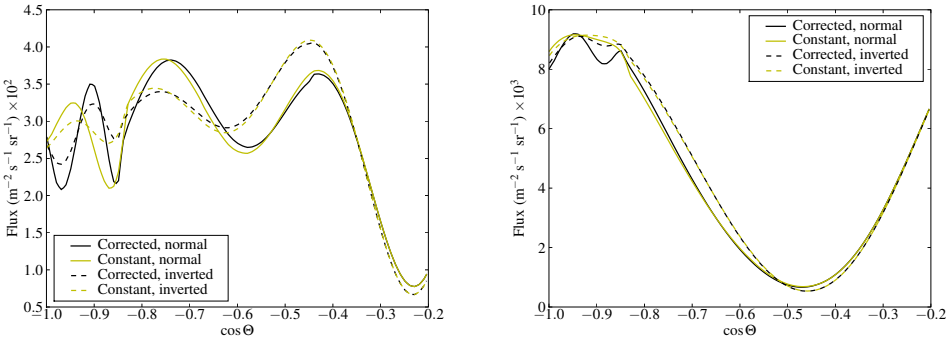

(a) 5–10 GeV

(b) 10–15 GeV

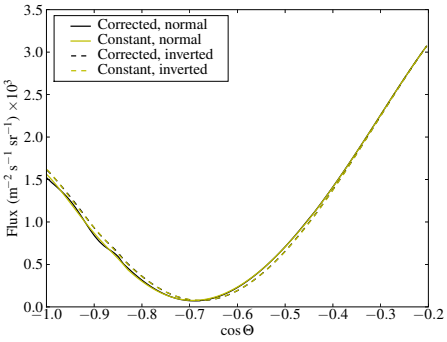

(c) 15–20 GeV

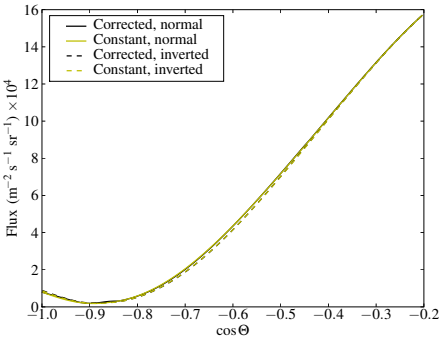

(d) 20–25 GeV

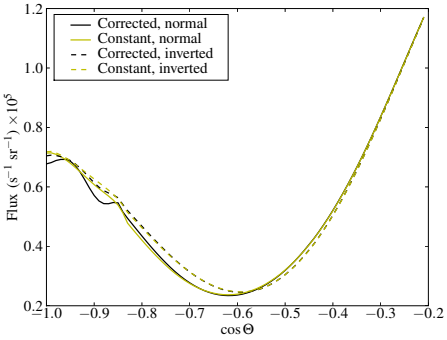

(e) 10–25 GeV with A_{eff} factor.

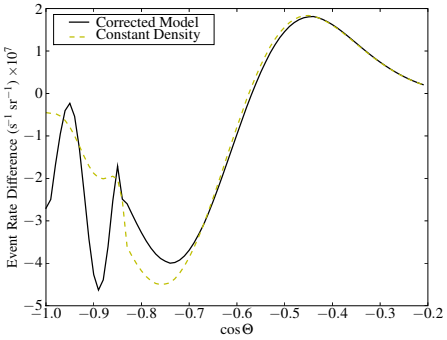

(f) Hierarchy difference, 10–25 GeV

Figure 3.8: Predicted atmospheric neutrino flux for normal and inverted hierarchy in 5 GeV energy bins, comparing the constant-density and corrected two-layer models. The lowest two figures include the energy-dependent effective area of Deep Core. The bottom right figure shows the difference between normal and inverted hierarchy rates for the two models. These plots are for $\sin^2 2\theta_{13} = 0.15$.

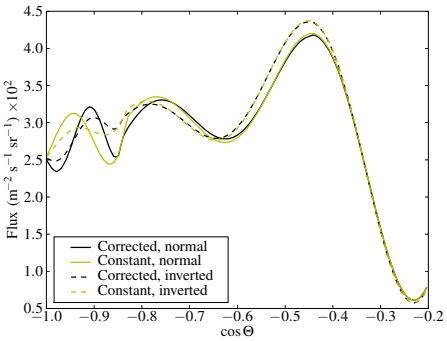

(a) 5–10 GeV

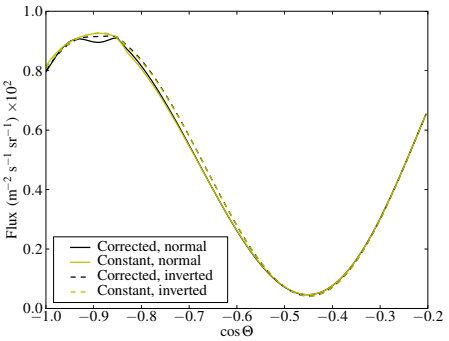

(b) 10–15 GeV

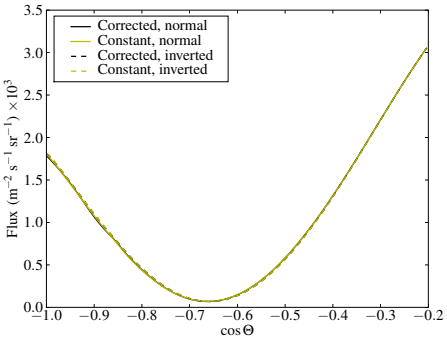

(c) 15–20 GeV

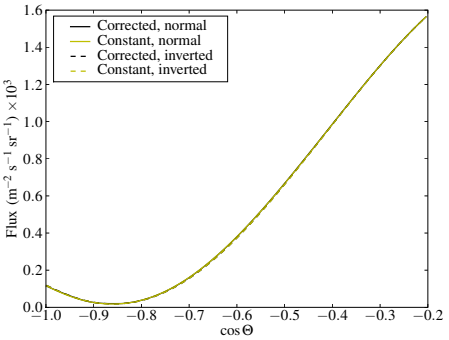

(d) 20–25 GeV

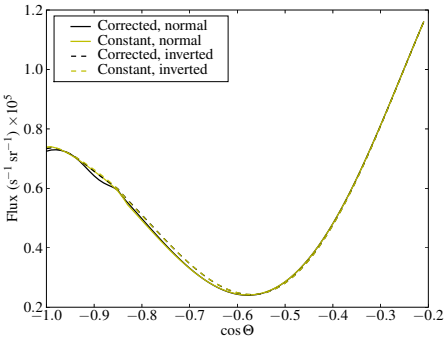

(e) 10–25 GeV with A_{eff} factor.

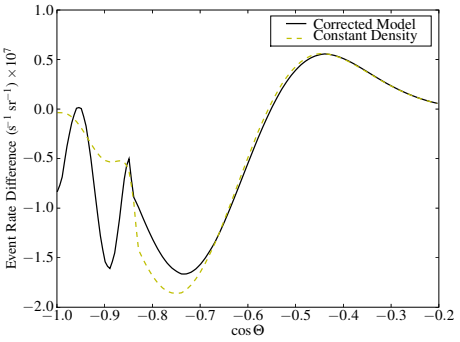

(f) Hierarchy difference, 10–25 GeV

Figure 3.9: The same as Figure 3.8 with $\sin^2 2\theta_{13} = 0.05$.

The dependence of the hierarchy difference on the magnitude of θ_{13} is apparent from a comparison with the same figures for $\sin^2 2\theta_{13} = 0.05$ shown in Figure 3.9. The main effect of decreasing the mixing angle is to reduce the amplitude of the peaks in the normal hierarchy oscillations. The inverted hierarchy flux peaks show some differences as well, but the difference is less pronounced. The overall effect of the hierarchy on the flux as a function of angle is very similar for both values of the mixing angle, up to an overall scaling. This suggests that it is this variation in angular flux as a function of angle that will be the best way to determine the hierarchy, since the absolute flux numbers have quite large uncertainties and are strongly dependent on the value of θ_{13} and the density model.

3.4 The IceCube Deep Core Extension

IceCube is a neutrino detector with an instrumented volume of approximately one cubic kilometre at the South Pole. When finished it will consist of 80 strings, each a cable with 60 photomultiplier detectors attached to it. These strings are lowered into holes drilled into the ice, and the detector modules are evenly spaced between depths of about 1500 to 2500 m below the surface. The detector's main goal is to measure neutrinos from various astrophysical sources such as gamma ray bursts, dark matter decays, and very high-energy cosmic rays. The detector should be fully completed during the next Southern Hemisphere summer [39].

The main IceCube detector is not sensitive to neutrinos with energies lower than 100 GeV. However, the Deep Core extension to the main detector is sensitive to much lower energies down to perhaps 10 GeV, with pointing resolution of a few degrees for muon neutrino events [38–40]. The first motivation for this extension was to look for the lower-energy neutrinos that would be produced by the decay of WIMPs, but there are also plans to use it to study neutrino oscillations in the Earth with high statistics at higher energies than other experiments to date. Work by Mena *et al.* [41], building upon earlier work relating to water and iron detectors such as Hyper-Kamiokande and the Indian Neutrino Observatory [35–37], has considered the possibility of measuring the neutrino mass hierarchy using Deep Core. The lowest part of the detector's energy range will be valuable for studies of the effects of the adiabatic matter density in the Earth and the oscillations of neutrinos at higher energies than have been measured by previous detectors even if the neutrino mixing parameters do not allow

the hierarchy to be measured.

The Deep Core extension is comprised of six new strings equally spaced around an existing IceCube string at a distance of 72 m. The new strings have 50 of their 60 detector modules concentrated at 7 m spacing in the deeper, clearer ice layers at around 2100-2500m depth. In contrast, the main detector strings have a 17 m module spacing and are 125 m apart. Other neighbouring IceCube strings will be used as a veto to help eliminate unwanted background events such as downgoing atmospheric muons. The collaboration's studies indicate that it will be possible to identify and measure muon-type neutrinos with energies of 10–100 GeV with relatively good efficiency using this recently-completed extension, though the energy resolution may not be particularly good.

According to recent simulations, the effective area of the detector is approximately $4 \times 10^{-4}\,\mathrm{m}^2$ at 10 GeV, rising to $7 \times 10^{-2}\,\mathrm{m}^2$ at 100 GeV [39]. The pointing resolution is expected to be of the order of a few degrees for muon neutrinos. For our study, we parametrized the effective area as a power law, in a similar manner to the neutrino fluxes. Our expression for the effective area as a function of energy is

$$A_{\mathrm{eff}}(E_\nu) = 10^{-5.64} \times (E_\nu/\mathrm{GeV})^{2.24}\,\mathrm{m}^2. \tag{3.46}$$

The effective area increases rapidly with neutrino energy, but because the matter effects are strongest for low energy neutrinos a high sensitivity to neutrinos with energies above 30 GeV is not directly useful for oscillation studies, and if the energy resolution is particularly poor it may prove to be detrimental to the hierarchy sensitivity. However, the neutrino flux also decreases rapidly with increasing energy, which helps to counterbalance the decreasing detector area at low energies. Measuring the flux of the higher-energy atmospheric neutrinos will also help to calibrate the flux models for low energy neutrinos.

In Figure 3.8 and Figure 3.9 we show the expected flux at the detector for energy bins from 5 to 25 GeV, and a sum of the neutrino flux in the range from 10–25 GeV which would allow for a large uncertainty in the detector's energy measurements. In the 20–25 GeV bin the hierarchy and density-dependent effects are practically invisible, whereas 10–20 GeV neutrinos are noticeably altered by changes in the density model and hierarchy.

Our simulation suggests that the difference in event rates for the two hierarchies will be of the order of a few percent in total flux if the flux is integrated

PREM Density Profile

	$-\cos\Theta$ Bin							
	1.0–0.9		0.9–0.8		0.8–0.7		0.6–0.5	
Model	Hits	Δ	Hits	Δ	Hits	Δ	Hits	Δ
	$\sin^2 2\theta_{13} = 0.15$							
c_{norm}	4507	2.35%	3494	6.12%	2286	10.8%	1128	−0.797%
c_{inv}	4613		3708		2534		1119	
d_{norm}	4514	2.24%	3464	6.73%	2231	12.7%	1138	−1.43%
d_{inv}	4615		3697		2515		1122	
s_{norm}	4589	1.26%	3561	4.75%	2231	12.7%	1138	−1.43%
s_{inv}	4647		3730		2515		1122	
	$\sin^2 2\theta_{13} = 0.05$							
c_{norm}	4782	0.669%	3908	1.89%	2697	3.71%	1076	0.372%
c_{inv}	4814		3982		2797		1080	
d_{norm}	4785	0.627%	3896	2.08%	2674	4.30%	1080	0.093%
d_{inv}	4815		3977		2784		1081	
s_{norm}	4813	0.291%	3935	1.42%	2674	4.30%	1081	0.093%
s_{inv}	4827		3991		2789		1080	

Table 3.2: The predicted number of detector interactions for a ten-year experimental run with the Deep Core detector integrated over the energy range 10–25 GeV. The models are c, the corrected two-layer density model, d, the two-layer path-dependent average density model, and s, the single-layer path-dependent average density model. The percentage difference between predicted events in the normal and inverted hierarchies are also shown.

over this energy range from $\cos\Theta = -1.0$ to $\cos\Theta = -0.7$. If the events are separated into angular bins covering a range of 0.1 in $\cos\Theta$, as in Mena *et al.* [41], the relative differences in rates in these bins between normal and inverted hierarchy are increased for our corrected model compared to the constant density model in the two highest zenith angle bins, and slightly decreased in the third bin. Because the event rate and angular resolution are higher for the higher zenith-angle bins, this means that overall the resonant oscillations caused by the layering of the Earth increase the sensitivity of the experiment to the hierarchy. We show our calculated event numbers for a ten year experiment run for $\sin^2 2\theta_{13} = 0.15$ and $\sin^2 2\theta_{13} = 0.05$ in Table 3.2.

3.4.1 The Effect of θ_{13} Uncertainty

As mentioned in the previous section, for different values of θ_{13} the difference in event rates for the two hierarchies changes significantly in magnitude but not in shape. Because the angular resolution of the Deep Core detector is expected to be very good, especially in comparison to its energy resolution, this suggests that the most model- and parameter-independent method of measuring the hierarchy will be to compare the count rates in different angular bins rather than measuring absolute rates. For example, as shown in Table 3.2 and the graph of the hierarchy difference, the event rate in a bin which spans the zero point of the hierarchy difference at around $\cos\Theta = -0.6$ will stay close to constant in the two hierarchies, allowing a reference point for the more strongly-affected bins. By carefully selecting the angular bins and calibrating the flux models using measurements of the flux in the regions of the angular distribution where the hierarchy is less influential it may be possible to measure the hierarchy without extremely accurate models of the raw number of neutrinos produced in the atmosphere. For additional calibration the experiment can also make use of neutrinos with energies of 30 GeV and above where the matter and hierarchy effects are very weak.

The value of θ_{13} must be fit to the observational data along with the hierarchy choice, but it appears from our results and previous work that as long as $\sin^2\theta_{13} \gtrsim 0.05$ variations in the precise value will not be too difficult to disentangle from the hierarchy assuming that there are no other confounding factors [41].

3.4.2 Density Model Variations

Mena *et al.* [41] do not describe in detail the density model they used for their probability calculations, but by comparing their figures to our own calculations and examining their references we infer that they used a numerical model based on the standard PREM density values first published in 1981 [72], and did not consider possible errors in this model. This model of the Earth is now quite old, and due to the sensitivity of the neutrino oscillation resonances to the density variations and layer thicknesses the results computed from it may vary considerably from newer models. For instance, the size of the inner core density step is not particularly well constrained [78], and local variations of the order of a few percent due to convection probably exist in the mantle [79]. It has even

been proposed that neutrino experiments may be able to give a measurement of the core density with accuracy comparable to more standard techniques [80]. In this section we study the effects of possible density variations on the hierarchy measurement that may be made with Deep Core.

Akhmedov *et al.* [33] consider the effect of Earth model variations, such as changing the ratio of the densities of the mantle and core, or changing the size of the core. In each case there are changes to the neutrino survival probabilities, though there are not large qualitative differences. The Earth's total mass must remain fixed, so for our model we changed the core density from the base PREM value by multiplying by a factor X so that the PREM density ρ_{core} becomes $X\rho_{\text{core}}$. The mantle density is multiplied by a similar factor Y, given by

$$Y = \frac{M_\oplus - XV_c\rho_c}{\rho_m V_\oplus - \rho_m V_c}, \tag{3.47}$$

where V_c and V_m are the volumes of the core and mantle and ρ_c and ρ_m are the average densities in the two layers. $M_\oplus$ is the fixed mass of the Earth. Because the uncertainties in the Earth's density are relatively small, the most relevant values of the density multipliers we tested were $X = 0.95$, $Y = 1.024$ and $X = 1.05$, $Y = 0.976$, representing 5% changes in the core density. We also considered more extreme models with $X = 1.1$ and $X = 1.2$, although the actual Earth density is very unlikely to vary this much from the PREM values.

A cruder Earth model difference is provided by the two-layer average density model. This is an extreme case of changing the slope of the Earth's density as a function of radius, so the difference between the corrected model and the two-layer model can be used as a limit on the effect of uncertainty in the rate of change of density in the Earth. In our calculations we find that the corrected model is very similar to the flat two-layer model, especially in comparison to the single-layer model and the differences caused by changes in the average density. This is as expected from the argument given in the earlier sections where we showed that the error in the simple two layer model is roughly proportional to the value of $\sin 2\theta_m$, which decreases with increasing neutrino energy. Our results thus show explicitly that the perturbation expansion is very accurate for neutrino energies above 10 GeV.

In Figure 3.10 we compare the oscillograms calculated using the PREM density profile with those that result from changing the core density by 5%. These density changes result in shifts in the positions of the resonant peaks.

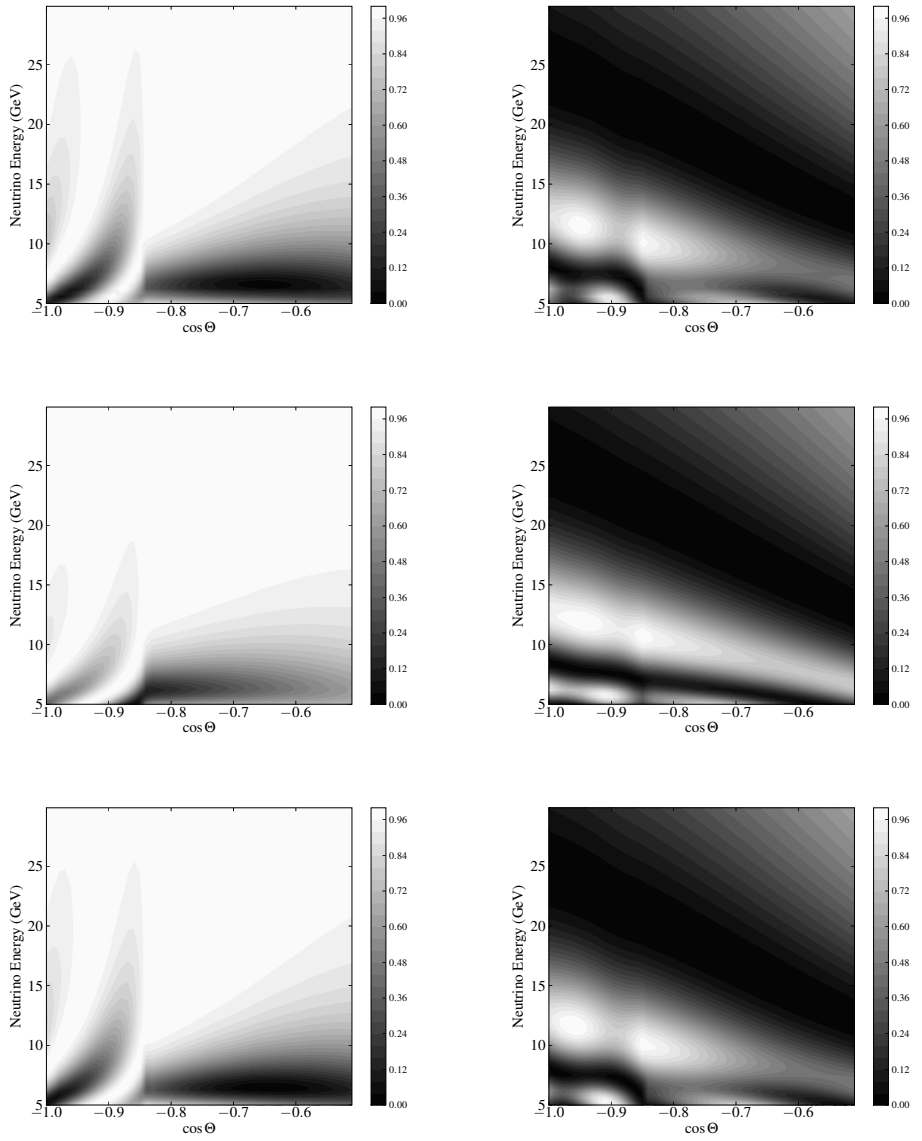

Figure 3.10: Oscillograms showing the effect of changes in the Earth density with $\sin^2\theta_{13} = 0.15$. The upper figures are for the PREM density, the middle figures have the core density increased by 5%, and the lower figures have the core density decreased by 5%. The mantle density is adjusted to hold the Earth mass constant. The left-hand figures are the ν_e survival probability and the right-hand figures are the ν_μ survival probability, with white representing 100% survival and black 0%.

Increased Core Density Profile

	$-\cos\Theta$ Bin							
	1.0–0.9		0.9–0.8		0.8–0.7		0.6–0.5	
Model	Hits	Δ	Hits	Δ	Hits	Δ	Hits	Δ
				$\sin^2 2\theta_{13} = 0.15$				
c_{norm}	4473	2.53%	3438	6.60%	2237	11.7%	1158	−1.30%
c_{inv}	4586		3665		2499		1143	
d_{norm}	4478	2.43%	3410	7.16%	2188	13.4%	1168	−1.88%
d_{inv}	4587		3654		2482		1146	
s_{norm}	4566	1.27%	3510	5.07%	2188	13.4%	1168	−1.88%
s_{inv}	4624		3688		2482		1146	
				$\sin^2 2\theta_{13} = 0.05$				
c_{norm}	4759	0.714%	3863	2.07%	2655	4.03%	1097	0.091%
c_{inv}	4793		3943		2762		1098	
d_{norm}	4761	0.672%	3851	2.28%	2635	4.55%	1100	−0.091%
d_{inv}	4793		3939		2755		1099	
s_{norm}	4794	0.292%	3893	1.54%	2635	4.55%	1100	−0.091%
s_{inv}	4808		3953		2755		1099	

Table 3.3: The predicted number of detector interactions for a ten-year experimental run with the Deep Core detector. The table is calculated in the same way as Table 3.2 but with the density of the core increased by 5% and the mantle density correspondingly reduced to keep the Earth's mass constant.

These are particularly noticeable in the electron neutrino survival probability. This shift also changes the shape and magnitude of the resonance peaks in the muon neutrino survival probabilities. Increasing density tends to move the main core peak towards smaller zenith angles and also affects the shape of the resonance at the core-mantle boundary. Although these alterations are small the changes due to the hierarchy are of a similar size, so it is important to consider the effect of density model changes on the event rates.

In Table 3.3 and Table 3.4 we show the number of events expected in the Deep Core detector during a ten year run with these modified density models using the single layer average-density approximation, the two-layer approximation and the corrected perturbative model. In both modified density models the event rate in the detector is predicted to decrease slightly in both the normal and inverted hierarchy, except in the $-0.6 < \cos\Theta < 0.5$ bin where the rate increases slightly.

Decreased Core Density Profile

	$-\cos\Theta$ Bin							
	1.0–0.9		0.9–0.8		0.8–0.7		0.6–0.5	
Model	Hits	Δ	Hits	Δ	Hits	Δ	Hits	Δ
				$\sin^2 2\theta_{13} = 0.15$				
c_{norm}	4485	2.36%	3486	5.68%	2291	9.82%	1145	0.704%
c_{inv}	4591		3684		2516		1137	
d_{norm}	4496	2.18%	3455	6.28%	2235	11.7%	1156	1.40%
d_{inv}	4594		3672		2496		1140	
s_{norm}	4556	1.40%	3539	4.58%	2235	11.7%	1156	1.40%
s_{inv}	4620		3701		2496		1140	
				$\sin^2 2\theta_{13} = 0.05$				
c_{norm}	4762	0.693%	3886	1.70%	2679	3.40%	1092	0.366%
c_{inv}	4795		3952		2770		1096	
d_{norm}	4767	0.608%	3873	1.91%	2656	3.99%	1096	0.091%
d_{inv}	4896		3947		2762		1097	
s_{norm}	4791	0.334%	3906	1.36%	2656	3.99%	1096	0.091%
s_{inv}	4807		3959		2762		1097	

Table 3.4: The predicted number of detector interactions for a ten-year experimental run with the Deep Core detector. The table is calculated in the same way as Table 3.2 but with the density of the core decreased by 5% and the mantle density correspondingly increased to keep the Earth's mass constant.

The change in rate caused by density variation is smaller than the difference caused by the hierarchy choice, so while density variations do bring the inverted hierarchy in the modified density model closer to the normal hierarchy with the PREM density profile the difference between the two is still significant. The percentage difference in event rates for the two hierarchies in the increased core density model is slightly larger than for the PREM, but for the decreased core density model it is slightly smaller.

These density model changes are fairly realistic and should be considered in the analysis of the Deep Core data. This will reduce the sensitivity of the experiment to the hierarchy. For instance, if the PREM model is fixed then the percentage difference in flux caused by the hierarchy change in the highest zenith angle bin is 2.35%, but the difference between the inverted hierarchy in the decreased core density model and the normal hierarchy in the PREM case is

reduced to 1.86%. The figure is 1.75% for the increased density model compared to the PREM density profile.

The change in flux caused by density variations may be difficult to extract from the effect of a smaller mixing angle, since the decrease in flux from a lower core density can be counterbalanced by a smaller value of the mixing angle. The most obvious method of disentangling these two effects is to use accurate measurements of the flux as a function of angle and use smaller angular bins. However, this will tend to reduce the sensitivity of the detector to the mass hierarchy due to the lower statistics in the smaller bins.

In Figure 3.11 we plot the raw flux and the difference in flux caused by the hierarchy choice as a function of angle for the Deep Core detector in the various density models. The shifting of the resonance peaks resulting from the changing density is clearly seen. We find that the flux in the inverted hierarchy is much less affected by the density model than the normal hierarchy flux. The flux for lower-angle neutrinos is also less sensitive to the density model, which is convenient for calibration since we have seen that this flux is also relatively insensitive to the hierarchy and the mixing angle. With increasing density the minima in the flux caused by the resonance peaks becomes sharper and deeper. The shift in angle is quite large even for the 5% change in density, and results in significant changes in the shape of the hierarchy difference. However, as seen in the tables of the predicted event counts the integrated difference between the two hierarchies is small. The behaviour of the second peak that occurs closer to the core-mantle boundary is very similar. The density modifications also have an effect on neutrinos that do not cross the core. For zenith angles between about $\cos\Theta = -0.82$ and $\cos\Theta = -0.7$ the entire flux curve moves downwards roughly linearly with increasing density. The effect in the normal hierarchy is once again larger than in the inverted hierarchy.

The sensitivity of the Deep Core detector to the neutrino hierarchy will be reduced when uncertainties in the Earth's structure are taken into account. However, according to our results the effects of density profile uncertainties on the shape of the flux as a function of angle are different to the effects of mixing angle uncertainties. In particular, the position of the resonance peaks for core-crossing neutrinos is affected by the Earth density model, but not by the mixing angle. This will interfere with measurements that depend on taking ratios of the flux in different bins to cancel out uncertainties in the mixing angle and the unoscillated atmospheric flux. If the angular resolution of Deep Core does

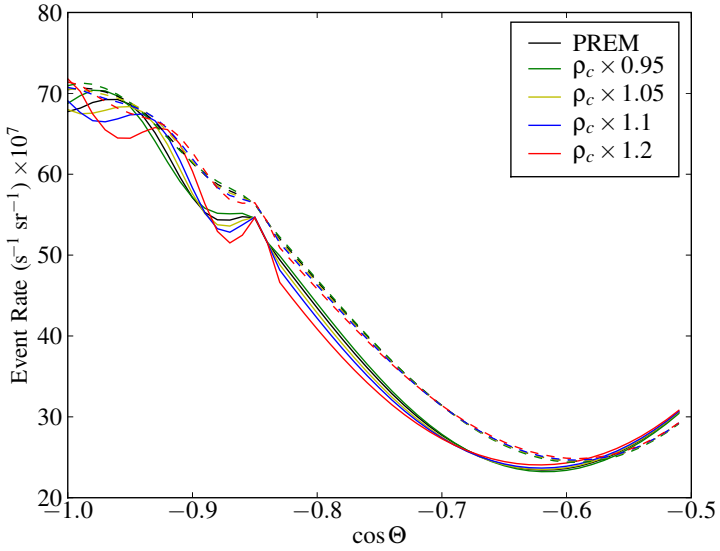

(a) Total flux in Deep Core, 10–25 GeV

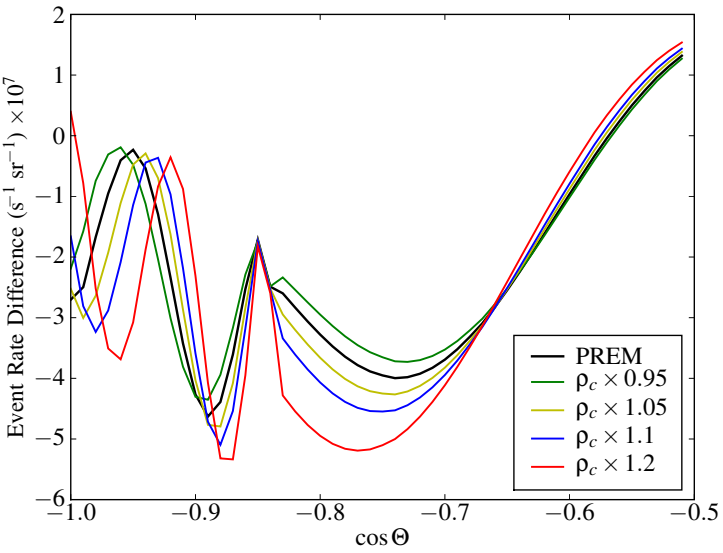

(b) Difference between normal and inverted hierarchy fluxes.

Figure 3.11: Event rates in the Deep Core detector as a function of zenith angle, Earth density, and hierarchy. In the upper figure dashed lines are for the inverted hierarchy and solid lines are for the normal hierarchy. Earth models with core densities altered relative to the PREM values are compared. These plots are for $\sin^2 2\theta_{13} = 0.15$.

turn out to be of the order of a few degrees for the lowest energy neutrinos then it may be possible to use a finer binning than we have presented here to roughly measure the shape of the resonance peaks. By taking the angular flux distribution into account the loss in sensitivity due to the Earth density model uncertainty could be compensated for to some extent, and in the best case could even be used as a sensitive probe of the density profile of the Earth. Better data on the detector capabilities is required to determine the best way to measure the hierarchy and the density profile. However, our results suggest that Deep Core will be able to determine the hierarchy if the mixing angle is not too much smaller than the current upper limit, as well as making very useful measurements of the structure of the Earth.

3.5 Summary

The oscillations of neutrinos in the Earth are described by a matter background term in the neutrino Hamiltonian, and because of the particular density variations that exist in the Earth the oscillation patterns are quite complex. The electron neutrino survival probability shows strong resonant effects because of the sharp step in density at the core-mantle boundary. The neutrino oscillation resonances result in two strong minima in the electron neutrino survival probability for core-crossing neutrinos. These minima occur for neutrinos passing close to the centre of the Earth and neutrinos with paths that graze inside the core-mantle boundary with zenith angle $\Theta \simeq 155^\circ$. If the density of the Earth is taken to be constant then this resonance does not occur and the oscillation probability is significantly altered, particularly in the inner peak. However, a basic two-layer model is remarkably accurate for neutrinos with energies above 10 GeV.

Because the resonant effects are strongest for neutrinos with energies between 5 and 20 GeV, it is very likely that the new Deep Core extension to the IceCube detector will be able measure the oscillations of atmospheric neutrinos above 10 GeV and identify the signatures of the resonance. Furthermore, because of the flavour asymmetries of the initial neutrino flux and the flavour- and hierarchy-dependent nature of the oscillation probabilities Deep Core may be able to collect high enough event statistics to determine the neutrino mass hierarchy, assuming that θ_{13} is not too small. Mena *et al.* [41] examined this possibility and found that the Deep Core detector has a reasonable discriminating power

using the PREM density profile. Using our own model with updated figures from the collaboration we have shown that the sensitivity of the detector to the hierarchy is somewhat reduced if the uncertainties in the PREM model are taken into account. However, the errors caused by Earth model uncertainties are different in several ways to the errors introduced by uncertainties in the mixing angle θ_{13}. It may be possible to disentangle the two effects and make very useful independent measurements of the Earth's density if the angular resolution of the detector is of the order of a few degrees. We have also shown that the sensitivity of the Deep Core measurement to the rate of change of density in the Earth is small. The average density of the two main layers has a much stronger influence on the oscillation probabilities in the sensitive energy range.

Conclusion

Neutrino oscillations in dense backgrounds have been a rich area of study in recent years. We have studied two astrophysical scenarios which demonstrate the complexity of neutrino flavour changes. Both systems provide opportunities for future detectors to determine neutrino mixing parameters such as the mass hierarchy. Our examples also show how the properties of the underlying physical structures can be probed by the unique signals provided by neutrinos.

The novel effects found in theoretical studies of the collective interactions of neutrinos at extremely high densities can only be directly tested using supernova neutrinos. However, before any measurements of neutrinos from nearby supernovae can be properly interpreted we will require a thorough understanding of the dependence of the flux received on Earth on the initial neutrino spectra and the background conditions near the supernova. We have shown that even very large-amplitude background density fluctuations still leave the major features of the final neutrino spectrum intact, though there are many interesting dynamic effects on the neutrino flavour evolution.

The oscillations of atmospheric neutrinos that pass through the Eath's core are also surprisingly complicated. We have described how the Deep Core detector may be able to measure the neutrino mass hierarchy by measuring the flux of atmospheric muon-type neutrinos that survives passage through the Earth. We also considered the complications that can result from uncertainties in the density profile of the Earth, which is still relatively poorly-known.

There is no doubt that the theoretical study of neutrino oscillations will continue to be an active and interesting field. As was the case before the first accurate measurements of the Solar neutrino flux were made, the literature is brimming with interesting predictions that eagerly await the release of the next helping of experimental results.

Bibliography

[1] B. Pontecorvo, Zh. Exp. Teor. Fiz. **33**, 549 (1957).

[2] B. Pontecorvo, Zh. Exp. Teor. Fiz. **53**, 1717 (1967).

[3] R. Davis, D. S. Harmer, and K. C. Hoffman, Phys. Rev. Lett. **20**, 1205 (1968).

[4] S. Fukuda *et al.*, Phys. Rev. Lett. **86**, 5651 (2001).

[5] Q. R. Ahmad *et al.*, Phys. Rev. Lett. **87**, 071301 (2001).

[6] S. Mikheyev and A. Smirnov, Soviet Journal of Nuclear Physics **42**, 913 (1985).

[7] L. Wolfenstein, Phys. Rev. D **17**, 2369 (1978).

[8] J. T. Pantaleone, Phys. Lett. **B287**, 128 (1992).

[9] S. Samuel, Phys. Rev. **D48**, 1462 (1993).

[10] V. A. Kostelecky and S. Samuel, Phys. Lett. **B318**, 127 (1993).

[11] V. A. Kostelecky, J. T. Pantaleone, and S. Samuel, Phys. Lett. **B315**, 46 (1993).

[12] S. Pastor, G. G. Raffelt, and D. V. Semikoz, Phys. Rev. **D65**, 053011 (2002), `arXiv:hep-ph/0109035`.

[13] H. Duan, G. M. Fuller, and Y.-Z. Qian, Phys. Rev. **D74**, 123004 (2006), `arXiv:astro-ph/0511275`.

[14] B. Dasgupta and A. Dighe, Phys. Rev. **D77**, 113002 (2008), `arXiv:0712.3798`.

[15] G. L. Fogli, E. Lisi, A. Marrone, and A. Mirizzi, JCAP **0712**, 010 (2007), arXiv:0707.1998.

[16] H. Duan, G. M. Fuller, and Y.-Z. Qian, (2010), arXiv:1001.2799.

[17] A. Dighe, J. Phys. Conf. Ser. **203**, 012015 (2010), arXiv:0912.4167.

[18] A. D. Dolgov *et al.*, Nucl. Phys. **B632**, 363 (2002), arXiv:hep-ph/0201287.

[19] A. D. Dolgov, Phys. Rept. **370**, 333 (2002), arXiv:hep-ph/0202122.

[20] C. Lunardini and A. Y. Smirnov, Phys. Rev. **D64**, 073006 (2001), arXiv:hep-ph/0012056.

[21] G. L. Fogli, E. Lisi, D. Montanino, and A. Mirizzi, Phys. Rev. **D68**, 033005 (2003), arXiv:hep-ph/0304056.

[22] J. P. Kneller and G. C. McLaughlin, Phys. Rev. **D73**, 056003 (2006), arXiv:hep-ph/0509356.

[23] J. P. Kneller, G. C. McLaughlin, and J. Brockman, Phys. Rev. **D77**, 045023 (2008), arXiv:0705.3835.

[24] J. Gava, J. Kneller, C. Volpe, and G. C. McLaughlin, Phys. Rev. Lett. **103**, 071101 (2009), arXiv:0902.0317.

[25] F. N. Loreti, Y. Z. Qian, G. M. Fuller, and A. B. Balantekin, Phys. Rev. **D52**, 6664 (1995), arXiv:astro-ph/9508106.

[26] G. L. Fogli, E. Lisi, A. Mirizzi, and D. Montanino, JCAP **0606**, 012 (2006), arXiv:hep-ph/0603033.

[27] A. Friedland and A. Gruzinov, (2006), arXiv:astro-ph/0607244.

[28] A. B. Balantekin, J. M. Fetter, and F. N. Loreti, Phys. Rev. **D54**, 3941 (1996), arXiv:astro-ph/9604061.

[29] W. C. Haxton and W. M. Zhang, Phys. Rev. **D43**, 2484 (1991).

[30] E. K. Akhmedov, M. Maltoni, and A. Y. Smirnov, Phys. Rev. Lett. **95**, 211801 (2005), arXiv:hep-ph/0506064.

[31] E. K. Akhmedov, A. Dighe, P. Lipari, and A. Y. Smirnov, Nucl. Phys. **B542**, 3 (1999), arXiv:hep-ph/9808270.

[32] E. K. Akhmedov, Nucl. Phys. **B538**, 25 (1999), arXiv:hep-ph/9805272.

[33] E. K. Akhmedov, M. Maltoni, and A. Y. Smirnov, JHEP **05**, 077 (2007), arXiv:hep-ph/0612285.

[34] E. K. Akhmedov, M. Maltoni, and A. Y. Smirnov, JHEP **06**, 072 (2008), arXiv:0804.1466.

[35] R. Gandhi *et al.*, Phys. Rev. **D76**, 073012 (2007), arXiv:0707.1723.

[36] R. Gandhi, P. Ghoshal, S. Goswami, P. Mehta, and S. Uma Sankar, (2005), arXiv:hep-ph/0506145.

[37] R. Gandhi, P. Ghoshal, S. Goswami, P. Mehta, and S. Uma Sankar, Phys. Rev. **D73**, 053001 (2006), arXiv:hep-ph/0411252.

[38] T. DeYoung, Mod. Phys. Lett. **A24**, 1543 (2009), arXiv:0906.4530.

[39] IceCube Collaboration, K. Hultqvist, (2010), arXiv:1003.2300.

[40] F. Halzen, J. Phys. Conf. Ser. **171**, 012014 (2009), arXiv:0901.4722.

[41] O. Mena, I. Mocioiu, and S. Razzaque, Phys. Rev. **D78**, 093003 (2008), arXiv:0803.3044.

[42] E. Komatsu *et al.*, (2010), arXiv:1001.4538.

[43] W.-M. Yao *et al.*, Journal of Physics G **33**, 1+ (2006).

[44] A. Friedland, Phys. Rev. **D64**, 013008 (2001), arXiv:hep-ph/0010231.

[45] G. G. Raffelt and A. Y. Smirnov, Phys. Rev. **D76**, 081301 (2007), arXiv:0705.1830.

[46] G. Fogli, E. Lisi, A. Marrone, and I. Tamborra, (2008), arXiv:0812.3031.

[47] G. Sigl and G. Raffelt, Nucl. Phys. **B406**, 423 (1993).

[48] H. Duan, G. M. Fuller, J. Carlson, and Y.-Z. Qian, Phys. Rev. **D74**, 105014 (2006), arXiv:astro-ph/0606616.

[49] B. Dasgupta, A. Dighe, A. Mirizzi, and G. G. Raffelt, Phys. Rev. **D78**, 033014 (2008), arXiv:0805.3300.

[50] S. Hannestad, G. G. Raffelt, G. Sigl, and Y. Y. Y. Wong, Phys. Rev. **D74**, 105010 (2006), arXiv:astro-ph/0608695.

[51] G. G. Raffelt, Phys. Rev. **D78**, 125015 (2008), arXiv:0810.1407.

[52] B. Dasgupta, A. Dighe, A. Mirizzi, and G. G. Raffelt, Phys. Rev. **D77**, 113007 (2008), arXiv:0801.1660.

[53] A. Friedland, Phys. Rev. Lett. **104**, 191102 (2010), arXiv:1001.0996.

[54] H. Duan, G. M. Fuller, and Y.-Z. Qian, Phys. Rev. **D77**, 085016 (2008), arXiv:0801.1363.

[55] B. Dasgupta, A. Mirizzi, I. Tamborra, and R. Tomas, (2010), arXiv:1002.2943.

[56] B. Dasgupta, G. G. Raffelt, and I. Tamborra, Phys. Rev. **D81**, 073004 (2010), arXiv:1001.5396.

[57] H. Duan, G. M. Fuller, J. Carlson, and Y.-Z. Qian, Phys. Rev. **D75**, 125005 (2007), arXiv:astro-ph/0703776.

[58] H. Goldstein, C. Poole, and J. Safko, *Classical Mechanics*, Third ed. (Addison Wesley, 2002).

[59] L. Landau and E. Lifshitz, *Mechanics*, 2nd ed. (Pergamon Press Ltd., 1969).

[60] B. Dasgupta, A. Dighe, G. G. Raffelt, and A. Y. Smirnov, Phys. Rev. Lett. **103**, 051105 (2009), arXiv:0904.3542.

[61] A. Esteban-Pretel, S. Pastor, R. Tomàs, G. G. Raffelt, and G. Sigl, Phys. Rev. D **76**, 125018 (2007).

[62] G. Fogli, E. Lisi, A. Marrone, and I. Tamborra, JCAP **0910**, 002 (2009), arXiv:0907.5115.

[63] G. G. Raffelt, M. T. Keil, R. Buras, H.-T. Janka, and M. Rampp, (2003), arXiv:astro-ph/0303226.

[64] L. Scheck, K. Kifonidis, H. T. Janka, and E. Mueller, (2006), arXiv:astro-ph/0601302.

[65] A. J. T. Poelarends, F. Herwig, N. Langer, and A. Heger, (2007), arXiv:0705.4643.

[66] C. Lunardini, B. Muller, and H. T. Janka, Phys. Rev. **D78**, 023016 (2008), arXiv:0712.3000.

[67] J. P. Kneller and C. Volpe, (2010), arXiv:1006.0913.

[68] A. N. Kolmogorov, Doklady Akad. Nauk SSSR **32**, 141 (1941).

[69] G. Pagliaroli, F. Vissani, E. Coccia, and W. Fulgione, Phys. Rev. Lett. **103**, 031102 (2009).

[70] F. Halzen and G. G. Raffelt, Phys. Rev. **D80**, 087301 (2009), arXiv:0908.2317.

[71] H. Duan, G. M. Fuller, J. Carlson, and Y.-Z. Qian, Phys. Rev. Lett. **100**, 021101 (2008), arXiv:0710.1271.

[72] A. M. Dziewonski and D. L. Anderson, Physics of The Earth and Planetary Interiors **25**, 297 (1981).

[73] F. D. Stacey, *Physics of the Earth* (Watson Ferguson and Company, 1992).

[74] M. Honda, T. Kajita, K. Kasahara, S. Midorikawa, and T. Sanuki, Phys. Rev. **D75**, 043006 (2007), arXiv:astro-ph/0611418.

[75] G. Barr, Nucl. Phys. Proc. Suppl. **143**, 89 (2005).

[76] T. K. Gaisser, Nucl. Phys. Proc. Suppl. **118**, 109 (2003), arXiv:hep-ph/0209195.

[77] R. Gandhi, C. Quigg, M. H. Reno, and I. Sarcevic, Phys. Rev. **D58**, 093009 (1998), arXiv:hep-ph/9807264.

[78] G. Masters and D. Gubbins, Physics of The Earth and Planetary Interiors **140**, 159 (2003).

[79] W. Su, R. Woodward, and A. Dziewonski, J. Geophys. Res. **99**, 6945 (1994).

[80] W. Winter, Phys. Rev. D **72**, 037302 (2005).